TISSUE ENGINEERING OF LIGAMENT THROUGH REHABILITATIVE MECHANICAL CONDITIONING OF MECHANO-ACTIVE HYBRID SILK SCAFFOLDS

Teh Kok Hiong, Thomas

B.Eng. (Hons.), NUS

A THESIS SUBMITTED FOR THE DEGREE OF

DOCTOR OF PHILOSOPHY

DIVISION OF BIOENGINEERING

NATIONAL UNIVERSITY OF SINGAPORE

2010

Preface

This thesis is submitted for the degree of Doctor of Philosophy in the Division of Bioengineering at the National University of Singapore under the supervision of Associate Professor Toh Siew Lok and Professor James Goh Cho Hong. No part of this thesis has been submitted for other degree at other university or institution. To the best of the author's knowledge, all the work presented in this thesis is original unless reference is made to other works. Parts of this thesis have been published or presented in the List of Publications shown in the subsequent section.

Teh Kok Hiong, Thomas

Singapore, July 2010

List of Publications

International Journal Publications

1. Toh SL, Teh TKH, Vallaya S, Goh JCH. Novel silk scaffolds for ligament tissue engineering applications. In: Lee SB, Kim YJ, editors. Experimental Mechanics in Nano and Biotechnology, Pts 1 and 2, 2006. p. 727-730.

2. Teh TK, Toh SL, Goh JC. Optimization of the silk scaffold sericin removal process for retention of silk fibroin protein structure and mechanical properties. Biomed Mater 2010; 5(3):035008.

3. Teh TK, Toh SL, Goh JC. Aligned Hybrid Silk Scaffold for Enhanced Differentiation of Mesenchymal Stem Cells into Ligament Fibroblasts. Tissue Eng Part C Methods 2011.

4. Sahoo S, Teh TK, He P, Toh SL, Goh JC. Interface Tissue Engineering: Next Phase in Musculoskeletal Tissue Repair. Annals, Academy of Medicine, Singapore 2011; 40(5).
5. Shi P, He P, Teh TK, Morsi YS, Goh JCH. Parametric analysis of shape changes of alginate beads. Powder Technology 2011; 210:60.

International Conferences

1. Teh TK, Toh SL, Goh JC. Novel Knitted Silk Scaffolds with Electrospun PLGA for Ligament Tissue Engineering Applications. (6th International Symposium on Ligaments & Tendons, Chicago IL, Mar 2006)

2. Toh SL, Teh TKH, Vallaya S, Goh JCH. Novel Silk Scaffolds for Ligament Tissue Engineering Applications. (The International Conference on Experimental Mechanics 2006. The 5th Asian Conference on Experimental Mechanics (ACEM5), Jeju , Korea, Sep 2006)

3. Teh TK, Toh SL, Kyaw M, Goh JC. Advanced Bioreactor System for Tendon or Ligament Regeneration. (2nd International Symposium on Biomedical Engineering, Bangkok, Thailand, Nov 2006)

4. Teh TK, Toh SL, Goh JC. Novel Nano-microfibrous Silk Scaffolds for Tendon-ligament Tissue Engineering Applications. (2nd Tohoku-NUS Joint Symposium on the Future Nano-medicine and Bioengineering in East-Asian Region, Singapore, Dec 2006)

5. Teh TK, Goh JC, Toh SL. Advanced Nano-micro Fibrous Silk Scaffold System for Tendon/Ligament Tissue Engineering. (International Society of Biomechanics XXI Congress, Taipei, Taiwan, 1 – 5 July 2007)

6. Teh TK, Goh JC, Toh SL. Characterization of Nano-Microfibrous Knitted Silk Hybrid Scaffold Systems for Tendon/Ligament Tissue Engineering Applications. (3rd WACBE World Congress on Bioengineering, Bangkok, Thailand, 9 – 11 July 2007)

7. Teh TK, Goh JC, Toh SL. The Effects of Nanofibers Arrangement in a Novel Hybrid Knitted Silk Scaffold System for Tendon/Ligament Tissue Engineering Applications. (Tissue Engineering & Regenerative Medicine International Society Asian-Pacific Chapter Meeting 2007, Tokyo, Japan, 3 – 5 December 2007)

8. Teh TK, Goh JC, Toh SL. The Effects of Nanofibers Arrangement on BMSC Growth in a Hybrid Knitted Silk Scaffold System for Tendon/Ligament Tissue Engineering Applications. (3rd Tohoku-NUS Joint Symposium on Nano-Biomedical Engineering in the East Asian-Pacific Rim Region, Singapore, 10 – 11 December 2007)

9. Teh TK, Goh JC, Toh SL. Comparative Study of Random and Aligned Nanofibrous Scaffolds for Tendon/Ligament Tissue Engineering. (7th Asian-Pacific Conference on Medical and Biological Engineering, Beijing, China, 22-25 April 2008)

10. Teh TK, Goh JC, Toh SL. Comparative Study of Random and Aligned Submicron Fibrous Scaffolds for Tendon/Ligament Tissue Engineering. (16th Congress of the European Society of Biomechanics, Lucerne, Switzerland, 6-9 July 2008)

11. Teh TK, Goh JC, Toh SL. Aligned Electrospun Substrates for Ligament Regeneration using Bone Marrow Stromal Cells. (Tissue Engineering and Regenerative Medicine International Society Asian-Pacific Chapter Meeting 2008, Taipei, Taiwan, 6-8 November 2008)

12. Teh TK, Goh JC, Toh SL. Characterization of Electrospun Substrates for Ligament Regeneration using Bone Marrow Stromal Cells. (13th International Conference on Biomedical Engineering, Singapore, 3-6 December 2008)

13. Teh TK, Toh SL, Goh JC. A comparative study of different mechanical conditioning regimes for the development of tissue engineered anterior cruciate ligament. (Tissue Engineering and Regenerative Medicine International Society Asian-Pacific Chapter Meeting 2010, Sydney, Australia, 15-17 September 2010). *Best Poster Award (3rd Prize)

14. Teh TK, Toh SL, Goh JC. Rehabilitative Mechanical Conditioning Regime for Tendon/Ligament Tissue Regeneration. (11th International Symposium on Ligaments and Tendons, Long Beach, California, USA, 12 January 2011) *Finalist for Savio L-Y. Woo Young Researcher Award

Acknowledgements

I would like to express my deepest gratitude to my mentors, Associate Professor Toh Siew Lok and Professor James Goh, who have led and inspired me towards research in the exciting and multidisciplinary field of tissue engineering and orthopaedic research. I am blessed to have their tireless support and guidance through the years of academic pursuit in the National University of Singapore. I am also grateful to the committee members of my qualifying examination, Prof Lim Chwee Teck and Associate Professor Tong Yen Wah, for their guidance and valuable feedback on this research undertaking. I am deeply appreciative of Dr Liu Haifeng and Dr Fan Hongbin, who as my post-docs, assisted and guided me in the early days of my research pursuit.

This project would not have been realized if not for the help, support and valuable discussion made with my colleagues at the Tissue Repair Lab and NUSTEP Lab. Special thanks have to be given to our Laboratory Technologists, Ms Lee Yee Wei and Ms Serene Goh, who have conscientiously ensured that the lab is always in order and have supported efficiently in the logistical aspect of this study. I would like to thank my fellow lab mates, Moe, Zheng Ye, Sambit, Bibhu, Eugene, Kian Siang, Peng Fei, Kelei, Pamela, Yuwei and Sujata for their support through both the exhilarating and challenging times of my research pursuit. Acknowledgement also needs to be given to the four undergraduate students, Sin Chang, Joanne, Zhihong and Alfred, who have assisted in parts of this study as fulfillment of their final year projects.

I would like to thank Mdm Zhong Xiangli from the Materials Lab for her help in SEM characterizations, Mr Chiam from the Experimental Mechanics Lab for his help in

the fabrication of jigs and components of the electrospinning and bioreactor setups, Dr Zhang Yanzhong and Hock Wei for their help in the biomechanical characterizations, Ms Eunice Tan from the Nano Biomechanics lab for her help in nano mechanical characterizations, and lastly Ms Amy Chee and Mr Cheng from the Dynamics Lab for their help in the use of the mechanical vibrator for degumming.

Last but not least, I am extremely grateful to my parents who have supported and nurtured me through my life. Together with my sister, Michelle, they have been my pillar of support through happiness and woes in my life endeavors. Another pillar of support of mine is my wife, who not only shares my enthusiasm and aspiration in research, but also bears undying faith in my abilities. Thank you, Erin, for trusting in me even in the most difficult of times.

Summary

The use of appropriate mechanically viable scaffold and the provision of appropriate biophysical environment has always been one of the keys to successful regeneration of ligament tissues. With the aim to biomimic the native environment, an aligned hybrid silk fibroin (SF) scaffold and a rehabilitative mechanical conditioning regime were studied. It was hypothesized that the mechano-active hybrid SF scaffold (AL) consisting of knitted SF integrated with aligned SF electrospun fibers (AL-SFEF) could enhance tissue regeneration by first promoting cellular alignment, which in turn facilitated effective mechano-transduction when the cell-seeded AL scaffolds were mechanically conditioned rehabilitatively. The study was grouped into four stages: (i) design and development of the SF knit, (ii) development of the AL scaffold, (iii) *in vitro* characterization of the AL scaffold, and (iv) rehabilitative mechanical conditioning of the AL scaffolds.

The first stage involved evaluation of the SF mechanical properties as an initial step to the design of the SF knit. Upon selecting the mechanical properties of the optimally degummed SF fibers, design of the SF knit revealed that 240 SF count was necessary. The designed silk knits were subsequently optimally degummed for overall structural/mechanical properties retention and effective sericin removal.

The second stage then involved electrospinning SFEF meshes and physically incorporating them to the knitted SF. Highly aligned SFEF meshes were obtained by using a customized electrospinning setup. The meshes were subsequently integrated physically with the SF knit via sequential and localized application of methanol to

produce inherent contractile forces of the SFEF meshes. Characterization of the completed hybrid SF scaffolds revealed that the AL scaffolds had SFEF meshes well-integrated with the knitted structure and were mechanically superior.

The third stage involved *in vitro* characterization of the AL scaffolds using rabbit mesenchymal stem cells (MSCs). It was shown that the AL scaffolds stimulated increased proliferation and collagen synthesis via providing favorable topographical conditions for cell and ECM alignment. Consequently, cells expressed up-regulation of ligament-related genes and deposition of the related ECM components, which were indicative of a differentiative phase. Mechanically superior AL constructs were obtained after 14 days of culture. These effects were intensified synergistically when the mechano-active AL scaffolds were dynamically cultured.

The fourth stage involved the optimization of the mechanical stimulation approach to further enhance tenogenic differentiation. Dynamic conditioning was also performed over a longer duration to examine its prolonged effect on MSC differentiation and development in the AL hybrid SF scaffold. Leveled mechanical stimulation regimes were used to compare with the rehabilitative approach, which in contrast with level state stimulations, involved gradual application of dynamic cues with increasing intensities in terms of cyclic frequency. Through the up-regulation and deposition of ligament-related genes and ECM components, it was shown that the rehabilitative approach to dynamic conditioning AL scaffolds allowed timely introduction of appropriate stimulation intensities, which allowed early introduction of the synergistic mechanical cues to the MSC-seeded mechano-active AL scaffold to effect an accelerated tenogenic profile.

Table of Contents

List of Abbreviations

2D	2 Dimensional
3D	3 Dimensional
ACL	Anterior Cruciate Ligament
AD	Angular Deviation
AL	Aligned/Aligned Hybrid Silk Fibroin Scaffold
AL-SFEF	Aligned Silk Fibroin Electrospun Fibers
ANOVA	Analysis of Variance
bFGF	Basic Fibroblast Growth Factor
BMSCs	Bone Marrow Stromal Cells
cDNA	Complementary DNA
CFU-F	Colony Forming Unit for Fibroblast
CO_2	Carbon Dioxide
DAB	3, 3' diaminobenzidine
DAC	Data Acquisition Card
DAPI	4′, 6-diamidino-2-phenylindole, dihydrochloride
DMEM	Dulbecco's Modified Eagle Medium
DNA	Deoxy Ribonucleic Acid
DO	Dissolved Oxygen
DTT	Dithiothreitol
E	Young's Modulus
ECL	Enhanced Chemiluminescence
ECM	Extracellular Matrix
ES	Elastic Stiffness

FBS	Fetal Bovine Serum
FDA	Food and Drug Administration of the United States
FTIR-ATR	Fourier-transformed infrared spectroscopy, using the attenuated total reflection method
GAG	Glucosaminoglycans
GAPDH	Glyceraldehydes 3-phosphate Dehydrogenase
H	Horizontal Length
H&E	Hematoxylin and Eosin
HC	Heavy Chain
HFIP	1,1,1,3,3,3-hexafluoro-2-propanol
HLA	Human Leukocyte Antigen
HLF	Human Ligament Fibroblasts
HRP	Horseradish Peroxidase
INF-γ	Interferon γ
ISCT	International Society for Cellular Therapy
LAD	Ligament Augmentation Device
LARS	Ligament Advanced Reinforcement System
LC	Light Chain
LCL	Lateral Collateral Ligament
L-PLA	L-polylactic Acid
LPS	Lipopolysaccharide
MA	Mechanical Agitation
MCL	Medial Collateral Ligament
MLC	Mixed Lymphocyte Culture
MSCs	Mesenchymal Stem Cells

MW	Molecular Weight
Na_2CO_3	Sodium Carbonate
NZW	New Zealand White
O_2	Oxygen
PBS	Phosphate Buffer Solution
PCL	Posterior Cruciate Ligament
PDS	Polyparadioxanone
PGA	Poly(glycolide)
PLAGA	Poly(lactide-co-glycolide)
PLLA	Poly(L-lactide)
PU	Polyurethane
qRT-PCR	Quantitative Reverse Transcription Polymerase Chain Reaction
RD	Random/Randomly-arranged Hybrid Silk Fibroin Scaffold
RD-SFEF	Randomly-arranged Silk Fibroin Electrospun Fibers
RNA	Ribonucleic Acid
SD	Standard Deviation
SDS	Sodium Dodecyl Sulfate
SDS-PAGE	Sodium Dodecyl Sulfate-Polyacrylamide Gel Electrophoresis
SEM	Scanning Electron Microscope
SER	Sericin
SF	Silk Fibroin
SFEF	Silk Fibroin Electrospun Fiber
SIS	Small Intestinal Submucosa
SMC	Smooth Muscle Cell
TCP	Tissue Culture Polystyrene

TGF-β	Transforming Growth Factor β
UTL	Ultimate Tensile Load
UTS	Ultimate Tensile Strength
V	Vertical Length

List of Tables

List of Figures

Chapter 1

INTRODUCTION

1.1. Background and Significance

Ligaments are dense regular connective tissue consisting of mainly collagenous fibers of collagen types I and III primarily [1-3], which functions to connect one bone to another or at the internal organs to provide stability at joints or to maintain position of internal organs respectively [2]. The microscopic structure of ligaments is characterized by parallel collagenous fibrils, consisting of triple helix tropocollagen molecules, arranged in a multi-level hierarchy ranging from submicron fibrils to micron level fibers and to larger entities. Such an organization provides the tissues excellent axial tensile load bearing capacity [1, 4, 5].

Of the various ligament tissues, the anterior cruciate ligament (ACL) is one of the most highly stressed structures of the body. It plays a central role in maintaining physiological knee mechanics and joint stability by resisting the anterior tibial translation and rotational loads [6-8]. While the ACL functions optimally under normal physiological loading, it is one of the most frequently injured structures [9]. It has been estimated recently that 11 in 1000 people, out of the general population, suffer knee ligament injuries per year [10]. Out of the total occurrence of knee ligament injuries, the ACL is the most commonly injured, contributing to 80% of total knee ligament injuries, with 65% of the operated injured ACLs predominantly associated with sports and recreational activities [10]. The rupture or tear of ACL can cause significant knee joint instability, which can lead to injuries of other ligaments and development of degenerative joint diseases subsequently, such as knee instability, meniscus tears and eventual osteoarthritis [11, 12].

Despite the high occurrence rate, the ACL does not heal spontaneously when torn. This is largely due to the lack of vasculature at the tissue, causing inadequate supply of essential reparative factors or agents should the tissue be torn [13]. Consequently, the disruption of the ACL remains one of the more challenging medical issues. Surgical reconstruction has been the standard treatment modality in the field of sports medicine [14], which very often succumb to the phenomenon of ineffective tissue self regeneration and looks at providing "immediate" functional restoration. These methods however often fail with time. The use of autografts, allografts or synthetic grafts has been practiced for the restoration of knee joint function, with the persistence of several disadvantages and risks, such as ligament laxity, donor site morbidity, pathogen transfer, mechanical mismatch, poor tissue integration and foreign body inflammation [15-17]. These complications often necessitate repeat surgeries, which interrupts site recovery and burdens not only the patients financially but also the medical services of its resources. Consequently, there is an increased need to research for alternative treatment solutions [18, 19] and tissue engineering has evoked much interest as it offers the potential of regenerating functional tissues of autologous origin [1, 3, 11, 20-22].

For the purpose of tissue engineering ligament tissues, the goal will be to generate neotissue from autologous cells grown on biocompatible and biodegradable scaffolds. Scaffolds of this purpose will have to provide structural template for neo-tissue development, exhibit comparable mechanical strength to that of the natural tissue and degrade at a rate that allows both optimal neo-tissue growth and progressive load transfer to neo-tissue without causing rupture of the construct. Paradoxical to the mechanical requirement, the scaffold should have sufficient void volume for cell

infiltration and extracellular matrix (ECM) deposition to promote gradual load transfer from scaffold to the neo-tissue [1, 23]. It is therefore clear that advancement in tissue engineering of ligament depends very much upon strategic application of materials engineering knowledge, involving the selection of appropriate biomaterial and scaffold architecture.

A variety of scaffold materials have been explored for this application, with popular choices ranging from synthetic poly (L-Lactide) based biomaterials to natural polymer such as collagen. Nevertheless, these materials have exhibited poor mechanical strengths and short degradation periods, both of which are disadvantageous for scaffold materials in the development of tissue engineered ligaments [24]. On the other hand, silk fibroin (SF) of *Bombyx mori* origin has been shown to be a promising candidate for this application after removal of the hyper-allergenic sericin component from raw silk [1, 3, 21, 25-27] and has compatible degradation rate that involves a gradual loss of tensile strength over 1 year *in vivo* due to proteolytic actions [1, 28]. More importantly, SF has outstanding and customizable mechanical properties, with superior strength and elasticity, making it suitable for use in constructs with high porosity without compromising the overall mechanical robustness of the construct [1, 23, 26-28]. As a structural template, SF has been shown to bear equivalence to collagen in supporting cell attachment, inducing appropriate morphology and growth since it is a natural protein as well [5, 28, 29]. To further mimic the ECM structure, SF has been successfully electrospun to form sub-micron nonwoven meshes and is found to enhance cell adhesion and spreading of type I collagen due to its high surface to volume ratio [25, 30, 31].

From the architectural perspective, ligament tissue engineered scaffolds need to be mechanically sound and bear similar loading responses to the native tissue such that mechanical cues that resemble the native environment can be transduced to the developing neo-tissue. Typical scaffold architectures used for this application include the braided, woven and knitted structures. Studies performed using the braided and woven structures have shown incompetence of these architectures in supporting uniform tissue regeneration resulting from poor nutrient transmission, cell attachment, infiltration and matrix production, especially in the early tissue regeneration phases [32-34]. The knitted scaffolds have however shown to possess good mechanical strength, encourage cell-cell signaling and promote uniform tissue formation due to sufficient scaffold porosity (>50%), thereby have been effectively used for tendon tissue engineering [35].

From a biomimetic perspective, ligament anatomy suggests fibrous structures apposite templates as an important consideration for ligament tissue engineering scaffold design. Although it may be unclear as to what exact dimensional order should structural cues be present for collagen-hierarchy reconstitution such that neo-ligament function can be optimized, recent studies have preliminarily demonstrated the positive effects of fiber alignment at the nanometer to sub-micron level on cell morphology and ECM production [23, 36, 37]. It was further discovered that alignment and elongation of cells along electrospun fibers sensitize them for effective mechano-transduction by tensioning cytoskeletal filaments [38]. The orientation of fibroblasts along a ligament has also been shown to improve its tensile strength [36]. Nonetheless, it is noted that there has been limited work in translating and utilizing this fundamental knowledge for

functional ligament tissue engineered constructs that are viable in both the mechanical and cellular aspects to allow early implantation without the need for long term *ex vivo* culture. Furthermore, assessments for the differentiative potential of bone marrow derived mesenchymal stems cells (MSCs) down the ligament fibroblast cell lineage as induced by aligned 3-dimensional (3D) scaffolds have also been limited and inconclusive.

In this study, a full SF hybrid scaffold system composing of a knitted SF fibrous mesh integrated with SF electrospun fibers (SFEFs) of aligned arrangement and seeded with MSCs is investigated for functional ligament tissue engineering applications. The aligned hybrid SF scaffold will be fully characterized prior to evaluating its feasibility *in vitro* under static and dynamic culture conditions. The purpose of the dynamic culture condition is to further enhance the positive effects due to the aligned SFEFs by utilizing it to transduce mechanical cues effectively to the seeded cells. The dynamic conditions should thus be optimized to mimic the native loading environment, while being implemented incrementally to allow optimal tissue regeneration. As such, a rehabilitative mechanical conditioning approach to ligament regeneration is envisioned to synergistically complement the aligned hybrid SF scaffold. It is anticipated that the aligned hybrid SF scaffold will combine the excellent biomechanical properties of the knitted SF mesh with the inducing ability of mechano-active aligned SFEFs, as enhanced by the rehabilitative dynamic culture conditions, to promote effective tenogenic differentiation of the seeded MSCs to regenerate functional tissue engineered ligaments.

To summarize, the specific factors affecting successful ligament tissue engineering are listed, which are addressed by the respective aspects of this study as follows:

Table 1-1: List of specific factors affecting successful tissue engineering of ligament with the aspects studied in this project to satisfy them.

Factors	Proposed to be satisfied by
Cells	Mesenchymal Stem Cells (MSCs)
Mechanically viable material	Silk fibroin (SF)
Mechanically sound architecture	Knitted structure
Biomimetic cell attachment substrate	Aligned silk fibroin electrospun fibers (AL-SFEF)
Mechanical cues	Rehabilitative approach to mechanical conditioning

1.2. Objectives

This research study is aimed at developing a novel hybrid SF scaffold that encompasses micron-scale knitted SF integrated with sub-micron aligned electrospun SF, to achieve mechanically robust construct that is capable of inducing cellular and ECM alignment. As such, the hybrid scaffold is mechano-active since mechanical cues from dynamic culture will effectively stimulate the oriented cells and matrix to further induce differentiation of MSCs towards the ligament fibroblast lineage. The novel rehabilitative mechanical conditioning regime will be designed to enhance the dynamic

culture process, which is aimed at accelerating the differentiation process to realize tissue engineered ligament at a shorter duration *in vitro*. The specific aims thus derived are:

1. Design and development of the SF knit

To design and customize SF knits to bear suitable mechanical properties for functional ligament tissue engineering applications and optimize the degumming protocol such that the mechanical properties of the SF knits can be retained.

2. Development of the aligned hybrid SF scaffold

To develop the AL-SFEF via a customized electrospinning setup which consists of a rotating grounded collector frame with two positively charged plates to limit the spinneret path. A well integrated hybrid SF scaffold structure is then obtained via physical contractile forces generated from contraction of SFEF onto SF knit upon methanol treatment for SF crystallization.

3. *In vitro* characterization of the aligned hybrid SF scaffold

To characterize and assess the differentiative potential of the MSC-seeded aligned hybrid SF scaffolds cultured in both static and dynamic conditions and compare it with the random hybrid SF scaffolds cultured in similar conditions.

Hypothesis 1: The aligned hybrid SF scaffold will be able to induce prominent tenogenic differentiation due to its positive topographical cues that cause cellular and ECM alignment.

Hypothesis 2: Enhanced tenogenic differentiation will be effected due to the synergistic effect of dynamic conditioning with the positive topographical cues of the aligned hybrid SF scaffold.

4. Rehabilitative mechanical conditioning of the aligned hybrid SF scaffolds

To optimize the parameters used for dynamic conditioning of the aligned hybrid SF scaffold such that it follows a rehabilitative approach for timely supplementation of mechanical cues at appropriate intensities. This approach will be compared with the "continuous low" and "continuous high" stimulation regime and be assessed for their effect on tenogenic differentiation.

Hypothesis 3: The rehabilitative approach to dynamic conditioning allows timely introduction of appropriate stimulation intensities, which allows early introduction of mechanical cues to the MSCs to effect an accelerated differentiative profile towards ligament fibroblasts.

1.3. Scope of Dissertation

This thesis composes of six chapters and is organized as follows:

Chapter 1 gives an introduction of the research background, objectives and scope of dissertation.

Chapter 2 is a literature review on the anatomy and function of the ligament, with insights given for the biochemical constituents and biomechanical properties of the tissue. Injury and current treatment modalities of the tissue will also be presented with

emphasis given on motivation towards the tissue engineering approach. The specific factors towards the success of ligament tissue engineering will also be reviewed in details.

Chapter 3 will focus on the design and development of the SF knit. The design process of the knitted SF with the aim to achieve mechanically viable construct that will be able to provide functional support during ligament tissue regeneration will be presented. This is followed by an optimization study of the degumming process to attain optimal retention of SF mechanical and structural properties.

Chapter 4 will present the development and characterization study of the aligned hybrid SF scaffold by assessing its mechano-active capabilities in inducing tenogenic differentiation in a static and dynamic environment.

Chapter 5 will provide an analysis of the rehabilitative mechanical conditioning regime and compare it with the continuous execution of "low" and "high" intensity stimulation profiles. Insights of this novel approach will also be presented and discussed, followed by assessing its feasibility for application in the ligament tissue engineering application.

Chapter 6 provides a conclusion of this study as well as recommendations for future works.

Chapter 2

LITERATURE REVIEW

2.1. Introduction

To gain an appreciation of the challenges involved in tissue engineering the ligament, it is essential to understand the anatomy and physiology of the tissue. Specifically, the ACL will be focused upon due to the substantial stresses it experiences and the high injury prevalence. Insights will be presented with respect to the biochemical constituents and the effective biomechanical properties of the tissue. The various modes of injury and the treatment modalities currently employed will be compared, with the tissue engineering approach being highlighted with the specific factors contributing to its success. These factors, as reviewed in this chapter, include the cell source, scaffold material, scaffold architecture and topography and dynamic culture conditions.

2.2. Ligament Anatomy and Function

Ligaments are short bundles of tough fibrous connective tissues, which serve as restraining elements in the musculoskeletal system by providing bone to bone attachment at joints, as shown in Figure 2-1 [39-43]. During motion, the contraction of a muscle results in transmission of the load from muscle, via its tendon, to a bone across a joint, which results in movement of the bone around the joints. This strains the ligaments between the bones. Therefore tendons operate to bring around movements of the joints while the ligaments prevent excessive motion of the joints and thereby provide stability [39-43]. Typically, ACL functions as the primary stabilizer of the knee motion (Figure 2-1).

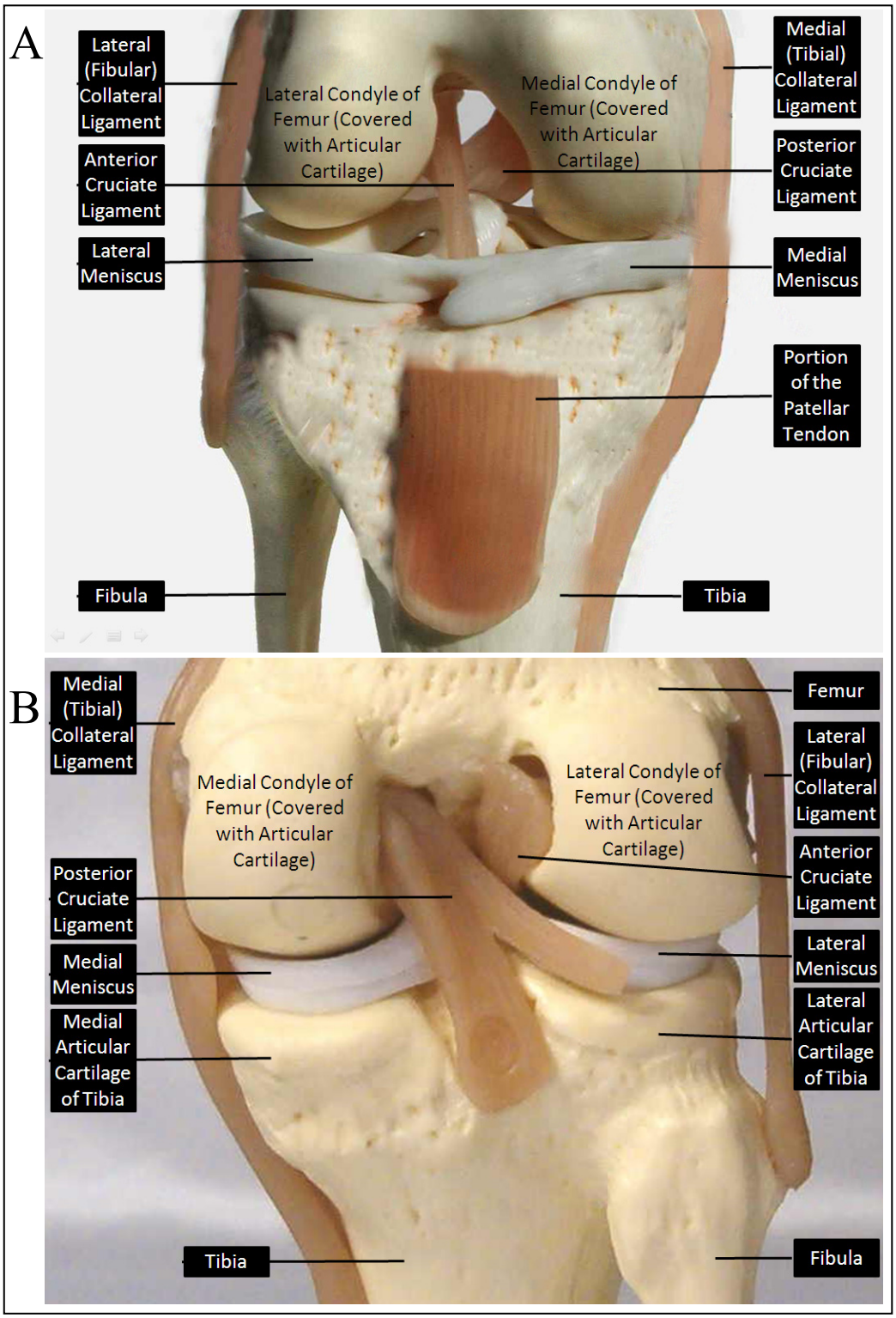

Figure 2-1: (A) Anterior view and (B) Posterior view of the knee joint with portion of the patellar tendon removed. Anterior cruciate ligament (ACL) limits rotation and forward motion of the tibia, posterior cruciate ligament (PCL) limits backward motion of the tibia, medial collateral ligament (MCL) and lateral collateral ligament (LCL) limits side motions, articular cartilage lines bones and cushions joint.

Ligaments are collagenous tissues with tropocollagen molecules as their primary building units [44]. Tropocollagen molecules are organized hierarchically into long cross-striated fibrils that are arranged into bundles to form fibers, which are further grouped into bundles called fascicles. Bundles of fascicles are then grouped together to form the ligament (Figure 2-2) [24, 45-48]. A large number of fibroblasts are scattered amongst and aligned in the direction of collagen fibers [2]. Collagen fiber bundles are arranged in the direction of functional need and act in conjunction with elastic and reticular fibers along with ground substance, composed of glycosaminoglycans (GAG) and tissue fluid, to give ligaments their mechanical characteristics, which are characteristic features of fiber reinforced composites [49]. In unstressed ligaments, collagen fibers take on a sinusoidal pattern. This pattern is referred to as a "crimp" pattern and is believed to be created by the cross-linking or binding of collagen fibers with elastic and reticular fibers. A structure, as such, optimizes axial tensile load bearing by imparting great strengths with limited extensibility and is essential for ligaments to perform their function [1, 4, 50].

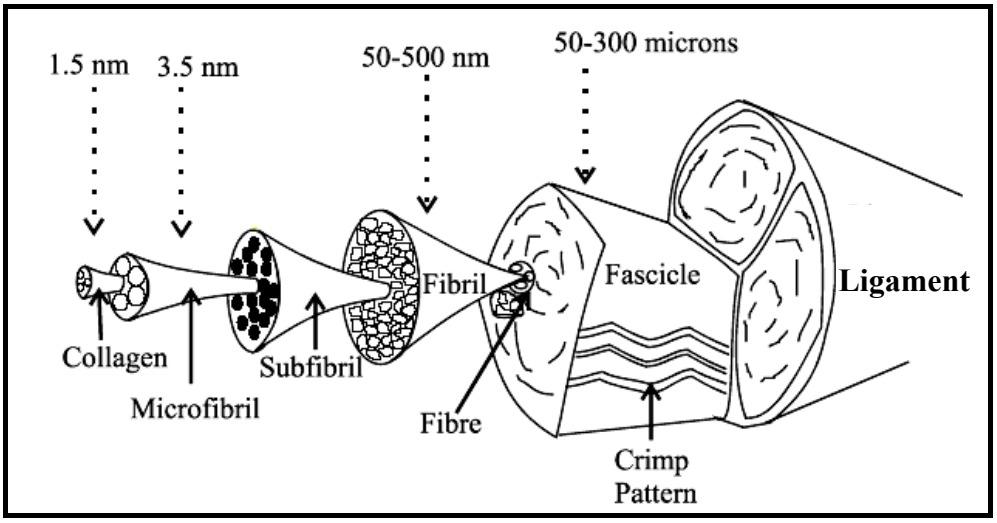

Figure 2-2: Schematic diagram of the structural hierarchy of ligament. Adapted from [51].

Specifically, the ACL of the knee is the major intra-articular ligament responsible for normal kinematics and stability of the knee joint [39-43]. It connects the femur to the tibia and is completely enveloped by synovium. Anatomical observations revealed that the tibial insertion point is broad and irregular at the front of the intercondylar area, while the femoral attachment is semicircular at the posteromedial part of the lateral femoral condylar area [39-43]. The human ACL is approximately 10-13 mm wide and is 30-38 mm long [24, 39-41, 43, 45, 52, 53], with large number of fiber bundles arranged into the anteromedial, posterolateral and intermedial portions [39-43]. Consequently, low friction and low tension during normal range of motion is achieved with such arrangements, with the anteromedial bundle becomes taut only during flexion, while the posterolateral bundle tautens only during extension. At the insertion sites the ligament gradually transforms from the midsubstance, to the fibrocartilage, and to the calcified fibrocartilage that inserts into the bone. The epiligament, containing cells, nerves and blood vessels wraps around the periphery of the ligament tissue, with blood supplied mainly from the middle geniculate artery and fat pad [41, 48]. Physiologically, the fascicles of the ACL are arranged helically near the bone junction and in parallel alignment internally to allow load distribution, such that different zones of the ligaments are loaded with varying degrees at different time of loading [41, 45]. This prevents the tissue from getting point stresses and rupture during normal physiological loading.

2.3. Biochemical Constituents of Ligament

Collagen, elastin, glycoproteins, protein polysaccharides, glycolipids, water and cells form the major constituents of the ligament [54]. Out of which water makes up 60-80 % of the wet weight of ligaments as compared to that of 55% for tendons. The approximate compositions are given in Table 2-1.

Table 2-1: ECM composition of ligaments [24, 41, 45, 55].

Major constituents	Approximate amount, % dry weight	Characteristics or functions
Type I collagen	80	Fibril bundles
Type III collagen	5-15	Thin fibrils
Type IV collagen, laminin, nidogen	<5	In basal laminae under epithelium and endothelium
Types V, VI, and VII collagens	<5	Type VII forms anchoring fibrils; others unknown
Elastin, fibrillin	<5	Provides elasticity
Fibronectin	<5	Associated with collagen fibers and cell surfaces
Proteoglycans, hyaluronate	0.5	Provide resiliency

2.4. Mechanical Properties

As a result of the unique organization and arrangement of fibers and fascicles within the ligament, the mechanical behavior of the tissue follows a viscoelastic trend, that is, there is increasing stress with increasing strain rate applied to the tissue. Therefore, injury to the ligament depends upon the absolute load, as well as the rate of at which the load is given or impact sustained by the tissue. Before the mechanisms of

ligament injury can be appreciated, it will be critical to understand the mechanical properties of the tissue. Furthermore, to effectively devise a suitable graft for repair of the ligament, a good understanding of the mechanical properties of the native tissue will be beneficial.

With the main function to transmit tensile loads across joints, largely in a uniaxial direction, the material properties of the ligament is highly anisotropic in nature, as contributed by the parallel collagen fibers. Their mechanical properties are usually described in the axial direction, and can be grouped as (1) structural properties (2) time- and history-dependent viscoelastic properties.

2.4.1. Structural Properties

The structural properties of ligament are extrinsic measures of the tensile behavior of the overall structure. As a result, they depend on the structural attributes, that is, the size and shape of the ligament. In addition, it also depends on the variations of zonal properties from tissue to the bone insertion zones. Structural properties are obtained by loading the tissue to failure, with load and elongation readings charted to attain the resulting load-elongation curve and the derived stress- strain curve as shown in Figure 2-3. Stress-strain curves are derived upon measurement of the tissue cross-sectional area using laser micrometry method, which is employed for accurate measurement of the tissues without deforming the cross-section of tissues [56]. The structural properties obtained from these curves are described in the Table 2-2.

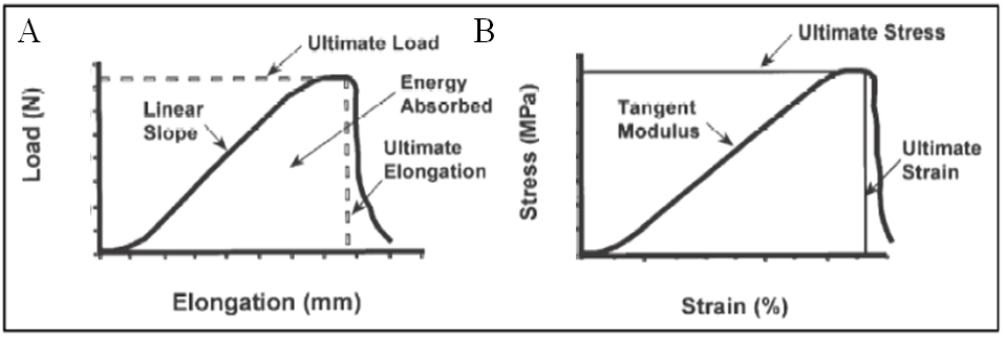

Figure 2-3: A typical (A) load-elongation curve and (B) stress-strain curve for ligament.

Table 2-2: Structural properties from the load-elongation curve and stress-strain curve of ligament [24, 41, 45, 55].

	Structural Properties	Description
Properties obtained from load-elongation curves	Ultimate tensile load (UTL)	Maximum load placed on tissue before failure occurs
	Ultimate elongation	Maximum elongation taken at point of failure
	Elastic stiffness (ES)	Slope of the load-elongation curve taken during the linear elastic phase
	Energy absorbed at failure	Area under the load-elongation curve up to point of failure
Properties obtained from stress-strain curves	Ultimate tensile strength (UTS)	Maximum stress achieved by tissue before failure occurs
	Ultimate strain	Strain achieved at failure
	Young's modulus (E)	Tangent modulus in the linear region of the stress-strain curve
	Toughness	Area under the stress-strain curve

Tissue stiffness is noted to be constant at forces above 50% of the ultimate load, while a pronounced "toe region" is observed at forces below ~25% of ultimate load. At this region, stiffness increases as the ligament unit is lengthened that is associated with the straightening of the "crimp" pattern of the collagen fibers.

The peak stress to which a ligament is subjected varies according to its anatomical site and the species. Values obtained vary with the testing protocol and conditions, and are enumerated in Table 2-3 for some tendons and ligaments of human and rabbits [24, 39, 42, 43, 57-78]. It should be noted that the human patellar tendon is often regarded as the gold standard for allogeneic ACL graft repair [74, 79].

Table 2-3: Mechanical properties of human tendons and ligaments [24, 39, 42, 43, 57-78].

Tissue	UTL (N)	UTS (MPa)	Ultimate Strain (%)	Stiffness (N/mm)	E (MPa)	Length (mm)	Cross-sectional area (mm^2)
Immature human ACL (22-35 years old)	1725-2200	38 ± 4	44.3 ± 9.0	182-292	----	26.9 ± 1.0	44.4 ± 4.0
Mature human ACL (35-50 years old)	1160-1503	13-46	9-44	192-220	65-541	33	----
Mature human ACL (60-97 years old)	495-734	13.3 ± 5.0	30 ± 10	124-180	----	27.5 ± 3.0	57.5 ± 16.0
Human Patellar tendon	2900 ± 260	24-69	14-27	1154 ± 193	143-660	48.7 ± 4.0	50.5 ± 3.0
Human Achilles tendon (Ankle)	----	14-61	24-59	----	65	----	----
Human Inferior glenohumeral ligament (Shoulder)	----	5-6	8-15	----	30-42	----	----
Human Anterior Longitudinal ligament (Spine)	----	8-37	10-57	----	286-724	----	----
Immature rabbit ACL (2.5kg)	218 ± 33		----	109 ± 10	----	8.2 ± 0.8	----
Mature rabbit ACL (4-5kg)	369 ± 53 (251 ± 47)	516 ± 69 (49 ± 20)	----	130 ± 19	----	11.7 ± 1.0	3.3-3.7 (5.3 ± 0.6)

The stress-in-life ranges of adult mammalian limb tendons vary from 10-70 MPa, with 13MPa being the most common stress value. Ultimate tensile strength of 50–100 MPa and ultimate strain of 2-5% has been reported in tendon tissues [80]. Amongst the ligaments, the ACL is the strongest with the human ACL shown to possess values of Young's Modulus of 345.0 ± 22.4 MPa, UTS of 36.4 ± 2.5 MPa and ultimate strain of 15.0 ± 0.8 % [81]. In terms of breaking loads, the UTL of normal human ACL ranges between 1,730-2,200 N [41, 45] and allows 7% to 16% of creep before permanent deformation and ligament damage occurs [82]. Cyclic loads of approximately 300 N is experienced by ACLs about 1 to 2 million times per year, with regular exposure to tensile forces ranging from 67 N (for ascending stairs) to 630 N (for jogging) [83-85]. For young human, breaking loads for ACL range from 1725N to 2160N. With that, it should be noted that ultimate mechanical properties of ligaments usually increase during development and decrease with aging.

2.4.2. Time- and History-Dependent Viscoelastic Properties

Ligament, like many other biological materials, possesses time-dependent and history-dependent viscoelastic properties [81]. As such, the loading and unloading of a specimen yields different paths on the load-elongation curve for each testing cycle, forming a hysteresis loop that represents the energy lost as a result of a non-conservative or dissipative process, as shown in Figure 2-4. This viscoelastic behavior is assumed to be due to complex interactions of the biochemical constituents of the tissues, of mainly collagen, water, surrounding protein, and ground substance (GAG).

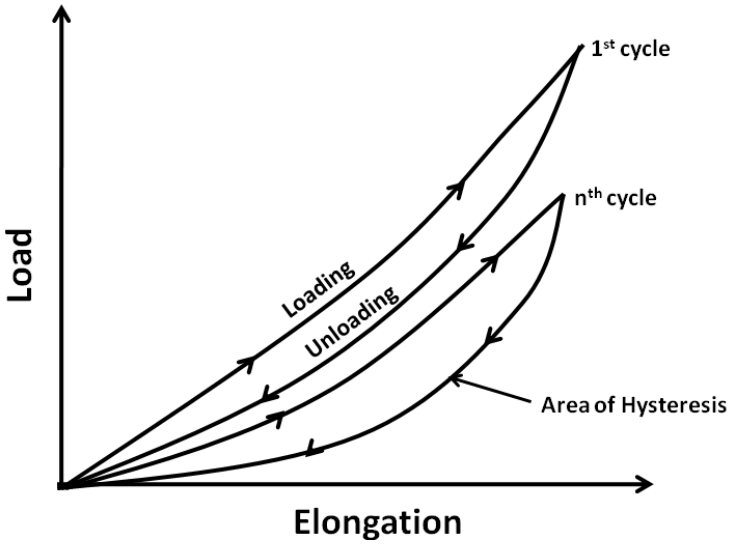

Figure 2-4: Cyclic load-elongation behavior shows that during cyclic loading, the loading and unloading curves do not follow the same path and create hysteresis loops indicating the absorption of energy; the energy loss is approximately 7% of the loading energy; however as the cycle number increases, the hysteresis decreases.

The viscoelastic behavior can be illustrated by two classic experimental tests: stress relaxation and creep tests. A stress relaxation test involves stretching the specimen to a constant length and allowing the measured stress to vary with time. A creep test involves subjecting a specimen to a constant force while the measured length gradually increases with time. Many researchers [86-89] have mathematically modeled the results of these tests better understand the time-dependent and nonlinear behaviors of ligament.

2.5. Ligament Injury

Ligaments, such as the knee collateral and cruciate ligaments, are frequently injured [9]. In the United States, more than 100,000 patients per year undergo surgery to repair tendon or ligament injuries [59]. Injuries to the ACL and the medial collateral ligament (MCL) of the knee (Figure 2-1) account for approximately 90% of all knee ligament injuries in young and active individuals, which occurred primarily during sports activities [9]. It is not surprising for the ACL to rupture or tear due to shocks sustained through contact sports, as it takes approximately 75% of the anterior shock load at the knee. Injury of such nature can cause pain and discomfort, with joint instability and even degenerative joint diseases over time. With an estimated 200,000 patients in America who required reconstructive surgery of the ligaments in 2002, billing over five billion dollars [90], there is a need to understand the mechanism involved in the tissue injury and repair, to devise effective treatment methodologies for the reconstruction of the tissue.

2.5.1. Mechanism of injury

Both the tendons and ligaments are injured primarily by two mechanisms:

1. Single impact macro-trauma

Single impact macro-trauma rupture generally occurs when there is a sudden overload strain of more than 8% applied to the tissue. This typically occurs in tendons like the Achilles tendon when occasional athlete makes an explosive push-off maneuver. Although this occurs typically in middle-aged male engaging intermittent

activities, it has been seen in young, high performance athletes as well. This mode of injury is also possible in cases where there is a direct blow onto the tendon when it is in a state of contraction [91]. For ligaments, this mechanism is typical for rupture of the ACL due to impact during contact sports, when the tissue experiences sudden overload strain, often due to twisting of the knee joint [10].

2. Repetitive exposure to low magnitude force

This mechanism of failure is often associated with repetitive loading of the tendon/ligament at 3-8% strain, leading to damage that cannot be regenerated at as fast a rate as that of the damage. With repetitive overuse, microscopic failure of the collagen fibrils or bundles begins to occur, leading to an inflammatory process at the tissue [9]. Tendons of the lower limbs are typical damaged due to this reason, especially due to extensive physical activity, which results in overuse injuries of the tendon [92]. Conditions as such are known as tendonitis, which is frequent in both occupational and athletic settings. It has been estimated that as high as 30-50% of all sports injuries can be classified as overuse injuries. In most cases, patients respond well to conservative treatment involving weeks to months of rests and therapeutic exercises. However, surgical restoration is necessary for the other patients to resume function of the tissue.

2.5.2. Healing of Ligament Injuries

The injured ligament has poor ability to heal intrinsically. This is because of the lack of vascularity in the tissues [93, 94]. Factors that can moderate the rate of healing include age, systematic factors and local factors such as blood supply synovial environment for ligaments within synovial capsules, mechanical stresses and

inflammatory cellular response [95]. Despite these factors, the healing process generally encompasses three phases of varying duration and rates: the acute inflammatory or reactive response phase, the regenerative or repair phase, and the tissue remodeling or maturation phase [9, 24, 39, 43, 47, 96-98].

Upon injury, acute inflammatory response starts within the first 72 hours with hypercellular activity involving the migration of inflammatory cells and erythrocytes to the site. Inflammatory cells such as polymorphonuclear leukocytes, lymphocytes, monocytes and macrophages phagocytize necrotic tissue and cell debris of the injured tissue. There is then a cellular concentration shift nearing the end of this phase from inflammatory cells to fibroblasts, leading to the formation of healing matrix consisting of randomly arranged collagen, and amorphous ground substances.

The healing matrix becomes gradually more organized over the next 6 weeks post injury during the repair and regeneration phase. This phase is characterized by active fibroblast proliferation and consequently further matrix deposition. Other cell types present include the macrophages and mast cells. To accelerate the regeneration of the healing matrix, a proliferating scar tissue or fibrous capsule is formed around the injured areas with development of vascularity in the wound. The scar tissue is thicker and is more cellular compared with the native tissue. There is also higher percentage of collagen III as compared to collagen I, which is typical of disorganized collagen fibrils. Leading to the next phase, the amount of fibrous capsule, vascularity and cellular density will decrease gradually.

The final phase is the tissue remodeling or maturation phase, which can last up to a year or longer from the initial injury. During this phase, the density of collagen increases as alignment of fibrils along the axis of the ligament improves, with the proportion of collagen I increasing over collagen III. Although there is gradual alignment of collagen fibrils over time, slight disorganization and abnormalities persist due to environment and mechanical factors, with the tissue never to regain its original properties.

2.6. Current Treatment Modalities

As a result of the less than optimal intrinsic regeneration capability of the ligament, surgical interventions using grafts are often necessary for full rupture of the tissue midsubstance or if the tissue is severed from the bone insertion points. Thus far, torn ligaments are usually sutured back while rupture ligaments are reconstructed or replaced by biological grafts or non-degradable synthetic prostheses [24].

Particularly for the ACL, the first surgical repair dates back to the late 1890's, when Robeson and Battle sutured torn ACL using silk and catgut sutures [99-101]. Subsequently, ligament reconstructions were performed using autogenous tissues such as fascia lata and tendons [99-101]. From then on, several reconstruction options for the ruptured ligaments are available and can be classified largely into three categories, which includes the permanent grafts, biological grafts, and degradable grafts [41, 45, 47, 55, 59, 102-109].

2.6.1. Permanent Grafts

Development of synthetic grafts started in the late 1950's when nylon ligament replacements were used only to find out later that it had carcinogenic side effects, consequence of its extreme foreign body reactions. During the 1970's, a polyethylene replacement called Polyflex prosthesis was approved by the FDA but was eventually retracted from the market in 1977 due to fatigue failure. Since then, new graft devices and procedures were developed based on a FDA guidance document for intra-articular prosthetic knee ligament devices in 1987 [99-101]. Several FDA approved ligament synthetic grafts had developed since then, as listed in Table 2-4, which included the Gore-Tex® Cruciate Ligament Prosthesis (polytetrafluoroethylene) by W.L. Gore and Associates, the Stryker Dacron® Ligament Prosthesis by Meadox Medicals, Inc., the 3M Kennedy Ligament Augmentation Device® (LAD, polypropylene) by 3M for Marshall-Macintosh procedure, the Surgicraft ABC carbon prosthetic ACL by Surgicraft Ltd, the Leeds-Keio artificial ligament (polyethylene terephthalate) and the ligament advanced reinforcement system (LARS) artificial ligament [24, 105, 108, 110-112], many of which are no longer suitable for human ACL replacement.

Table 2-4: Synthetic ACL prosthesis with their advantages and disadvantages.

Prosthesis	Advantages	Disadvantages
Gore-Tex	Tensile strength 3x native human ACL	Progressive long term loosening
Dacron	Polyester coating can protect implant from abrasion	Poor long-term stability
Kennedy LAD	Protects autogenous graft from excessive stresses	Weak implant-graft interface Can cause intra-articular inflammation, resulting in synovitis and effusions
Carbon	Stress reduction and uniform distribution between graft and soft tissue attachment Polylactic acid coat protects graft during implantation	Migration of carbon wear particles Poor long-term functional outcome resulting from implant stretching and rupture
Leeds-Keio Artificial Ligament	Acts as a scaffold for soft tissue ingrowth Excellent maximum tensile strength which exceeds that of native ACL	Stress-shielding effect leads to lack of tissue ingrowth and maturation Large number of long-term graft ruptures
LARS Artificial Ligament	Mimics natural ACL structure and orientation with porosity to encourage tissue ingrowth Reduces shearing forces on the implant	Residual post-operative laxity persists No long-term follow-up study as yet

These non-degradable grafts can be further classified into three categories: permanent replacements, augmentation devices and scaffolds [45].

The Gore-Tex® prosthesis is an example of permanent replacements. It is made of a single long strand of expanded polytetrafluorethylene that is wound into multiple loops and jointed to a three-strand braid. Designed with ultimate tensile strength of

greater than 4448 N to give immediate fixation with early load-bearing capabilities, this prosthesis gives patients early mobilization and activity [41, 45, 100, 101, 107, 113-115]. Gore-Tex® graft ultimately failed from material fatigue owing to the lack of tissue ingrowth, consequence of both the graft design and material properties. Failure of the graft is apparent from observations of fraying at the bone tunnels and consequently chronic effusions [41, 116]. It is thus apparent that although permanent synthetic ACL replacements provide the function of the ligament it replaces, it does not encourage tissue ingrowth, resulting in long-term mechanical failure due to creep and fatigue.

The Kennedy Ligament-Augmentation Device® (LAD) consists of a cylindrical prosthesis of diamond braided poly(propylene) yarns and was designed to provide protection to a weak portion of the quadriceps patellar tendon autograft or allografts during early postoperative period of the ACL reconstruction [45, 100, 101, 105]. The resulting construct has ultimate tensile strength of 1730 N and works by simply stacking over the autograft and has been used as primary repair of partially torn ACLs. LADs had high rate of complications in primary ACL reconstructions (up to 63%) and was reportedly causing delay in ligament maturation because of stress shielding [117].

An example of scaffold prosthesis is the Leeds-Keio ligament replacement, which consists of a porous woven tube of poly(ethylene) terephthalate to allow tissue ingrowth [45, 100, 101, 108]. The ultimate tensile strength of the Leeds-Keio ligament is 2600 N, giving it enough strength to protect the knee during early stage remodeling. This device allows for early post-operative mobilization [100, 101] but problems of stress shielding to the neoligament tissue persist.

The Dacron® ligament was designed as hybrid prosthesis to solve the problems of stiffness or stress-shielding that led to high failure rates in earlier devices [118]. Although tissue ingrowth was significant, the graft did not provide knee stability because organized collagenous ingrowth was not observed. This is probably due to eventual stress shielding from the synthetic material and nondirectionality of the sheath covering.

To date, no permanent ligament prostheses have met the requirements for long term ACL substitutes [24, 45]. They have shown problems ranging from long-term failure, indicative by synovitis, arthritis and mechanical deterioration, to lack of supportive tissue ingrowth and organization due to stress shielding [41, 45]. Therefore ideal ligament reconstruction should involve devices that are biodegradable to allow gradual transfer of mechanical load to the biological graft or neoligament tissue.

2.6.2. Biological Grafts

Current ACL reconstructions involving the use of autografts are typically collagenous tissues from the patient's own patellar tendon, hamstring tendon and quadriceps tendons [47, 55, 79, 90, 104, 119-124]. The success of these biological grafts often depends on the revascularization and remodelling of these transplanted tissues, which will eventually be covered by the synovial membrane. The use of central 1/3 or lateral 1/3 section from patellar tendon is still considered the gold standard for ACL reconstruction and has been approved for use in patients since 1992 [55]. It is often harvested in a bone-patellar tendon-bone configuration with small piece of bone from both the patella end and the insertion area at the tibia. This construct is then anchored at

both the femur and tibia bone tunnels, which will heal in 6-8weeks. The tensile strength of the graft is approximately 2950 N to failure [61, 63] and is reportedly able to withstand upcoming stresses after proper rehabilitation. The key limitation of autografts is donor site morbidity. Several other considerations include the limited sites at which suitable autogenous tissues can be harvested, unpredictable graft resorption characteristics, increased recovery time due to damage to additional tissue harvest site and potential failure or injury of the harvest site.

Other sources for biological grafts include allografts such as patellar tendon, hamstring tendon and Achilles tendon from cadevers [55, 64, 103, 104, 106, 125-129]. This graft source is especially useful for surgeries involving multiple grafts and in revision surgeries when autografts have previously been harvested. Although the patient's problem of site morbidity is removed, the main limitation of allograft use lies in the risk of disease transmission such as HIV and Hepatitis, bacterial infection and immunogenic response elicited in the host, which can hinder tissue remodeling [47, 63, 130]. These limitations are largely due to the inability of the graft to be sterilized as it will then be weakened [45, 128]. The current processing steps involved in preparing allografts for implantation include harvesting, cleaning, screening for HIV and Hepatitis, and finally frozen and stored in liquid nitrogen. Consequently, the tissue is cleared of disease with a probability of infection at 1:1,000,000.

It is thus clear that both sources for biological grafts are limited by several uncontrollable factors. It is these limitations that drive the search for more robust reconstruction solutions, which very often utilize synthetic materials that can promote tissue ingrowth and biodegradable to allow neotissue regeneration [41, 45, 55, 59, 109].

With the knowledge that ACL autografts are remodelled by 8 weeks and are complete by 20 weeks post-implantation [24], the goal will thus be to devise a solution that achieves this in shorter or comparable duration.

2.6.3. Biodegradable Grafts

The application of reconstructive surgery for ruptured ligament is undoubtedly necessary due to the lack of intrinsic reparative ability of the tissue. Although there is limited success in the reconstruction of ligament, particularly the ACL, using permanent prosthesis and biological grafts, many of the limitations can be overcome with the advancement in biodegradable grafts. In particular, tissue derived materials such as collagen and synthetic biodegradable materials have shown to be promising in ACL replacements.

For collagen based grafts, collagen type I has been extracted from bovine and porcine tissues and processed into fibers to fabricate biodegradable scaffolds [45, 131-137]. These scaffolds can be modified in its resorption rate via controlling the degree of cross-linkages formed. Furthermore, since the scaffolds are collagen-based, they tend to not elicit antigenic reactions to cells involved in tissue repair and are able to promote remodeling between the 10-20 weeks phase to strengths similar to autografts.

Biodegradable polymers have gained popularity in this application due to its ability to be engineered to control its degradation rates and mechanical properties. Through chemical modifications, a variety of mechanical properties is possible with tensile strengths ranging between 0.6-500 MPa and modulus of 10-6500 MPa [24, 41, 45], the biodegradation times can be controlled to last over days or months [24, 138,

139]. Different strategies to the use of biodegradable polymers have arisen for the case of ACL reconstruction, which can be classified into the acellular and the cellular approach.

The acellular approach often involved resorbable LAD, whereby the synthetic material is needed for strengthening purpose of the autograft tissue. An example is the L-polylactic acid (L-PLA) resorbable LAD (3M, MN), which is made from L-PLA parallel fiber cords and surrounded by a braid of six yarns of the same material [100, 101]. Resorption study of the material over two years showed no major complications, other than formation of seroma around the L-PLA osteosynthesis devices used for fixation at the bones, which was a result of the release of large amount of acidic products during the degradation process that could not be removed over the period of implantation. Another example is the Vicryl (Polyglactin 910) with PDS (Polyparadioxanone) cords and flat braids developed by ETHICON, NJ [100, 101, 140], which likewise had seroma and local infections observed due to a change in pH resulting from the degradation products. This resulted in the lack of native soft tissue coverage over the synthetic material and it did not support effective tissue remodeling as tissue only manage to fully remodel after 8 weeks postoperation. From these studies, it is apparent that concerns raised with regards to implantation of degradable polymeric materials should not only be limited to the mechanical aspect of the degradation kinetics, but also the degradation products and its rate of assimilation such that neotissue development will not be hindered or delayed.

The cellular approach, on the other hand, needs to be concerned not only with degradation issues, but also cell related issues, which includes cell source and concerns

similar to that of autograft and allograft implants. Very often, this approach is referred to as the tissue engineering approach, which generally involves the use of a biodegradable scaffold to support initial seeded cell development and be stimulated either *in vivo* or *in vitro* using various cues ranging from mechanical and topographical to chemical cues for successful and functional tissue regeneration. Early attempts to improve the regeneration ability of implanted ligament prostheses involved the use of canine fibroblast cell-seeded knitted Dacron ligament prostheses by Brody *et al.* [141]. They showed that the seeded prostheses demonstrated a more uniform and abundant connective tissue encapsulation as compared to the unseeded counterparts. From then, investigators begun to look into using biodegradable materials instead of non-degradable prostheses for graft application to support immediate stabilization of the ruptured ligament while acting as a scaffold for ingrowth and replacement by host cells eventually [34, 41, 45, 59, 109, 142-149]. Very often, studies relating to tissue engineering aims to provide a viable environment for early healing, improved remodeling and biomechanical function of the regenerated construct, which will be described further in the following sections.

2.7. Tissue Engineered Ligament Grafts

With advancement in medical sciences, coupled with the maturation of supporting technologies, regenerative approach towards treatment of tissue trauma, which is the basis for tissue engineering, is now regarded superior over the current reparative approach using permanent prostheses. Although the latter may offer faster healing, the generation of scar or weak fibrotic tissue is a definite minus point for ligament tissues.

Not limiting to that, the active regenerative approach is clearly more appropriate as compared to the passive reparative approach. While the regenerative approach attempts to bridge the discontinuous connective tissue to give a faster and complete heal, the reparative approach will not be capable of this feat if the trauma is greater than the critical size for passive self healing to occur.

The strategy for treatment of ruptured ligament thus lies in the minimization of the above-mentioned problems in current treatment modalities and the development of a closer or similar substitute to that of the native ligament. This result in much research interest in functional tissue engineering of the ligament, which involves the use of reparative cells, seeded onto supporting template structure or scaffold, together with the use of appropriate biochemical and physical regulatory signals to generate normal and functional tissue development *in vitro* or *in vivo* [150]. The goal will therefore be to generate neotissue of autologous cells grown on biocompatible and degradable scaffolds, which is mechanically loaded, characteristic to that of the *in vivo* environment, to trigger development of functional ligament reconstruction implants.

Amongst the various systems used for tissue engineering of the ligament, collagen is often the starting material for scaffold development [57, 147, 151, 152]. These include works by Dunn *et al.* who developed fibroblast-seeded collagen scaffolds for ACL reconstruction. Collagen fibers of 60 μm diameter were made by extrusion, rinsed, dried under tension, treated with cyanamide vapor or glutaraldehyde vapor and combined in an aligned fashion to form the scaffold. The autogenous fibroblasts sourced from rabbit ACL, synovium, patellar tendon and skin were seeded and evaluated *in vitro* and *in vivo* using the rabbit model. It was found that collagen fibers used in the scaffold

for ACL reconstruction had to be thin, strong and resorbable. ACL fibroblasts were also found to adhere better than other fibroblast types but proliferated slowest, while patellar tendon fibroblasts proliferated fastest. All fibroblast types secreted protein and collagen within the scaffold and was verified to be viable *in vivo*. Nevertheless, limitations persist with the use of collagen-based scaffolds, which includes allogenicity of the collagen, batch-to-batch variability and the lack of flexibility in fabrication and modification as compared to other biodegradable polymers [149]. In yet another study, Auger *et al.* developed collagen based scaffolds made from bovine Type I collagen and seeded them with fibroblasts isolated from ACL biopsies of patients undergoing total knee arthroplasty (ages 60-67 yrs) [45, 59]. Upon culturing vertically and horizontally, histological and immunofluorescence observations indicated that parallel orientation of the fibers of Type I collagen were formed in the applied tension. They had thus concluded that the histological organization of the structure can be modulated by the seeded fibroblasts and the tension applied *in vitro*.

Through these studies and many others performed by various groups in the pursuit of functional tissue engineering of the ligament, several factors have been identified as essential [11, 50]. They include the general factors such as cell source, the various aspects of the scaffold, and the stimulatory biochemical/mechanical cues. Of the different aspects involved for scaffold design, the architecture and the material used remain significant. The synergistic effect of these factors is represented in Figure 2-5. Of these factors, this study will focus on the scaffold and biomechanical aspect to stimulate MSCs towards tenogenic differentiation, which will be discussed in the subsequent sections.

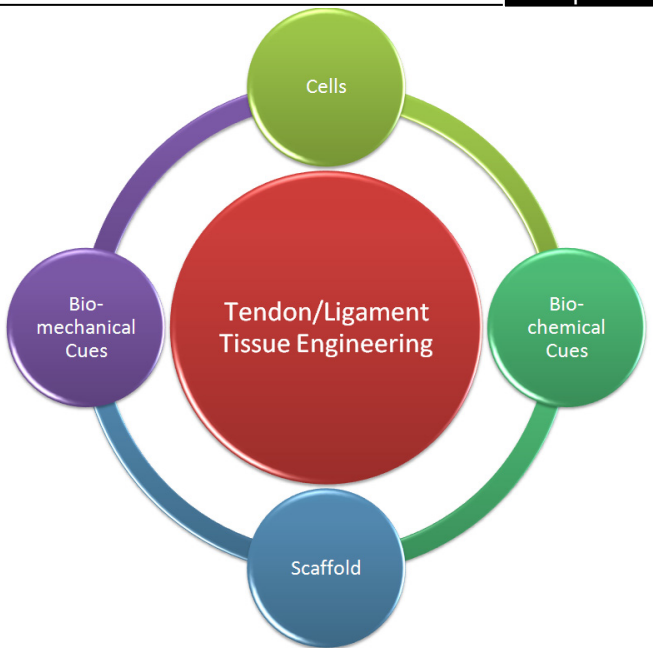

Figure 2-5: Diagram representing synergistic effect of various factors contributing to tissue engineering of ligament.

2.7.1. Cells

The use of appropriate cells is important for successful tissue engineering and regeneration of the ligament. As discussed previously, the presence of cell ingrowth is crucial for the remodeling and prolonged function of reconstructed ligament. The concept of tissue engineering puts forward the use of cell-seeded constructs instead of the acellular approach to accelerate and facilitate the cell infiltration process. With the presence of seeded cells, the potential for proliferation, cell-to-cell signaling, biomolecule production and the formation of ECM can be improved [34, 41, 59, 142-149]. From these reports, it is apparent that the number of cells seeded can influence the nature of cell-mediated processes involved in tissue formation and the rate of the developmental and physiological processes occurring. In fact, a minimum threshold cell density exists for normal neotissue formation.

A variety of cell source exist, including autogenic, allogeneic and xenogeneic sources; and of different cell types, including differentiated cells, stem or progenitor cell and genetically modified cells that can make specific molecules [153]. Typically, the cells exploited for ligament regeneration include skin fibroblasts, ACL fibroblasts and mesenchymal stem cells or bone marrow stromal cells (BMSCs), of which the BMSCs showed highest DNA content and collagen production, making it most suitable for ligament tissue engineering applications [32].

Mesenchymal stem cells (MSC), also known as marrow stromal cell or colony forming unit for fibroblast (CFU-F), were more recently named as multipotent mesenchymal stromal cells by the International Society for Cellular Therapy (ISCT) [154]. They were first identified and isolated from adult bone marrow by Friedenstein *et al.* [155, 156] and have since then been considered a promising cell source for tissue engineering applications. MSCs are rare cells and exist in a very low concentration in human adult bone marrow, accounting for only 0.00001% to 0.001% of mononuclear cells in bone marrow. Being non-haemopoietic in nature, they can be separated from the haemopoietic fraction of the bone marrow via their ability to adhere to tissue culture plastic and be cultured. Being multipotent, MSCs have the potential to differentiate into various types of mesenchymal cell phenotypes, including osteoblasts, chondroblasts, myoblasts and fibroblasts [157].

Very often, MSCs contain a heterogeneous population of cells, with varying colony sizes, proliferation rate, cellular morphology and multipotency both *in vitro* and *in vivo* even though they may be of single colony derived strain [158, 159]. This phenomenon exists even with more sophisticated isolation methods, including immuno-

depletion techniques [160] or selection via STRO-1 and CD 271 antibodies [161, 162]. Specifically, varied cell morphologies ranging from spindle-shaped to broad stromal-like cells were observed using these isolation and purification techniques [163-165]. There is thus inter-culture and inter-species differences in the potential of MSCs to self renew or form fibroblast colonies in low density cultures [163, 166-168].

MSCs are also inherently non-immunogenic, giving them the potential to be used in allogeneic transplantation strategies [169]. Being human leukocyte antigen (HLA) Class I positive and Class II negative, and that they do not express co-stimulatory molecules of CD40, CD40L, CD80, or CD86 [170], MSCs are widely regarded as non-immunogenic and may even be effective at inducing tolerance. When tested via mixed lymphocyte culture (MLC) assay, MSCs did not trigger a proliferation response of allogeneic lymphocytes [171, 172]. Even with induction to express HLA Class II via interferon γ (INF-γ), MSCs could still escape recognition from alloreactive T-cells [170, 173]. It was observed that the differentiated MSCs (adipocytes, chondrocytes and osteocytes) remained non-immunogenic as well [174].

Other than being non-immunogenic, MSCs showed strong immunomodulatory effect both *in vitro* and *in vivo* as well. It was found that MSCs exhibited immunosuppressive effects and inhibited T-cell alloreactivity *in vitro* [157, 171, 175-177]. The effect was relayed *in vivo* whereby MSCs have been reportedly shown to successfully cure the graft-versus-host disease after allogeneic hematopoietic stem cell transplantation [178, 179]. Although the governing mechanism is not understood fully, it is possible that the paracrine effect of MSCs played a significant role. This is so as it was shown that MSCs may inhibit T-cell recognition and expansion by inhibiting TNF-

α and INF-γ production, which consequently increase IL-10 levels [169, 177, 180]. Inhibition of TNF-α and promotion of IL-10 was found to affect dendritic cell maturation state and their functional properties, which will result in skewing the immune response towards an anti-inflammatory or tolerant phenotype [180].

In summary, from the perspective of ligament tissue engineering, the MSCs from bone marrow sources are selected for use in this study due to the following:

1. MSCs can be isolated easily using the plastic adhesion method or simple antibody selection techniques [161].

2. MSCs and differentiated MSCs are reported to be non-immunogenic and suitable for allogenic applications [173], which is a promising strategy for future clinical applications.

3. MSCs proliferate faster than other potential cell sources (fibroblasts from skin and ACL), thereby shortening *ex vivo* culture duration [32, 181].

4. MSCs exhibited elevated transcript levels for ligament phenotypic markers, which translated to increased amount of ligament-related ECM components produced during *in vitro* culture [181].

2.7.2. Scaffold

The scaffold is an important component of a tissue engineered ligament as it translates two-dimensional (2D) cell culture towards forming a three-dimensional (3D) structure and thereby mimicking the ECM and facilitating the development of

functional neotissue. Specific to the ligament tissue, it should be designed to meet the immediate functional mechanical demands of the reconstructed knee and yet be able to degrade at a rate similar to tissue ingrowth. In other words, the ligament scaffold should lose its mechanical integrity gradually while allowing the remodeled tissue regenerate and gain strength by gradually loading it.

An ideal scaffold typically possesses the following characteristics:

1. Biocompatible and biodegradable material that is suited for distinctive applications
2. Suitable porosity that allows cell infiltration and medium perfusion into the scaffold
3. Sufficient surface area for cell attachment, growth and proliferation
4. Architecture or geometry that facilitates tissue attachment and regeneration, while imparting the required mechanical properties at various stages of tissue regeneration.

To achieve these goals, the material and the architecture of ligament tissue engineered scaffolds have been extensively studied, which will be presented in the following sections.

2.7.2.1. Common Ligament Tissue Engineering Scaffold Materials

Current research into the tissue engineering approach of ligament reconstruction has focused on seeding either collagen-based scaffolds or synthetic biodegradable polymers with a variety of cell types. The intention of achieving biodegradability in these scaffolds is motivated by the disadvantages of previous non-degradable materials,

which have released wear particles and other materials into the surrounding tissue structure causing inflammatory responses and rendering the need for revision surgeries.

Collagen ligament implants have been used experimentally and was found to degrade by a sequential attack from lysosomal enzymes [133]. The rate of collagen scaffold degradation can be controlled via the extent of cross-linking involved. However, limitations such as allogenicity of the collagen, batch-to-batch variability and the lack of flexibility in fabrication and modification persist with the use of this material, as discussed previously.

Synthetic biodegradable polymers have been popularly used for orthopedic applications. They include poly(α-hydroxy) acids, poly(ε-caprolactone), poly(orthoester), copoly(ether-ester), poly(carbonate), poly(iminocarbonate) and poly(dioxanone) [182, 183]. The advantages of these materials include controllable chemical uniformity and physical properties, with the degradation and mechanical properties modifiable through chemical manipulations [138, 139] to make them suitable for specified applications. In particular, the poly(α-hydroxyester) family is often used for ligament tissue engineering applications since they are FDA approved and commercially available in fibrous form. The family is made up of poly(glycolide) (PGA), poly(L-lactide) (PLLA) and their copolymers of poly(lactide-co-glycolide) (PLAGA), which can be synthesized in a variety of methods [184, 185]. Table 2-5 lists the physical and mechanical properties of some of these polymers [101, 182, 184, 186-188].

Table 2-5: Physical and mechanical properties of the poly(α-hydroxyester) family.

Polymer	PGA	Copolymer			PLLA
		PLAGA	DL-PLAGA	DL-PLAGA	
Composition	100	(10:90)	(50:50)	(85:15)	100
Chemical Structure	$[C_2H_2O_2]y$	$[C_3H_4O_2]10$ $[C_2H_2O_2]90$	$[C_3H_4O_2]50$ $[C_2H_2O_2]50$	$[C_3H_4O_2]85$ $[C_2H_2O_2]15$	$[C_3H_4O_2]x$
Tensile Strength (MPa)	339-394 (fibers)	570-910 (fibers)	41.4-55.2	41.4-55.2	<870 (fibers)
Maximum Strain (%)	15-35 (fibers)	18-25	3-10	3-10	25 (fibers)
Approximate Resorption Duration (months)	Loss of mech. prop.: 1 month Full resorption: 50-75 days	Loss of mech. prop.: 90 days	1-2	5-6	>24

The poly(α-hydroxyester) family degrades via hydrolysis of the ester bonds and bulk erosion, with a loss of mechanical strength over a period of 2-4 weeks for PGA to 24 weeks for PLLA in pH 7 fluid at 37°C [186, 188, 189]. Lactic acid is released during the course of degradation for PLLA and its copolymers. Specifically for PLAGA polymers, the pH of the degradation solution (mainly lactic acid) can cause autocatalysis, whereby the lowered pH in the local environment can cause increase in degradation rate [182, 190]. Although cellular and tissue biocompatibility of polylactides have been shown in several toxicological studies and the American Gentox program [182], problems persist to limit their application as biodegradable polymers. These problems include issues due to the progress of resorption process *in vivo*, control of mechanical properties with degradation *in vivo*, effect of local pH decrease, burst

phenomenon and the possibility of mutagenicity due to the degradation products [100, 101, 182, 184, 187, 191-194].

Apart from these materials, the use of natural materials such as silk has fast becoming a popular biomaterial of choice for ligament tissue engineering [3, 13, 21, 27, 195-197]. This is largely due to the extraordinary mechanical properties and enhanced implant stability of silk. The following section will give further insights to the application of silk fibroin, the biocompatible component of silk, as used for tissue engineering ligament.

2.7.2.2. Silk Fibroin as Ligament Tissue Engineering Scaffold Material

Silk fibroin (SF) of the *Bombyx mori* has long been recognized as a valuable material in the textile and biomedical industries. It is utilized in many biomedical applications including sutures, whereby its excellent mechanical strength and elasticity are utilized [28, 198, 199]. The superior mechanical properties of SF are attributed to their protein structural arrangements. It has been proposed that SF exists in two different phases, which are identified as Silk I and Silk II [200, 201]. Silk II has been identified to be anti-parallel β-sheets, whereby the polypeptide main chains are aligned and adjacent chains connected by hydrogen bonds. Silk I, on the other hand, has been suggested to compose of α-helix and random coil structures [202, 203]. When subjected to external stimulation such as heating and shearing, metastable Silk I will be converted to the more stable and mechanically viable Silk II [204-206].

Despite the excellent mechanical properties, SF is only sought recently for use as scaffold material in tissue engineering [28, 198, 199]. This is partly due to confusion in the past, whereby concerns were raised on *Bombyx mori* silk for invoking inflammatory responses in certain biomedical applications [207-215]. Coupled with the misconception that SF is non-degradable *in vivo*, having retained majority of its tensile strength beyond 60 days, it was being sidelined by other biocompatible synthetics of shorter degradation period and was wrongly classified as a permanent implant material.

Now however, there is a clearer understanding of *Bombyx mori* silk, making it possible for SF to be used as an implantable scaffold material for tissue engineering. It is realized that SF will not likely induce hypersensitivity if the wax-like sericin coating is removed [28, 199, 212, 216-218]. A degumming process is used to remove the sericin component from raw silk. Moreover, since silk is a protein, it will be susceptible to proteolytic degradation *in vivo* and be absorbed, though a longer period of time is required. With the enhanced environmental stability due to the extensive hydrogen bonding and significant crystallinity in the SF protein structure, there is potential for SF to be used for scaffolds in tissue engineering where mechanical robustness and long term degradation is required. This is why silk is typically used in musculoskeletal and orthopedic applications, such as ligament repairs [3, 21, 27, 197], where a very gradual transfer of load from the scaffold to the growing tissue is desired. Furthermore, SF has been shown to bear equivalence to collagen in supporting cell attachment, inducing appropriate morphology and growth since it is a natural protein as well [36, 37, 219]. In fact, the size ranges of SF fibers (8-14 μm) used in this study fell within the range of collagen fibers (1-20 μm) seen in natural ligament tissue [24]. To further mimic the

ECM structure, SF has been successfully electrospun to form nonwoven meshes of sub-micron diameters and is found to enhance cell adhesion and spreading of Type I collagen due to its high surface to volume ratio [5, 38, 199].

However, in the process of removing sericin from raw silk, typically using the thermo-chemical treatment approach, the structural state of SF is affected. Consequently, there will be changes in the SF microstructure, which will inevitably alter the mechanical and degradation properties of SF. Indeed, it has been reported that degumming affects the mechanical properties of silk and Pe'rez-Rigueiro *et al.* have reported the effects of degumming with distilled water on the tensile strength of forcibly reeled silkworm silk fibers [220, 221]. Jiang *et al.* have also investigated the tensile behavior and morphology of SF upon degumming using different solution types [222].

The various degumming chemical solution types can be largely classified into two categories: alkaline and enzymatic. Both of these types of chemical degumming uses a combination of sericin removal approach, which includes dispersion, solubilization and hydrolysis of the various sericin polypeptides [223]. The primary mechanism utilized by alkaline degumming is hydrolysis. Since hydrolytic agents are used, it is important that moderation of the conditions be done when this method of degumming is performed. Although recent studies have looked into using proteolytic enzymes for degumming purpose, there exist several limitations to the method [224-227]. These limitations include higher shear and bending rigidity of resultant SF, the presence of residual sericin at the overlap points and core of processed silk structures [228] and the higher cost of enzymes as compared to chemicals used for alkaline degumming.

Even though it has been shown by investigators that amongst the various degumming methods, alkaline degumming using Na_2CO_3 causes significant structural and mechanical changes [222, 229], it remains as a popular method due to the high effectiveness of sericin removal within a relatively short duration [28, 199]. Moreover, it is often necessary to degum silk of a processed form, such as knits or braids. These architectures are generating much interest in recent load-bearing tissue engineering development, especially in combination with the silk fibroin material, whereby the inherent superior mechanical properties of the fibroin fibers are fully exploited, to form the load bearing component of a functional scaffold [3, 21, 27, 28, 197, 199]. Although fabricating scaffold from raw silk instead of degummed silk can ease fabrication process and better protect SF by the sericin coating during the fabrication process, it poses new challenges. This is so as it will then be difficult to remove sericin from the core of these structures, where raw silk is not exposed to the degumming solution. In these cases, degumming using the Na_2CO_3 alkaline method proves to be effective and produces scaffolds with negligible hypersensitivity and inflammatory reactions [3, 27, 197]. To maximize the benefits of using SF as scaffold material in this study, the challenge thus lies in optimizing the degumming method and identifying a set of conditions, such that SF hydrolytic damage, together with the resultant mechanical and structural deterioration, is reduced. This is essential for the production of functional scaffolds in tissue engineering applications, especially that for ligament tissue regeneration whereby the mechanical aspect is crucial.

2.7.2.3. Scaffold Architecture

There are several architectures, resulting from the different fabrication methods, which have been used for scaffolds in tissue engineering. Very often, scaffolds made from biodegradable polymers are fabricated using techniques such as particulate leaching, textile technologies or 3D printing techniques. In the traditional particulate leaching method, a particulate-matrix mix is created by casting a polymer solution over water-soluble particles such as sodium chloride salt, which is followed by solvent evaporation and salt leaching to yield a porous scaffold. However, this method is limited by the lack of interconnectivity between the pores and difficulty in controlling pore dispersion and porosity, leading to uncontrollable morphologies in pore walls [230].

Textile technologies have also been used to fabricate woven or non-woven fabrics as scaffolds [231, 232]. Some of the textile technique that have been used for ligament tissue engineering scaffolds include axial fiber structures, woven structures, 2-D braids and knitted structures. Axial fiber replacements have been used in carbon-based total ligament replacements such as ABC (Surgicraft, UK) and collagen-based scaffolds developed by Dunn *et al.* [45, 57, 113]. Being just structures of collated fibers plied and fixed parallel to each other, the axial fiber architecture is susceptible to axial splitting due to flexural and torsional fatigue, and surface peeling as a result of yarn-on-yarn or yarn-on-bone abrasion [113]. Woven fibrous structures, on the other hand, are 2D interlaced yarn systems with an “over” and “under” weave pattern and have been used in the Stryker and Lygeron ligament replacements [45, 100, 101]. The disadvantage of this structure however is low extensibility, poor collagen infiltration and orientation,

and similar problems to axial fiber structures such as axial splitting and abrasive wear due to tight weaving [113]. 2-D braids are made using two braiding yarns in the through thickness direction of the braid and have been used in the Gore-Tex, Proflex and Kennedy LAD devices [45, 100, 101, 105, 113]. Although the structure can transfer high loads and provide for structural elongation, it fundamentally inhibits collagen infiltration due to the tightly braided construct [33, 34]. As such, there will be loss of structural integrity, and problems of surface peeling, axial splitting of fibers and stability issues.

Knitted fibrous structures are made by interlocking a series of loops of one or more yarns to create a porous fabric for tissue ingrowth and have been used in LARS and Stryker ligaments [45, 100, 101, 113, 233]. The structure have also been made with PLGA and have been shown to have high porosity and more internal connective voids compared to braided structures, especially during tensioned states [35]. These spaces allow effective cell adhesion and medium perfusion, thereby stimulating uniform ECM formation, which is critical during the repair process and helps functional integration of the engineered tissue into the surrounding tissues. Furthermore, the knitted structure can be designed to suit individual applications and in this study, it will be designed to cater to the loading conditions involved in ACL regeneration using SF as the material of choice. Although it may not have as high a loading capacity as the braided structures, the use of a mechanically superior material such as SF can compensate for this limitation. Even though the knitted structure may not be capable of supporting orientation in the collagen tissue formed, it can be incorporated with aligned

electrospun SF fibers, as in this study, to provide topographical cues for cell guidance such that oriented collagen tissue can be achieved eventually.

2.7.2.4. Scaffold Topography

In this study, the main knitted structure requires a matrix for effective cell seeding and subsequent tissue development due to the large pores (1mm) inherent of the structure. In common practice, a gel system, such as fibrin or collagen gel, is used, but such system was found to be unstable in a dynamic environment, especially that of the knee joint [234]. Moreover, problems of nutrient transmission occur in such systems, whereby cells seeded in a 3D gel system are observed to proliferate only near the periphery surfaces [235, 236]. A more effective matrix based on electrospinning technology is used to produce electrospun ultra-fine fibers of sub-micron diameters, which have high surface area-volume ratio and mimics the ECM of native tissue. This matrix type has been shown to facilitate cell attachment, proliferation and ECM deposition [237].

The addition of an electrospun matrix not only facilitates cell attachment, but also introduces a mean to provide cell guidance to the attached cells. From a biomimetic perspective, ligament anatomy suggests fibrous structures apposite templates as an important consideration for ligament scaffold design. Although it may be unclear as to what dimensional order should structural cues be present for collagen-hierarchy reconstitution such that neo-ligament function can be optimized, recent studies have preliminarily demonstrated the positive effects of fiber alignment at the nanometer to sub-micron level on cell morphology and ECM production [23, 36, 37]. The correlation

of cellular spreading and orientation with electrospun fiber topography is demonstrated by Lee *et al.* [37]. They have found that human ligament fibroblasts (HLFs) cultured on electrospun aligned polyurethane (PU) fibers (657±183nm) were spindle-shaped, oriented in the fiber direction and secreted significantly more collagen than on randomly oriented fibers. Under cyclic strain in the direction of alignment, 150% more collagen was produced. As mechanical interactions between cells and the underlying substrate can take several forms, including topographic interactions and surface tensile forces, aligned electrospun fibers can sensitize these cells for effective mechano-transduction by tensioning cytoskeletal filaments [38]. The orientation of fibroblasts along a ligament has also been shown to improve its tensile strength [36].

Nevertheless, there has been limited work in translating and utilizing this fundamental knowledge for functional ligament constructs that are viable in both the mechanical and cellular aspects to allow early implantation without the need for long term *ex vivo* culture. Furthermore, assessments for the differentiative potential of bone marrow derived MSCs down the ligament fibroblast cell lineage as induced by aligned 3D scaffolds have also been limited and inconclusive. On top of that, the synergistic effects of mechanical conditioning on a 3D aligned scaffold has also not been studied and understood. It is thus the aim of this study to provide further insights into these issues.

2.7.3. Biomechanical Cues

The use of bioreactors in tissue engineering applications has been widely studied, often with the aim of providing a closer resemblance of the *in vivo* environment *ex vivo*.

Very often, it is designed with the ability to provide physiologically relevant biochemical and biomechanical cues to achieve the conversion of a cell type to another specific tissue phenotype or to trigger tissue maturation by "working" the tissue engineered construct *in vitro*. Specifically, the tissue engineering bioreactor should function to [238-240]:

1. Increase mass transport to alleviate diffusion limitation of 3D scaffolds; that is, to provide adequate nutrient, oxygen and regulatory molecules to cells while removing waste such as metabolites and CO_2.

2. Stimulate the tissue engineered construct physiologically to provide mechanical cues to trigger the mechano-transduction process towards the differentiated cell lineage.

Similar to the conventional bioreactors commonly used in the industries for food processing, fermentation, and production of pharmaceuticals and recombinant proteins, bioreactors for tissue engineering should also allow close monitoring and tight environmental controls. Environmental parameters such as temperature, pH, oxygen concentration, nutrient supply and waste removal are particularly essential to be controlled. Other than these, tissue engineering bioreactors should also provide an avenue to control the introduction and conclusion of biochemical and physical regulatory signals to guide cell proliferation, differentiation or tissue development. The bioreactor thus offers possibilities of providing controlled tissue development *in vitro*, which could be scaled up for commercial production of engineered tissues.

The essential function of a bioreactor for tissue engineering the ligament is to provide mechanical stimulus to modulate the cell physiology and increase overall biosynthetic activity in the 3D constructs for effective tissue regeneration *in vitro* [150]. Mechanical conditioning is necessary for ligament tissues in order to mimic the constant loading due to locomotion and regenerate the hierarchical structure present in these tissues. In particular, Altman *et al.* reported the use of directed multi-dimensional strains to mimic the physiological environment [241]. They had implemented both translational and rotational strains with the attempt to develop tissue engineered ACL with the unique helical fiber organization and structure of the native ACL. By so doing, the resultant tissue engineered ACL would have better mechanical attributes to make it suitable for its stabilizing functions. In the same light, cellular alignment and ECM orientation have been achieved in many studies involving mechanical loading of fibroblasts; while other studies have demonstrated enhanced cell proliferation, increased ECM synthesis, and promotion of MSC differentiation to ligament fibroblast phenotypes [242-247]. Mechanical stimulation is thus considered by many as crucial to the successful development of tissue engineered ligament [1, 13, 142, 241, 244].

There are several approaches to providing mechanical stimulation of the ligament; with most studies following the approach of providing physiological loading to condition cell-seeded constructs *in vitro* [248-252]. Many of these studies were based on works performed by Morrison and Fleming *et al.* [248, 249, 251, 252], whereby the strain behavior of the ACL was being tested during a variety of activities ranging from level walking, stair climbing and descending, walking up and down a ramp and bicycling. It was found that the ACL forces ranged from 169 N during level walking to

a high of 447 N during stair descending. This corresponded to a 3.1% to 6.9% ACL strains determined from load-extension graphs of young human ACLs. Other studies reported strain amplitudes of 2% to 10% for human cruciate ligaments and Achilles tendon [84, 253, 254]. Consequently, the general consensus of physiological ACL strain is set at 5% as deduced from studies related to mechanical conditioning of the ACL [241, 244, 245, 255-260].

However, other than the strain value, a cyclic strain profile is characterized by several other variables, whereby considerable diversity has been reported [241, 244, 245, 255-261]. This is further complicated by the different cell types, scaffold materials and designs, and bioreactor designs involved. Therefore, it may be feasible to understand and try to optimize a general profile that will be optimal for ligament regeneration. In this way, the selection of stimulation parameters, such as cyclic strain amplitude (maximum extension with respect to original length), cyclic frequency (number of cycles per second), duration of total stimulation period and periodic frequency (duration of stimulation period per day) will be based on a specific profile intended for the tissue construct during a particular developmental stage, rather than trying to moderate individual parameters separately. In other words, it may be more feasible and likely more effective to identify groups of stimulation parameters that contribute to “low” or “high” stimulation intensities respectively and timely implement these intensities in series, rather than implementing a particular optimized parameter continuously throughout the stimulation period. Not only is the latter a generalization of the stimulation effect to the contribution of a single parameter, it may also not be suitable throughout all the tissue’s developmental phases. Indeed, this is motivated by

the fact that physiological loading parameters are often used in many studies, which may be sub-optimal to the regenerating ligament tissue construct since they are not matured tissues to begin with. It is therefore critical to first indentify conditioning parameters that will provide “low” and “high” stimulation intensities and subsequently execute a series of timely implementations of these different intensities in the stimulation regime.

As such, the cyclic frequency will be varied in this study, with 0.1 Hz identified for the “low” intensity profile and 0.5 Hz for the “high” intensity profile. Consequently, the number of cycles per day based on 12 hours daily activity for “low” intensity profile was 4320 and that for “high” intensity profile was 21600. These values were selected to substantially mark the upper and lower boundaries by positioning above and below the physiological range as reported in pedometer studies whereby human walking activity per day is 6700 to 11900 cycles per day [262]. Other parameters including the cyclic strain amplitude and periodic frequency would be kept constant at the physiological values, which were 5% and 12 hours/day respectively. Although not part of the scope of this study, the values of these respective parameters accounting for “low” or “high” intensity profiles should be obtained experimentally to describe the different stimulation intensities more comprehensively.

The onset of the “low” and “high” intensity profiles would follow a rehabilitative approach as inspired from the rehabilitation treatment rendered to patients who have undergone ACL reconstruction surgeries [54, 263]. A carefully tailored postsurgical rehabilitation protocol is often developed with the patient’s individual unique situation and type of surgery that has ensued so that full restoration of limb function can be

achieved [264]. The balanced amount of exercise is essential for functional restoration, while introducing exercises that are less or more than optimal may be ineffective or even detrimental to subsequent recovery of the tissue function [265]. The exercise dosage in terms of the amount of repetitions done in a given duration is a particularly important condition to moderate as an inappropriate exercise dosage performed to the extent of muscle fatigue may not only cause knee joint stability [266], but also put the newly constructed graft at risk of failure [267].

Although the concept of rehabilitation has been well studied and implemented as a standard post-surgical treatment for ACL reconstruction, it was generally not studied and realized in tissue engineering applications of ACL as many studies focused on the execution of level stimulation profile throughout the conditioning period [241, 244, 245, 255-261]. In relation to this, a rehabilitative stimulation regime, which included static culture and "low" intensity biomechanical stimulation would be implemented in the first 7 days post-seeding to allow initial cell attachment, proliferation and stimulated differentiation onset in a relatively mild mechanical environment. Subsequently, the "high" intensity biomechanical stimulation would be in place to further accelerate the tissue differentiation and maturation stages. The onset of the "high" intensity profile was proposed to be after 7 days post-seeding as consensus from several studies demonstrated that positive changes to tissue constructs were often effected if mechanical conditioning is started after this duration of cell acclimatization [245, 268-271]. It was only then that MSCs could respond positively to the dynamic culture environment. With appropriate temporal tissue conditioning at the respective phase of growth, it was likely that seeded MSCs could be induced to proliferate and differentiate

with collagen laid down in an organized manner to attain functional ligament in a shorter duration.

2.8. Summary

In the investigation of ligament tissue engineering, it is essential to first understand the tissue's anatomical and physiological functions. The unique macroscopic mechanical properties of the tissue are contributed by the hierarchical organization of the microscopic components. Despite the superior mechanical adaptation of the tissue to its working environment, the ligament is prone to injury either due to single impact trauma or repetitive exposure to low magnitude forces. Subsequent healing of the tissue is often suboptimal as inherently repaired torn ligament will never be as strong as the original tissue. Furthermore, it is necessary for ruptured ligament to be surgically reconstructed. However, current surgical treatment modalities, which include permanent grafts and biological grafts, often bear many limitations including long-term implant failure, donor site morbidity, graft rejection and infection. This motivated the use of biodegradable grafts, which contributed to the interest in tissue engineering solutions. Of the factors affecting tissue engineering success in ligament applications, the cell source, scaffold and biomechanical cues are focused in this study. MSCs derived from bone marrow are chosen for the cell source used in this investigation, which will be seeded onto knitted SF scaffolds with aligned electrospun SF. This hybrid SF scaffold will thus support tissue regeneration both mechanically by the strong SF material and biologically by providing suitable cell attachment topography from the aligned electrospun SF. This cell seeded construct will then be dynamically cultured in a

rehabilitative manner multi-dimensionally to gradually load the construct physiologically. It is envisioned that these topographical and mechanical cues will work synergistically to promote tenogenic differentiation for successful functional tissue engineering of the ligament.

Chapter 3

DESIGN AND DEVELOPMENT OF THE SILK FIBROIN KNIT

3.1. Introduction

The knitted architecture has been shown to be advantageous over other textile based architectures, such as the braided and woven structures, and has been widely used in prosthetic ACL such as the LARS and Stryker ligaments [45, 100, 101, 113, 233]. Being highly porous and more extensible, this architecture was selected for the main load-bearing structure and was customized using SF to support physiological loading of the ACL. The ACL was chosen as the tissue of interest to be focused in this study, amongst the ligament tissues, due to the high mechanical loading that it has to undertake. Hence making it one of the more challenging ligament tissue types to design for mechanically and regenerate successfully.

A series of steps was necessary to ensure that the final degummed SF knit would be functional as a tissue engineered ACL *in vivo* in a rabbit model. These steps include:

1. Tensile tests of single SFs extracted from degummed silk yarns to preliminarily determine the mechanical properties of the SF material to facilitate design of functional SF knit in the next step.

2. Custom design of the load bearing knitted SF that would be capable of supporting functional loading in the rabbit model *in vivo*. Design would be performed theoretically based on the fully extended knit, with SF material properties determined from previous step and safety factors to cater for *in vivo* degradation of the SF material.

3. Maximize the mechanical properties of the knitted SF structure after degumming. This final step was necessary as harsher degumming conditions would be required for a knitted structure as compared to the silk yarns that the custom design was based on. This final stage of the design steps would therefore aim to preserve SF mechanical integrity after degumming from the knitted structure, by reducing mechanical depreciation resulting from the harsher degumming conditions, such that the mechanical properties of the final degummed SF knit could be as close to theoretical design values as possible.

3.2. Mechanical Properties of SF from Degummed Silk Yarns

3.2.1. Materials and Methods

3.2.1.1. Sample Preparation and Degumming

Raw silk fibers of 80 fibroin counts were reeled onto a water-filled 50 ml Falcon tube (BD Biosciences, CA, USA) and immersed into degumming solution of aqueous Na_2CO_3 and SDS, 0.25% w/v each (Sigma-Aldrich, St. Louis, USA) at 98-100°C. Pure aqueous Na_2CO_3 solution, without SDS, was used as the negative control degumming condition. Unlike the degumming procedure used for silk knits, reeled silk yarns were not mechanically agitated since the degumming solution could reach the silk fibers readily. A variety of degumming duration ranging from 5-90 min was used to assess the shortest duration at which the raw silk was degummed. 90 min was used to degum silk fibers of the control group as preliminary works showed that degumming using plain

aqueous Na_2CO_3 solution could not achieve effective sericin removal in durations shorter than 90 min. Degummed silk fibers from the different groups were all rinsed in warmed distilled water after removal from the respective degumming solution and left to air dry for at least 24 h before further tests were conducted.

3.2.1.2. Observation of SF Morphology and Cross-Section

The degummed silk fibers were gold-sputtered and observed at 15 kV in a scanning electron microscope (SEM, JEOL Ltd, JSM-5600 LV, Japan) to characterize their surface morphology and cross-sectional areas. SFs of the silk fiber yarn were carefully spread for observation of sericin presence at two different positions, followed by a 90° rotation about the longitudinal axis for observation on the cross-section. Cross-sectional areas were then obtained pictorially using imaging software (ImageJ 1.38x, Wayne Rasband, NIH, USA). Data was collected over 20 samples.

3.2.1.3. Nanotensile Tests

To gain accurate representation of the mechanical strength of SF, single fibroins (n=10 each group) were carefully extracted from degummed silk yarns and mechanically tested to failure using a nanotensile tester (MTS Systems Corporation, Nano Bionix UTM® Testing System, MN, USA) under standard environmental conditions (20°C, 60% relative humidity) as shown in Figure 3-1. The reason for testing single fibroins instead of the 80 fibroin yarns was because testing of fibroin yarns would result in slippages of individual fibroins, leading to inaccurate tensile results. The single SF fibers were first mounted onto a rectangular paper frame using a masking tape to

give a gauge length of 20 mm. After mounting the frame with the SF fiber within the grips of the nanotensile tester, the side columns of the paper frame were cut and the samples stretched to failure at strain rate of 1 $\%s^{-1}$. Load (mN) and extension (mm) were recorded and stress-strain behaviors of SF were derived, as detailed in Appendix A, using cross-sectional areas measured via SEM prior the tensile tests. Care was taken to avoid stretching the fibers plastically prior to testing.

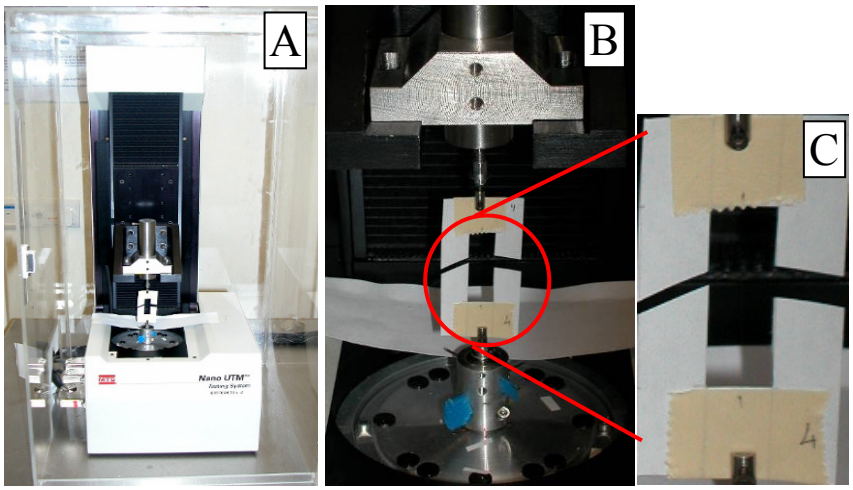

Figure 3-1: (A) Nanotensile testing of single SF fiber using nanotensile tester, with (B) single SF fiber mounted on rectangular paper frame that was cut on the sides before tensile testing the fiber. (C) Care was taken to mount the fiber such that it was in line with the clamps of the nanotensile tester.

3.2.1.4. Statistical Analysis

All data were expressed as means ± standard deviation (SD). The single factor analysis of variance (ANOVA) technique was used to assess the statistical significance of results between groups. For pairwise comparisons, two-tailed, unpaired Student's t-tests were used. GraphPad Prism ver. 5 (GraphPad Software, Inc., CA, USA) was used to implement the statistical analysis. A $p<0.05$ was considered statistically significant.

3.2.2. Results and Discussion

3.2.2.1. Degummed Silk Morphology

Upon degumming for different durations, the degummed silk fibers were observed using the SEM to assess the effectiveness of sericin removal. It was noted that sericin remnants persisted in samples that were degummed for less than 30 min (Figure 3-2A), while smooth SF fibers were observed in samples degummed for 30 min or more (Figure 3-2B). Since effective degumming of silk yarns could be attained by degumming for 30 min, it would not be necessary to degum for longer durations. This observation would be used to complement the data for mechanical properties of silk, to ascertain the group with the optimal degumming duration that would be selected for its mechanical properties in the design of SF knits.

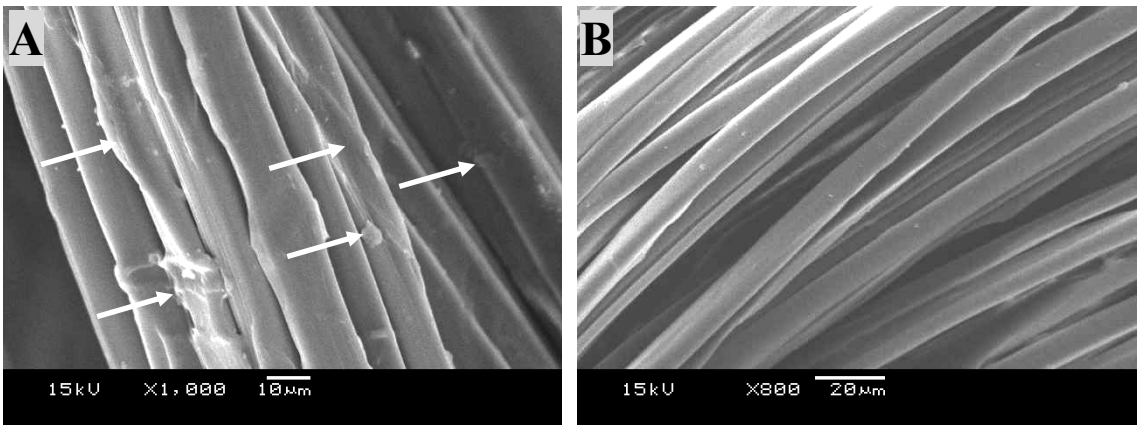

Figure 3-2: (A) Silk fibers degummed for 15 min with remnant sericin present as shown by the arrows and (B) silk fibers degummed for 30 min with smooth SF and no observable sericin. Magnification: (A) 1000× and (B) 800×.

3.2.2.2. Cross-Sectional Area

Before mechanical test was carried out for single SF filaments, the average cross-sectional area of single SF filament would have to be determined and the value was used to represent the cross-sectional area of all the tested samples. Since silk is a natural fiber, standard deviation for the cross-sectional area of SF was not expected to be very small. The cross-sectional areas were measured for SF using SEM images of SF cross-sections (Figure 3-3). From the measurements made (data from 20 samples), the SF cross-sectional area was typically 102 $\pm$ 25 μm^2. This corresponded to a diameter of 11.4 ± 1.3 μm, when the cross-section was assumed to have a circular profile. This result also matched, within acceptable range, to that performed by Pe´rez-Rigueiro *et al.*, whereby a value of 9.3 ± 0.3μm was determined [272]. This thus highlighted the existence of batch to batch variance in fibroin diameters due to their natural origin.

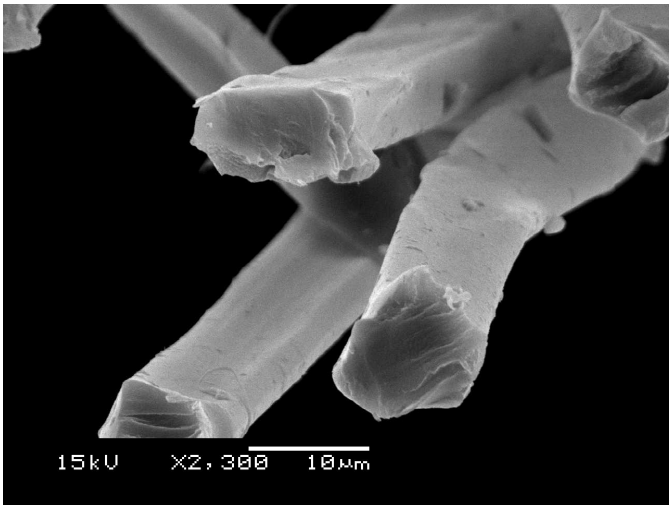

Figure 3-3: Representative SEM micrograph of SF cross-section used for determining cross-sectional area. Magnification: 2300×. [26]

SEM was used for imaging the cross-section of cleanly degummed SF fibers for pictorial measurement of the fiber cross-sectional area, which would be used in the determination of mechanical properties of various SF specimen,. The cross-sectional area measured was used for deriving the stress-strain curve of the differently degummed samples based on the assumption that samples of various groups had comparable SF cross-sectional area before and after degumming and regardless of the degumming protocol. This was shown by Pe'rez-Rigueiro *et al.* whose investigations demonstrated that the diameter of silkworm silk was reproducible after degumming [220]; thereby revealing that degumming had very little effect on changing the cross-sectional area of SF. Although the cross-sectional area of a mildly degummed sample would be greater due to sericin presence, the contribution of any remnant sericin coating to the mechanical properties of SF would be negligible as the load bearing capacity of sericin was deemed negligible compared to fibroin [273]. Therefore, the tensile parameters measured were considered that of SF and any variations in these measured parameters would imply modification to the mechanical integrity of SF, regardless of amount of sericin present.

3.2.2.3. SF Mechanical Properties

The stress-strain behaviors of degummed SF by different degumming durations were plotted as shown in Figure 3-4. "SDS5 (fibers)" indicates the experimental silk fiber group degummed with aqueous Na_2CO_3 and SDS degumming solution for 5 min and so on, while "Sod Carb 90 (fibers)" indicates the control silk fiber group degummed with aqueous Na_2CO_3 degumming solution for 90 min. The corresponding mechanical properties obtained for the groups were tabulated as shown in Table 3-1.

It was observed that the mechanical properties of SF generally depreciated with increased degumming duration. This was also observed by Pe´rez-Rigueiro *et al.* [220, 221] and could be attributed by the hydrolytic actions due to water and the chemicals used, which acted as plasticizers [221]. Furthermore, it was noted that SF in the fiber form exhibited two yield points as indicated by the arrows in Figure 3-4. Such a complex stress-strain curve was not observed in the knitted SF form, when compared retrospectively, and could be attributed to the reeling process during sample preparation, as previously described for silkworm silk obtained via reeling degummed cocoons [221, 274].

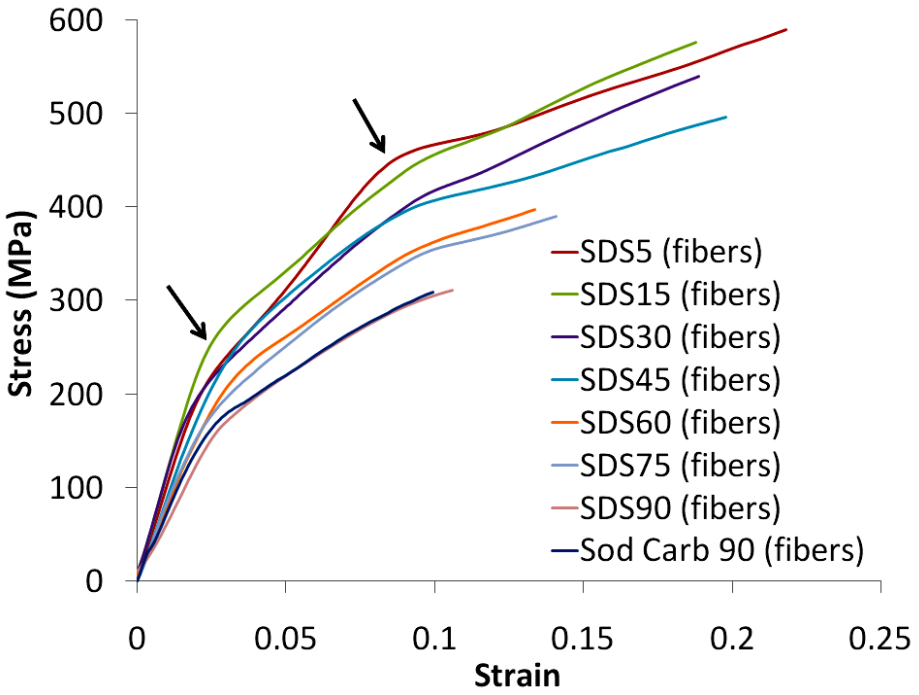

Figure 3-4: Stress-strain curves of degummed single SF filament subjected to different degumming durations (mean of ten contiguous samples for each group).

Table 3-1: Tensile properties of differently degummed SF fibers (data from ten degummed samples for each group).

Degummed Samples	Young's Modulus (GPa)	Yield Strength (MPa)	Yield Strain (mm/mm)	Breaking Strength (MPa)	Breaking Strain (mm/mm)
SDS5 (Fibers)	9.4 ± 1.1	231 ± 30	0.026 ± 0.003	434 ± 45	0.19 ± 0.07
SDS15 (Fibers)	10.5 ± 1.4	235 ± 44	0.024 ± 0.004	456 ± 70	0.20 ± 0.04
SDS30 (Fibers)	9.6 ± 1.2	205 ± 26	0.023 ± 0.004	430 ± 75	0.20 ± 0.04
SDS45 (Fibers)	9.1 ± 0.8	174 ± 19	0.021 ± 0.003	361 ± 66	0.13 ± 0.05
SDS60 (Fibers)	8.9 ± 1.8	204 ± 33	0.022 ± 0.003	366 ± 59	0.17 ± 0.07
SDS75 (Fibers)	8.8 ± 1.6	197 ± 60	0.026 ± 0.012	359 ± 49	0.14 ± 0.04
SDS90 (Fibers)	7.7 ± 1.2	208 ± 86	0.028 ± 0.007	274 ± 49	0.12 ± 0.03
$Na_2CO_3$90 (Fibers)	8.1 ± 1.7	146 ± 43	0.020 ± 0.003	309 ± 51	0.13 ± 0.07

When compared with the mechanical properties of SF as obtained by Pe´rez-Rigueiro *et al.* (Breaking strength: 650 ± 40 MPa, Young's modulus: 16 ± 1 GPa) [272], the breaking strengths and Young's modulus measured in this study were all relatively lower. However, it was comparable to the ultimate tensile strength or breaking strength commonly quoted for *Bombyx mori* silk of 500 MPa [272]. The reason for the slight discrepancy could be attributed to the difference in the source of silk used for different project groups. Moreover, the conditions at which the experiments were conducted were usually not specific, rendering slight differences in the results obtained.

From the mechanical properties obtained for SF degummed in different durations, the properties for "SDS30 (fibers)" was chosen for use in the design of the SF knit. This decision was made based on the observation that sericin was clearly removed from the silk fibers by 30 min of degumming (determined by SEM) and prolonged degumming would only weaken the SF material further (determined by tensile tests performed).

3.3. Design of Knitted SF Architecture

3.3.1. Design Purpose and Specifications

The purpose set for this stage was to design the knitted SF in terms of its dimensions, pore size and choose the optimal number of yarns for physiological loading as a rabbit ACL total replacement *in vivo*. The principle of the design was to macroscopically and physically match the construct to the native tissue in terms its mechanical attributes. It was important to consider contribution from *in vivo* proteolytic degradation in the design such that the construct could remain mechanically viable throughout the tissue regeneration phase *in vivo*.

It was estimated that the maximum rabbit ACL force experienced was at 40 N, which was about 138.6 % of rabbit body weight (2.5 – 3.0 kg) [12]. Although proteolytic degradation of SF was minimal for *in vitro* cultures, drastic decrease in tensile strength had been reported to range from 55% at 6 weeks to 73% at 30 days after subcutaneous implantation of silk scaffolds [28, 275]. A 50% decrease in SF scaffold failure load was also observed after 24 weeks in an *in vivo* study conducted by our group for rabbit ACL replacement [3]. Since the rate of degradation would very much depend on the implantation site, mechanical environment and scaffold structure, it would be more accurate to expect a 50% decrease in SF knitted scaffold loading capacity after 24 weeks *in vivo* when applied for ACL replacement. Although ultimately, the tensile properties of the regenerated construct should come from the regenerated tissue instead of from the scaffold, the scaffold should last a minimum of 6 months *in vivo* to allow time for tissue growth and maturation [9, 24, 39, 43, 47, 96-98].

Of the whole hybrid SF scaffold, the SF knit would contribute the bulk of the mechanical loading involved. Therefore the knitted SF structure in this study should be able withstand the maximum ACL load even if there was a 50% decrease in loading capacity due to proteolytic degradation of the knit. This was done by customizing the SF knit to support more than twice the maximum ACL force in rabbits; that was to support more than 80 N of loading within its elastic limits.

The tensile stiffness of knitted SF, on the other hand, should be less than half of the native ACL tissue, which was measured to be 47.07 ± 14.84 N/mm [3]. Having lower scaffold stiffness as such could prevent stress shielding and allowed mechanical forces that were subjected to the scaffolds to be effectively conducted to the attached cells. This strategy fell in line with the principles of functional tissue engineering [150] and would be especially important when the cell-seeded scaffolds were to be mechanically conditioned either *in vitro* or *in vivo* to further enhance the proliferative and differentiative potential of MSCs on the hybrid SF scaffolds. Stiffness of the knitted SF was therefore designed to be less than 25 N/mm.

3.3.2. Design Development

The dimensional attributes of the SF knits were first determined. With due considerations given to the native tissue dimension, surgical implantation feasibility and ease of handling, the length of the SF knit was set at 40 mm while the width at 20 mm. This would give a cylindrical ACL analogue of length 40 mm with circular cross-section of 5 mm outer diameter when the knit was rolled up along its width as shown in

Figure 3-5. Due to the limitation of the knitting machine, the minimum pore size attainable for the knitted structure was 1 mm.

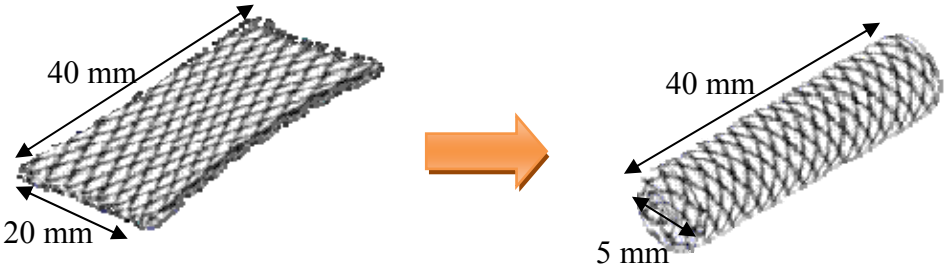

Figure 3-5: Dimensions of knitted SF in the flat rectangular profile and the cylindrical profile when rolled up along its width.

With these parameters set, the optimum number of SF filaments that would be required to withstand the rabbit ACL physiological loads *in vivo* could then be determined theoretically. Although the mechanical strength of the knitted structure would increase by increasing the number of SF filaments used, the porosity and voids available for cell and tissue ingrowth would also decrease. This was notwithstanding the fact that overall structure stiffness would increase with increasing filament count, leading to stress shielding of the regenerating tissue.

Optimization of the number of SF filaments would thus be necessary to determine the minimal filament number necessary for the application. Calculations for the required number of SF filaments to achieve this were based on the loading of SF knit in a taut state, whereby the individual struts of the loading direction were oriented to the direction of loading (Figure 3-6). It should also be noted that there was pore narrowing with force applied. In this state, the individual SF filaments would be tensioned and contributed to loading capacity of the knitted structure in a linear elastic manner. With

reference to load-extension curve for knitted structures, the start of this tensioned state would also mark the start of the linear elastic region (Figure A-1C, Appendix A) and the toe region before that would indicate that the knitted struts were not all in tension and loaded yet. It was thus assumed that failure of the knitted structure would require fully loading the individual SF filaments of the tensioned struts to failure. To further simplify the calculations, it was assumed that the SF filaments were loaded uniformly, rendering them to extend and fail in unison upon stretching the knitted structure to failure.

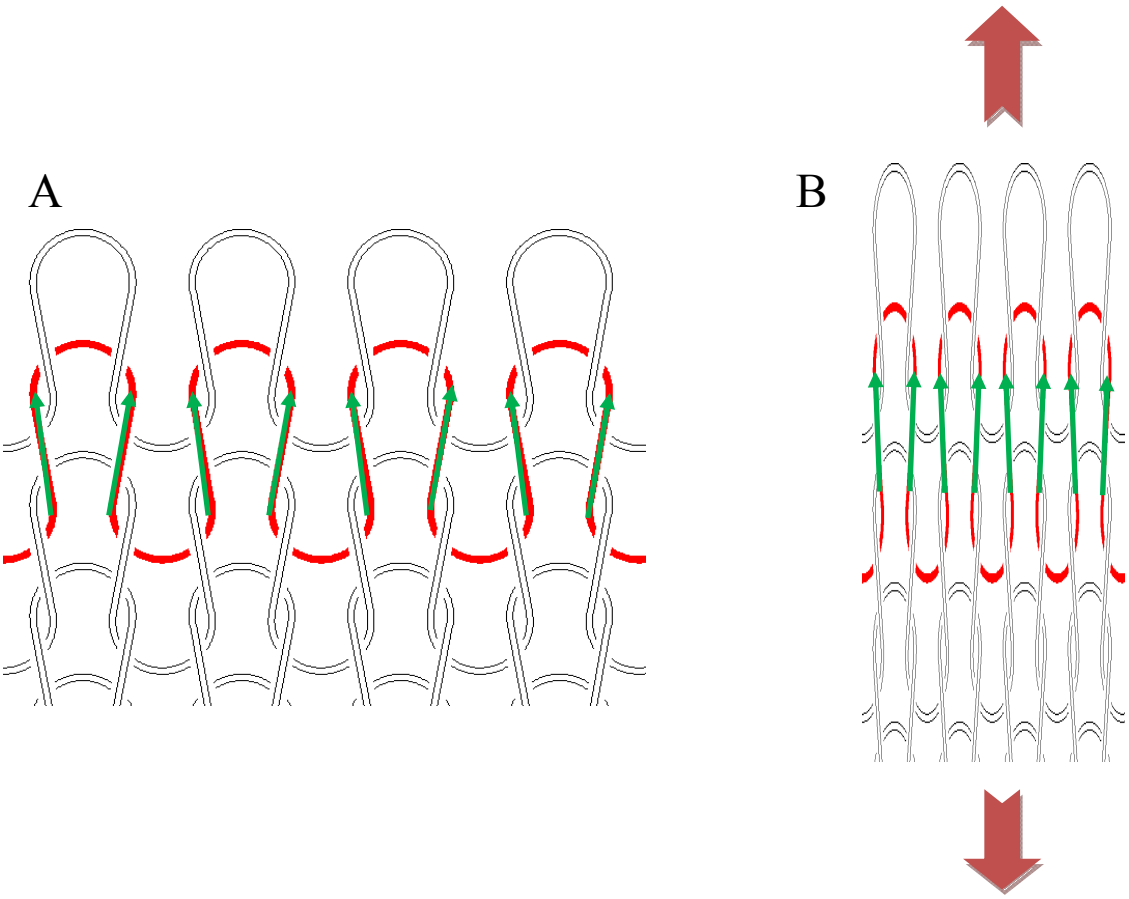

Figure 3-6: Knitted structure in a (A) relaxed state, and in a (B) tensioned state with applied force. The green arrows indicate the change in direction of orientation of the loaded struts with applied force, which makes these struts orientate in the direction of force applied. Red arrow: Direction of applied force.

Theoretical Calculation for the Optimal SF Filament Count

The design specifications in terms of the yield point load and stiffness are listed in Table 3-2. The material mechanical and physical properties of SF as determined via single filament tensile test of silk degummed for 30 min and SEM measurements are as tabulated in Table 3-3 and the designed knitted SF parameters are tabulated in Table 3-4.

Table 3-2: Design specifications for knitted SF.

Yield Point Load and Stiffness Requirement	
Yield Point Load	> 80 N
Stiffness	< 25 N/mm

Table 3-3: Tensile properties of SF fibers degummed for 30 min.

Tensile Properties of Degummed SF	
Young's Modulus (GPa)	9.6 ± 1.2
Yield Strength (MPa)	205 ± 26
Yield Strain (mm/mm)	0.023 ± 0.004
Breaking Strength (MPa)	430 ± 75
Breaking Strain (mm/mm)	0.20 ± 0.04
Cross-sectional Area (μm^2)	102 ± 25

Table 3-4: Designed knitted SF parameters.

Knitted SF Parameters	
Dimension (mm)	40 × 20
Average pore size (mm)	1
Needle/stroke setting	12 needles 27 strokes

From the mean values of the tensile properties of SF filaments, the yield point load and elastic stiffness of the single SF filaments could be derived (Table 3-5) using the measured filament cross-sectional area and gauge length when the filaments were tested.

Table 3-5: Calculated yield point load and stiffness of SF filament.

Yield Point Load and Stiffness of SF Filament	
Yield Point Load	20.9 mN
Stiffness	49.0 mN/mm

With a safety factor of 1.5 derived empirically from preliminary single yarn knit tensile measurement to cater for stress concentration factors at the knots of the knitted structure and degumming damages, and assuming that the tensioned struts were oriented parallel to the directional force,

$$Total\ no.of\ filaments\ required = \frac{Yield\ point\ load\ required}{Yield\ point\ load\ of\ single\ SF\ filament} \times Safety\ factor$$

$$= \frac{80}{20.9\times10^{-3}} \times 1.5 = 5742$$

Therefore, given that 2 struts were associated with each needle,

$$No.of\ filaments\ per\ strut = \frac{Total\ no.of\ filaments\ required}{No.of\ needles\ \times 2}$$

$$= \frac{5742}{12\times2} = 239$$

Since each yarn of raw silk fiber that was provided had a SF count of 80, 3 yarns of silk would be used to generate SF knit that would be strong enough for rabbit ACL physiological loading. Using 240 SF filaments for fabrication of the SF knits, the theoretical stiffness of the structure could be determined as follows, which was lower than 25 N/mm and thus met the design requirement.

$$Stiffness = 240 \times 49 \times 10^{-3} = 11.8\ N/mm$$

3.3.3. Summary of Design Outcome

In the design of the knitted SF to cater for mechanical viability of the rabbit ACL, it was important to consider degradation issues *in vivo*, such that the structure could last as long as it was intended for in the body. It was determined that 3 yarns of silk, totalling to 240 SF filaments, would be sufficient to cater to the maximum load observed in rabbit ACL during normal function. Although the design approach used involved both empirical methods of preliminarily tensile testing single yarn SF knits to determine the safety factor, and theoretical calculations, it would be necessary to experimentally test the designed knits to ascertain its loading capacity.

3.4. Optimization of Knitted SF Degumming

3.4.1. Introduction

Upon determining the number of yarns to be used for the SF knit in this study, it would be necessary to investigate the effects of degumming on SF knit mechanical depreciation. Since harsher degumming conditions would be necessary to degum knitted structure made of 3 yarns of SF, the purpose of this part of the study was to optimize the degumming procedure to preserve knitted SF mechanical integrity. Moreover, current literature had shown limited work in investigating the effects of the different factors or degumming conditions in alkaline degumming that would directly contribute to the degradation of SF mechanical properties and morphology. The optimization and control of these factors or conditions to yield sericin-free and mechanically viable processed SF scaffolds had also been lacking.

Therefore, the specific aim of this part of the study was to identify the factors or conditions in alkaline degumming that contribute to mechanical deterioration and protein structural modification. They were specifically identified as (1) duration, (2) presence of mechanical agitation, (3) thermal conditions, (4), use of refreshed solution and (5) post degumming structural modification of SF. Through a series of phases, investigating only a specific factor (presence of mechanical agitation, thermal conditions, use of refreshed solution and post degumming structural modification of SF) in each phase with varying durations, the effects of these factors on the SF tensile properties, SF morphology, effectiveness of sericin removal and SF protein structure were evaluated. Based on these material characterizations of single SF filaments, we

then attempted to provide a set of optimized parameters for degumming knitted silk structure. Using this set of optimized degumming parameters, the mechanical properties of the overall SF knit would then be determined and compared with the required yield point load and stiffness of SF knit to verify the theoretical calculations of the SF filament count. The percentage of sericin removed from knitted raw silk structures using such an optimized degumming protocol would also be quantified.

The optimization phases thus investigated the impact of different degumming factors on knitted SF from a material aspect by measuring single SF filaments extracted from the differently degummed knitted structures. The optimization process and the optimized degumming parameters obtained were transferrable for degumming of similar processed structures since the material aspect was investigated. Upon finding the optimal degumming parameters via these optimization phases, the overall knitted structure degummed using this set of parameters would then be characterized and be used to verify that the designed SF knit would be mechanically sufficient to serve its purpose.

3.4.2. Materials and Methods

3.4.2.1. Sample Preparation and Degumming

Raw *Bombyx mori* silk fibers (*Nang Lai* silk) were provided by the Silk Innovation Center at Mahasarakham University, Thailand. With the aid of the Silver Reed SK270 (Suzhou, China) Knitting Machine, as shown in Figure 3-7, 3 yarns of 80 fibroin raw silk (total of 240 fibroins) was fabricated into knitted silk meshes of

dimensions about 40 mm by 20 mm, with a setting of 12 needles and 27 strokes. The pore diameter was 1 mm on average, which was the minimum pore size available on the machine. At this stage of knitting, sericin was not removed from the silk material but was deliberately left unremoved as sericin acted as a 'gumming' agent that surrounded fibroin fibers, binding these fibers together. By doing so, the protein would provide a protective coating over the fibroin filament, necessary in the knitting process, while it prevented fraying of the fiber, allowing ease in knitting. Silk fibers, when treated, might fray and get caught in the complex mechanism of the knitting machine (Figure 3-7B). This strategy of sericin retention is typically used in silk processing of the textile industry [276].

However, these silk knits tended to curl up and thus custom-made U-shaped stainless steel wire frames of 1 mm diameter (Global Orthopaedics, Hampshire, England) were used to open up the knits (Figure 3-7A).

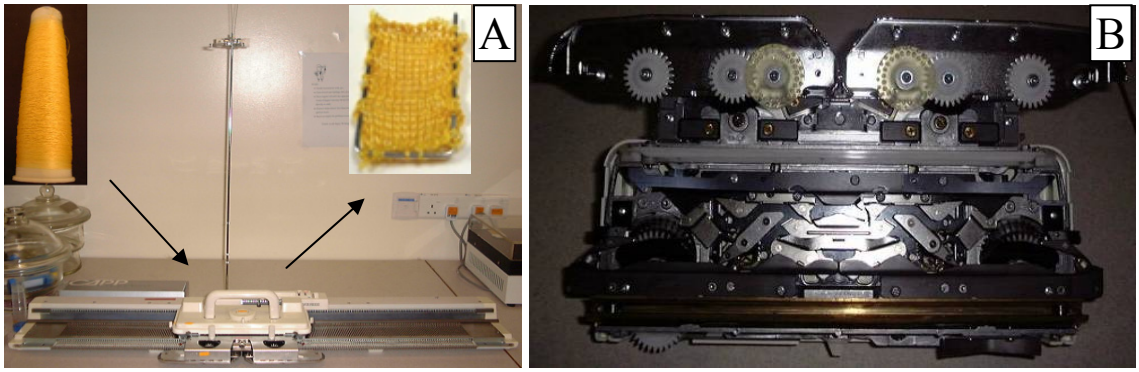

Figure 3-7: (A) Hand-operated knitting machine used for the fabrication of knitted silk scaffolds from silk yarns with (B) the complex knitting mechanism that would catch frayed degummed silk fibers causing damage to the knit.

Due to the antigenic nature of sericin, it is necessary to remove it cleanly from the knitted silk structure before the material can be made suitable for use in tissue engineering applications. The process of removing sericin from silk is also known as

silk degumming and often involves mechanical weakening of the fibroin structure [220-222]. Alkaline degumming was the mode of degumming chosen for use in this study. It involved the use of alkaline degumming solution, which consisted of aqueous sodium carbonate (Na_2CO_3) and sodium dodecyl sulphate (SDS), 0.25 %w/v each (Sigma-Aldrich St. Louis, USA). The addition of chemical surfactant such as SDS would reduce surface tension at the water–silk interface due to its hydrophilic and hydrophobic components, thereby improving the sticking and adsorbing properties of the cleaning solution onto raw silk. SDS is also a known anionic surfactant, which has been often used in protein separations by binding protein and disrupting the non-covalent bonds, making proteins lose their native conformation. Hence, SDS was added to reduce degumming duration by improving the efficiency of sericin removal.

The SF knits were degummed under either presence or absence of mechanical agitation, different duration, different thermal conditions, with or without use of refreshed solution, and with or without post-degumming SF structural modification. The control group, on the other hand, was degummed with pure aqueous Na_2CO_3 solution (SDS-free) for 90 min at 100°C with mechanical agitation.

Using SDS containing degumming solution, the various factors identified to affect the effectiveness of degumming and the physical outcome of degummed SF were each investigated in a series of phases (Table 3-6). It should be noted that Table 3-6 was compiled retrospectively, with the optimal parameter obtained after each phase applied to the subsequent phases.

Table 3-6: Classification of sample groups and the degumming conditions subjected to each group. The different factors were optimized under different phases (Phase I: Mechanical agitation, Phase II: Degumming thermal conditions, Phase III: Use of refreshed solution and Phase IV: Use of post-degumming SF structural modification). Degumming durations were varied within each phase. Numbers following "SDS" or "Na_2CO_3" of sample group names indicate degumming duration pattern, while items in bracket indicate degumming temperature and whether mechanical agitation is present (MA) or absent (Static).

Factors Optimized		Samples	Parameters				
			Total Duration (min)	Temp. (°C)	Refreshed Soln (Y/N)	Mechanical Agitation (Y/N)	SF Struc. Mod. (Y/N)
Control		$Na_2CO_3$90 (100°C, MA)	90	100	N	Y	N
Phase I							
Mechanical Agitation	**Duration**	SDS15 (100°C, MA)	15	100	N	**Y**	N
		SDS30 (100°C, MA)	30	100	N	**Y**	N
		SDS60 (100°C, MA)	60	100	N	**Y**	N
		SDS90 (100°C, MA)	90	100	N	**Y**	N
	Duration	SDS15 (100°C, Static)	15	100	N	**N**	N
		SDS30 (100°C, Static)	30	100	N	**N**	N
		SDS60 (100°C, Static)	60	100	N	**N**	N
		SDS90 (100°C, Static)	90	100	N	**N**	N
Phase II							
Degumming Thermal Conditions	**Duration**	SDS30 (100°C, MA)	30	**100**	N	Y	N
		SDS60 (100°C, MA)	60	**100**	N	Y	N
		SDS90 (100°C, MA)	90	**100**	N	Y	N
	Duration	SDS30 (75°C. MA)	30	**75**	N	Y	N
		SDS45 (75°C, MA)	45	**75**	N	Y	N
		SDS60 (75°C, MA)	60	**75**	N	Y	N
		SDS90 (75°C, MA)	90	**75**	N	Y	N
	Duration	SDS45 (60°C, MA)	45	**60**	N	Y	N
		SDS90 (60°C, MA)	90	**60**	N	Y	N
Phase III							
Use of Refreshed Solutions	**Duration**	SDS15 (100°C, MA)	15	100	**N**	Y	N
		SDS30 (100°C, MA)	30	100	**N**	Y	N
		SDS60 (100°C, MA)	60	100	**N**	Y	N
	Duration	SDS7.5+7.5 (100°C, MA)	15	100	**Y**	Y	N
		SDS15+15 (100°C, MA)	30	100	**Y**	Y	N
		SDS30+30 (100°C, MA)	60	100	**Y**	Y	N
Phase IV							
SF Struc. Mod.	**Duration**	SDS30 (100°C, MA)	30	100	N	Y	**N**
		SDS30 (100°C, MA)	30	100	N	Y	**Y**

Phase I was aimed at identifying the need for mechanical agitation in the process of degumming knitted SF. Mechanical agitation of raw silk knits involved the attachment of the knits to a customized mechanical vibrator and immersed in a beaker of degumming solution, which was in turn placed on a heating magnetic stirrer (Figure 3-8A). The mechanical vibrator would thus generate vibrational agitation (amplitude: 5 mm, frequency: 12 Hz) in the vertical plane, whereas the heating magnetic stirrer (rotational speed: 800 rpm) would generate agitation currents normal to the knit surface and provide heat for the degumming process.

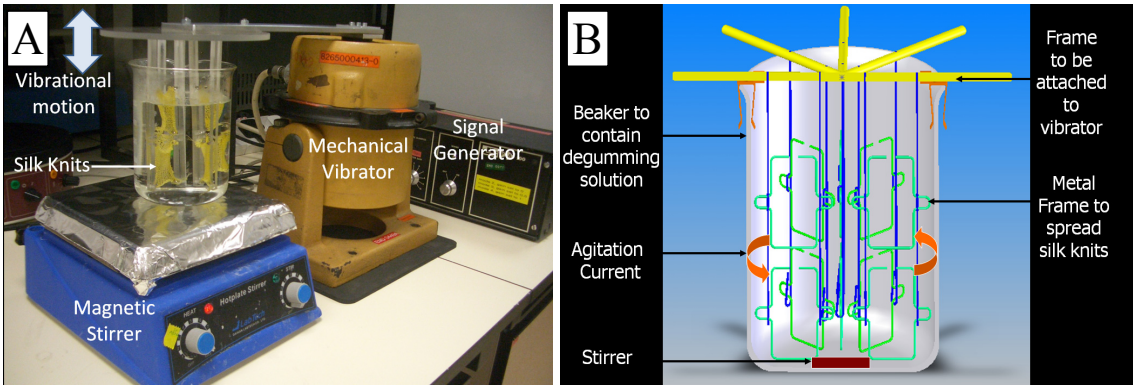

Figure 3-8: (A) Mechanical vibrator and magnetic stirrer setup to provide agitation during degumming. (B) Schematic diagram of knit attachments with annular agitation currents provided by magnetic stirring action.

During this process, the raw silk knits were spread open via a metal frame (Figure 3-8B), so that the exposed area can be maximized to allow effective sericin removal by the degumming solution. These metal frames were attached to a supporting framework and arranged efficiently to allow multiple knitted silk structures to be degummed simultaneously. The knits were positioned vertically so that the larger surfaces would be normal to the stirring current provided by a magnetic stirrer. Doing this would thus allow relative motion between the degumming solution current and the knitted structure itself, which would lead to more effective sericin removal especially at the 'knots' of

the knitted scaffold. Moreover, the secured knits would also not be swirled in the current, which could possibly entangle or damage the structure. The purpose of the vibrational agitation was to loosen the knitted structures such that the degumming agents could reach the 'knots' and yarn core of the knits.

Sample groups without mechanical agitation were simply immersed in degumming solution for similar durations. Within this phase, the degumming duration was varied (15-90 min) while factors of thermal conditions and use of refreshed solution were kept constant (100°C, without use of refreshed solution). Upon establishing the necessity of having mechanical agitation, it would be applied in subsequent phases.

Phase II would then involve optimizing the degumming thermal conditions using 3 different thermal conditions (60°C, 75°C and 100°C), while keeping other factors constant. Likewise, duration was varied from 30-90 min while other factors were kept constant. Mechanical agitation was applied as determined from Phase I and no refreshment of solution was applied for all samples within this phase.

Upon obtaining the optimal thermal condition, it would be applied to Phase III to determine the need to refresh degumming solution. This was performed by changing similar volume of fresh degumming solution, with same SDS and Na_2CO_3 concentrations, midway through the degumming durations with total durations of 15, 30 and 60 min. All other factors were kept constant as determined from previous phases (100°C with mechanical agitation).

Degummed SF knits from the optimized protocol would then be treated for post-degumming methanol treatment to induce structural modification and crystallization of

SF in Phase IV and evaluate to see if this structural modification and crystallization would aid in further improving the mechanical properties of the degummed SF. This was done by immersing dried degummed SF samples in methanol (Thermo Fisher Scientific Inc., MA, USA) for 10 min and dried in room temperature and relative humidity (25°C, 60% respectively).

All sample groups were rinsed in warmed distilled water after removal from degumming solution and left to air dry for at least 24 h before further tests were conducted.

3.4.2.2. Observation of SF morphology

The sample groups were gold-sputtered and observed at 15 kV in a SEM (JEOL Ltd, JSM-5600 LV, Japan) to characterize their surface morphology and cross-sectional areas. SFs at the core of the knits were carefully exposed for observation of sericin presence at two different positions. Data was collected over 20 samples.

3.4.2.3. Single Fibroin Mechanical Test

Single SF filaments were carefully extracted from the knitted structure at various locations, and tensile tested to failure using the nanotensile tester as described in section 3.2.1.3. Data was collected over 10 samples for each degumming method. Stress-strain behaviors of SFs subjected to various alkaline degumming conditions were thus obtained from force-displacement data as described in Appendix A using the cross-sectional area measured.

3.4.2.4. Knitted SF Mechanical Test

The overall knitted structure obtained by degumming using the "SDS30 (100°C, MA)" set of parameters was tested mechanically using a universal testing machine (Instron 3345 Tester, Instron, Norwood, MA, USA) with 1000 N load cell at standard environmental conditions (20°C, 60% relative humidity) (Figure 3-9A). "SDS30 (100°C, MA)" was selected as an optimized set of degumming protocol for knitted silk structures after having performed sample assessments through the first 3 phases via SEM and mechanical tensile tests of single SF filaments extracted from degummed knits.

Each cylindrical samples (5 mm outer diameter, 20 mm gauge length) were rolled from their laminar form along the widths prior testing (Figure 3-9B). Cylindrical forms were tested as this form would be analogous to the ligament tissue and would also be the functional form *in vivo*. The samples were kept moist with phosphate buffer saline (PBS) solution and loaded to failure by increasing the tensile load continuously at a crosshead speed of 10 mm/min without any pretension or preconditioning. Masking tapes were used to secure the specimens and aid to prevent slippages at the grips during testing. Samples were generally noted to fail from the central portions of the gauge length, indicative uniform loading profile through the gauge length and non-slipping at the grips (Figure 3-9C).

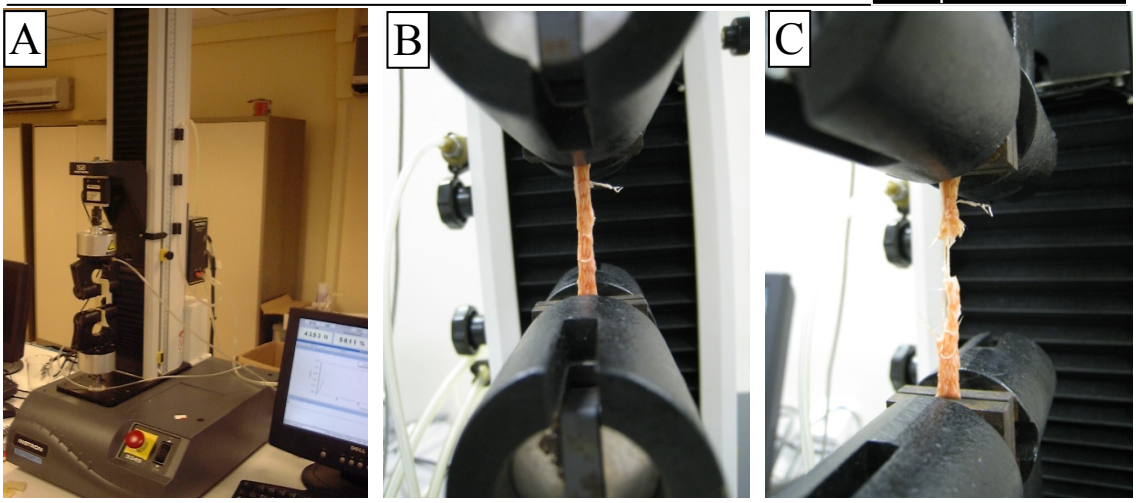

Figure 3-9: (A) Tensile testing of SF knits, scaffolds or cultured constructs using universal testing machine, with (B) cylindrical form of the specimens placed centrally at the grips for testing. (C) Failure was generally noted to initiate from the central portion of the tested specimens.

Tensile load and elongation were recorded as represented by the load-displacement curves, where the failure load, linear stiffness and extension at failure load were determined from. The ultimate tensile load (UTL) or failure load is defined as the highest load in load-extension graph, while the elastic stiffness of the constructs were obtained from the gradient of the line that fitted to the best linear region of the load-extension graph and is expressed in N/mm. The stiffness in the elastic region was found by the method as detailed in Appendix A.

The extent of the toe region relative to extension was also determined to indicate the degree at which the different specimens could be stretched prior to linear extension, method of identification is as described in Appendix A as well.

3.4.2.5. Silk Protein Identification and Fractionation using SDS-PAGE

SDS-PAGE was performed for the SF knits degummed for different durations ranging from 5 min to 90 min at 100°C with mechanical agitation (i.e. "SDS5 (100°C, MA)", "SDS15 (100°C, MA)", "SDS30 (100°C, MA)", "SDS45 (100°C, MA)", "SDS60 (100°C, MA)", "SDS75 (100°C, MA)", "SDS90 (100°C, MA)"). This was done to determine the changes in the protein structure involved due to extended degumming. Particularly, it was used to determine and ascertain the removal of sericin in the optimal degumming condition and subsequently deduce the efficiency of sericin removal in the optimized degumming protocol. Sample solutions were obtained from raw silk, sericin and the differently degummed SF knits (n=5 each). Pure sericin was used as negative control in these analyses to indicate the molecular weights of sericin bands and compare it to the degummed silk specimens.

A general protocol for the SDS-PAGE analysis is described below.

a. **Dissolution.** Sericin was extracted from 0.5 g of finely cut raw silk pieces using 8M urea containing 2% 2-mercaptoethanol (Sigma-Aldrich, St. Louis, USA) at 80°C for 5 min [277]. Fiber residues were then removed and the extract was centrifuged to obtain the sericin solution as supernatant. Sericin was precipitated by adding three times volume of ethanol, and the extracted sericin precipitate was redissolved in 10 ml saturated LiSCN (250% w/v, Sigma-Aldrich, St. Louis, USA) with 2% 2-mercaptoethanol. It was assumed that the sericin extracted through this process reflected the total amount of sericin present in the raw silk sample.

Degummed silk solutions of specimens that had undergone various degumming conditions and treatments, on the other hand, were obtained from dissolution of the corresponding finely cut degummed SF sample, which was derived from 0.5 g of knitted raw silk, in 10 ml saturated LiSCN with 2% 2-mercaptoethanol. The amount of raw silk at which the sericin or the degummed silk specimens were obtained from was the same at 0.5 g to allow subsequent comparison of the protein bands. Upon centrifugation of the dissolved silk at 3000 rpm for 10 min, degummed silk solutions were obtained as supernatant.

b. **Running the gel.** Sample solutions for SDS–PAGE were prepared by adding an equal volume of sample buffer (0.5 M Tris–HCl buffer of pH 6.8, containing glycerol, 10 %w/v SDS and 0.5 %w/v bromophenol blue, Bio-rad, CA, USA) to individual protein solutions, vortexed and centrifuged briefly. The sample solutions were then loaded to a 12% gel (Bio-rad, CA, USA) and electrophoresis was performed in the Tris/glycine/SDS solution (Bio-rad, CA, USA) at a voltage of 100 V.

c. **Gel staining.** Upon completion of the electrosphresis, polypeptides were then stained with Coomassie Brilliant Blue R (Pierce, Thermo Scientific, MA, USA), which made up 0.2 % in 45:45:10 of methanol: water: acetic acid mix. The gel was covered with staining solution, sealed in plastic box and left overnight on shaker at room temperature. It was then destained with 25:65:10 of methanol: water: acetic acid mix, with agitation. The bands were compared to 10–250 kDa protein ladder (New England BioLabs, #P7703S, MA, USA). After which, the polyacrylamide gel

was photographed in a gel documentation system (Gel Doc 2000, BioRad, CA, USA).

d. Gel analysis. The smear intensities of the individual specimens were normalized to the standard molecular marker band intensities (set as the 80 kDa marker of the protein ladder) before the relative intensities could be compared between different gels for different specimens.

On the other hand, fractionations of sericin (SER) and "SDS30 (100°C, MA)" proteins using ethanol and SDS-PAGE were performed to ascertain the removal of sericin in the "SDS30 (100°C, MA)" sample. To perform the fractionation of silk proteins from the "SER" and "SDS30 (100°C, MA)" solutions, pure ethanol was added stepwise (final concentrations of 77.8%, 81.1%, 83.6%, 84.1%, 85.9%, 87.3%, and 89.0% v/v), with the generated precipitate at each step redissolved in 2ml saturated LiSCN for analysis using SDS-PAGE. At different volumes of ethanol added, sericin and SF proteins would be precipitated independently and identified using SDS-PAGE. As the proteins extracted were from a constant amount of raw silk (0.5 g), comparison of the polypeptide bands between "SER" and "SDS30 (100°C, MA)" fractions could be made to give indication of the amount of protein components within each sample. Smear intensities were normalized to standard molecular marker band intensities before the relative intensities could be compared. Through the comparison of any remnant sericin smears from "SDS30 (100°C, MA)" and sericin smears from "SER", evaluation on the amount of sericin removed from "SDS30 (100°C, MA)" could be performed. For statistical significance in the evaluation, extractions, ethanol fractionations and gel separation of "SER" and "SDS30 (100°C, MA)" were independently repeated (n=5).

3.4.2.6. Conformational Structure Analysis of Degummed SF using FTIR-ATR

FTIR-ATR was performed to determine the secondary structure and conformational changes of degummed SF, and the effects of post-degumming methanol treatment on SF protein structure. FTIR-ATR spectra were obtained in the spectral region of 1000-2000cm^{-1} (Thermo Nicolet, Avatar 360 FTIR spectrometer, USA). The specimens to be tested were first dried thoroughly in vacuum set at 37°C for 24 h to remove any remnant water. Upon complete drying, the crystal and tip of the FTIR spectrometer were cleaned with distilled water and dried prior to placing the specimens in between for scanning. Upon obtaining the absorbance waveform for each specimen, absorption peaks for the amide I, amide II and amide III (corresponding to C = O, N – H and C – N stretching) of Silk I random coil and Silk II β-sheet conformation were determined respectively. Specific to the secondary protein structure of SF, strong absorption bands at 1655 cm-1 (amide I), 1540 cm-1 (amide II) and 1230 cm-1 (amide III) were attributed to the random coil conformation, whereas absorption bands of 1628 cm-1 (amide I), 1533 cm-1 (amide II) and 1260 cm-1 (amide III) were assigned to the β-sheet conformation [219, 278, 279]. To quantitatively analyze the degree of crystallization of the specimens, the crystalline index was calculated using the intensity ratio of the absorbance wavenumbers of 1260cm^{-1} to 1230cm^{-1} (amide III peaks) [278].

$$Crystalline\ Index = \frac{Peak\ Intensity_{1260cm^{-1}}}{Peak\ Intensity_{1230cm^{-1}}}$$

The peak intensities of absorbance were determined from the area bounded by the respective peaks with the baseline absorbance.

3.4.2.7. Statistical Analysis

All data were expressed as means ± SD. Single factor ANOVA technique was used to assess the statistical significance of results between groups. For pair-wise comparisons, two-tailed, unpaired Student's *t* tests were used. GraphPad Prism ver. 5 (GraphPad Software, Inc., CA, USA) was used to implement the statistical analysis. A $p<0.05$ was considered statistically significant.

3.4.3. Results

3.4.3.1. Degummed SF Morphology

From the SEM images obtained (Figure 3-10), sericin was observed to be effectively removed from "SDS30 (100°C, MA)" sample, as indicated by the smooth SF fibers (Figure 3-10A). Sericin remnants were observed to be present for samples with the same degumming duration of 30 min but without mechanical agitation, "SDS30 (100°C, Static)" (Figure 3-10B). Remnant sericin could be observed in samples degummed shorter than 30 min, with or without mechanical agitation (Figure 3-10B). Although sericin was removed for samples degummed longer than 30 min, with or without mechanical agitation, fibrillations were observed in the fibroin filaments, indicative of fibroin degradation due to excessive degumming (Figure 3-10C). The same was observed for the control group, which was degummed using pure Na_2CO_3 in the absence of SDS for extended durations (90 min) with mechanical agitation (Figure 3-

10C). Shorter durations (15, 30, 60 min) of degumming using pure Na_2CO_3 (without SDS) with mechanical agitation at 100°C were performed preliminarily, which produced samples with presence of sericin remnants (Figure 3-10B). In addition to the remnant sericin, fibrillations were also observed in the samples degummed for 60 min (Figure 3-10D). Consequently, effective sericin removal using purely Na_2CO_3 could only be achieved after 90 min, by which extended fibrillations would have occurred.

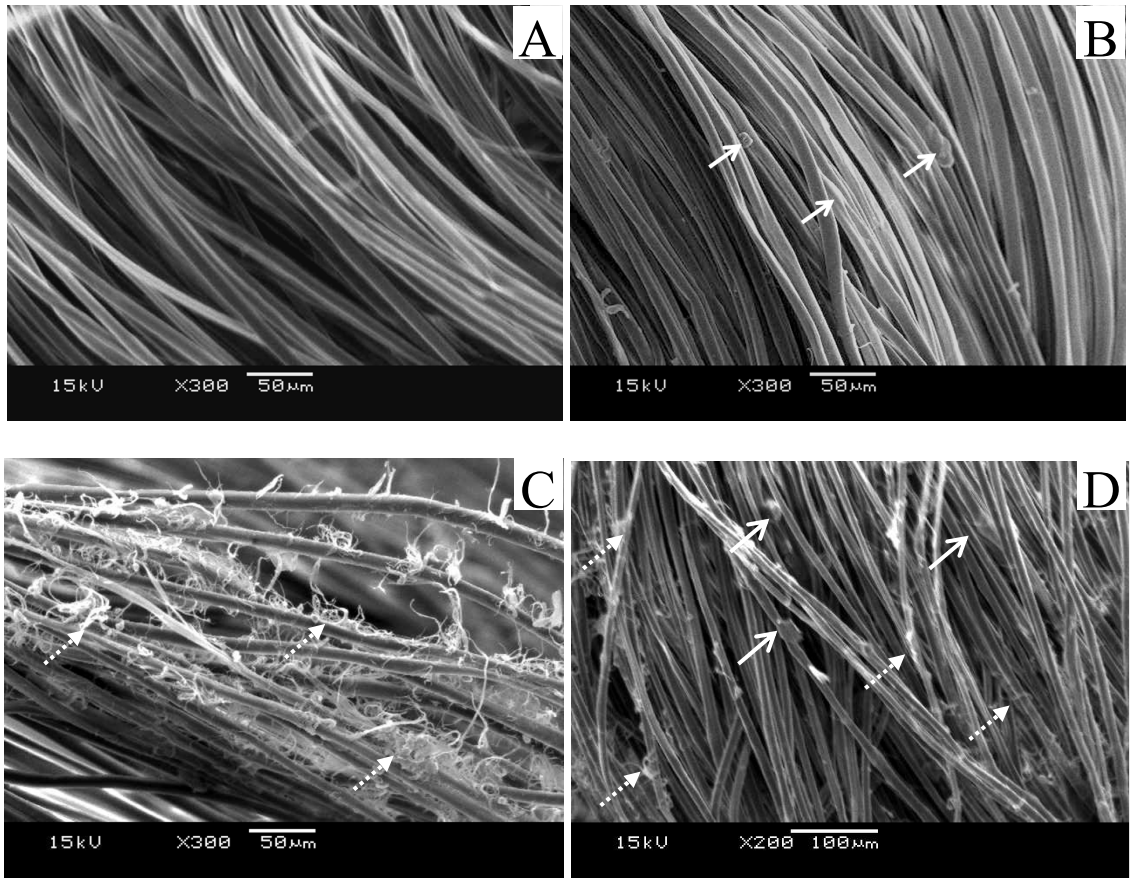

Figure 3-10: (A) SEM of "SDS30 (100°C, MA)" showing smooth SF filaments. (B) Representative image showing remnant sericin typical in "SDS30 (100°C, Static)", "SDS15 (100°C, MA)", "SDS15 (100°C, Static)", "SDS30 (75°C, MA)", "SDS90 (60°C, MA)" and "SDS7.5+7.5 (100°C, MA)". (C) Representative image showing SF fibrillations typical in "SDS60 (100°C, MA)", "SDS60 (100°C, Static)", "SDS15+15 (100°C, MA)"and "$Na_2CO_3$90 (100°C, MA)". (D) Representative image showing remnant sericin with signs of SF fibrillations typical in SF knits degummed in Na_2CO_3 for 60 min at 100°C. Remnant sericin indicated by solid arrows and fibrillations indicated by dashed arrows. Magnification: (A-C) 300×, (D) 200×. Data collected over 20 samples. [26]

Sericin remnants were observed in sample groups degummed with mechanical agitation at temperatures below 100°C (75°C and 60°C), regardless of the duration of degumming (Figure 3-10B). Prolonged degumming at 60°C for 90 min with mechanical agitation did not lead to fibrillations nor yield effective sericin removal as sericin was observed to be present (Figure 3-10B).

Fibrillation of SF also occurred in sample groups "SDS15+15 (100°C, MA)" degummed in mechanical agitation for 30 min and having one change of fresh degumming solution midway through the 30 min duration (Figure 3-10C). Sericin remnants were observed in both "SDS15 (100°C, MA)" and "SDS7.5+7.5 (100°C, MA)" (Figure 3-10B), indicating that sericin removal could not be done within 15 min, with or without refreshment of solution.

3.4.3.2. Degummed SF Mechanical Properties

The effect of mechanical deterioration due to prolonged degumming of knitted scaffolds was observed for the first 3 phases whereby the different factors were investigated (Figure 3-11 A-E). Qualitatively, the elastic modulus, the elastic limit (yield point), the breaking strength (ultimate tensile strength, UTS), and breaking strain were shown to decline. Table 3-7 summarizes the tensile properties of various samples subjected to different degumming conditions, which indicates a general decline in mechanical integrity with prolonged degumming durations, regardless of other contributing factors, such as degumming temperature or presence of mechanical agitation. Interestingly, there was a significant decrease ($p<0.05$) in yield stress, UTS and breaking strain with SF degummed more than 30 min as compared to the "SDS30

(100°C, MA)" group, but no significant difference ($p>0.05$) was found between the "SDS15 (100°C, MA)" and "SDS30 (100°C, MA)" groups.

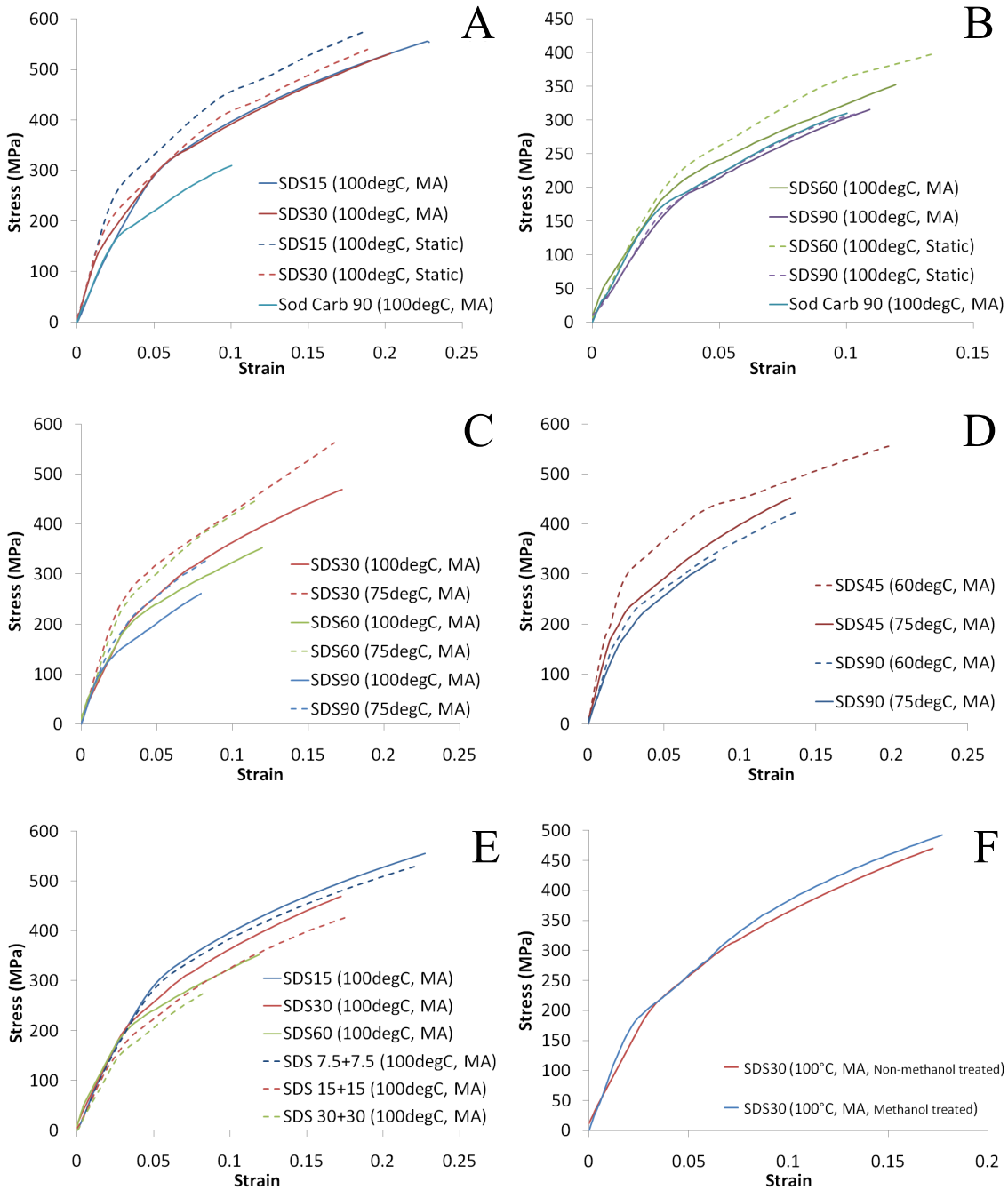

Figure 3-11: Stress-strain curves of single fibroins extracted from degummed knitted silk (representative samples) (A & B) subjected to different degumming durations with and without mechanical agitation, (C & D) subjected to different degumming thermal conditions, (E) with and without degumming solution refreshed, and (F) with and without methanol treatment. Samples degummed using only aqueous Na_2CO_3 for 90 min was assigned as the control group (A & B). [26]

Table 3-7: Tensile parameters of differently degummed SF (data from 10 degummed samples for each group) with the data from the group with optimal degumming highlighted in bold.

Samples	Young's Modulus (GPa)	Yield Strength (MPa)	Yield Strain (mm/mm)	Breaking Strength (MPa)	Breaking Strain (mm/mm)
$Na_2CO_3$90 (100°C, MA)	8.1 ± 1.7	146 ± 43	0.020 ± 0.003	309 ± 51	0.13 ± 0.07
SDS15 (100°C, MA)	9.5 ± 2.4	186 ± 52	0.022 ± 0.005	482 ± 70	0.19 ± 0.06
SDS30 (100°C, MA)	**10.1 ± 3.1**	**172 ± 38**	**0.020 ± 0.006**	**466 ± 67**	**0.16 ± 0.04**
SDS60 (100°C, MA)	8.9 ± 1.8	129 ± 64	0.017 ± 0.007	366 ± 101	0.12 ± 0.06
SDS90 (100°C, MA)	8.5 ± 2.1	136 ± 25	0.019 ± 0.005	318 ± 79	0.11 ± 0.06
SDS15 (100°C, Static)	10.4 ± 2.2	197 ± 48	0.024 ± 0.008	502 ± 89	0.18 ± 0.07
SDS30 (100°C, Static)	10.5 ± 2.6	184 ± 32	0.021 ± 0.005	489 ± 73	0.20 ± 0.04
SDS60 (100°C, Static)	9.1 ± 1.9	141 ± 54	0.018 ± 0.004	380 ± 98	0.13 ± 0.05
SDS90 (100°C, Static)	8.8 ± 2.0	132 ± 45	0.018 ± 0.003	320 ± 59	0.12 ± 0.03
SDS45 (60°C, MA)	14.6 ± 1.8	174 ± 17	0.014 ± 0.002	533 ± 104	0.15 ± 0.06
SDS90 (60°C, MA)	9.8 ± 2.7	218 ± 54	0.026 ± 0.009	521 ± 103	0.19 ± 0.08
SDS30 (75°C, MA)	9.0 ± 2.8	159 ± 53	0.021 ± 0.010	471 ± 90	0.29 ± 0.13
SDS45 (75°C, MA)	10.5 ± 1.8	156 ± 33	0.017 ± 0.005	436 ± 40	0.15 ± 0.06
SDS60 (75°C, MA)	8.9 ± 2.0	169 ± 24	0.022 ± 0.004	414 ± 64	0.18 ± 0.08
SDS90 (75°C, MA)	9.1 ± 1.7	175 ± 30	0.021 ± 0.004	394 ± 65	0.11 ± 0.04
SDS7.5+7.5 (100°C, MA)	9.8 ± 1.9	177 ± 39	0.023 ± 0.005	495 ± 67	0.19 ± 0.06
SDS15+15 (100°C, MA)	8.3 ± 1.4	140 ± 37	0.019 ± 0.004	378 ± 55	0.17 ± 0.07
SDS30+30 (100°C, MA)	7.0 ± 1.7	166 ± 56	0.026 ± 0.006	367 ± 44	0.11 ± 0.02
SDS30 (100°C, MA) (Methanol Treated)	10.3 ± 3.4	151 ± 34	0.018 ± 0.005	449 ± 60	0.16 ± 0.07

With the presence of mechanical agitation, degummed SF exhibited significant decrease ($p<0.05$) in yield stress as compared to the sample groups without mechanical agitation (Figure 3-11A-B and Table 3-7). This was consistently observed across sample groups with different degumming durations (15-90 min).

The mechanical properties of SF changed with variation in the degumming thermal conditions used (Figure 3-11C-D and Table 3-7). Between the groups degummed at 100°C and 75°C, significant differences ($p<0.05$) in the UTS and yield stress existed only after 90 min of degumming. On the other hand, significant differences ($p<0.05$) in the UTS and yield stress existed in all groups degummed at 60°C when compared with the groups of similar durations degummed at 100°C and 75°C. These results indicated that degumming at 75°C yielded similar reduction in mechanical properties of SF as that of 100°C, but with prolonged degumming of 90 min, the decline in UTS and yield stress of the groups degummed at 100°C was significantly more ($p<0.05$) than that of the 75°C group. Conversely, SFs degummed at 60°C were significantly stronger ($p<0.05$) in terms of UTS and yield stress even after prolonged degumming of 90 min.

The stress-strain curve of samples degummed with the same degumming solution throughout the process ("SDS15 (100°C, MA)", "SDS30 (100°C, MA)" and "SDS60 (100°C, MA)") and that of samples with degumming solutions refreshed at the midpoint of the process ("SDS7.5+7.5 (100°C, MA)", "SDS15+15 (100°C, MA)" and "SDS30+30 (100°C, MA)") is illustrated (Figure 3-11E and Table 3-7). A significant drop ($p<0.05$) in the tensile properties, specifically the UTS, yield stress and yield strain, was observed in the groups that had refreshed degumming solutions ("SDS15+15

(100°C, MA)" and "SDS30+30 (100°C, MA)") as compared to their counterparts of similar total degumming durations ("SDS30 (100°C, MA)" and "SDS60 (100°C, MA)"). No statistical significant differences ($p>0.05$) in tensile properties were found between "SDS7.5+7.5 (100°C, MA)" and "SDS15 (100°C, MA)".

From stress-strain curves and tensile properties of "SDS30 (100°C, MA)" treated with methanol and that without methanol treatment (Figure 3-11F and Table 3-7), no significant differences ($p>0.05$) existed in the tensile properties of the two groups. This indicated that methanol treatment had statistically negligible effects in improving the tensile properties of degummed "SDS30 (100°C, MA)" SF.

3.4.3.3. Degummed SF Knit Mechanical Properties

From the SEM and mechanical tests performed through the first 3 phases of the optimization process, it was shown that the optimal degumming condition for processed silk forms such as the knitted structure was that of "SDS30 (100°C, MA)". Using this optimal degumming condition, the optimal degummed SF knit was obtained for mechanical testing. The load-extension graph for the optimally degummed silk structure (Figure 3-12) and the mechanical properties of this structure (Table 3-8) were determined. It was experimentally verified that the designed SF knit could meet the design requisite of being able to support 80 N of yield point load and having a stiffness of less than 25 N/mm by having yield point load of 82.35 ± 4.55 N and stiffness of 16.24 ± 0.81 N/mm.

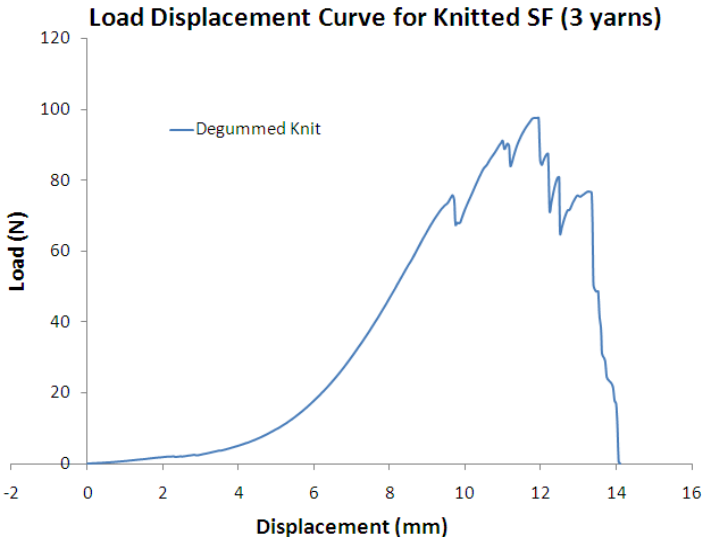

Figure 3-12: Load-displacement curve of SF knit degummed using the conditions of "SDS30 (100°C, MA)" (representative sample).

Table 3-8: Mechanical properties of degummed SF knit using the "SDS30 (100°C, MA)" degumming condition (n=5).

Yield point load (N)	Displacement at yield point (mm)	Stiffness (N/mm)	Maximum load (N)	Displacement at maximum load (mm)
82.35 ± 4.55	7.93 ± 1.82	16.24 ± 0.81	93.24 ± 5.62	9.24 ± 3.12

3.4.3.4. Silk Protein Identification and Fractionation

From the SDS-PAGE performed for samples degummed for different durations, it was shown that raw silk (lane 1) exhibited smears and bands at ~150 kDa and 30 kDa respectively, indicating mixture of sericin, heavy-chain (HC) fibroin and light-chain (LC) fibroin components (Figure 3-13). Sericin (lane 2) had a smear at ~150 kDa. Silk knits were degummed for various durations of 5, 15, 30, 45, 60, 75 and 90 min (lanes 3-9 respectively), leading to increased LC fibroin (30 kDa) degradation with degumming duration. Relative to volume intensity of the 30 kDa band in raw silk, the volume

intensities of corresponding bands in samples degummed for 5-90 min were 82%, 52%, 49%, 43%, 37%, 32% and 29% respectively. Consequently, there was an increase in peptide fragments at 20 kDa with degumming duration, whereby the volume intensities with respect to that of raw silk was 107%, 194%, 284%, 235%, 241%, 289% and 387% respectively.

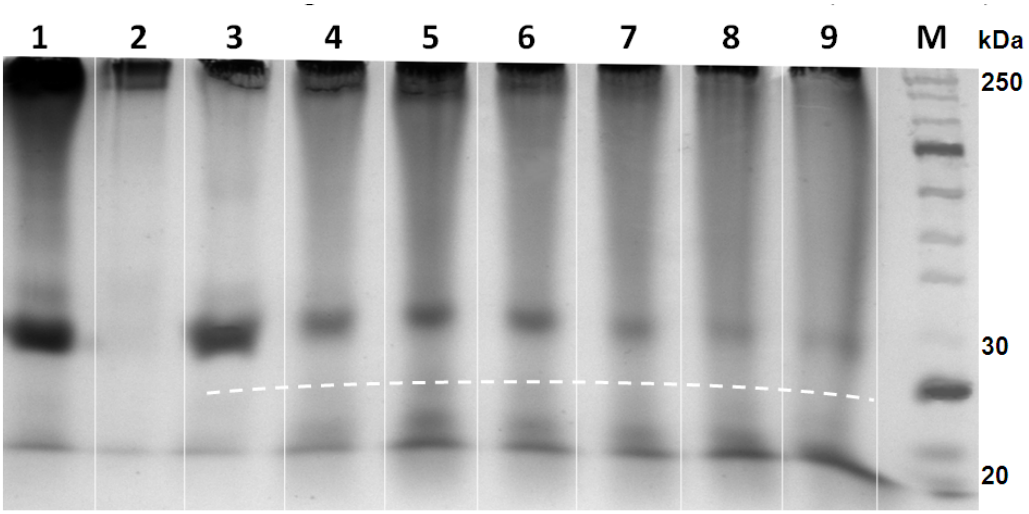

Figure 3-13: SDS-PAGE of raw silk (lane 1), sericin (lane 2), "SDS5 (100°C, MA)" (lane 3) "SDS15 (100°C, MA)" (lane 4) "SDS30 (100°C, MA)" (lane 5) "SDS45 (100°C, MA)" (lane 6) "SDS60 (100°C, MA)" (lane 7) "SDS75 (100°C, MA)" (lane 8) "SDS90 (100°C, MA)" (lane 9). Molecular marker (10-250 kDa) (lane M).

Upon determining the optimal parameters to be used for degumming knitted silk with retention in the SF mechanical properties (i.e. "SDS30 (100°C, MA)"), the efficacy of sericin removal of this protocol was determined via a comparison of fractionated sericin and "SDS30 (100°C, MA)" proteins using SDS-PAGE analysis. Fractionation of "SER" by ethanol precipitation in saturated LiSCN (Figure 3-14) showed intense smears in lanes 1-2 with reduction in intensity in subsequent lanes indicating that sericin was predominately fractionated when final ethanol concentration of 77.8% - 81.1% was added. Lanes 1-2 of "SDS30 (100°C, MA)", corresponding to remnant

sericin, were relatively clear (Figure 3-15), as compared to the corresponding lanes in "SER".

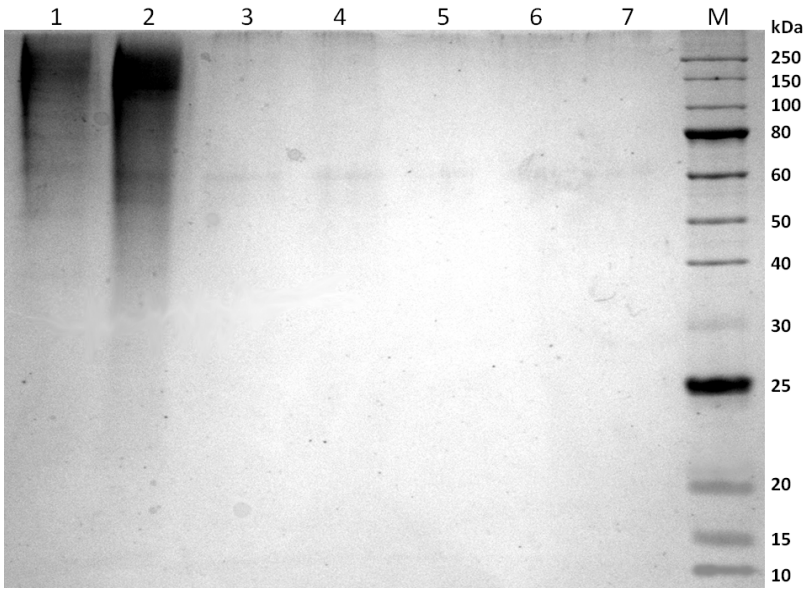

Figure 3-14: SDS-PAGE of fractionated "SER" by ethanol precipitation in saturated LiSCN. Concentrations of ethanol added were 77.8%, 81.1%, 83.6%, 84.1%, 85.9%, 87.3%, and 89.0% corresponding to lanes 1-7 respectively. Molecular marker (10-250 kDa) (lane M). [26]

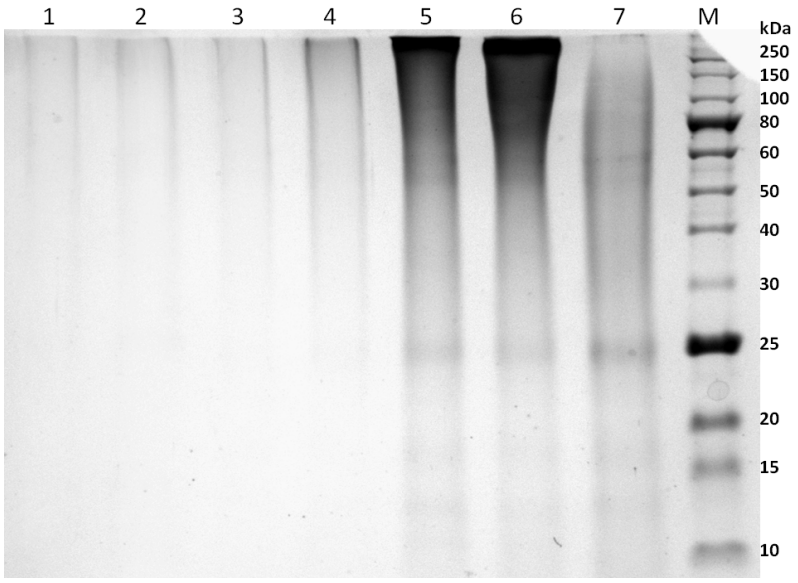

Figure 3-15: SDS-PAGE of fractionated "SDS30 (100°C, MA)" by ethanol precipitation in saturated LiSCN. Concentrations of ethanol added were 77.8%, 81.1%, 83.6%, 84.1%, 85.9%, 87.3%, and 89.0% corresponding to lanes 1-7 respectively, which were similar that added to fractionate "SER". Molecular marker (10-250 kDa) (lane M). [26]

By comparing the normalized smear intensities of the respective lanes 1-2 of "SER" and "SDS30 (100°C, MA)" samples, it was determined that 91.2 ± 3.4% of total sericin was removed from the "SDS30 (100°C, MA)" samples (n=5). There was a gradual increase in smear intensity at around 150 kDa for lanes 4-6 of "SDS30 (100°C, MA)" (predominantly HC fibroin and its fragments) and 30 kDa bands for lanes 5-7 (LC fibroin). It should be noted that these smears and bands were not apparent in the "SER" fractions.

3.4.3.5. Degummed SF Conformational Structure Analysis

From the FTIR-ATR spectra obtained (Figure 3-16), it was observed that "SDS30 (100°C)" upon degumming exhibited peaks at 1655cm^{-1}, which corresponds to the amide I region of the random coil structure. Upon methanol treatment, there was a conformational transformation by reduction in random coils to greater proportion in β-sheets, as observed from the FTIR-ATR spectra. This is indicated by the absence of peaks corresponding to random coil structures, especially at the amide I regions.

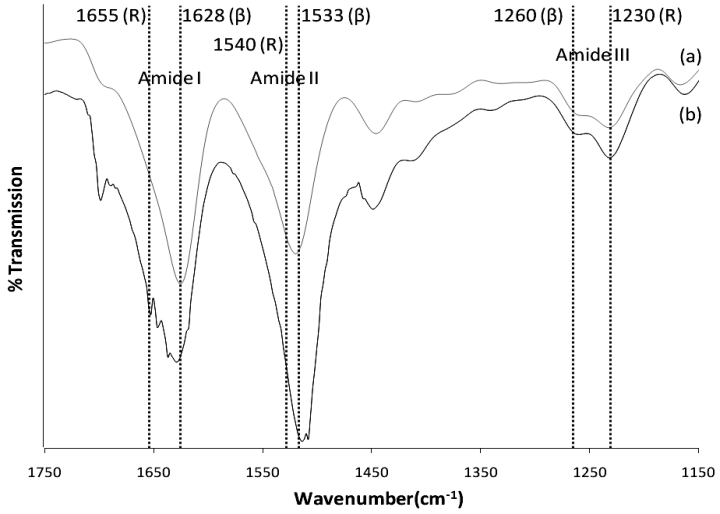

Figure 3-16: FTIR-ATR spectra of "SDS30 (100°C)" (a) with and (b) without methanol treatment.

To quantitatively analyze the degree of β-conformational transition, the amount of β-sheet structure was determined as the crystalline index for degummed SF with and without methanol treatment. Crystalline index for methanol treated "SDS30 (100°C)" was calculated to be 0.86 while that without methanol treatment was 0.79. Methanol treatment of "SDS30 (100°C)" thus led to an 8% increase in crystalline index, indicating that there was increased β-sheet conformation in SF upon methanol treatment.

3.4.4. Discussion

Alkaline degumming was chosen amongst other methods, based on its high throughput and suitability in degumming processed scaffolds for tissue engineering purposes. It was with the aim of achieving effective sericin removal while retaining the mechanical and structural properties of SF that an optimization study was performed to assess the effects of various factors and conditions involved in alkaline degumming. Particularly, the optimization was performed on processed silk forms, which proved to be harder to degum due to the difficulty in removing sericin from the core of the processed fibers. The various factors and conditions identified in this study include the duration, presence of mechanical agitation, thermal conditions and the use of refreshed solution. These four factors were studied in a series of three phases, each of which looked at effects of a specific factor. The effect of duration was investigated within each these three phases. Within each phase, the morphology of SF, sericin presence and tensile properties were determined via observations using SEM and single SF tensile tests.

3.4.4.1. Rationale for Mechanically Testing Both Single SF Filaments and Knitted SF

It should be highlighted that mechanical properties of a processed silk form, such as the knit in this case, are based on two aspects: architectural properties and material properties. Hence, the motivation for tensile testing single SF fiber extracted from a knitted structure and not the whole knitted structure lies in the fact that the mechanical properties of knits or any processed silk forms depend very much on their architectural properties. As such, mechanical properties of these silk forms will depend largely on the effective cross-sectional area experienced during loading. Not only is it very challenging to determine the effective cross-sectional area of a processed silk form accurately, the mechanical properties obtained are also limited to illustrate that for knitted structures and not other processed silk forms. On the other hand, single filaments extracted from the degummed knits could be tested to give a more accurate depiction of the mechanical integrity of SF. Testing single filaments also prevented effects of relative fiber slippage/movement from contributing to the tensile test profile. Given these concerns, it was of interest to first perform the *material* mechanical characterization prior to the *architectural* mechanical characterization of the knitted form. A material mechanical characterization as such could then aid in understanding the issues of degumming general processed structures, while providing an accurate assessment of the effects of different degumming factors on the mechanical properties of SF, and not be limited to just the knitted structure.

3.4.4.2. Effects of Prolonged Degumming

From the SEM images and mechanical studies conducted on SF degummed using the different conditions, it was observed across the three phases that although sericin was effectively removed by degumming at 100°C in durations more than, and inclusive of, 30 min, it was not mechanically and structurally optimal to degum over extended durations. This was so as prolonged degumming at 100°C (beyond and includes 60 min) led to fibrillations, regardless of the type of alkaline degumming solution used (aqueous Na_2CO_3 with or without SDS). Fibrillations, as such, were likely to be caused by weakening of at least one type of the non-covalent interactions (hydrogen bonds and Van der Waal's forces). Consequently, this weakening of the intrinsic molecular order of SF translates to reduction in UTS and yield points of the SF fiber. In this case, extended degumming at high temperatures was the cause of this weakening. This phenomenon was further illustrated by the SDS-PAGE analysis conducted for various degumming durations, which indicated that the 30 kDa fibroin LC was degraded with increased exposure to boiling degumming solution. The volume intensity of the 30 kDa band decreased with time, suggesting cleavage of the 30 kDa chain with prolonged degumming at boiling temperature. 30 kDa band volume intensity of the various degumming durations as a percentage to that of raw silk showed a decreasing trend from 82% for "SDS5 (100°C, MA)" to 29% for "SDS90 (100°C, MA)". Furthermore, there was a 30 kDa to 150 kDa smear for samples degummed longer than 5 min, which was likely due to degradation of the HC fibroin, which became more prominent after 5 min of boiling. This is supported by observations of Yamada *et al.* who indicated that prolonged heating beyond 5 min at 100°C degraded fibroin heavy chains [229].

In conjunction with that, it was observed from FTIR-ATR scans performed for degummed knitted silk, spectral peaks at 1655cm^{-1}, corresponding to the amide I region of the random coil structure (Silk I), were exhibited even though SF consists of mechanically viable Silk II predominantly. This indicated that during the degumming process, certain degree of SF degradation has taken place via penetration of the degumming agents into microvoids and amorphous non-crystalline region of SF's intermolecular structure [280, 281]. This is consistent with Jiang *et al.*'s results, whereby it was found that the process of degumming affects the intrinsic molecular order, which is the amount and perfection of crystallinity in SF [222]. With this disruption in the SF secondary structure, leading to an increase in the amorphous random coil regions, the tensile behavior and other physical properties of SF will be altered. Other than the deterioration of mechanical properties, one other specific physical property that could be affected is the degradation kinetics of SF. It will thus be interesting to look at the differing degrees of Silk II to Silk I shift that is contributed by different degumming conditions in the future.

Nevertheless, with the aim to prevent SF fibrillation and preserve their secondary structure, it was important to shorten the duration at which SF was exposed to boiling temperatures without compromising the efficacy of sericin removal.

One way to achieve this was the use of SDS in the degumming solution. As compared to the control group, which used a common degumming protocol involving just pure Na_2CO_3, sericin removal could be made within a shorter duration with the addition of SDS (all other factors kept constant) and hence attained mechanically more desirable SF scaffolds. "SDS30 (100°C, MA)" was sufficient for sericin removal from a

processed structure, such as the knitted form, without causing fibrillations in the SF fibers. As such there was no significant deterioration ($p>0.05$) in SF mechanical properties as compared to "SDS15 (100°C, MA)", whereby SF properties were retained. Without SDS, effective sericin removal from a knitted structure could only be achieved after 90 min of degumming (control group), by which the degummed SF already had significant mechanical deterioration, indicated by both the morphology and the tensile properties.

3.4.4.3. Effects of Mechanical Agitation during Degumming

The "SDS30 (100°C, MA)" protocol involved the use of mechanical agitation. After investigating the necessity for having mechanical agitation in Phase I, it was shown that knitted silk could not be effectively degummed in a static environment within 30 min. The purpose of including mechanical agitation during degumming was thus to promote efficient transfer of degumming solution into the core of processed silk such that sericin in the core of silk bundles could be effectively removed. In this case, knitted structure was subjected to mechanical agitation in the multidimensional form, comprising of vertical vibration and lateral solution flow motion. However, with mechanical agitation, SF was shown to have reduced mechanical properties when compared with that degummed in a static environment for the same duration. This could be attributed to the increased penetration and exposure of SF to hydrolytic degraders such as SDS and water, which acted as plasticisers [221] and attacked the amorphous regions to disrupt the inter- and intra-molecular hydrogen bonding. As a result, there was increased probability for relative protein chain segment displacements, leading to stress relaxation and subsequent drop in tensile properties. Although the effects of

mechanical agitation and inclusion of SDS into degumming solution were as such, they were necessary for removal of sericin within a short duration. Otherwise, prolonged degumming would be required, leading to a general decline in mechanical integrity. In other words, one can do without mechanical agitation and increase degumming duration to achieve SF clear of sericin, but this will lead to an even greater depreciation in tensile properties than that contributed by mechanical agitation done at shorter duration. This was apparent based on two observations. One was from the SEM image for "SDS30 (100°C, Static)", which showed that sericin removal was sub-optimal as compared to that for "SDS30 (100°C, MA)". The other was from the tensile properties of "SDS60 (100°C, Static)", which exemplified a significant decline ($p<0.05$) when compared to the "SDS30 (100°C, MA)" group.

3.4.4.4. Effects of Thermal Conditions during Degumming

Phase II was set for investigation as degumming at lower temperatures was thought to aid in preserving SF structure. It was believed that with lower temperatures, hydrolytic degradation of the fibroin would be limited. However, though this might be the case, as shown by the absence of fibrillations in the SEM images, the efficacy of sericin removal was undermined as remnant sericin was observed in samples that were degummed at lower temperatures (60°C and 75°C), even in those which were degummed over longer durations (>60 min). It should also be noted that there was mechanical deterioration after prolonged duration (>30 min) even when degumming was conducted at lower thermal conditions. Therefore, a feasible strategy would be to conduct alkaline degumming at high temperatures but within short duration to both

effectively remove sericin and preserve the structural morphology of the SF protein, which would affect its physical and mechanical properties.

3.4.4.5. Effects of Refreshing Degumming Solution

In the attempt to further shorten the degumming duration, a change of fresh degumming solution in the process of degumming was envisaged and investigated in Phase III. This was thought to shorten degumming duration as it was observed that in the course of degumming, sericin was often removed at an accelerated rate initially, which gradually reduced over time. This was indicated by a rapid change in degumming solution color, contributed by the leeched sericin, at the initial degumming stage. Hence the step to refresh degumming solution at the midpoint of the degumming process was initially thought of to create greater diffusion gradient for remnant sericin to leech out into the solution system after the sericin bulk was removed. Nevertheless, as indicated by the SEM images, sericin could not be removed when degumming was performed for 15 min (with and without refreshment of solution). On the other hand, fibrillation of the SF occurred in the "SDS15+15 (100°C, MA)" samples, while no fibrillation was observed in the "SDS30 (100°C, MA)" samples. It was thus hypothesized that with the degumming solution refreshed midway through degumming, there was increased hydrolytic degradation at the non covalent bonds of fibroin. This was due to the introduction of fresh SDS that not only bound remnant sericin, but also bound the main fibroin protein chain and denatured fibroin, leading to the fibrillation observed. Moreover, the presence of sericin in degumming solution could act to protect fibroin from hydrolytic attack by binding to the existing SDS. Hence a change in the sericin-rich degumming solution would lead to fibroin fibrillation caused by the fresh solution.

Upon determining the optimal parameters via a systematic optimization process involving the first three phases, "SDS30 (100°C, MA)" was selected as optimal and assessed for its construct mechanical properties, sericin removal efficiency using a fractionation method with SDS-PAGE analysis and examine the effect of SF protein conformational modification on SF mechanical properties.

3.4.4.6. Effects of Post-Degumming SF Protein Structural Modification

In the attempt to improve the physical properties, especially the tensile properties, of SF after degumming, methanol was used to induce crystallization of SF molecules and to transform random coils to β-sheets. This was based on the hypothesis that through the degumming process, certain degree of SF degradation had taken place via penetration of the degumming agents into microvoids and amorphous non-crystalline region of SF's intermolecular structure [280, 281]. With this disruption in the SF secondary structure, leading to an increase in the amorphous random coil regions, the tensile behavior and physical properties of SF would be altered. This was consistent with Jiang *et al.*'s results, whereby it was found that the process of degumming affected the intrinsic molecular order, that was, the amount and perfection of crystallinity in SF [222]. Crystallization of SF molecules was thus performed via immersion of degummed SF in methanol. The mechanism was proposed as that methanol, due to its polar properties, could attract water from SF molecules and induced swelling and weakening of the hydrogen bonds [196, 282, 283]. With the main chain SF acquiring mobility, the energetically favorable aggregation of hydrophobic amino acids, such as Ala and Gly,

was promoted. As the Gly-Ala sequence existed as unit dimension of the SF crystal structure, methanol could thus induce stable β-sheet crystallization of SF. As such, methanol treatment was performed post-degumming to induce structural modification of SF and increased SF crystallinity, which would have a direct relationship to the tensile properties of SF [220, 221].

To verify this conformational transition and determine the crystalline index of degummed SF, prior and post methanol treatment, a FTIR-ATR analysis was performed. This method was chosen due to its relative ease of use in determining the secondary structure of peptides and proteins. Protein conformation was determined from specific spectral regions, which arose from coupled and uncoupled stretching and bending modes of amide bonds. These specific spectral regions were most sensitive to changes due to secondary structure folding and had been identified as the amide I (1700-1600 cm^{-1}) and amide III (1350-1200 cm^{-1}) spectral bands, which corresponded to predominantly C=O and in-phase combination of N-H in-plane bending and C-N stretching vibrations respectively [284]. Although the intensity of amide II (1600-1450 cm^{-1}) region due to C-N stretching was relatively strong, it was not as sensitive to changes in protein secondary structure as compared to the other two spectral regions. This was especially so as amide II bands overlapped with bands due to amino acid side chain vibrations [285]. Between amide I and amide III bands, the signal of amide III seemed to be more reliable in estimating protein secondary structure as it was not affected by water interference, whereas amide I band overlapped that for water, which exhibited strong absorption in the range of 1640-1650cm^{-1}. As such, the crystalline index at amide III was determined as a quantitative assessment of the degree of β-

conformational transition of SF upon methanol treatment. This was shown to be increased for degummed "SDS30 (100°C)" SF sample after methanol treatment was performed, indicating that there was an increase in β-sheet formation due to the treatment.

However, from the tensile tests performed, no significant improvement of mechanical properties was observed for methanol treated "SDS30 (100°C)" SF sample. The reason for the increased crystallinity not translating to improved tensile properties could be attributed to structural imperfection in SF as a result of the degumming process. In other words, the process of degumming would likely induce a certain degree of structural imperfections and defects via several agents such as heat and hydrolytic degraders, the effect of which superseded the increased crystallinity in SF. Nevertheless, the increase in β-sheet formation after methanol treatment could possibly prolong its degradation period *in vivo* and therefore affect the implant life of SF scaffolds using the "SDS30 (100°C)" degumming conditions. Further investigations will be required to verify this hypothesis.

3.4.4.7. Sericin Removal Efficiency

From the SEM images obtained, sericin was observed to be removed from "SDS30 (100°C, MA)" samples. Particularly, smooth SF fibers were observed. Ethanol fractionation of the "SDS30 (100°C, MA)" and "SER" samples further illustrated that sericin was effectively removed, with approximately 90% of total sericin present in the raw silk sample removed. Fractionation of silk proteins was introduced by Takasu *et al.* for the purpose of isolation of various sericin components [277]. They had added similar

concentrations of ethanol as those used in this study to obtain the respective peptides. However, in this study, we adopted the method for the purpose of assessing sericin presence in our degummed SF samples.

The rationale for adopting the ethanol fractionation method to determine sericin removal efficacy lies in the observation that sericin and heavy-chain fibroin have very close molecular weights, making it challenging to ascertain sericin removal from the degummed samples using SDS-PAGE analysis. When raw silk was analyzed using SDS-PAGE, smears and bands were exhibited at ~250 kDa and 25 kDa respectively, of which the smears indicated mixture of sericin and heavy-chain (HC) fibroin, while the band indicated light-chain (LC) fibroin components. It was noted that the smears larger than 150 kDa were attributed by both sericin (20 kDa – 350 kDa) and HC fibroin (~325 kDa). Typically when degummed SF was analyzed using SDS-PAGE, the volume intensity of the 150 kDa to 350 kDa smear reduces with increase in degumming duration. This could be attributed to either a gradual reduction in sericin content, or degradation of HC fibroin with extended degumming. Consequently, further purification methods would be necessary to ascertain removal of sericin for the "SDS30 (100°C, MA)" group, which had been observed to have sericin effectively removed via SEM while having its mechanical properties preserved. In this study, the ethanol fractionation method was used to serve this purpose. Silk protein fractionation was performed and by comparing ethanol fractionation concentrations used to isolate sericin, HC fibroin could be distinguished from sericin. This method thus allowed analysis on the presence and deduced the amount of sericin remaining in the "SDS30 (100°C, MA)" sample group.

Having quantified the amount of sericin removed from raw silk using an optimized set of parameters tailored to retain the SF mechanical properties, the next question would then be whether this efficiency of sericin removal was sufficient for tissue engineering purposes. From animal and clinical studies performed using raw/virgin silk, it was clear that sericin proteins, when associated with native SF fibers, would induce immune response as previously presented [207-215]. In support of this, Panilaitis *et al.* were able to show that there was strong macrophage response to lipopolysaccharide (LPS), as induced by sericin coated SF fibers [286]. This was not observed in sericin-coated tissue culture plates or with soluble sericin, even at high concentrations of sericin, illustrating the need for a physical association with SF for sericin induced immunological response to occur. The underlying mechanisms, as proposed, was that macrophages could adhere better onto sericin-coated fibers or that there was a conformational conversion of sericin when it was bound to SF, which in turn induced macrophageal responses. It was interesting to note that other studies have shown that extracted sericin, when not in association with SF, supported and increased cell attachment and proliferation instead [287, 288]. Specifically, sericin-S (MW 5-100 kDa) had been shown to be superior in its mitogenic effect as compared to other sericin types and was used as cell culture supplement to accelerate cell proliferation.

When sericin was removed via a degumming process, the remaining SF had been shown to be suitable for use in a variety of biomedical and tissue engineering applications [3, 13, 21, 27, 28, 195-197, 199]. Upon the removal of sericin, macrophages were no longer activated by the SF fibers as phagocytosis of these large fibers was not possible. Even if phagocytosis was to occur, it was expected to occur at

lower degrees, limited to only the surfaces. In fact, it was observed that SF fibers did not induce significant up-regulation in transcript levels from a wide range of pro-inflammatory cytokines when cultured with macrophages [286]. Santin *et al.* had also compared the inflammatory potential of degummed SF to that of polystyrene and poly (2-hydroxyethyl methacrylate), showing that there was less adhesion of immuno-competent cells to SF [289].

However, it was not clear in current literature whether there was any correlation in the amount of SF associated sericin with the degree of macrophageal response induced. Although it might seem to be ideal to have sericin-free SF scaffolds to prevent any occurrence of hypersensitivity problems, it might not be practically necessary. In fact, most of the current silk scaffold related studies utilized alkaline degumming protocols with little quantitative substantiation on the degree of sericin removed [3, 13, 27, 195-197]. Although qualitatively, SEM images showed smooth fibers of SF similar to that observed in this study for "SDS30 (100°C, MA)", it was quantitatively unclear if there were any sericin remnants in their scaffolds. Even though this might be the case, many of these *in vivo* works reported little or no extensive hypersensitive issues. Amongst the *in vivo* studies conducted by our group (published and unpublished), similarly degummed silk scaffolds did not caused irrevocable hypersensitivity issues [3, 197]. Although some level of foreign body response would arise upon implantation of SF scaffolds as with other non-autologous materials, long term T-cell mediated hypersensitivity immune response due to sericin was not observed in these studies. SF derived after treating using the "SDS30 (100°C, MA)" was thus considered effectively degummed when compared with these studies. However, the lack of studies done on

correlation between the amounts of sericin remaining in degummed silk and the level of corresponding hypersensitivity evoked persist as a valid concern for possible future study.

3.5. Concluding Remarks

The focus of this chapter lies in the design and development of the SF knitted structure. The SF mechanical properties were first determined, which shed light into the mechanical attributes of the material. This was essential in the design of the SF knit and to determine the appropriate number of SF filaments to be used for a robust scaffold structure used for ACL replacement in a rabbit model. Upon determining the suitable SF filament count, it was essential to investigate the degumming factors that might influence the mechanical performance of the degummed SF knit. Of the factors investigated, degumming duration played a key role in influencing the mechanical and morphological outcome of degummed SF. Having considered and balanced the effectiveness of sericin removal with the retention of mechanical and structural properties, degumming of knitted silk was found to be optimal when performed using the "SDS30 (100°C)" protocol in the presence of mechanical agitation. Although the design process discussed herein revolved around the rabbit model due to the use of rabbit MSCs for seeding, the process could be translated readily for clinical applications by upscaling the number of yarns of SF and increasing the scaffold dimensions to cater to increased loading. SF knits designed for clinical applications using this method and seeded with human MSCs would thus have potential for functional tissue engineered ligament applications.

Chapter 4

DEVELOPMENT AND CHARACTERIZATION OF THE MECHANO-ACTIVE HYBRID SILK FIBROIN SCAFFOLD

4.1. Introduction

The mechano-active hybrid SF scaffold consisted of the main knitted SF that was designed to undertake the bulk physiological load during the early tissue development stages, and the AL-SFEF meshes that were integrated to facilitate cell seeding and hypothesized to provide topographical cues to stimulate positive tenogenic differentiation. With mechanical stimulation, the AL-SFEF meshes were hypothesized to provide more effective stimulation of the seeded cells, thereby synergistically work with the dynamic culture conditions to promote enhanced and accelerated tenogenic differentiation.

In this chapter, the AL scaffold would be fully characterized prior to evaluating its feasibility *in vitro* for application in ligament tissue engineering. To further exploit the advantageous topography of the AL scaffold, other than static culture of the MSC-seeded scaffold, the seeded scaffold was also used for dynamic culture to explore the synergistic effect of cues from both mechanical stimulation and topography. In these *in vitro* evaluations, the MSCs cultured in tissue culture polystyrene (TCP) was used as control to contrast the effects of 3D culture, rendered by the AL scaffold, on MSCs proliferation and differentiation. RD scaffold was also used to compare with the AL scaffold to exemplify the positive effects offered by the aligned topography of the AL scaffold in both static and dynamic culture conditions.

4.2. Materials and Methods

4.2.1. Fabrication of Hybrid SF Scaffolds

Raw *Bombyx mori* silk fibers (3 yarns) were used to fabricate the knitted structure as described in section 3.4.2.1. For the group of scaffolds to be used for dynamic culture, 60 × 20 mm silk knits were fabricated, while the dimension of 40 × 20 mm remained for the group used for static culture. The extra 20 mm length was to cater for attachment in the standalone bioreactor chamber. All the raw silk knits were then degummed using the optimized degumming protocol as described in section 3.4.

In order to close up the pores of the knitted structure to facilitate cell seeding, SFEF meshes with ultra-fine fibers were used to coat both sides of the SF knits to form the hybrid SF scaffold, as shown in Figure 4-1. These SFEF meshes would not only aid to provide more effective cell seeding but also provided topographical cues for subsequent ligament tissue development.

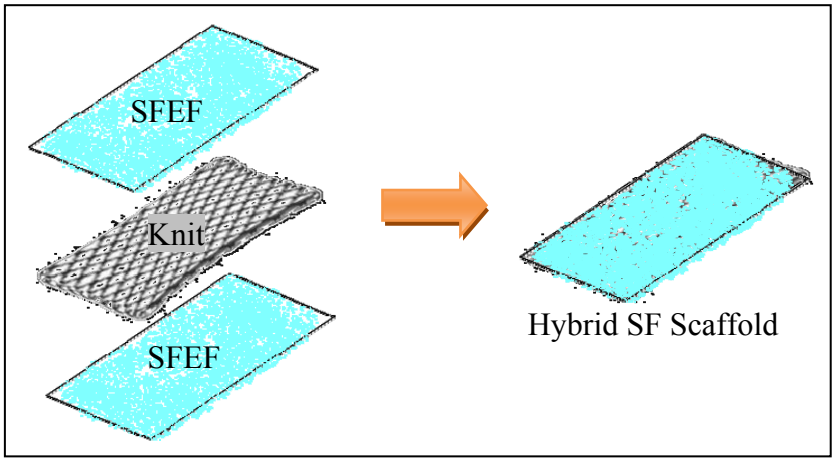

Figure 4-1: Schematic showing the process of integrating SFEF meshes to the knitted SF to produce the hybrid SF scaffold.

To fabricate SFEF meshes, electrospinnable SF solution was first obtained from a series of steps involving an initial dissolution of dried SF in saturated lithiumthiocyanate (LiSCN, 250 %w/v, Sigma-Aldrich, St. Louis, USA) to a final SF concentration of 20 %w/v. Upon full dissolution, any undissolved SF or particle impurities were removed by centrifugation at 3000rpm for 10 min. The supernatant obtained was dialyzed for 3 days against distilled water using Snakeskin™ pleated dialysis tubing (10,000 MWCO, Thermo Fisher Scientific Inc., MA, USA). The dialyzed aqueous SF solution was then lyophilized to obtain regenerated SF sponge. The SF sponge was then dissolved in 1,1,1,3,3,3-hexafluoro-2-propanol (HFIP, Fluka, Sigma-Aldrich, St. Louis, USA) at 9.5%w/v to obtain the electrospinnable SF solution. This SF solution would then be ready for use to electrospin two types of SFEF meshes: aligned fibers (AL-SFEFs) and randomly-arranged fibers (RD-SFEFs).

A closer look at the process of electrospinning reveals that it is a manufacturing method, which involves the formation of ultra-fine fibers of sub-micron diameters via an electrostatic technique. In brief, the phenomenon was attributed to the application of a strong electric field between a polymer solution (SF solution in this case) and a metallic surface on which the fiber was collected. This is illustrated in the schematic for the electrospin setup to obtain RD-SFEFs in Figure 4-2.

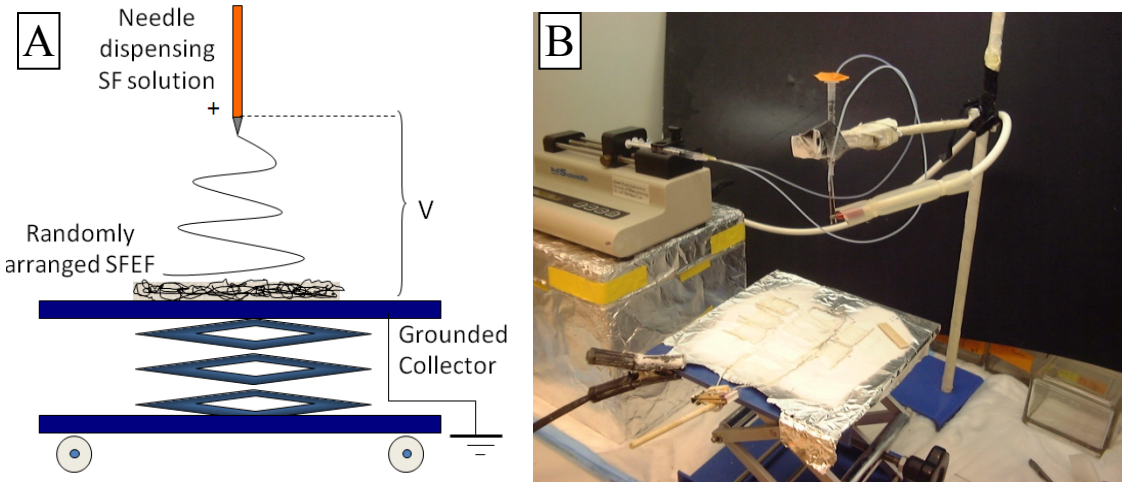

Figure 4-2: (A) Schematic of electrospin setup for RD-SFEFs and (B) actual electrospin setup to produce RD-SFEFs. V: vertical distance between the spinneret and the collector.

Typically, the metallic capillary tip which dispensed the SF solution was charged positively while the metallic collection screen was charged negatively or grounded. Upon adjustment to a critical potential difference between the two ends, the pendant droplet or Taylor cone of polymer solution formed at the tip would gain enough charges to overcome its surface tension, producing a jet. This electrically charged jet would be stretched and narrowed in diameter under electrohydrodynamic forces [290]. Further narrowing could be attributed to certain operating conditions, when the moving jet would experience a series of electrically induced bending instabilities, leading to extensive stretching of the jet. The diameter of the jet was further reduced by the rapid evaporation of solvent. Upon collection of these jets, a nonwoven mesh of RD-SFEFs, with diameters ranging from nanometers to micrometers, could be formed using this conventional electrospin setup. Certain parameters or variables could affect the morphology and size of the fibers. For example, the charge density and the SF solution concentration could alter the fiber diameter to a certain extent. On the other hand, the

thickness of the deposited mesh depended on the duration of the electrospin process [291]. Other important variables included polymer feed rate, pendant drop-collector distance, solution viscosity and polymer molecular weight [292].

Modifications to the conventional electrospin setup were made to produce AL-SFEFs. Essentially, a customized rotational electrospin setup involving a combination of positive electric field plates and a rotating collector device was made (Figure 4-3 and 4-4). Using such a setup, the path of the polymer jet was restricted by the positive electric field plates, such that highly aligned SFEFs could be obtained on the grounded rotating frame (800 rpm) comprising of 2 parallel steel rods. The spinneret needle was placed at an angle from the axis of the rotating frame with horizontal (H) and vertical (V) distances optimized (Figure 4-3A) to achieve smooth collection of aligned SF fibers and prevent stray SF droplets from damaging the collected fibers. The spinneret needle tip was also constantly cleaned with an insulator while electrospinning, as accumulation of dried polymer pendant at the tip would disrupt steady flow and force a circumventing trajectory.

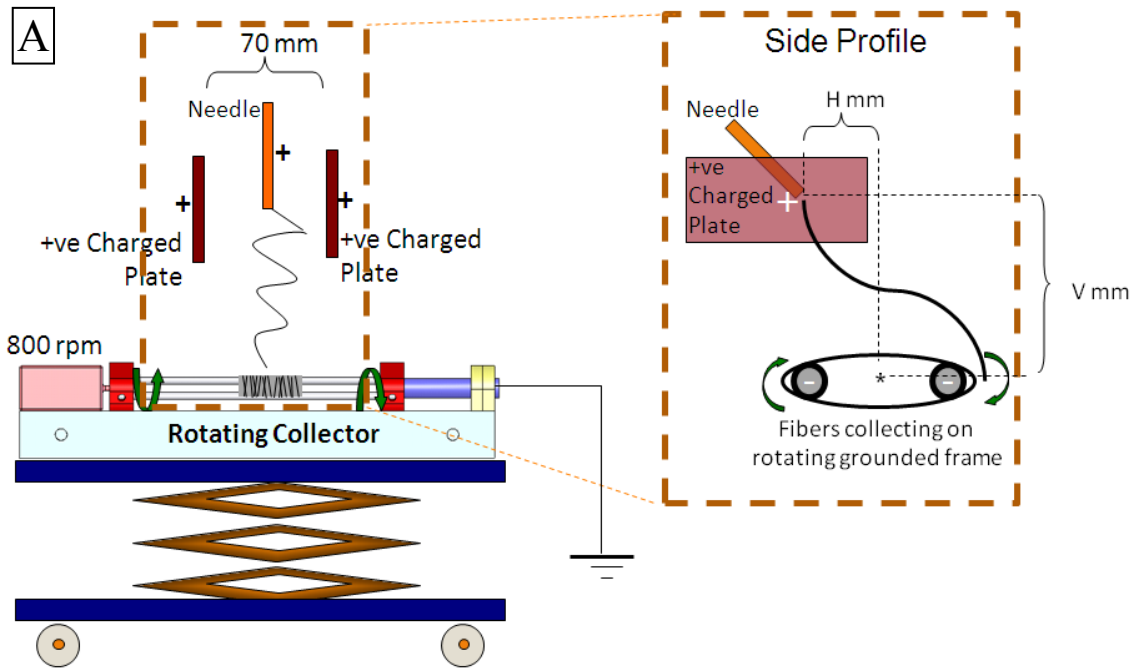

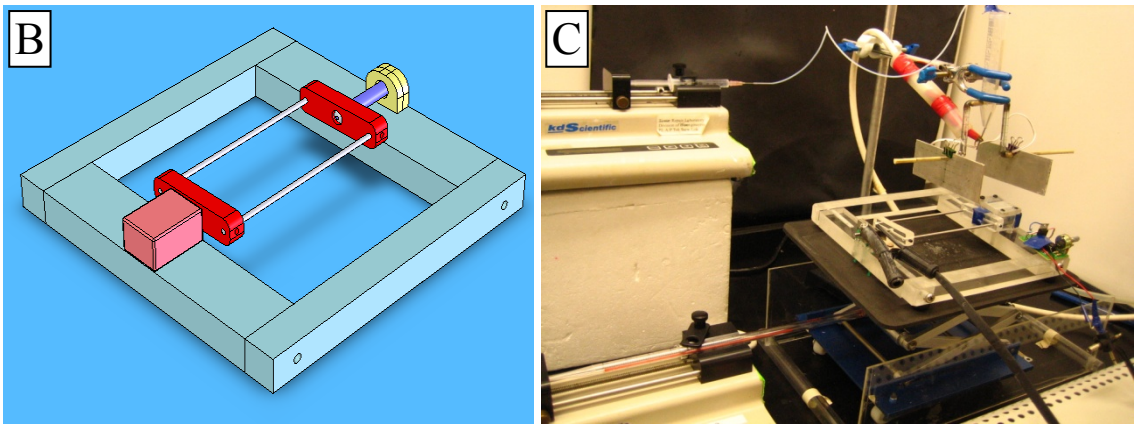

Figure 4-3: (A) Schematic of electrospin setup for AL-SFEFs with the front and side profiles, (B) using a customized rotating frame attachment to the existing conventional electrospin setup. (C) Actual electrospin setup to produce AL-SFEFs.

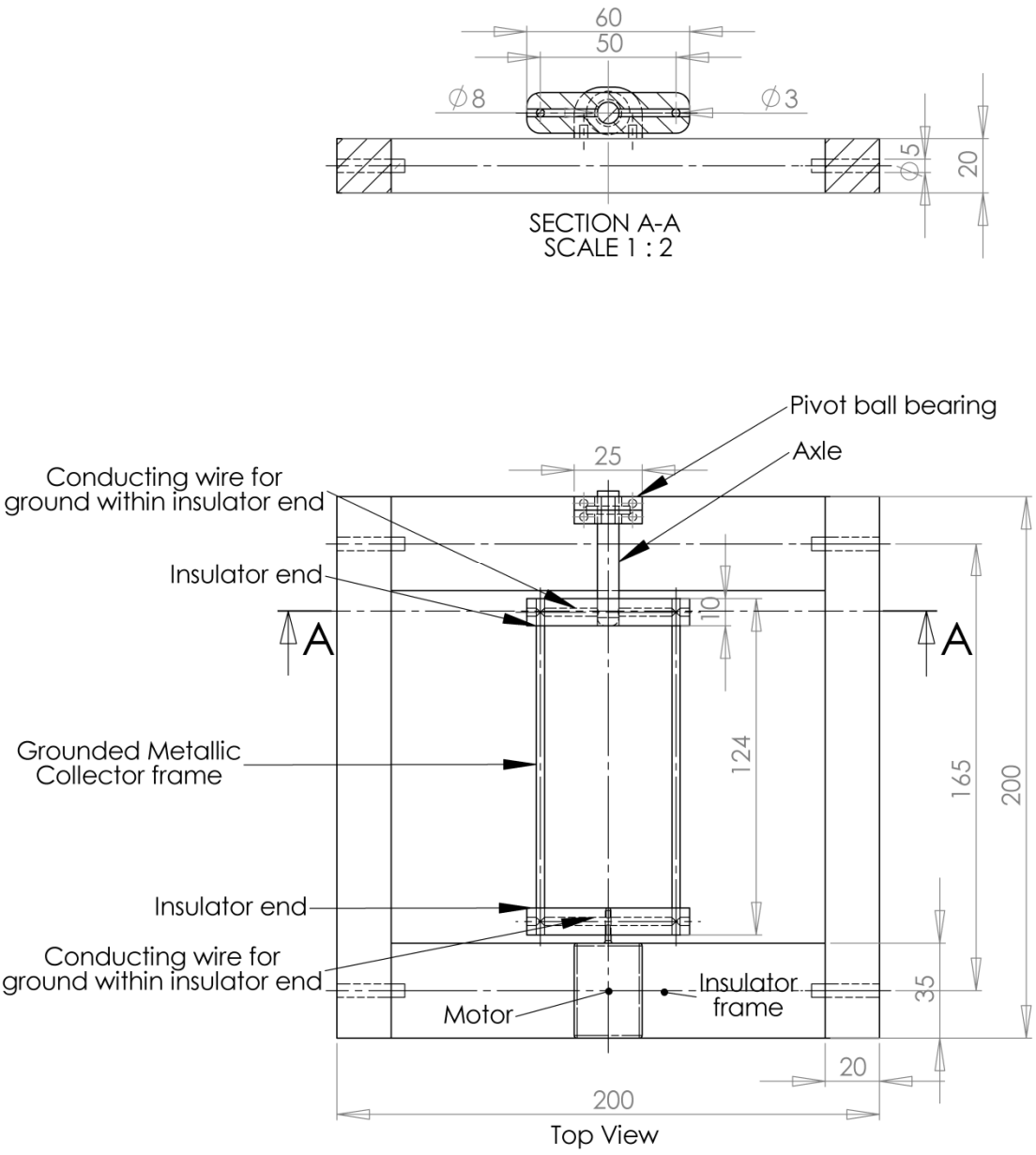

Figure 4-4: Detailed technical drawing of the rotating frame attachment. Dimensions in mm.

The parameters at which the two types of SFEF meshes were collected were collated in the following Table 4-1.

Table 4-1: Electrospinning operating parameters.

Operating parameter	RD-SFEFs	AL-SFEFs
Flow rate (ml/hr)	1.3-1.5	1.3-1.5
Voltage (kV)	9-11	9-11
Spinneret tip diameter	16.5 G	16.5 G
Positive plate distance apart (mm)	NA	70
Collector frame rotating speed (rpm)	NA	800
Vertical distance, V (mm)	150	100
Horizontal distance, H (mm)	NA	45
Temperature (°C)	25	25
Collection duration per layer (min)	5	5
Number of layers per complete mesh	2	6
Mass of complete mesh (mg)	10-12	10-12

To minimize large angular deviations caused by electrical repulsion and isotropic deposition, AL-SFEFs were collected at regular short intervals (5 min) onto a glass slide and amassed to the desired amount as standardized by final mass (~12 mg). Similarly, the RD-SFEFs collected from the grounded metallic collector were amassed to a comparable mass of ~12 mg. The two groups of SFEF meshes were collected on 44 x 22 mm glass slides.

Subsequently, the meshes were integrated with the degummed SF knits to produce the complete hybrid SF scaffolds. To produce aligned hybrid scaffolds (AL), two pieces of AL-SFEF meshes were obtained by gently peeling them off from their respective glass slides and laid flatly on both sides of a degummed SF knit, taking note that the SFEFs' alignment direction was in line with the longitudinal axis of the knit (Fig. 4-5A). Methanol treatment was performed next to allow crystallization and insolubilization of SFEF meshes by transforming amorphous Silk I into regular β-sheet secondary structures of Silk II [28, 30, 199]. As SFEFs have been reported to form a denser structure by methanol treatment [30], it was exploited to allow the contracting SFEF meshes bind the knitted SF. A two step process was used to securely bind SFEF meshes onto the knitted SF. The first step involved applying methanol selectively to the borders where the two layers of SFEF meshes overlapped (Figure 4-5A) to generate localized wetting and contraction, which formed a tight seal between contacting SFEFs at the edges (Figure 4-5B). Such boundary contraction further tensioned the meshes over the knit, forming a well integrated structure. The hybrid scaffolds were dried before proceeding to the second step, whereby the whole hybrid scaffolds were immersed in methanol for 30 minutes under vacuum to promote further integration of the meshes into the SF knit. The completely treated hybrid aligned scaffold is as shown in Figure 4-5C. Hybrid scaffolds with RD-SFEFs (RD) were produced similarly as in the described steps for AL scaffolds but with the use of RD-SFEF meshes instead.

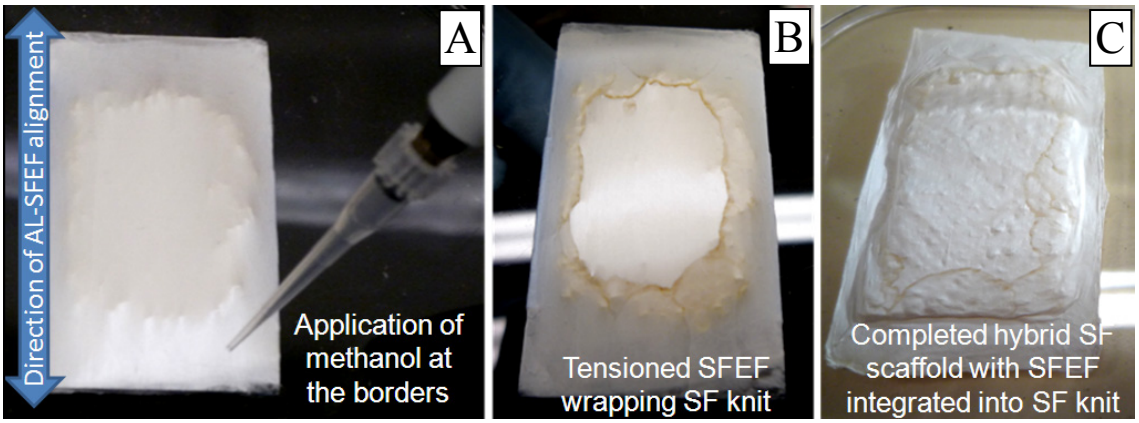

Figure 4-5: The process of SFEF integration with SF knit, (A) by first sandwiching knitted SF between 2 layers of SFEF noting direction of alignment for AL-SFEF and applying methanol to the SFEF borders. (B) Contracting SFEF at the borders will allow tensioned wrapping of SFEF with knit. (C) Hybrid SF scaffold is completed after overall methanol treatment under vacuum.

Prior to cell seeding, the hybrid scaffolds were sterilized by means of formaldehyde (37%) (Mallinckrodt Baker, Inc., NJ, USA) gassing for 24 h. All other sterile equipment was sterilized by steam autoclaving.

4.2.2. Scaffold Characterization

The general morphology of the hybrid scaffolds was observed and determined via phase contrast microscopy (IX71 Inverted Research Microscope, Olympus, Japan). Scanning electron microscopy (SEM) was conducted to observe the surface morphology of the knitted SF post-degumming and the hybrid scaffolds. Samples were gold-sputtered prior to observation in a SEM (JEOL Ltd, JSM-5600 LV, Japan). Plain knitted SF were observed after the degumming process for presence of sericin remnants to ascertain sericin removal, while the hybrid scaffolds were observed for the integration of the SFEFs with the knit and to determine the diameter and directional distribution of the SFEFs (RD-SFEF and AL-SFEF) using image analysis software (ImageJ 1.38x, Wayne Rasband, NIH, USA). Electrospun fiber diameters (300 sampling points) and the

angular deviation (AD, 500 sampling points) were determined independently for both the RD-SFEFs and the AL-SFEFs. For AD analysis, fiber orientations were referenced from a defined vertical direction (0°) and ranged from -90° to 90° referencing from the vertical datum. The AD value was then calculated from the angular measurements of fiber orientation using circular statistics as described by Fisher [293]. MATLAB (ver. 6.5 Mathworks Inc., Natick, MA, USA) was used to implement the circular statistics algorithms [294].

FTIR-ATR was performed to determine the secondary structure of SF at different processing stages and verify any conformational changes in the SFEFs as compared to the original degummed SF. Three samples: degummed SF, methanol treated SFEF mesh and hybrid SF scaffold were tested to obtain FTIR-ATR spectra in the spectral region of 1000-2000 cm^{-1} using materials and methods detailed in section 3.4.2.6.

Mechanical tests were conducted on the different scaffold types (RD and AL) with the knitted SF acting as control (n=5 for each group) using materials and methods described in section 3.4.2.4. From the tensile load and elongation recorded, the failure load or ultimate tensile load, stiffness, extension at failure load and extent of toe region were determined.

4.2.3. Isolation and Culture of MSCs

MSCs were generated from bone marrow aspirates of New Zealand White (NZW) rabbits based on a protocol approved by the Institutional Animal Care and Use Committee, National University of Singapore, using the techniques as reported [237]. Briefly, bone marrow was aspirated from the iliac crest of anesthetized (12 weeks old,

2.5–3.0 kg) NZW rabbits and collected into polypropylene tubes containing preservative-free heparin (1000 units/mL). The bone marrow was then diluted in an equal volume of culture medium containing Dulbecco's Modified Eagle Medium (DMEM) with low glucose (Gibco, Invitrogen, Carlsbad, CA, USA), L-glutamine, 110 mg/L Na-Pyruvate, Pyridoxine HCl (GIBCO, Invitrogen Corporation, CA, USA), 15% fetal bovine serum (FBS) (HyClone Logan, Utah, USA) and penicillin–streptomycin (100 U/mL) (GIBCO, Invitrogen Corporation, CA, USA), and plated into culture flasks. Mononuclear MSCs were selected by means of their short-term adherence to tissue culture polystyrene, on incubation at 37°C with 5% humidified CO_2. After 72 h, non-adherent cells were discarded by medium change and adherent cells cultured, changing the medium every 3 days. When culture flasks became 70-80% confluent after about 7 days, the adherent cells were detached using 0.05% trypsin (GIBCO, Invitrogen Corporation, CA, USA) and serially sub-cultured. A homogenous MSC population was obtained after 2 weeks of culture and MSCs (P3) were harvested for further use in seeding onto the respective hybrid SF scaffolds and TCP negative control.

4.2.4. Standalone Bioreactor for Dynamic Culture

The purpose of the standalone bioreactor was to provide mechanical stimulation to the seeded hybrid scaffold constructs, while maintaining optimal environmental conditions to sustain cell viability and promote tissue development. To achieve this, the tissue chamber and medium contacting components of the bioreactor system was made of biocompatible and sterilizable materials. It was also able to provide metabolite transport through active medium flow and maintain environmental conditions by constantly monitoring and moderating these conditions through a feedback system.

Multidimensional strain could also be provided through a computer system, which allowed modifications in the mechanical stimulation parameters to be made. This setup could thus provide means for extensive study of the physical and chemical outcomes of providing different mechanical cues and allow optimization to accomplish the conditions suitable for ligament regeneration.

The advanced bioreactor system consisted of several essential components, which could be categorized into two groups: the environmental control system and the multidimensional strain control system. The environmental control system consisted of specific components such as the peristaltic pump, the gas diffusion chamber, the medium conditioning water bath and the medium reservoirs, while the multidimensional strain control system consisted of the bioreactor vessels stand, the chamber vessels and the motors to provide tensional and torsional strains (Figure 4-6).

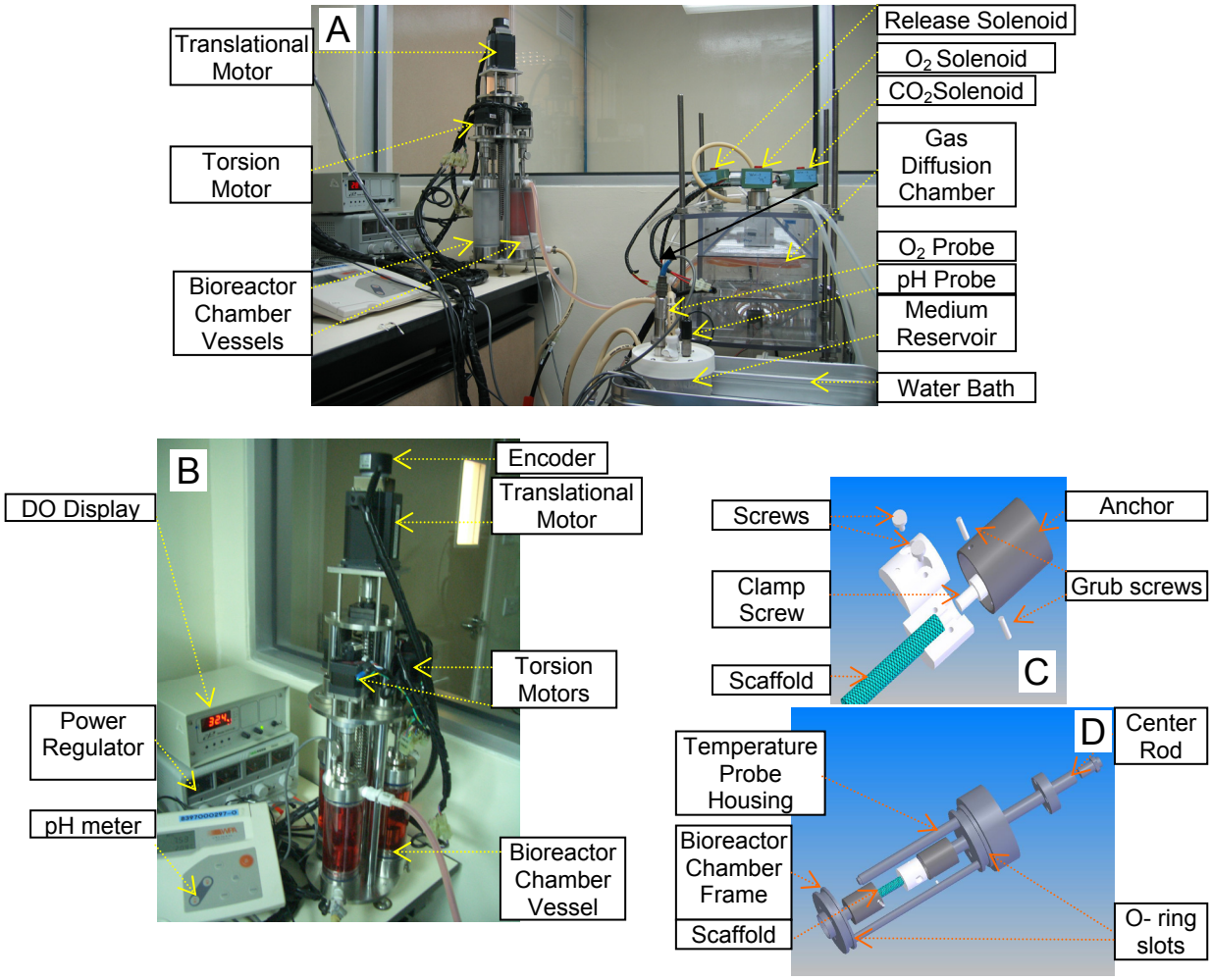

Figure 4-6: (A) Standalone bioreactor system setup. (B) Bioreactor vessels stand. (C) Mechanism and components of scaffold clamps within the bioreactor chambers. (D) Clamping mechanism affixed onto the bioreactor chamber frame.

4.2.4.1. Environmental Control System

One of the limitations of the current bioreactor system is that they require the setup to be situated in incubators [295, 296]. This takes up much space and provisions have to be made to electrically connect the monitoring setup from outside of the incubator to the bioreactor inside. pH and oxygen levels measured are also not real-time measurements taken of the medium but are monitored indirectly through the incubators instead. As such, end users are not able to monitor minute changes in medium

conditions. Moreover, current setups do not facilitate easy transportability and cannot be observed by the end users readily since it is situated within the incubator. As such, our research group had designed and constructed this standalone bioreactor system with the aim of providing the required environmental conditions independently, which was capable of providing feedback action and monitoring of the critical environmental parameters.

Figure 4-7 shows an overall schematic of the bioreactor setup. Medium from the reservoir would flow to the heat transfer tubes in the water bath, through which the medium inside could be heated up effectively due to increased surface area. Temperature of the water bath was monitored and feedback heating was provided to maintain the optimal medium temperature (37 °C). A peristaltic pump was placed after the water bath to generate flow within the tubes without contacting the medium. Medium then entered vessel chamber from below and filled it up before leaving through the top. The medium next entered the gas diffusion chamber to receive oxygen (O_2) and carbon dioxide (CO_2) before being returned to the reservoir.

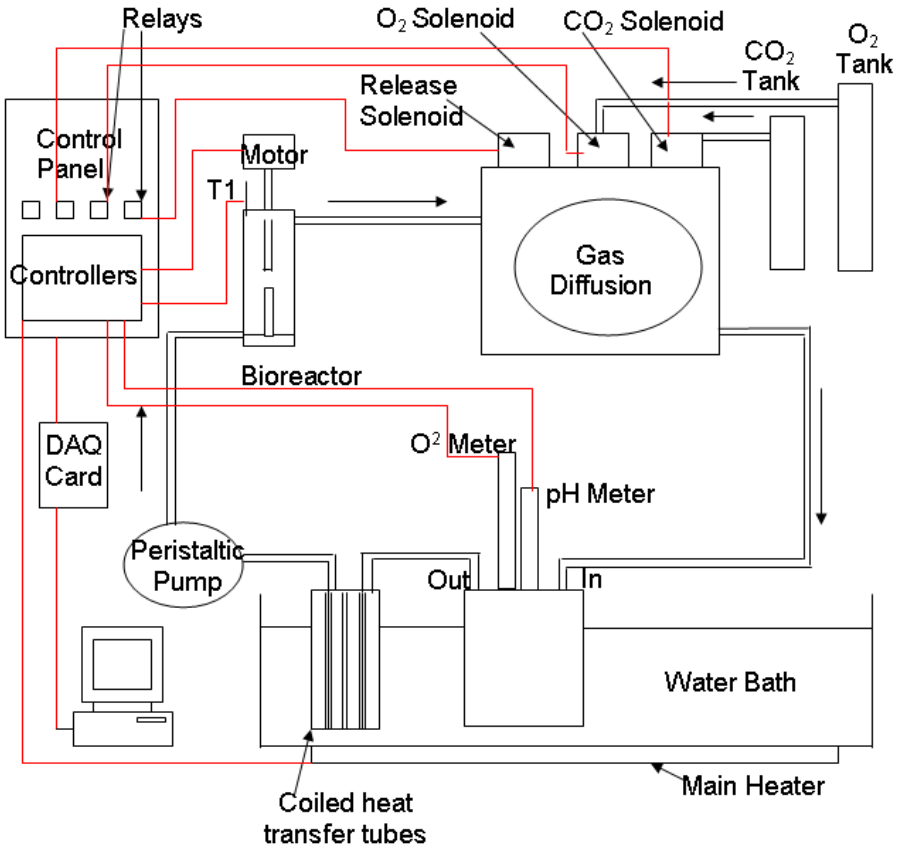

Figure 4-7: Schematic diagram of the bioreactor system.

The gas diffusion chamber served the function of conditioning medium with the optimal O_2 and CO_2 concentration, which would affect the pH value of the circulating culture medium. The optimal dissolved oxygen concentration (DO) and pH determined was 30% saturation and 7.4 respectively [297]. Through the sensor and feedback control of the environment control system, these values were maintained through the dynamic culture of the seeded hybrid scaffolds. Structurally, the chamber was fabricated with polycarbonate and had the capacity to hold three coils of silicone diffusion tubes, one for each culture chamber vessel, which allowed gaseous exchange of the medium within

the tubes with the gases outside. A rubber layer was utilized to line the seams of the gas chamber between compartments to prevent leakage of CO_2 and O_2 from the seams. Three solenoid valves were fixed at the top of the gas diffusion chamber (Figure 4-6A). Two of them infuse CO_2 and O_2 into the chamber, while the third releases gases from within the chamber when there is excess CO_2 or O_2 inside the chamber. Therefore, the input of gas was controlled by solenoid valves, which opened or closes depending on the pH and DO values measured by the probes in the reservoir and that registered by the control software, as will be described. To minimize risk of contamination, a completely closed system was designed using joint connectors to connect tubings between the different components of the medium circuit. Medium was circulated independently in each medium circuit for each chamber. The transport tubes (MasterFlex 06485 model, IL, USA) used outside the gas chamber and the coiled diffusion tubes used inside (diffusible and platinum cured, MasterFlex Silicon 96410, IL, USA) were biocompatible, non toxic, fungus resistant and could be steam sterilized. Tube lengths were kept minimal to reduce heat loss to the surrounding.

To achieve a stable environment, sensors and actuators were used to achieve feedback control loops. Actuating durations were optimized to obtain the desired range of temperature, pH, and DO levels. A safety control mechanism was added via programming to stop system when readings exceed the limits set. Parameter inputs, data acquisition and motion control were managed mainly through Labview software (National Instruments, TX, USA). Details of the mechanism for temperature, pH and oxygen feedback control are described in Appendix C.

4.2.4.2. Multidimensional Strain Control System

The bioreactor vessel stand was the main frame structure that supported the chamber vessels, the motors and allowed conversion of rotational motion to linear motion for effecting linear strains through the central screw gear. Three chamber vessels could be affixed vertically to the stainless steel bioreactor vessel stand. To stimulate these three chambers, three motors were housed on the vessel stand to provide for torsion on the scaffolds and one central motor was used to provide for tensile strain on all scaffolds via the central screw gear.

Torsional strains (set to 90° from the rest state) were provided together with tensile strains to provide the multidimensional straining environment that mimic the physiological environment of the ACL. It was demonstrated that such straining environment could specifically direct the differentiation of MSCs towards the ligament lineage [244]. It was relevant to apply both translational and rotational strains to developing ACL tissues as the ACL has a unique helical fiber organization and structure to allow it to perform its stabilizing functions. Together with the way the ACL is attached to the bones and the need for the knee joint to rotate about 140° (extension and flexion), the physiological angle of twist resulted in the ACL is about 90° [241]. This was thus provided to the loaded SF hybrid scaffolds by the torsion motors of the bioreactor setup. Although the rotational strains alone can act to translate individual fibers organized in a helical geometry, it was necessary to provide translational strains to both control the fiber pitch angle of this helicity and also to mimic the anterior draw loads that are stabilized by the ACL.

To successfully actuate mechanical strains onto the hybrid silk scaffolds, it would be necessary to secure the scaffolds firmly in the chamber vessels first. The chamber vessels were designed to provide firm and easy fixation of scaffolds to the clamp anchors, which were in turn attached onto the chamber vessel frame. These components were designed such that there was reduction in handling and exposure time to the surrounding to minimize contamination. Moreover, since the vessel frame could be detached from the main vessel stand, loading of scaffolds could be performed within the biosafety cabinet to reduce contamination risks. High density polyethylene clamps and the stainless steel clamp screws were used to secure the scaffold in a rolled-up cylindrical form (Figure 4-6C). Since the ends of the hybrid scaffolds were used for anchorage purposes, the groups of scaffolds used for dynamic cultures were 60 mm long instead of 40 mm long in the static group. The middle 40 mm of these scaffolds were seeded, which eventually formed the gauge length between the clamps after loading in the bioreactor. Upon securely fixing the scaffold ends onto the plastic clamps, they were then inserted into the stainless steel anchors, where two stainless steel grub screws were inserted to secure the plastic clamps to the chamber vessel frame (Figure 4-6D). The chamber vessel frame was then assembled with a glass chamber and stainless steel end before loading it onto the main bioreactor vessel stand. Mechanical stimulations of scaffolds were achieved via movements of the centre rods of the chamber vessels, which were attached to the motors at the bioreactor vessel stand. The scaffolds were stretched from slack to a point when they were not observably slack, which indicated the start position of the stimulation process.

A variety of mechanical stimulation parameters could then be applied to the loaded scaffolds, depending on the stimulation profile embarked for the experimental group. These parameters (including stroke, frequency, stroke delay, stimulus duration, stimulus interval, start delay and total stimulus) could be modified and changed to generate different stimulation strains, cyclic frequency, periodic frequency and duration (Figure 4-8).

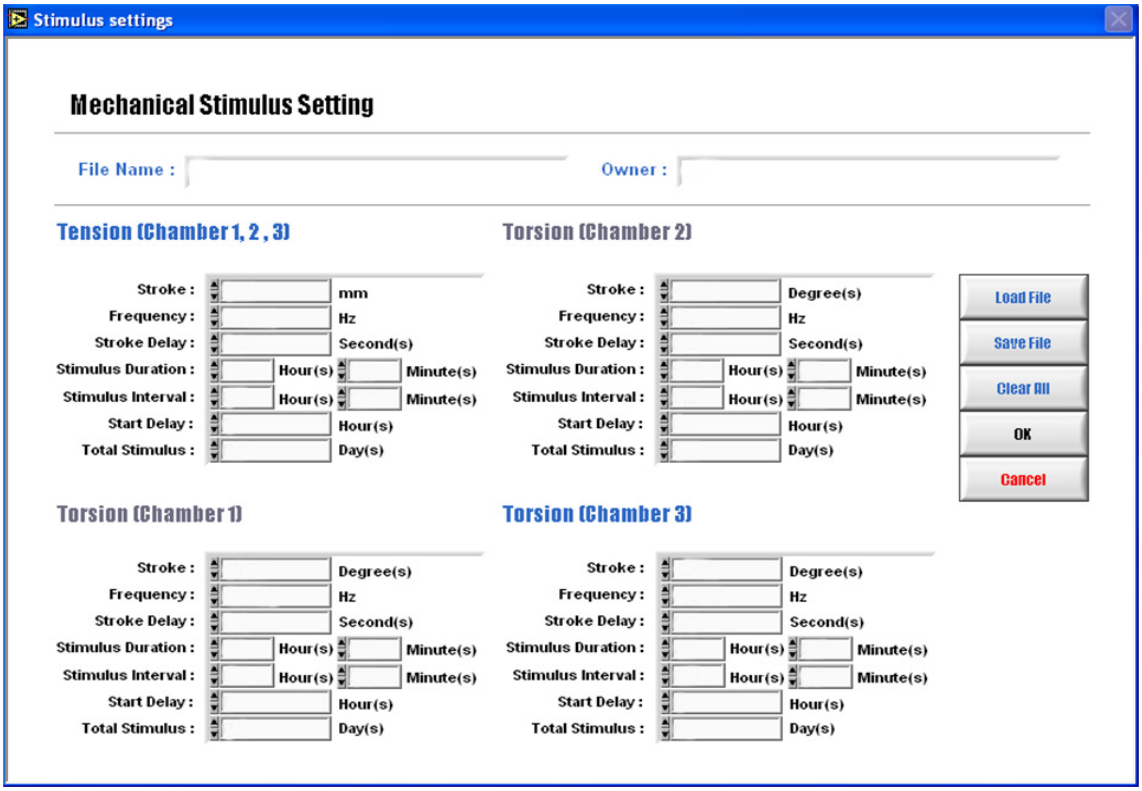

Figure 4-8: Interface for mechanical stimulus settings used in the bioreactor computer system to control mechanical cues provided to the scaffolds

4.2.5. MSC-seeded Scaffolds Cultured in Static and Dynamic Conditions

The MSCs (P3) were resuspended in complete culture medium containing DMEM with high glucose (Gibco, Invitrogen, Carlsbad, CA, USA) supplemented with 10% FBS (HyClone Logan, Utah, USA), L-glutamine (580 mg/L) and penicillin–streptomycin (100 U/mL). 1.5 x 10^6 cells were then seeded by simply pipetting onto one side of each sterile hybrid scaffold. The same amount of cells were placed into T175 TCP flasks and cultured concurrently as negative control group. The two experimental groups of hybrid scaffolds (RD and AL) were cultured in a laminar manner (Figure 4-9A) for 3 days before being rolled up with the cell-seeded surface in the inner core and secured at the ends with SF fibers (Figure 4-9B).

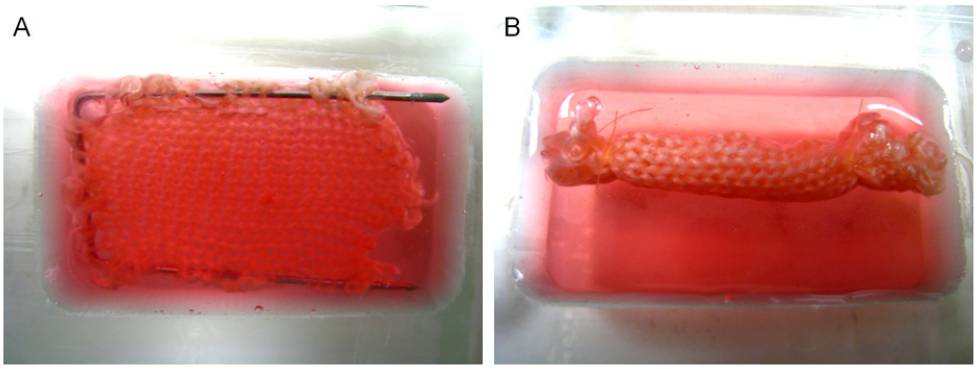

Figure 4-9: (A) MSCs-seeded hybrid SF scaffold cultured flat in a custom-made chamber for 3 days, (B) prior to rolling up into a cylindrical ligament analogue. [298]

For the group undergoing static culture, rolled-up scaffolds (RD and AL) then continued to be cultured separately in customized 6-well polycarbonate dishes for another 11 days (total experimental period of 14 days), with medium being changed twice a week.

For the group undergoing dynamic culture, rolled-up scaffolds (RD and AL) were loaded into steam-autoclaved standalone bioreactor chamber vessels. The chamber vessels were then affixed onto the bioreactor main bioreactor vessel stand (Figure 4-10), where dynamic culture conditions would be provided over the next 11 days period. Dedicated medium circulation for each chamber was provided by the environmental control system, which regulated the medium temperature, pH and DO level, to ensure that favorable culture conditions were provided to the cultured constructs. The dynamic culture conditions followed that of the "low" intensity type as identified in section 2.7.3, whereby the cyclic frequency was set at 0.1 Hz amounting to 4320 cycles per day based on a 12-hour daily activity rate. The various stimulation parameters used for the dynamic culture of hybrid scaffolds used in this part of the study are as listed in Table 4-2.

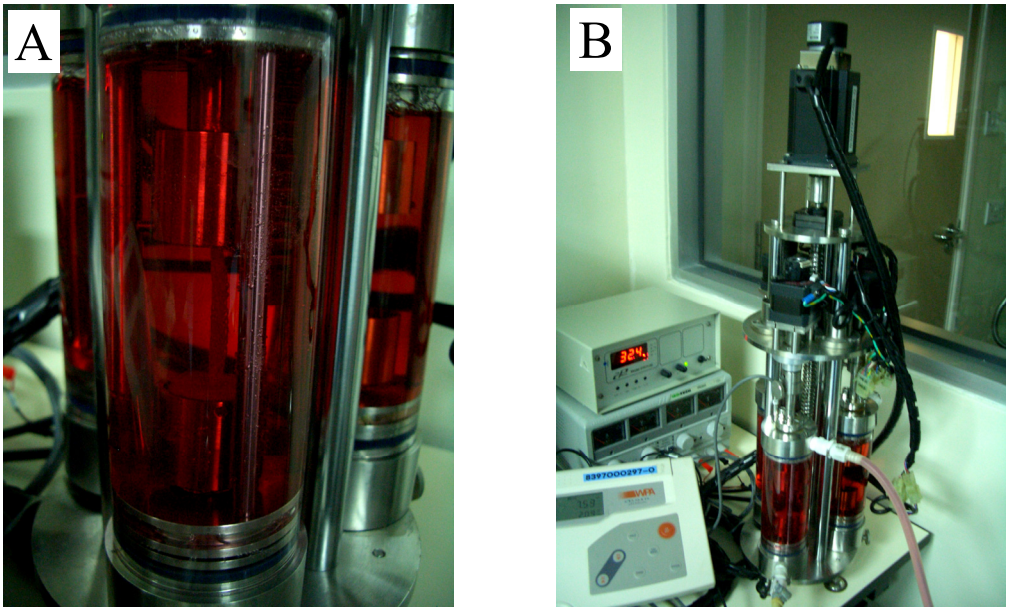

Figure 4-10: (A) Rolled-up SF hybrid scaffolds loaded into the bioreactor chamber vessel, (B) which was in turn affixed onto the bioreactor vessel stand to be environmentally conditioned and mechanically stimulated.

Table 4-2: Stimulation parameters used for dynamic culture of MSCs-seeded SF hybrid scaffolds to assess mechano-active effects of AL scaffolds.

Stimulation conditions	*Parameters*
Strain (%)	5
Cyclic frequency (Hz)	0.1
Periodic frequency (hours/day)	12
Cycles per day	4320

"Low" intensity type stimulation conditions were used, in this case, to provide a benchmark stimulation level for comparison with the static culture. Its purpose was to preliminarily assess the effect of mechanical conditioning on cells without over straining the cells to cause an adverse effect. It was important to ensure that cells were ready and mature enough for mechanical conditioning could be applied. Since the purpose of this chapter was to show that the AL type scaffolds were mechano-active and respond positively to mechanical stimulation, a low intensity would suffice. A more optimal stimulation approach would be evaluated and performed in the next chapter.

4.2.6. Cell Seeding Efficiency, Viability and Proliferation

Cell seeding efficiency was determined at 36 h after initial seeding, whereby the culture medium was collected from the wells or TCP (n=3) into separate centrifuge tubes. After centrifugation at 1500 rpm for 10 minutes, the cell pellets were re-suspended in 500 µL of medium respectively and cell counted using a hemocytometer as described in Appendix B1. The cell seeding efficiency was expressed as a percentage of the number of cells attached to the scaffold to the total number of cells seeded.

Each group of cultured scaffolds (static and dynamic culture conditions) and TCP was assayed for viability and cell proliferation (n=5) using Alamar Blue™ assay at days 3, 7 and 14 following the methods described in Appendix B2.

4.2.7. Cell Morphology

Cell morphology was assessed for the hybrid scaffold groups to specifically observe the cellular orientation, distribution and its interaction with the scaffold architecture. As such, assessment was made on statically cultured groups and not the dynamically cultured ones. To achieve this, at each time point (days 3, 7 and 14) , both groups of the static cultured samples (RD and AL) were fixed and had their F-actin filaments and nuclei fluorescence stained with Texas Red®-X phalloidin and DAPI respectively, as described in Appendix B3. The stained samples (n=3) were then washed and inspected via confocal microscopy as described.

To further observe the cell morphology and cellular interaction with the scaffolds, statically cultured samples at days 7 and 14 (n=3) were carefully unrolled and the seeded surface examined by SEM (JEOL Ltd, JSM-5600 LV, Japan).

4.2.8. Collagen Quantification

The collagen production and deposition of the MSCs in the statically and dynamically cultured hybrid scaffolds and TCP (n=3) were quantified using SirCol™ collagen assay at days 3, 7 and 14 following the method detailed in Appendix B4.

4.2.9. Histological Assessment

MSC-seeded RD and AL scaffolds of both the static and dynamic culture groups (n=3) were harvested for H&E staining after 7 and 14 days of culture according to methods described in Appendix B5a. The samples were fixed, paraffin blocked and sectioned longitudinally. As it was of interest to examine the core of the hybrid scaffolds for cell morphology and continued viability over the 14 days experimentation, longitudinal sections were taken from the core region and stained for histological evaluation. The slides were dehydrated before being mounted on glass cover slips.

4.2.10. Real-Time qRT-PCR Analysis

To assess tenogenic differentiation of the seeded MSCs, gene expressions for ligament-related ECM proteins such as collagen type I, collagen type III, tenascin-C and tenomodulin were analyzed and evaluated. After 7 and 14 days of culture, total RNA was extracted from the statically and dynamically cultured hybrid scaffolds (RD and AL) and TCP controls (n=3) as described in Appendix B6 for real-time qRT-PCR analysis.

4.2.11. Western Blot Analysis

After 7 and 14 days of culture, statically and dynamically cultured hybrid scaffold groups were processed for total protein extraction and Western blot performed for collagen I, collagen III and tenascin-C as detailed in Appendix B7. Band signals were detected and relative band intensities (with respect to the statically cultured RD scaffolds at day 7) were obtained and compared among the groups (n=3).

4.2.12. Biomechanical Test on Cultured Hybrid Scaffolds

The four groups of hybrid SF scaffolds (RD and AL; cultured statically and dynamically) were tensile tested to failure following the protocol described in section 3.4.2.4. at different time points (day 7 and 14). Unseeded hybrid scaffolds (blank RD and blank AL) were tested as control group. The load (N) and extension (mm) data was collected over 5 samples for each group and time point, and the failure load, elastic region stiffness, extension at maximum load and extent of toe region were determined after plotting the load displacement curves.

4.2.13. Statistical Analysis

Single factor ANOVA technique and post-hoc Tukey tests were used to assess the statistical significance of multiple comparisons. For pair-wise comparisons, two-tailed, unpaired Student's *t* tests were used. GraphPad Prism ver. 5 (GraphPad Software, Inc., CA, USA) was used to implement the statistical analysis. All data were expressed as means ± standard deviation (SD) and $p<0.05$ was considered statistically significant.

4.3. Results

4.3.1. Hybrid SF Scaffold Morphology

Gross observation of degummed knitted 3 yarns silk scaffold using the optimized "SDS30 (100°C, MA)" degumming protocol was made (Figure 4-11). It was shown that the degummed SF knit had a fairer appearance after the yellowish sericin coating had been removed from the knitted silk by degumming. When observed using the SEM, knitted SF obtained using this degumming protocol had smooth SF fibers and were clear of sericin after the degumming process as shown in the previous chapter.

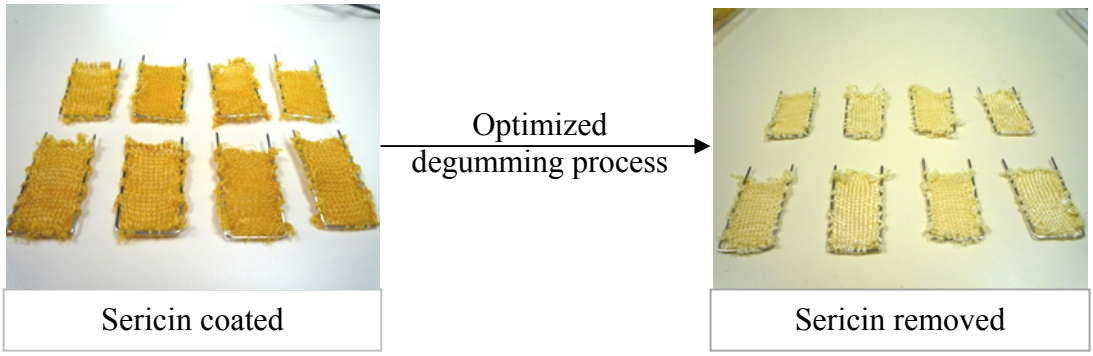

Figure 4-11: Change in appearance of knitted silk upon degumming using the "SDS30 (100°C, MA)" optimized degumming process, indicative of sericin removal.

Gross observations of the hybrid SF scaffolds (RD and AL) showed that the degummed knitted SFs had macro-pore sizes of about 1 mm diameter (Figure 4-12A), which were covered uniformly by the SFEF meshes on both sides of the knit to facilitate cell seeding (Figure 4-12B).

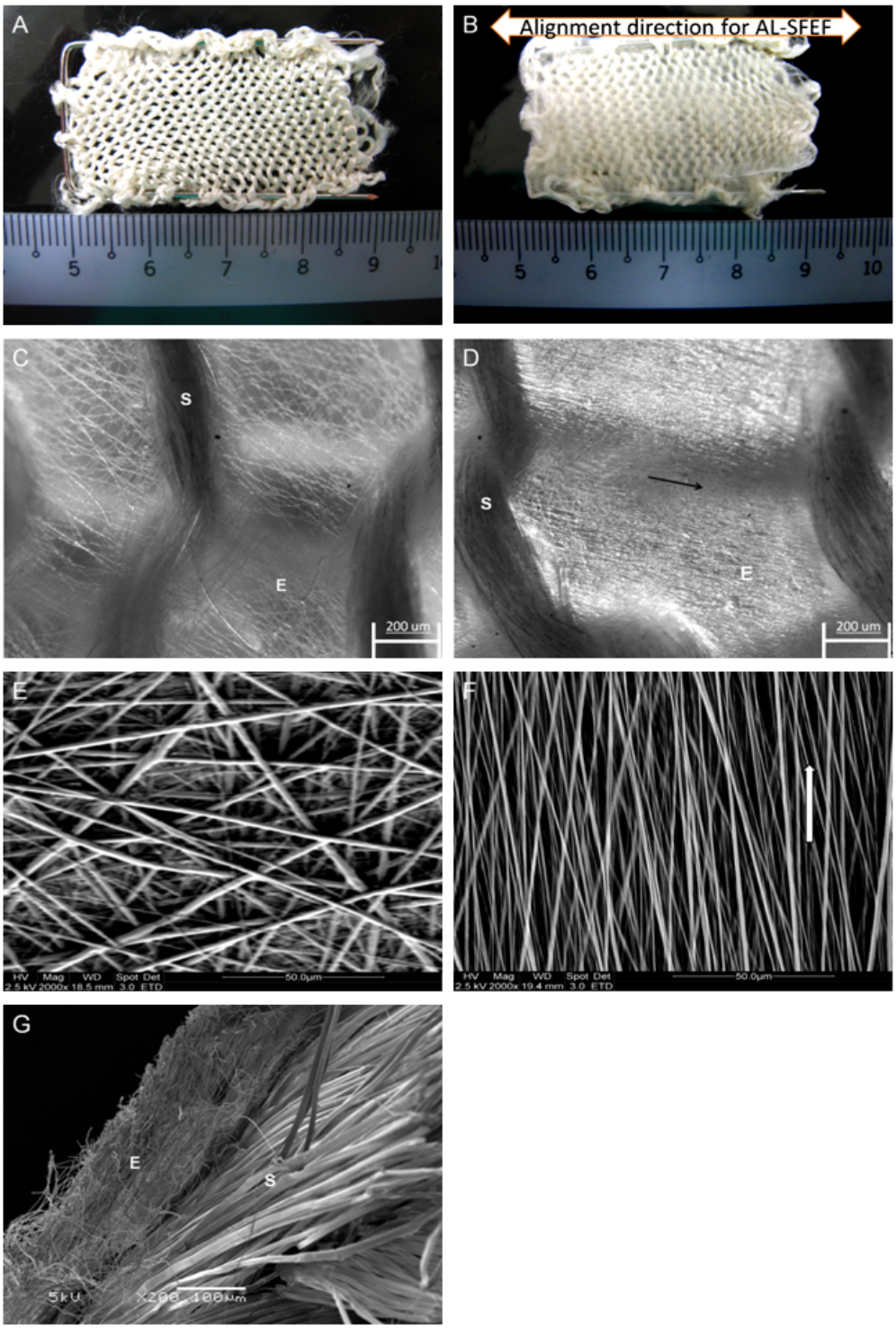

Figure 4-12: Gross observation of (A) knitted SF and (B) hybrid SF scaffold. Scaffold morphology of hybrid SF scaffolds: (C, E) RD and (D, F) AL. Phase contrast images (C, D) illustrate that the SFEF meshes were well integrated into the knitted SF, closing the large pores of the knitted structures. SEM images (E, F) illustrate the different SFEF morphology and arrangement. (G) The SFEFs were well integrated with the knitted structure as observed in SEM image. Magnification: (C, D) 64×, (E, F) 2000× and (G) 200×. Arrows indicate the direction of SFEF alignment, while "S" indicates knitted SF and "E" indicates electrospun SF. [298]

Both groups of the hybrid SF scaffold were revealed to be highly porous with interconnected pores uniformly distributed throughout the scaffold (Figure 4-12C, D). Pore sizes of the two groups of hybrid scaffolds ranged from 1 – 60 μm for the equiaxed pores of RD scaffolds, and 1 – 20 μm (minor axis) and 10 – 100 μm (major axis) for the elliptical pores of AL scaffolds. The SFEF meshes were also observed to be well integrated with knitted SFs after the two step binding process, which involved utilizing the contractile forces from methanol treated SFEF (Figure 4-12G). The dimensional difference of the SFEFs and the knitted SF fibers, both of which composed the hybrid SF scaffold, was also exhibited in this figure. Specifically, the SFEFs had diameters of 1211 ± 441 nm (RD-SFEFs) and 796 ± 111 nm (AL-SFEFs), while the degummed SF fibers had diameters of 11.7 ± 1.69 μm. The smaller AL-SFEF fiber diameter was due to the rotation of the grounded rotating frame, which collected and exerted a pulling force on the electrospun jet, and consequently reduced the dimensions of the AL-SFEF fibers.

4.3.2. SFEF Orientation

SFEFs of the AL hybrid scaffolds was observed to exhibit single directional alignment, while there was no observable alignment in the RD types (Figure 4-12C, D, E, F). Histograms plotted for the angular distributions of SFEFs (Figure 4-13) indicate significant alignment of the AL group (AD=4.8^{o}) as compared to RD group (AD=51.8^{o}).

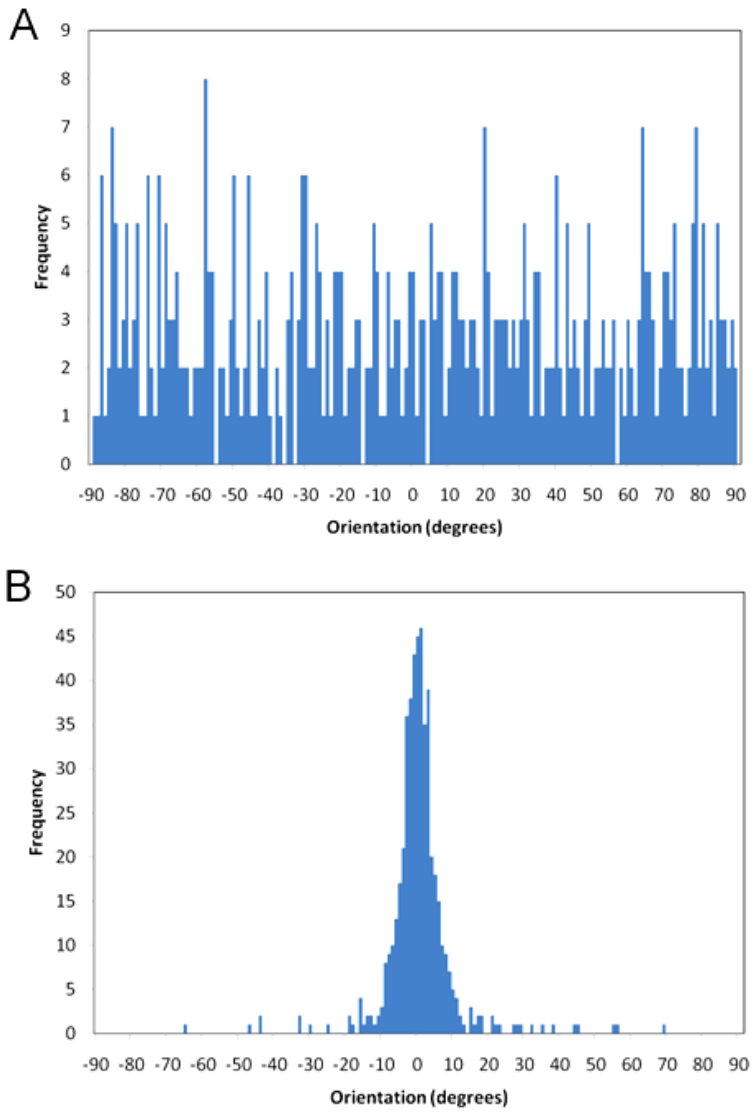

Figure 4-13: Histograms representing angular distributions of SFEFs: (A) randomly-arranged (AD = 51.8°, n=500) and (B) aligned (AD = 4.8°, n=500). [298]

4.3.3. Conformational Analysis of SF, SFEF and Hybrid SF Scaffold

Conformational analysis of SF at various stages of the scaffold fabrication process was performed using FTIR-ATR. From the FTIR-ATR spectra obtained (Figure 4-14), it was observed that SF upon degumming exhibited peaks at 1655cm^{-1}, which corresponded to the amide I region of the random coil structure (Figure 4-14(a)). Peaks

of the amide I region for random coil was not apparent in the methanol treated SFEF mesh (Figure 4-14(b)). Upon overall methanol treatment to the hybrid scaffold, there was an overall conformational transformation by reduction in random coils to greater proportion in β-sheets, as observed from the FTIR-ATR spectra (Fig. 4-14(c)). This was indicated by the absence of peaks corresponding to random coil structures, especially at the amide I regions. The spectra indicated that the dissolution and electrospinning process did not significantly alter the SF protein conformation as it was preserved as β-sheets, which is the native conformational state of SF fibers.

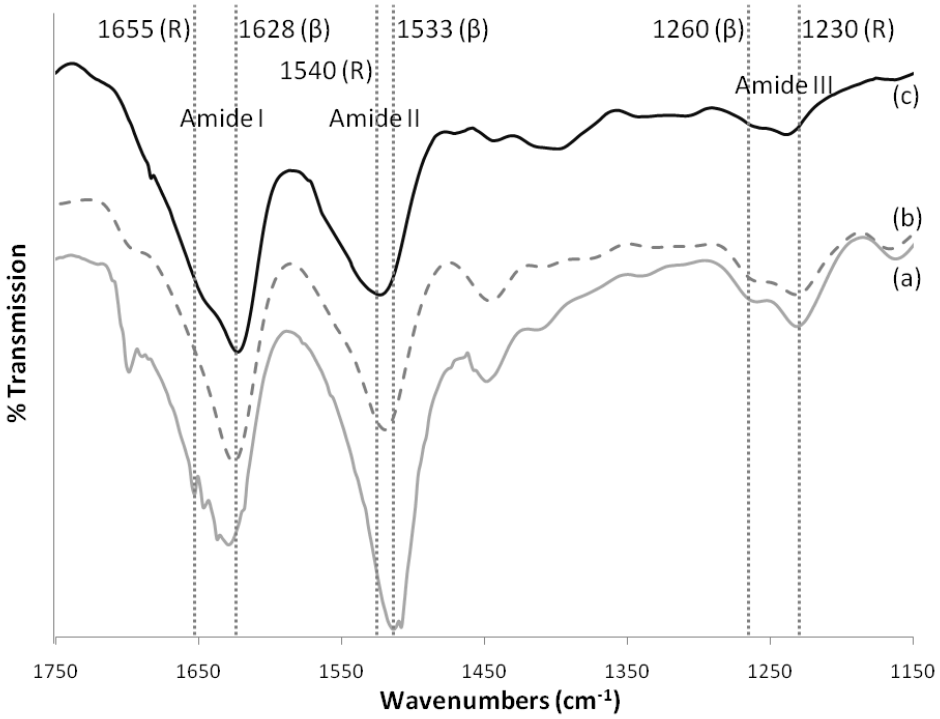

Figure 4-14: FTIR-ATR spectra of (a) degummed SF, (b) methanol treated SFEF mesh and (c) hybrid SF scaffold. [298]

4.3.4. Tensile Properties of AL and RD Hybrid Scaffolds

Rolled-up blank RD and AL hybrid scaffolds were tested for their tensile properties against rolled-up knitted SF (Table 4-3). All samples were tested to failure and the rupture sites were noted to consistently initiate at the mid zone of the gauge length. The load-deformation curves recorded comprised the toe region, linear region, microfailure region, and failure region, which were similar to the curve of native ACLs (Figure 4-15). The microfailures were generally attributed to the failure of knitted SF microfibers in tandem with extension of the construct.

Table 4-3: Mechanical properties of blank scaffold samples (n=5, data: mean ± SD). *p<0.05 when compared to knitted SF.

Samples	Maximum load (N)	Stiffness (N/mm)	Extension at maximum load (mm)
Knitted SF	93.24 ± 5.62	16.24 ± 0.81	9.24 ± 3.12
Blank RD	106.05 ± 6.23	19.21 ± 0.93 *	8.73 ± 2.67
Blank AL	129.21 ± 7.43 *	22.12 ± 1.22 *	9.25 ± 2.45

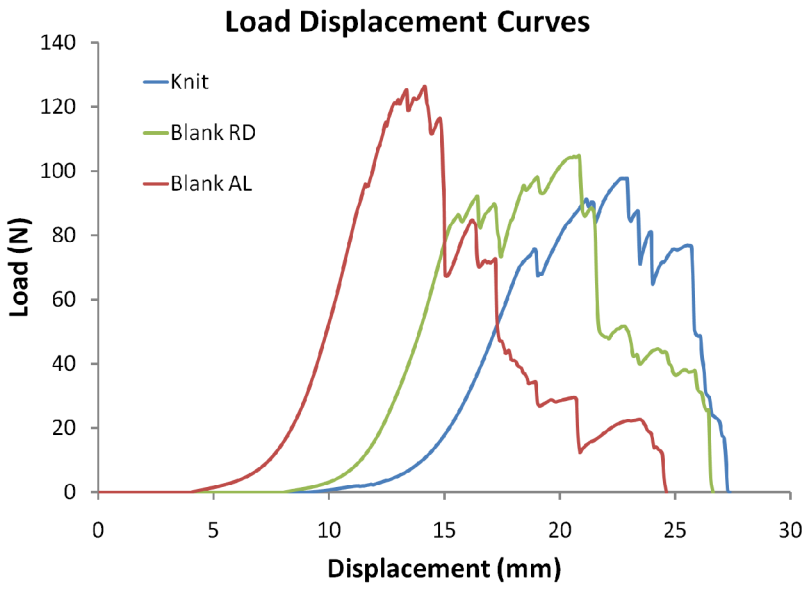

Figure 4-15: Representative load–displacement curves for different scaffold types. [298]

The tensile properties of blank AL were significantly better ($p<0.05$) than both the knitted SFs and blank RD in terms of the failure load (129.21 ± 7.43 N) and stiffness (22.12 ± 1.22 N/mm). No significant difference was noted for the extension at maximum load across the three groups ($p>0.05$). The extents of toe regions were 2.44 ± 0.94 mm, 3.30 ± 1.04 mm and 2.70 ± 1.11 mm for knit, blank AL and blank RD respectively, with no significant differences identified among the three groups ($p>0.05$).

4.3.5. Cell Adhesion, Viability and Proliferation

Cell attachment rate for all three groups (RD, AL, TCP) after 36 h from seeding was around 93% of the total amount of seeded MSCs per scaffold. Alamar Blue™ assay revealed that, as compared to the RD and TCP groups, cell viability for both culture conditions (static and dynamic) was significantly higher in the AL hybrid scaffolds after 7 days of culture (Figure 4-16). For the groups cultured in the static conditions, AL hybrid scaffolds had 24% (day 7) and 25% (day 14) more cells when compared to RD hybrid scaffolds ($p<0.01$), while for groups cultured in the dynamic conditions, AL hybrid scaffolds had 23% (day 7) and 27% (day 14) more cells when compared to RD hybrid scaffolds ($p<0.01$). Within each type of hybrid scaffold, significant difference was only seen on day 14 between AL hybrid scaffolds cultured in static and dynamic conditions ($p<0.05$), while no significant difference was observed in the RD hybrid scaffolds of the two culture conditions during this 14 day period ($p>0.05$).

The proliferation trends for different scaffold groups were also observed in Figure 4-16. There was also consistent proliferation in both the AL groups (static and dynamic) and also the dynamically cultured RD group through the 14 days culture period

($p<0.05$). However, there were no significant proliferations in the statically cultured RD and TCP groups ($p>0.05$) within the same 14 days culture period.

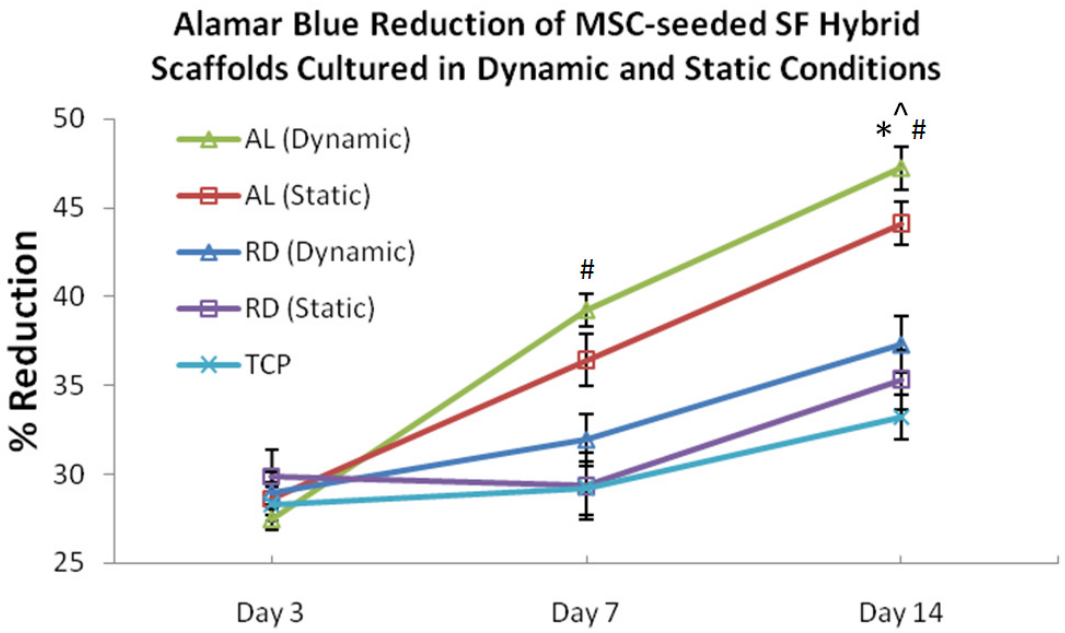

Figure 4-16: Alamar Blue™ assay illustrating consistent and significantly more viable cells in the AL groups (both static and dynamic) compared to other respective groups from day 7 onwards (#$p<0.01$, Student's t-test, n=5) and AL (dynamic) having more viable cells than AL (static) on day 14 (*$p<0.05$, Student's t-test, n=5). Significant proliferation (^$p<0.05$, ANOVA and post-hoc Tukey tests, n=5) was observed in AL (dynamic), AL (static) and RD (dynamic) through the 14-day culture.

4.3.6. Cell Morphology

After 3 days of static culture, the MSCs seeded onto AL hybrid scaffolds had already developed spindle-shaped morphologies and were oriented in the direction of SFEF alignment (Figure 4-17B). This was apparent when compared to the MSCs' equiaxed cell morphology with minimal ellipticity when cultured on RD (Figure 4-17A). From the confocal micrographs taken on days 7 and 14, cells cultured on statically cultured AL hybrid scaffolds continued to align along the length of the scaffolds (Figure 4-17D, F) after the hybrid scaffolds were rolled up to form ligament

analogues on day 3, while no apparent directionality was observed in cells cultured on RD hybrid scaffolds (Figure 4-17C, E). Increase in cell density was observed in both groups over the 14 days static culture period (Figure 4-17C, D, E, F), with near confluence observed at the cell-seeded layers by day 14.

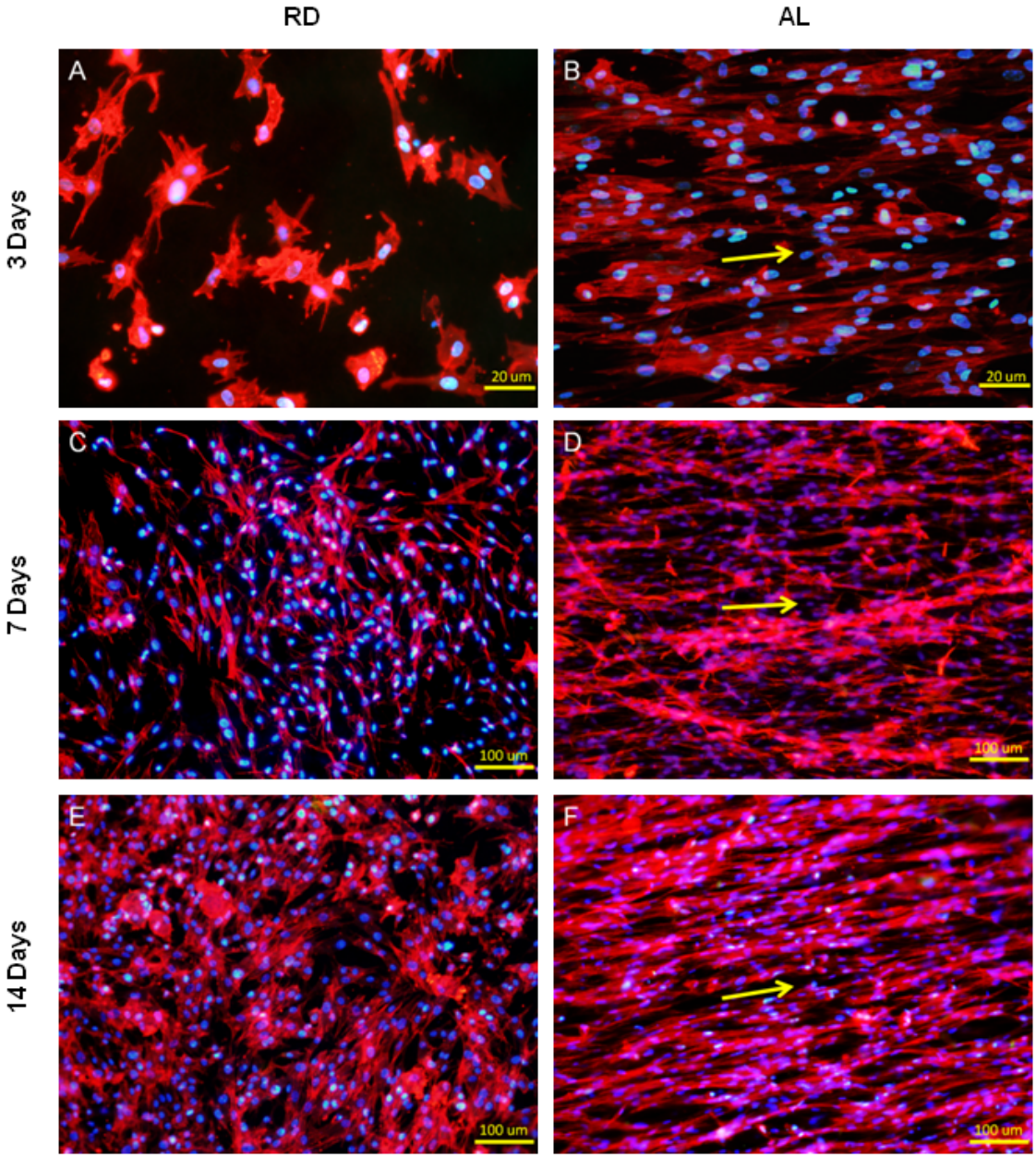

Figure 4-17: Confocal micrograph illustrating actin fibers (red) and nuclei (blue) of fluorescent stained MSCs seeded on (A,C,E) RD and (B,D,F) AL scaffolds and statically cultured for (A,B) 3 days, (C,D) 7 days and (E,F) 14 days. Magnification: (A,B) 400× and (C,E,E,F) 100×. [298]

SEM images taken for seeded surfaces, after carefully unrolling the hybrid scaffold constructs, revealed that MSCs were attached and elongated along the direction of localized SFEF orientation under static culture (Figure 4-18A, B). As compared to the AL hybrid scaffolds, MSCs attached to RD type formed projections along the SFEFs they were attached to, thereby unable to generate elongated morphologies as the surrounding SFEFs themselves were randomly arranged. As a result of cell alignment at an early stage of culture (3 days post seeding), MSCs on AL hybrid scaffolds began to form ECM network across cell colonies, while no obvious ECM network was formed in RD hybrid scaffolds (Figure 4-18C, D). More extensive ECM networks were seen at day 14, with more uniform and continuous ECM network observed for AL hybrid scaffolds as compared to the RD type (Figure 4-18E, F). In addition, MSCs on AL group began to form 3D tissue-like oriented bundles along the direction of SFEF alignment by day 14 of static culture, which was not apparent in the RD group (Figure 4-18G, H). Such 3D structures indicated that cross-layer ECM networks were being forged and cellular extensions were made to bridge with the adjacent AL-SFEF layer of the rolled-up AL hybrid scaffold.

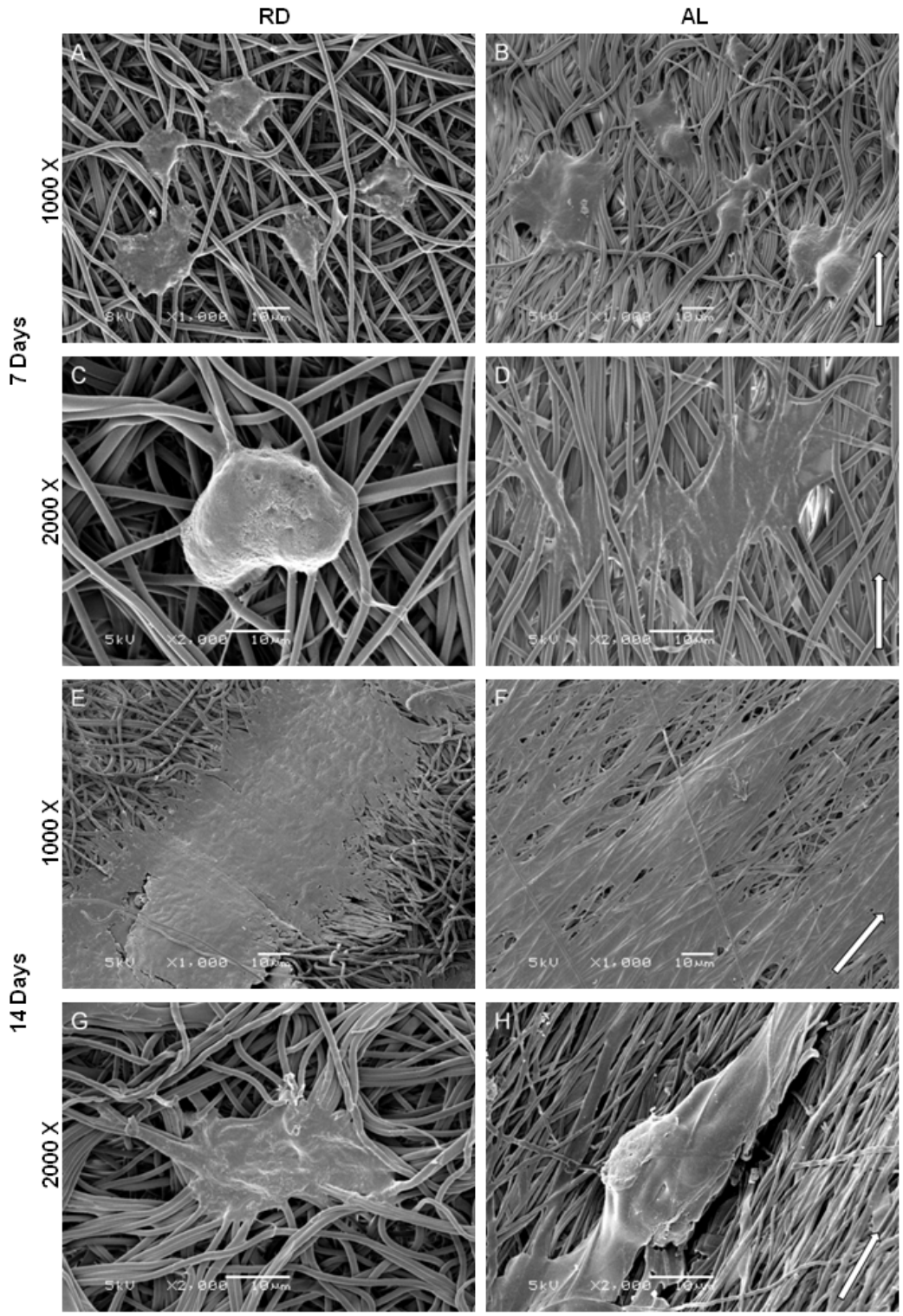

Figure 4-18: SEM images of MSCs-seeded (A,C,E,G) RD and (B,D,F,H) AL hybrid scaffolds after culturing statically for (A,B,C,D) 7 days and (E,F,G,H) 14 days. ECM deposition was initiated at day 7 for the AL scaffolds with uniform cellular elongation and aligned ECM deposition observed by day 14. Magnification: (A,B,E,F) 1000× and (C,D,G,H) 2000×. Arrows indicate the direction of SFEF alignment and the consequent cellular alignment, elongation and ECM deposition direction. [298]

4.3.7. Collagen Synthesis

Insoluble collagen assay was performed to determine the amount of deposited collagen on the hybrid scaffolds and TCP as an indication of the extent of ECM formation. This quantification assay revealed that there was significant increase ($p<0.05$) in collagen production and deposition in both the hybrid scaffold types over the culture duration (Figure 4-19) for both culture conditions. MSCs cultured on TCP, however, did not have significant increase in collagen deposited ($p>0.05$) until 14 days after seeding. It was also demonstrated that 3D hybrid scaffolds stimulated significantly more collagen deposition as compared to 2D TCP culture, regardless of the dynamic environment ($p<0.05$).

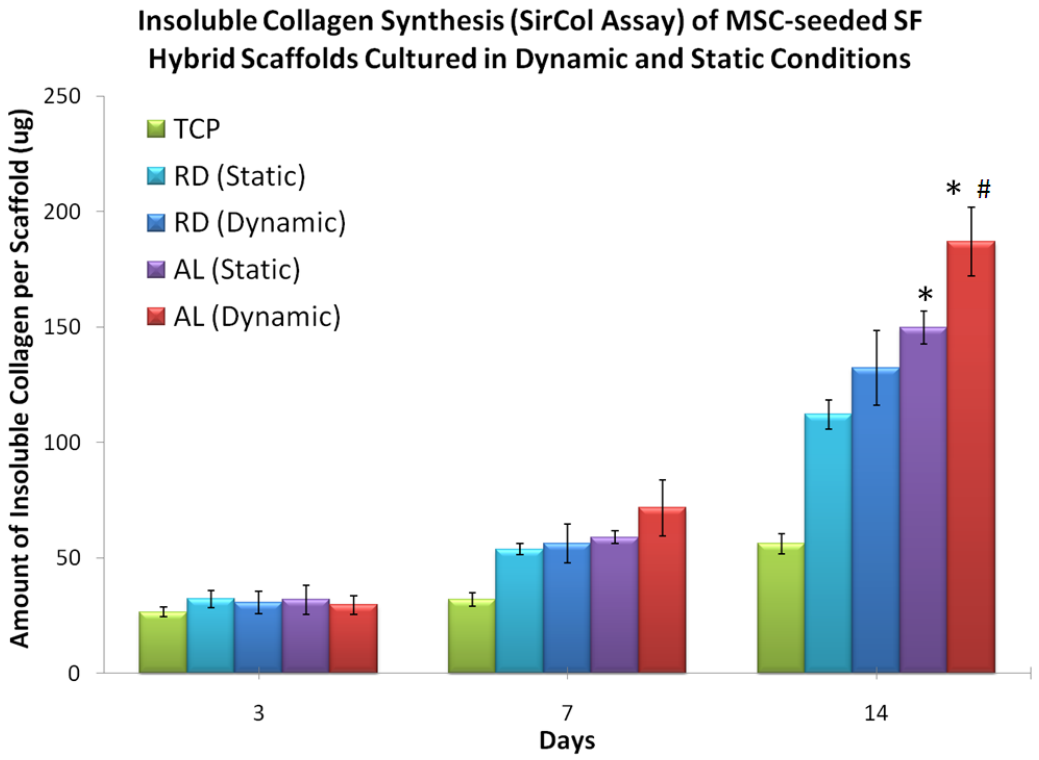

Figure 4-19: SirCol™ assay for amount of collagen deposited per scaffold/culture sample. Significant increase in collagen deposition was observed in the AL groups as compared to the RD groups at day 14 for the respective dynamic condition (*p < 0.01, Student's t-test, n=3). Significantly more collagen was deposited in the AL (dynamic) group as compared to AL (static) group at day 14 (#p < 0.01, Student's t-test, n=3).

Among the AL, RD and TCP groups cultured statically, significant difference was found between AL group and both RD and TCP groups at day 14 with AL hybrid scaffolds having 33.5% more collagen deposited than RD hybrid scaffolds and 66.3% more than TCP ($p<0.01$). With dynamic conditioning, significant differences in collagen deposition was found only in AL scaffold type after 14 days of culture, whereby dynamically cultured AL hybrid scaffolds had 24.9% more collagen deposited than the statically cultured counterpart ($p<0.01$). No significant difference was found for the RD hybrid scaffolds cultured using the two different conditions through the 14 days ($p>0.05$). Between the two scaffold types that were cultured dynamically, AL hybrid scaffolds demonstrated significantly more collagen deposition (41.3%) by day 14 as compared to the RD type ($p<0.01$).

4.3.8. Histological Analysis

HE staining was performed on longitudinal sections of the inner core of RD and AL hybrid scaffolds after 7 and 14 days of culture to assess cell proliferation and ECM production in the two groups qualitatively (Figure 4-20). Consistent with previous observations, aligned spindle-shaped cells with elongated processes were also observed in the both statically and dynamically cultured AL hybrid scaffold core sections (Figure 4-20B, D, F, H), while spherical or equiaxed cells were observed in the RD hybrid scaffold core sections (Figure 4-20A, C, E, G).

Histological images also revealed observable increase in cell density and distribution at the core of statically cultured AL hybrid scaffolds (Figure 4-20B, D); while interestingly, no observable increase in cellular distribution was found at the core

of statically cultured RD hybrid scaffolds (Figure 4-20A, C). This indicated that the cells remained viable and proliferative in the core of AL constructs during static culture but for the RD type, it was limited to just an increase in cell colony sizes, with minimal interconnected colonies formed. However, with dynamic culture, more uniform cell distribution was observed for RD hybrid scaffolds (Figure 4-20E, G), especially at day 14. This could be attributed to the improved medium uptake into the scaffold cores with dynamic culture. Despite the difference in proliferation rates between the two types of hybrid scaffolds during static culture, both were shown to be able to support cellular viability due to the interconnected porous structures of the hybrid scaffolds.

The effect of dynamic conditioning on cellular morphology was apparent in both the RD and AL hybrid scaffolds. Compared with the statically cultured counterparts, the dynamically cultured RD groups exhibited improved cellular elongation along the direction of mechanical strain. Nevertheless, the effect was more prominent in the AL groups. Increased cellular density and ECM deposition was also observed qualitatively in the dynamically stimulated AL group as compared to both the statically cultured AL group and the dynamically cultured RD group, demonstrating the effect of the mechano-active AL hybrid scaffold.

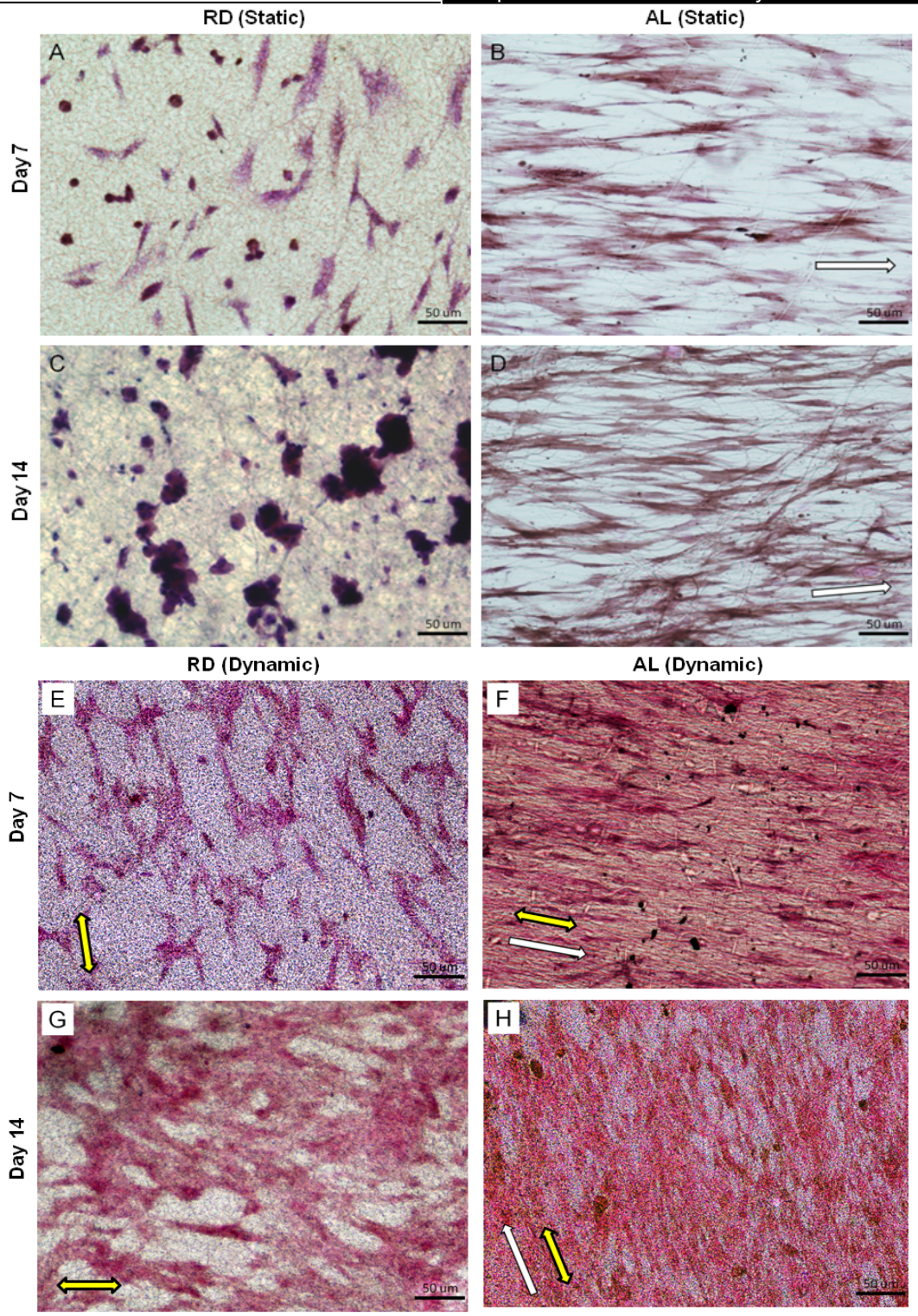

Figure 4-20: Histological evaluation of statically cultured (A, C) RD and (B, D) AL scaffolds, and dynamically cultured (E, G) RD and (F, H) AL scaffolds. HE staining of the fibrous core sections of the cylindrical analogues was done after having cultured for (A, B, E, F) 7 days and (C, D, G, H) 14 days. Magnification: 200×. White single-head arrows indicate the direction of SFEF alignment and the consequent cellular alignment, elongation and ECM deposition direction, while yellow double-head arrows indicate the direction of mechanical strain in the dynamically cultured groups. [298]

4.3.9. Gene Expression of Ligament-related ECM Proteins using Real-Time qRT-PCR

The expression of ligament-related genes in TCP, RD (static and dynamic) and AL (static and dynamic) were evaluated via real-time qRT-PCR. From results obtained for statically cultured groups, it was revealed that expression levels for collagen I was significantly up-regulated in the AL group compared to the RD and TCP groups from day 7 onwards (Figure 4-21A; $p<0.05$), while collagen III and tenascin-C expressions were significantly up-regulated in the AL group compared to the other two groups on day 14 only (Figure 4-21B, C; $p<0.05$). However, there was no significant difference in tenomodulin expression between the groups through the 14 day culture period (Figure 4-21D; $p>0.05$). All target genes were significantly up-regulated in the statically cultured AL group from day 7 to day 14 (collagen I: 92.7% higher, collagen III: 146.8% higher, tenascin-C: 19.6% higher and tenomodulin: 32.8% higher; $p<0.05$), which was not the case for the other two groups. These results indicated that the AL hybrid scaffold could stimulate up-regulation of ligament-related gene expression at a faster rate than the other two groups and enhanced differentiation of MSCs to ligament fibroblasts.

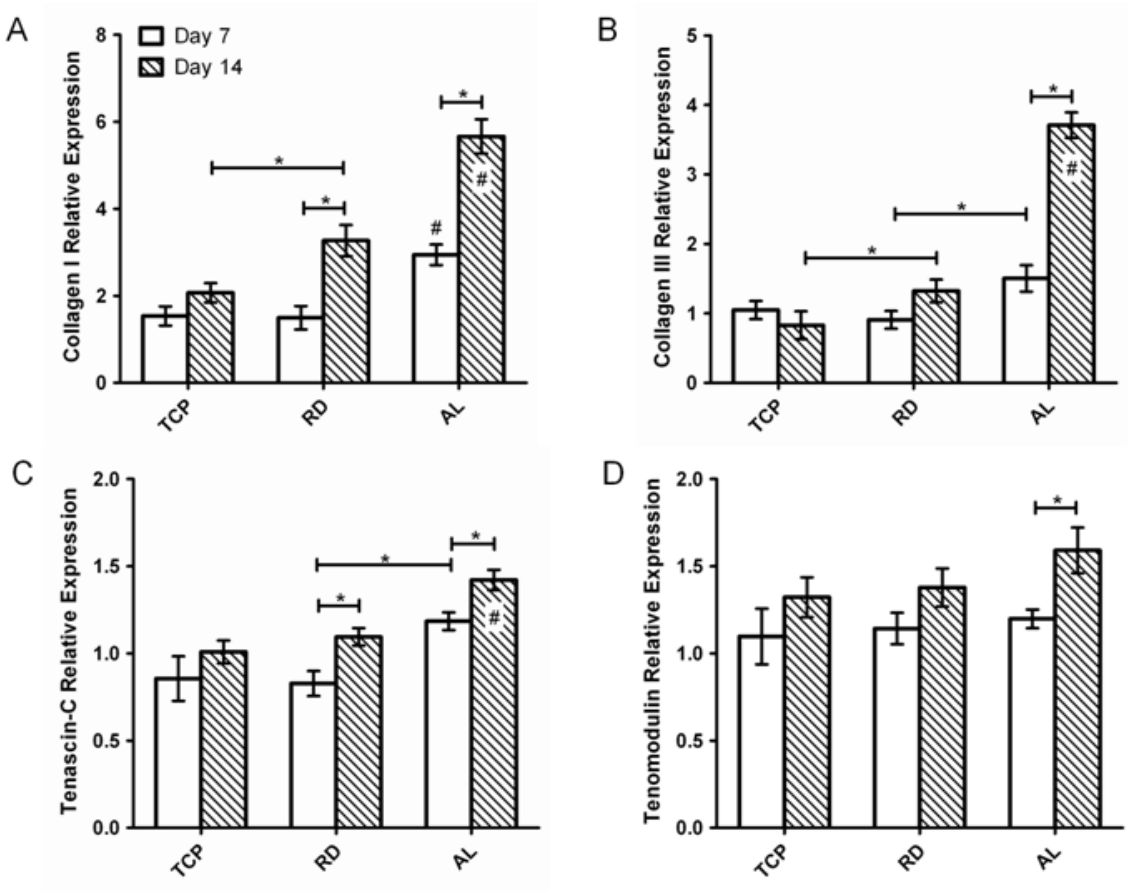

Figure 4-21: Type I collagen gene expression was significantly higher in the statically cultured AL scaffolds than the other 2 groups from day 7 onwards, while type III collagen and tenascin-C gene expression were significantly higher in statically cultured AL scaffolds than the other 2 groups only after 14 days (indicated by #). Levels were quantified using real time RT-PCR and were normalized to the housekeeping gene, GAPDH (n=3). Other statistically significant differences are indicated by * ($p < 0.05$). [298]

From results obtained for dynamically cultured hybrid scaffolds (Figure 4-22), gene expression for all targeted ligament-related genes were significantly up-regulated in both RD and AL groups by day 14, as compared to their respective statically cultured counterparts ($p<0.05$). Nevertheless, significantly higher expression for collagen I, tenascin-C and tenomodulin were observed in dynamically cultured AL group as early as day 7, compared to the static equivalent, which was not the case for the RD groups. With dynamic stimulation, all targeted genes were up-regulated in the AL groups as

compared to the RD groups by day 14, indicating that dynamic conditioning did synergistically complement the favorable topographical cues presented by the AL hybrid scaffolds in accelerating tenogenic differentiation.

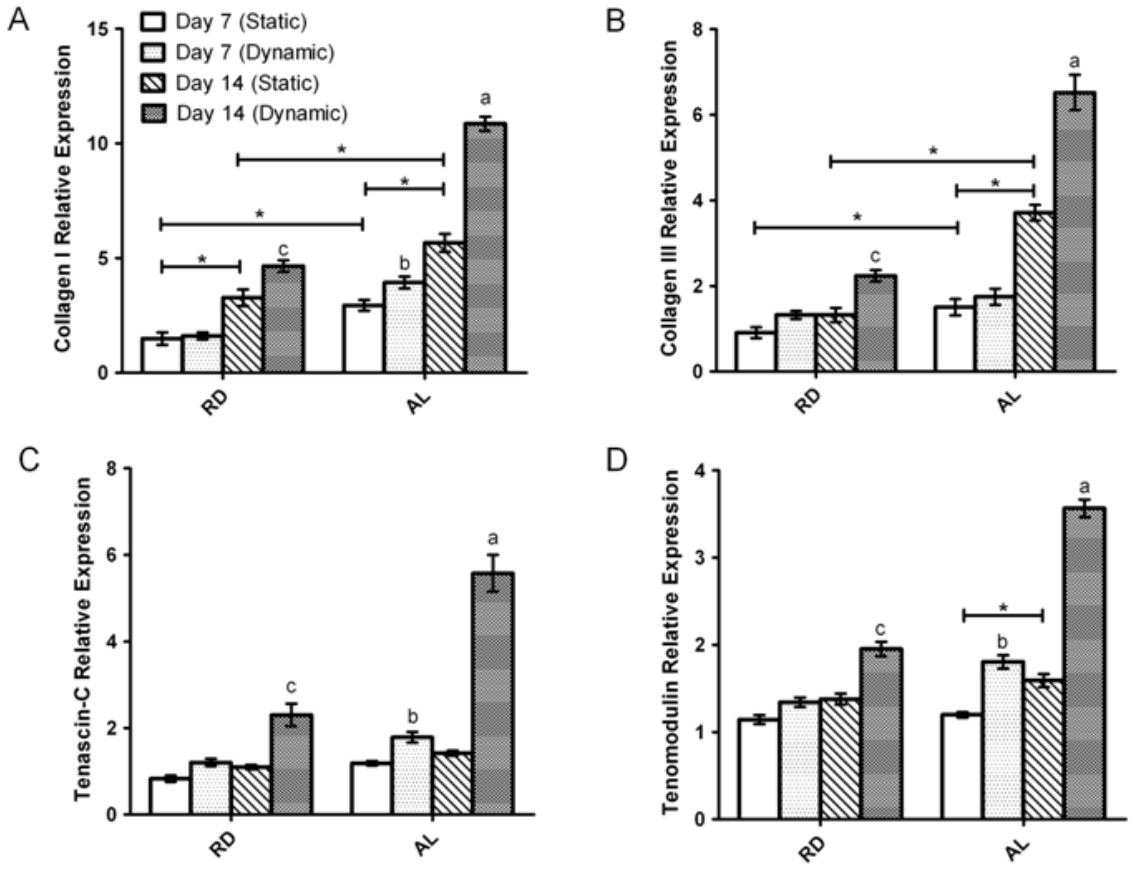

Figure 4-22: Collagen I, tenascin-C and tenomodulin were up-regulated in the dynamically cultured AL group by day 7 as compared to the RD groups and AL (static) at the same time point(indicated by "b"). Gene expressions of all targeted genes were significantly up-regulated in the dynamically cultured scaffold groups (RD and AL) by day 14 (indicated by "a" and "c"). Gene expressions for all targeted genes were significantly higher in the dynamically cultured AL group than the RD group by day 14 (indicated by "a"). Levels were quantified using real time RT-PCR and were normalized to the housekeeping gene, GAPDH (n=3). Other statistically significant differences are indicated by * ($p < 0.05$).

4.3.10. Western Blot Analysis

Protein expressions for collagen I, collagen III and tenascin-C were detected for RD and AL groups after 7 and 14 days of static culture (Figure 4-23). Analysis was performed on densitometric data of the optical intensity of each lane expressed in the Western blot membranes, which was normalized to RD group cultured for 7 days.

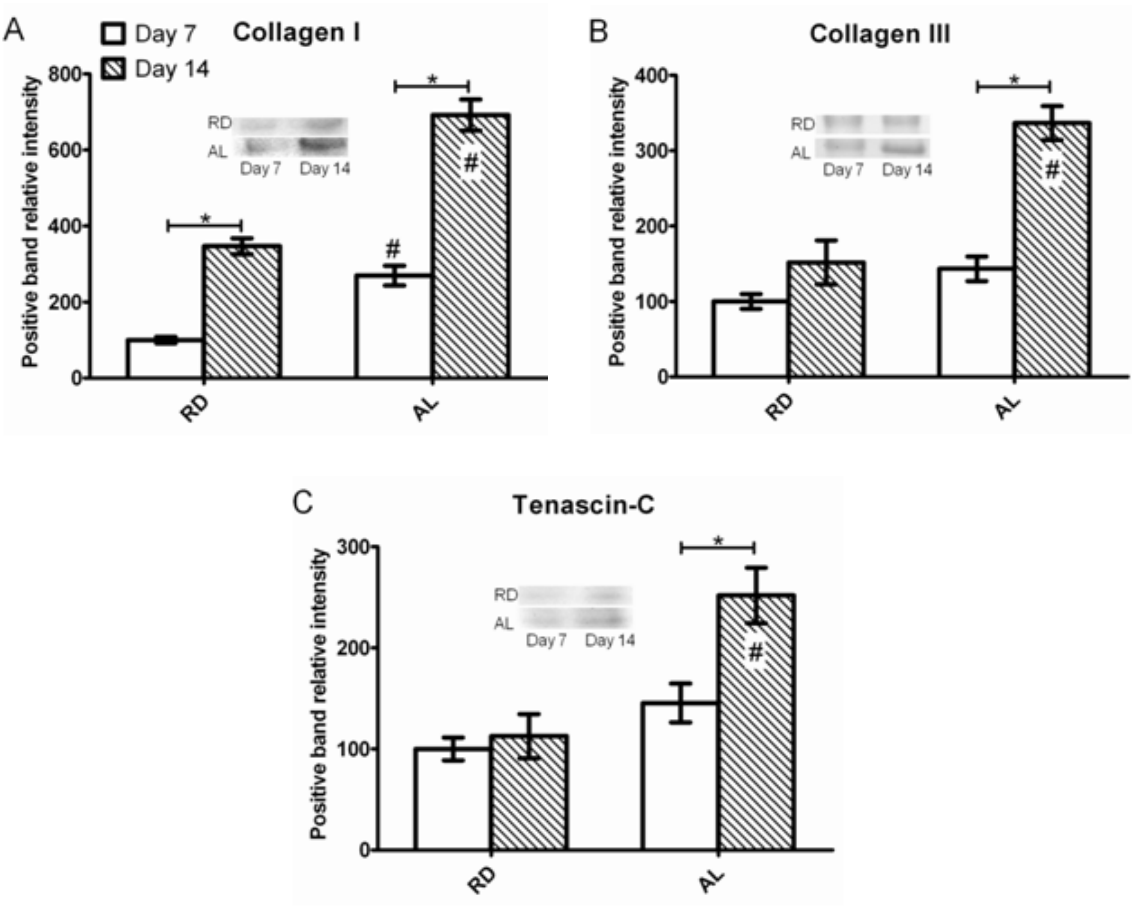

Figure 4-23: Western blot analysis of ligament-related ECM proteins produced by MSCs cultured on the RD and AL scaffolds and statically cultured for 7 and 14 days. The results were normalized to data obtained from RD scaffolds statically cultured for 7 days and evaluated on a relative basis for comparison between different samples (n=3). Significantly more type I collagen was produced in AL scaffolds from day 7 onwards, while significance was observed for type III collagen and tenascin-C after 14 days of static culture (#p < 0.05). *p<0.05 between 2 time points within each group. [298]

The results demonstrated that the matrix of the statically cultured ligament analogues composed of mainly type I and III collagen and tenascin-C, with collagen I being predominant as its expression was consistently higher in both RD and AL when compared to collagen III and tenascin-C. Significantly more collagen I was expressed in AL than RD from day 7 onwards (day 7: 169.7% more, day 14: 99.4% more), while significance was found for collagen III and tenascin-C on day 14 (collagen III: 121.8% more and tenascin-C: 123.6% more; $p<0.05$). For the RD group, significant increase from day 7 to day 14 was found for collagen I only (246.9% more; $p<0.05$) but for the AL group, it was found for all three proteins tested (collagen I: 156.5% more, collagen III: 134.8% more, tenascin-C: 73.2% more; $p<0.05$). Similar trends were observed in the RT-PCR results for statically cultured RD and AL scaffolds as shown previously.

This trend was altered with mechanical stimulation, as significant increase from day 7 to day 14 was found for all three proteins tested, for both RD (collagen I: 80.7% more, collagen III: 33.1% more, tenascin-C: 50.5% more; $p<0.05$) and AL (collagen I: 81.5% more, collagen III: 64.1% more, tenascin-C: 70.3% more; $p<0.05$) groups (Figure 4-24). Between RD and AL groups that were dynamically cultured, AL hybrid scaffolds could similarly stimulate increased type I collagen production since day 7 compared to RD types (day 7: 37.7% more, day 14: 38.3% more; $p<0.05$). Similar to static culture, significantly more type III collagen and tenascin-C was found for AL group relative to RD group on day 14 only (collagen III: 40.7% more and tenascin-C: 43.4% more; $p<0.05$). With mechanical conditioning, both RD and AL hybrid scaffolds composed of significantly more collagen I from day 7 onwards (For RD, day 7: 90.9% more, day 14: 26.7% more, and for AL, day 7: 60.0% more, day 14: 28.7% more;

p<0.05), and significantly more collagen I and tenascin-C on day 14 only (For RD, collagen III: 45.0% more and tenascin-C: 73.4% more, and for AL, collagen III: 24.7% more and tenascin-C: 19.7% more; p<0.05) . These results were indicative of the differentiative stimulatory effects of mechanical stimulation on the hybrid scaffolds, especially the aligned hybrid SF scaffolds.

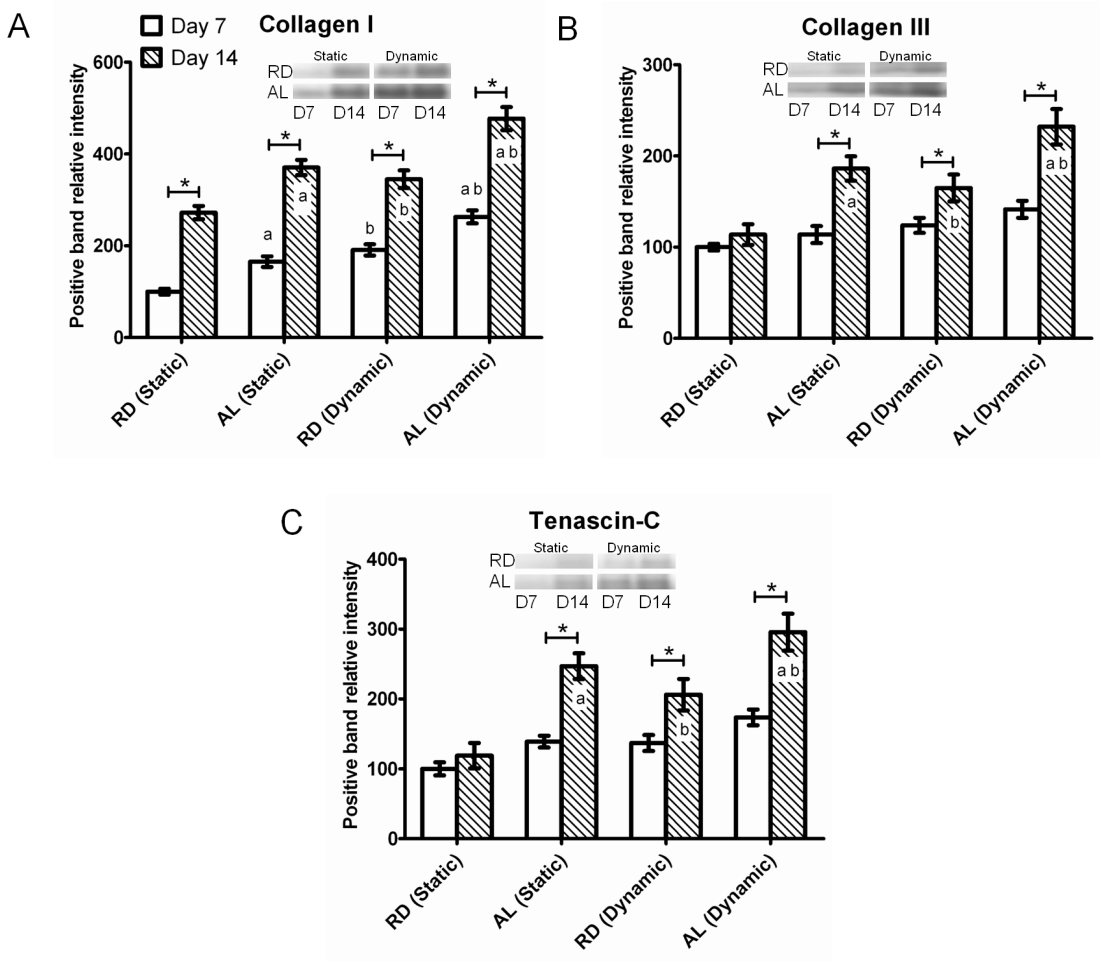

Figure 4-24: Western blot analysis of ligament-related ECM proteins produced by MSCs cultured on the RD and AL scaffolds and cultured (statically and dynamically) for 7 and 14 days. The results were normalized to data obtained from RD scaffolds statically cultured for 7 days and evaluated on a relative basis for comparison between different samples (n=3). a: significant difference (p<0.05) between the two hybrid scaffold types (RD and AL) at each time point; b: significant difference (p < 0.05) between the two stimulation conditions (static and dynamic) at each time point. *p<0.05 between 2 time points within each group.

4.3.11. Tensile Properties of Cultured Hybrid Scaffolds

Statically and dynamically cultured rolled-up hybrid scaffolds (RD and AL at day 7 and 14) were tested for their tensile properties as tabulated in Table 4-4. The samples were tested to failure and rupture was noted to initiate from the centre region of the entire gauge length, though exact rupture site was inconsistent across samples. Load-displacement curves plotted revealed the toe region, linear region, microfailure region and failure region, similar to that of native ACLs (Figure 4-25B). Similar to the blank scaffolds, microfailures were observed in the cultured hybrid scaffolds, which were generally attributed to SF knitted microfiber failure in tandem as the construct was extended.

Table 4-4: Mechanical properties of statically and dynamically cultured scaffold samples (n=5, data: mean ± SD). *p<0.05 when compared to RD scaffolds at each time point of the same culture condition (for static and dynamic cultures respectively). #p<0.05 when dynamically cultured scaffolds were compared to the statically cultured equivalent at the same time point.

	Samples	Maximum load (N)	Stiffness (N/mm)	Extension at maximum load (mm)
Static	RD (Day 7)	115.31 ± 4.75	18.85 ± 0.79	9.81 ± 3.54
	AL (Day 7)	138.53 ± 9.19 *	23.29 ± 1.38 *	9.39 ± 2.89
	RD (Day 14)	125.63 ± 5.34	21.45 ± 0.82	11.24 ± 3.24
	AL (Day 14)	158.14 ± 8.49 *	26.22 ± 0.92 *	12.45 ± 3.64
Dynamic	RD (Day 7)	122.35 ± 3.67	17.48 ± 0.93	10.35 ± 2.94
	AL (Day 7)	144.44 ± 5.03 *	24.33 ± 1.40 *	11.46 ± 3.51
	RD (Day 14)	138.67 ± 9.22	23.07 ± 2.54	11.33 ± 3.11
	AL (Day 14)	172.08 ± 6.28 *#	26.93 ± 2.40 *	10.99 ± 2.67

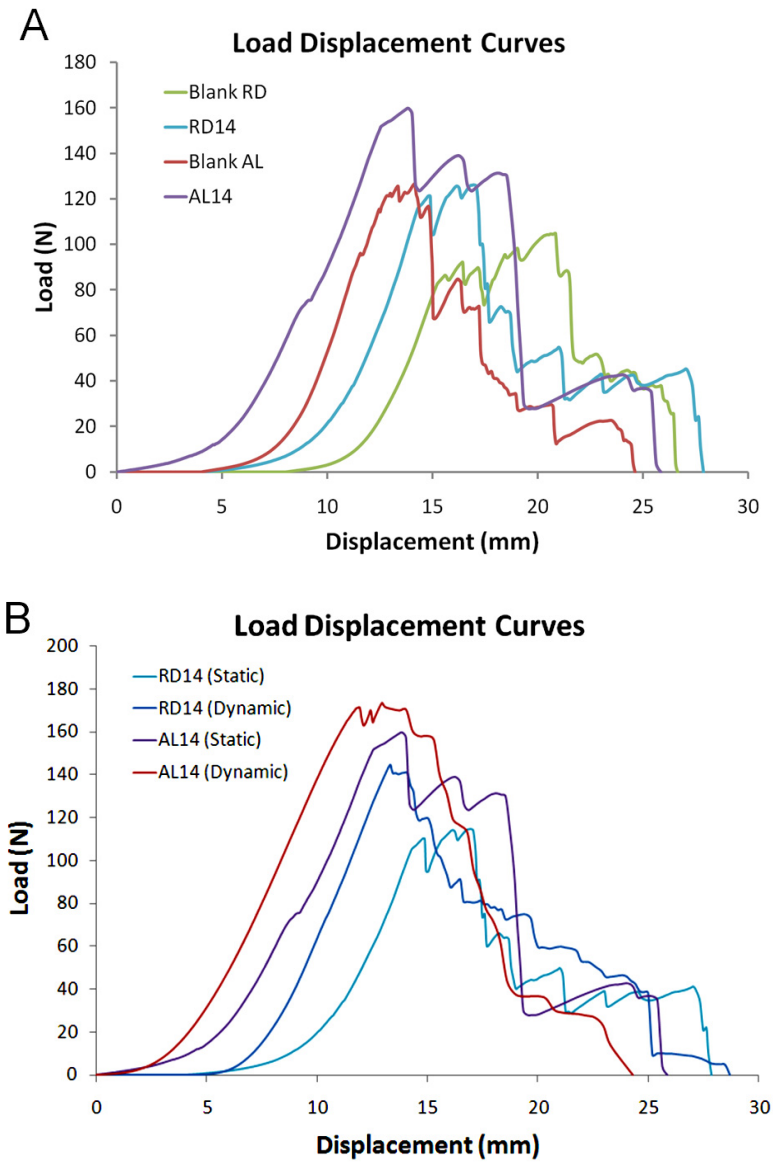

Figure 4-25: Representative load–displacement curves for (A) blank/MSC-seeded scaffolds (day 14, static cultured) and for (B) statically/dynamically cultured scaffolds (day 14).

When compared against rolled-up blank RD and AL hybrid scaffolds (Table 4-4), both statically cultured RD and AL groups had significant increase in maximum load (RD: 18.5% increase and AL: 22.6% increase) and stiffness (RD: 11.7% increase and AL: 18.5% increase) from the respective blank hybrid scaffolds only after 14 days of culture ($p<0.05$). Through the 14 days static culture period, AL group had significantly

higher maximum load and stiffness than its RD counterpart of the same culture duration (day 7 and day 14; $p<0.05$), with the AL group being 25.9% stronger and 22.2% stiffer than the RD group after 14 days of culture. Both the statically cultured RD and AL groups had significantly larger extents of toe region after the 14 days culture as compared to the respective blank hybrid scaffolds, with cultured RD scaffolds having 6.48 ± 1.45 mm and cultured AL scaffolds having 5.05 ± 1.23 mm by day 14 ($p<0.05$). This indicated that after culture for 14 days, both RD and AL hybrid scaffolds could be stretched over significantly larger displacements prior to linear extension than their cell-free counterparts. However, no significant difference was found in the toe region extents between RD and AL after 14 days of culture ($p>0.05$).

With mechanical stimulation, both RD and AL groups at day 14 had increased maximum load and stiffness from day 7 of the culture period (For RD, maximum load: 13.3% increase, stiffness: 32.0% increase; $p<0.05$ and for AL, maximum load: 19.1% increase, stiffness: 10.7% increase; $p<0.05$). This was not the case for RD when it was subjected to static culture, as there was no significant increase in maximum load and stiffness from day 7 to day 14 in this culture condition ($p>0.05$). Similar to static cultures, dynamically cultured AL hybrid scaffolds were also significantly stronger and stiffer than the RD group at both day 7 and 14 ($p<0.05$), with dynamically cultured AL group being 24.1% stronger and 16.7% stiffer than similarly cultured RD group. When compared to the statically cultured groups, dynamically cultured AL group was significantly stronger than the statically cultured AL group at day 14 (8.9% stronger, $p<0.05$), indicating the dynamic condition did have effect on strengthening the AL hybrid scaffolds. Nevertheless, no significant increase was found for stiffness when the

two culture conditions were compared based on the AL hybrid scaffold ($p>0.05$). This could be attributed to the freshly deposited collagen being not as stiff and required longer culture period for maturation and remodeling. Similarly, there was no significant difference in the extent of toe regions measured between the groups cultured dynamically and when cross comparisons were made with the statically cultured counterparts ($p>0.05$). Longer culture period might be necessary before significant changes in the extent of toe region could be observed.

No significant differences were noted for the extension at maximum load across all the groups and at different time points tested in this part of the experiment ($p>0.05$).

4.4. Discussion

In this part of the study, the focus was on the development and characterization of a mechanically functional full silk scaffold with customizable aligned topographical cues, which would be further stimulated mechanically to accelerate the tenogenic differentiation process with the aim of achieving the regeneration of ligament. Enhanced cell proliferation, cell viability and ECM production were observed in the AL hybrid scaffolds when compared with both the RD type and the 2D culture on TCP. MSCs were observed to attach in an aligned fashion in the direction of SFEF alignment from as early as 3 days post-seeding and continued to expand in cell density over the 14 days static culture period. This was further enhanced by mechanically stimulating the scaffolds, whereby more prominent increase in cell viability and proliferation was observed in the mechanically stimulated AL scaffolds. On top of that, there was no loss of directionality in cellular elongation as aligned spindle-shaped cells were observed

consistently after 7 and 14 days of culture in both static and dynamic conditions, whereby the hybrid scaffolds were rolled up into the cylindrical ligament analogues. The AL constructs stimulated upregulation of gene expression for ligament-related ECM proteins, which consequently induced increased deposition of collagen and aligned ligament-related ECM components. The increased aligned ECM deposition subsequently improved the overall mechanical properties of AL constructs. These effects were amplified in the mechanically stimulated AL constructs, whereby results showed that there was further upregulation of ligament-related ECM proteins, especially tenomodulin, which is responsible for ligament fibril maturation [299]. This was translated to improved strength observed for dynamically cultured AL scaffolds compared with the statically cultured counterpart after 14 days of culture. These results indicated that the hybrid SF scaffolds with aligned SFEFs were suitable for functional tissue engineering of the ligament and that the presence of dynamic conditioning would help accelerate the process of attaining viable and functional regenerated ligament for tissue replacement applications.

4.4.1. Knitted Mesh of the AL Hybrid SF Scaffold

The mechanical advantage of the hybrid SF scaffold was largely attributed to the knitted SF mesh. The SF fibers used to fabricate the knitted silk mesh of hybrid SF scaffolds were generally of the Silk II conformational state, which was the stronger and more stable β-sheet form. However, even though the degumming process had been controlled and optimized to reduce conformational transition of SF as discussed in Chapter 3, a small level of conformational shift from Silk II to Silk I occurred in the degummed SF knits as shown from the FTIR-ATR analysis performed. The

conformational change could be reversed upon immersion of methanol as observed in the FTIR-ATR performed for methanol treated hybrid SF scaffold (Figure 4-14). From the FTIR-ATR results obtained, it was also verified that the structural conformation of SFEFs was preserved as Silk II after methanol treatment.

4.4.2. AL-SFEF of the AL Hybrid SF Scaffold

The AL hybrid scaffold not only had the micron-scale SF knit, which catered to the mechanical aspect of the construct, but also composed of the sub-micron AL-SFEF mesh, which acted as a seeding substrate that provided topographical cues to stimulate cellular alignment and consequently aligned ECM deposition. The aligned surface topology is the typical native environment of ACL fibroblasts. In fact, preferential alignment forms the basis of anisotropicity, which is fundamental to musculoskeletal tissues [300]. This is apparent when normal ligaments are compared with repaired ligaments [9], whereby collagen fibrils laid down by the fibroblasts remained relatively disorganized and surrounded by amorphous ground substance in repaired ligaments. As a result of that, the properties of repaired ligaments are inferior to the normal ligaments. In actual fact, the lack of collagen alignment can shift the dynamics of continuous ligament remodeling towards degradation and reduction in the load-bearing capacity of newly formed tissue [1]. In view of this, the hybrid SF scaffold with AL-SFEFs for early cellular alignment and consequently alignment of the ECM and collagen fibrils may be relevant.

Using electrospinning, aligned fibers had been produced to act as topographical cues or guidance for cells. Xu *et al.* [301] compared the cell-cell adhesion and

proliferation of human coronary artery smooth muscle cells (SMC) on TCP, polymer film and aligned polymer fiber. They observed that SMCs migrated along the axis of the aligned fibers and expressed spindle-like contractile phenotype. On the other hand, Baker *et al.* [302] employed poly(ε-caprolactone) fibrous scaffolds for the tissue engineering of the meniscus. They seeded MSCs on aligned and random fibers, with results demonstrating that the aligned fibrous scaffolds could serve as a micro-pattern for directed tissue growth and produced constructs with improved mechanical properties compared to random scaffolds. Yim *et al.* [303] had also presented a comprehensive review of cellular interaction with nanoscale topography. Their findings also indicated that cells responded to topography of synthetic substrates of the nanometer and sub-micron range in terms of adhesion, proliferation, migration and gene expression. Other than these studies that utilized synthetic polymers, contact guidance had also been effected using naturally derived bioscaffolds. Almarza *et al.* [304] had demonstrated the use of elongated small intestinal submucosa (SIS) to create aligned SIS fibers and applied it as bioscaffold for ligament tissue engineering. Positive responses were seen in the cultured bone marrow derived cells seeded in such bioscaffolds as well. Nevertheless, issues pertaining the lack of the source, difficulty in controlling the quality or degree of fiber alignment and infection due to cross or intra-species transplantation persisted.

4.4.3. Mechano-Active AL Hybrid SF Scaffold Improved Cell Viability and Proliferation

The novelty of this study thus involved the development of a consistent and reproducible aligned hybrid SF scaffold that not only supported accelerated formation of aligned collagen fibers, but was also mechanically functional, making it suitable for ligament tissue engineering applications. The advantages of the AL hybrid SF scaffold were exemplified in the cellular viability and proliferation results, whereby cells seeded on AL were significantly more viable after 7 days of culture and had consistent proliferation throughout the 14 days culture, which was not apparent in the other 3D RD system or the 2D TCP system. As compared to 2D culture systems, the 3D culture systems could provide environmental cues closer to the native tissue to stimulate cell-surface receptors and adhesion sites that regulate cell cycle and gene expression for key ligament ECM components [1, 50, 305, 306]. The AL hybrid SF scaffold further enhanced these responses by bearing surface chemistry and topographical similarities with the native ECM. These effects were further improved when mechanical stimulation was provided, whereby increased differentiative activities were observed from the increased production of ligament-related genes and proteins in dynamically cultured AL hybrid scaffolds. This indicated that an essential benefit of culturing seeded AL scaffolds is the ability for AL-SFEFs to effectively transfer axial strain to the attached aligned MSCs. This was supported by works conducted by Lee *et al.* [37], whereby enhanced ECM production as a result of effective mechano-transduction due to aligned electrospun PU fibers were observed for HLFs.

The aligned architecture also facilitated medium intake into the core of the scaffold construct through active capillary action rendered by the aligned SFEFs. Consequently, higher cell densities with uniform cellular distribution were observed in the inner core of the AL group than the RD group. Nevertheless, with mechanical conditioning, medium intake was facilitated by the active strain actions rendered to the loaded constructs, which acted as a pumping action to bring about effective mass transfer within the constructs. This was why improved cell density and morphology was observed in the core of both AL and RD scaffolds when mechanical stimulation was present.

4.4.4. Mechano-Active AL Hybrid SF Scaffold Improved Cell/ECM Alignment and Collagen Fiber Formation

With the ability to stimulate elevated proliferation, high cell density of aligned spindle-shaped cells could be formed in AL scaffold types within the 14 days culture, contributing to the formation of extensive networks of aligned ECM as observed. Further to that, the formation of early stage collagen fiber bundles was apparent in the 3D culture of AL as bridging structures were discovered in the SEM images of carefully unrolled AL scaffolds. These bridging structures were possibly adhesion points with adjacent aligned ECM layers in the attempt to form 3D collagen fibers. This observation was complemented with the gene expression results, which indicated significant upregulation of ligament-related genes in the AL group after 14 days of culture. Although tenomodulin was not significantly up-regulated in the statically cultured AL group, there was significant upregulation at day 14 from day 7, indicating imminent

increase in expression of tenomodulin, which is associated with increase in collagen fibril diameter during ligament development [299]. This was brought forward with mechanical stimulation as significantly more tenomodulin was expressed in the dynamically cultured AL group compared to the dynamically cultured RD group from as early as day 7. Coupled with the increase in ligament-related ECM protein detected in the dynamically cultured AL group, it was clear that mechanically stimulated AL stimulated accelerated ligament tissue formation and maturation, with close structural similarity to the native tissue.

However, while the production of ligament-related proteins (collagen I, collagen III and tenascin-C) was clearly improved in the seeded AL constructs in both static and dynamic cultures, studies relating to the distribution pattern of these proteins within the scaffold would be necessary. It would also be interesting to investigate collagen fiber formation and distribution in the transverse cross-section of the constructs to identify the distribution pattern of mechanically contributing collagen fibers and ascertain collagen bundles formation.

4.4.5. Improved Mechanical Properties of MSC-Seeded Mechano-Active AL Hybrid SF Scaffold

The formation of aligned ECM structure was translated to the superior mechanical properties of the AL constructs. AL was observed to be significantly stronger and stiffer after being cultured with MSCs for 7 and 14 days as compared to the RD scaffold type under both static and dynamic conditions. Upon static culture for 14 days, the AL and RD hybrid scaffolds exhibited significantly extended toe regions of non-linear increase

in load-displacement than the respective blank hybrid scaffolds. It could thus be deduced that the ECM deposited in both the AL and RD contributed to the tensile loading, with the discontinuous and non-mature ECM structures being loaded prior to the hybrid scaffold. Interestingly, such loading pattern is also very similar to the native ACL, whereby wave or "crimp" patterns of the fibrils exist in the matrix to provide loading of fibrils in tandem via recruitment to "buffer" for slight elongations without incurring overall fibrous damage [53, 307] and to provide shock-absorbance for sudden lengthwise loading [308]. Tensile tests performed on native ACL also revealed similar nonlinear load-displacement curves, as a consequence of gradual increase of tissue stiffness [12]. Although the implementation of mechanical stimulation did not significantly increase the extent of the toe region measured from the statically cultured counterparts, equivalently higher values were observed compared to the blank scaffolds. It might be necessary for longer duration of mechanical conditioning be applied on the hybrid scaffolds before significant changes in this aspect could be seen.

Although the regenerated tissue contributed to the increase in tensile properties of the cultured hybrid scaffolds, majority of the loading capacity came from the hybrid SF scaffold itself. The hybrid SF scaffold had been designed to accommodate proteolytic degradation *in vivo* with the knit being customized to support more than twice the maximum ACL force in rabbits. This was notwithstanding the fact that the loading capacity was increased due to the SFEFs incorporated and the ECM that would be deposited as shown by the tensile tests performed. The tensile stiffness of knitted SF, on the other hand, was designed to be less than half of the native ACL tissue [3]. Stiffness was increased after SFEFs were incorporated to the SF knits, which was especially so

for the AL hybrid scaffold type as its stiffness was about 50% of the native tissue. Having lower scaffold stiffness as such can prevent stress shielding and allow mechanical forces that are subjected to the scaffolds to be effectively conducted to the attached cells. This strategy would be especially important when the cell-seeded scaffolds were to be mechanically conditioned either *in vitro* or *in vivo* to further enhance the differentiative potential of MSCs on the hybrid SF scaffolds. In this case, *in vitro* mechanical conditioning had been shown to be effective and had synergistically complemented the positive stiffness and mechano-transduction property of AL type hybrid scaffold to promote functional regeneration of the ligament tissue.

4.5. Concluding Remarks

In this study, a method of fabricating an aligned hybrid SF scaffold for ligament tissue engineering was presented. The hybrid SF scaffold consisted of knitted SF mesh with highly aligned AL-SFEFs produced via a custom-made rotating wire frame collector. With integration of the AL-SFEFs, the hybrid SF scaffold was shown to support MSC proliferation and provided favorable topographical and surface chemistry for cellular and ECM alignment. MSCs were consequently stimulated to produce elevated amounts of ligament-related proteins, indicative of ligament fibroblast differentiation. These effects were intensified when mechanical stimulation of the defined "low" intensity level was provided. With mechanical stimulation of the AL hybrid scaffolds, significantly stronger and stiffer constructs that displayed similar biomechanical characteristics as the native ACL were produced. The AL hybrid SF scaffold was thus shown to be mechano-active as it intensified the positive effects of mechanical stimulation and synergistically combined these effects with those provided by the aligned topography of the scaffold.

Further to this, works were performed as described in Chapter 5, whereby the mechanical stimulation approach was optimized to further enhance tenogenic differentiation and be carried out over a longer duration to examine the prolong effect of dynamic conditioning on MSC differentiation and development in the AL hybrid SF scaffold.

Chapter 5

REHABILITATIVE MECHANICAL CONDITIONING OF THE MECHANO-ACTIVE HYBRID SILK FIBROIN SCAFFOLD

5.1. Introduction

In the previous chapter, it has been shown that mechanical stimulation of the mechano-active AL hybrid SF scaffold enhanced ligament regeneration via effective mechano-transduction. Although the positive effects of dynamic culture using the AL hybrid scaffold has been shown, the stimulation parameters used may be less than optimal as the number of cycles provided per day (4320 cycles) was much lower than the lower boundary of the physiological range (6700 cycles) obtained from pedometer studies [262]. Although this might be the case, precipitous stimulation at the physiological level during the early stage of culture might be harmful as the seeded MSCs would not have developed sufficient and stable adhesions with the scaffold to respond positively. In view of these concerns, it was envisioned that the mechanical stimulation approach could be optimized to cater to timely supplementation of mechanical cues of the appropriate intensities in a rehabilitative manner. With successful implementation of this rehabilitative approach, it was hypothesized that early introduction of mechanical cues could be performed for the MSC-seeded mechano-active hybrid SF scaffold to effect an accelerated tenogenic differentiative profile.

In this study, the “low” and “high” intensity stimulation profile was identified to compose of 0.1 Hz and 0.5 Hz cyclic frequency respectively to effect 4320 and 21600 cycles per day respectively based on a 12 h stimulation period. These values were identified to mark the upper and lower boundaries by positioning substantially above and below the physiological range as reported in pedometer studies whereby human walking activity per day is 6700 to 11900 cycles per day [262]. Other stimulation

parameters were kept constant at the physiological values in these two stimulation profile. These two stimulation profile would be executed continuously for dynamic culture of AL hybrid SF scaffolds in the "continuous low" and "continuous high" regimes, and be contrasted with the "rehab" regime. The "rehab" regime would be composed of both the "low" and "high" stimulation profile, with the "low" stimulation profile executed 3 days post-seeding after initial static culture and the "high" stimulation profile executed 7 days post-seeding. Upon assessing the effect of these stimulation regimes on tenogenic differentiation of MSC-seeded AL hybrid constructs over a 28 day period, the optimal regime would be completely characterized and compared with the statically cultured MSC-seeded AL hybrid constructs.

5.2. Materials and Methods

5.2.1. Fabrication of AL Hybrid SF Scaffolds

Raw *Bombyx mori* silk fibers (3 yarns) were used to fabricate the knitted structure as described in section 3.4.2.1. For the experimental groups of scaffolds to be used for mechanical stimulation regime optimization, 60 × 20 mm silk knits were fabricated, while the dimension of 40 × 20 mm remained for the control group used for static culture. The excess 20 mm length for the experimental groups was to cater for attachment to the standalone bioreactor chamber. All the raw silk knits were then degummed using the optimized degumming protocol as described in section 3.4. To fabricate AL-SFEF components, electrospinnable SF solutions were first made using the method described in section 4.2.1. Subsequently the AL-SFEF meshes were fabricated, collected and integrated with the degummed SF knits to form AL hybrid SF scaffolds

respectively as described in the same section. It should be noted that corresponding to the longer SF knits used in the experimental groups, SFEF meshes that were used to integrate with the group of knits were also made longer.

Prior to cell seeding, the hybrid scaffolds were sterilized by means of formaldehyde (37%) (Mallinckrodt Baker, Inc., NJ, USA) gassing for 24 h. All other sterile equipment was sterilized by steam autoclaving.

5.2.2. Isolation and Culture of MSCs

MSCs were generated from bone marrow aspirates of NZW rabbits, isolated and cultured as described in section 4.2.3. A homogenous MSCs' population was obtained after 2 weeks of culture and MSCs (P3) were harvested for seeding onto the AL hybrid scaffolds.

5.2.3. MSC-seeded AL Scaffolds Cultured in Different Dynamic Conditioning Regimes and Static Conditions

The MSCs (P3) were resuspended in complete culture medium containing DMEM with high glucose (Gibco, Invitrogen, Carlsbad, CA, USA) supplemented with 10% FBS (HyClone Logan, Utah, USA), L-glutamine (580 mg/L) and penicillin–streptomycin (100 U/mL). 1.5 x 10^6 cells were then seeded by simply pipetting onto one side of each sterile AL hybrid scaffold. The same amount of cells was used for both the experimental groups ("continuous low", "continuous high" and "rehab") of the optimization study and the statically cultured control group. The AL hybrid scaffolds

were then statically cultured in a laminar manner for 3 days before being rolled up with the cell-seeded surface in the inner core and secured at the ends with SF fibers.

For the control group undergoing static culture, rolled-up AL hybrid scaffolds then continued to be cultured separately in customized 6-well polycarbonate dishes for another 25 days (total experimental period of 28 days), with medium being changed twice a week.

For the group undergoing dynamic culture for mechanical stimulation regime optimization, rolled-up scaffolds (RD and AL) were loaded into steam-autoclaved standalone bioreactor chamber vessels. The chamber vessels were then affixed onto the bioreactor main bioreactor vessel stand, as previously described, where dynamic culture conditions would be provided over the next 25 days period. Three dynamic culture regime was implemented, which included the “continuous low”, “continuous high” and “rehab”, whereby the “continuous low” and “continuous high” regimes were done by continuous supplementation of the “low” and “high” intensity stimulation profile through the 25 days stimulation period respectively, while the “rehab” regime was performed by executing the “low” stimulation profile for the first 4 days of dynamic culture and subsequently the “high” stimulation profile for the next 21 days of dynamic culture. The “low” and “high” stimulation profiles were described in detail in Table 5-1 and the temporal executions of the profiles in each of the regime were illustrated in Figure 5-1.

Table 5-1: Stimulation parameters of the "low" and "high" intensity stimulation profile used for optimization of the dynamic conditioning regime.

Stimulation conditions	*Parameters*	
	"Low"	"High"
Strain (%)	5	5
Cyclic frequency (Hz)	0.1	0.5
Periodic frequency (hours/day)	12	12
Cycles per day	4320	21600

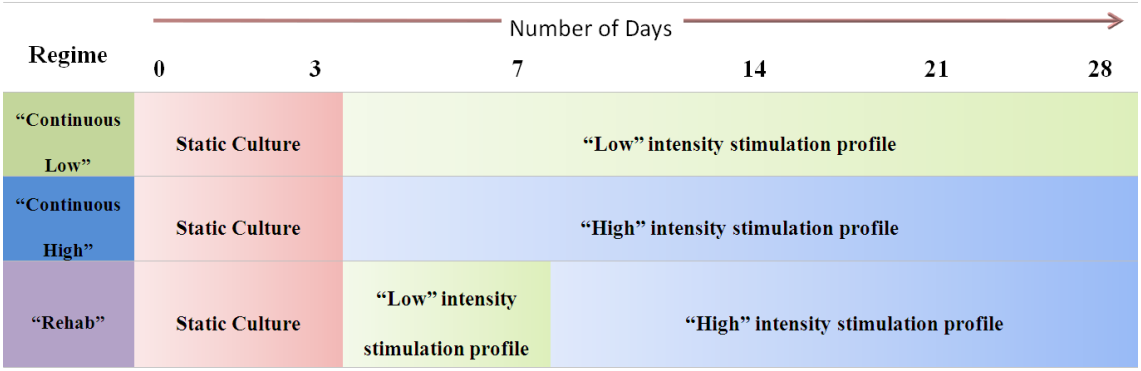

Figure 5-1: Timeline for illustrating the temporal execution of the "low" and "high" intensity stimulation profile for the different dynamic conditioning regimes.

Upon determining the optimal stimulation regime, it would be fully characterized and compared with the static culture of the MSC-seeded AL hybrid SF scaffold (control) over another 28 days of culture duration.

5.2.4. Cell Viability and Proliferation

Each group of the dynamically cultured AL scaffolds ("continuous low", "continuous high" and "rehab") were assayed for viability and cell proliferation using

Alamar Blue™ assay (n=5) at days 3, 7, 14, 21 and 28 following the methods described in Appendix B2. Upon determining the optimal stimulation regime based on all the assessments that would be performed, it would be used to compare with the static culture control (n=5) at days 3, 7, 14, 21 and 28 as well.

5.2.5. Collagen Quantification

The collagen production and deposition of the MSCs in the various dynamically cultured hybrid scaffolds were quantified using SirCol™ collagen assay (n=3) at days 7, 14, 21 and 28 following the method detailed in Appendix B4. Similar to the Alamar Blue™ assay, the optimal regime would be used for comparison with the static culture control at similar time points.

5.2.6. Histological Assessment

With the amount of collagen deposited in each dynamic condition group quantified, it would be of interest to determine their distribution and morphology within the AL scaffold structure. MSC-seeded AL hybrid scaffolds of the three stimulation regime groups (n=3) were harvested for Masson's trichrome staining after 14, 21 and 28 days of culture according to methods described in Appendix B5b. The samples were fixed, paraffin blocked and sectioned longitudinally and transversely as detailed in Appendix B5 prior to performing the staining protocol. Analysis, in terms of diameter measurement, of any collagen fibers formed was made using imaging software (ImageJ 1.38x, Wayne Rasband, NIH, USA) over 20 data points and compared between the experimental groups.

As it was of interest to examine the core of the rolled-up AL scaffolds for cell morphology, ECM protein/collagen production, and ECM protein/collagen distribution over the 28 days experimentation, longitudinal or transverse sections were taken from the core region of the cultured ligament analogues for histological evaluation. The respective stained slides were dehydrated before being mounted on glass cover slips for observation.

Constructs obtained from culturing in the optimal stimulation regime were further assessed for specific ECM proteins distribution within the cultured construct and compared with that of the statically cultured construct at day 28. Transverse construct sections were obtained via cryosection using methods described in Appendix B5. The sections were then immunohistochemically stained for collagen type I, collagen type III and tenascin-C as described in Appendix B5c.

5.2.7. Real-Time qRT-PCR Analysis

To assess the differential effect of various stimulation regime on tenogenic differentiation of the seeded MSCs, gene expressions for ligament-related ECM proteins such as collagen type I, collagen type III, tenascin-C and tenomodulin were analyzed and evaluated. After 14, 21 and 28 days of culture, total RNA was extracted from the cultured AL hybrid scaffolds of the different dynamic conditioning regimes (n=3) as described in Appendix B6 for real-time qRT-PCR analysis. Results from the optimal stimulation regime would then be used to compare with that of the statically cultured control group over the similar 28 days duration.

5.2.8. Western Blot Analysis

After 14, 21 and 28 days of culture, AL hybrid scaffold groups of the optimal stimulation regime and static control were processed for total protein extraction and Western blot performed for collagen I, collagen III and tenascin-C as detailed in Appendix B7. Band signals were detected and relative band intensities (compared to statically cultured AL scaffolds at day 14) were obtained and compared between the two groups.

5.2.9. Biomechanical Test

The AL hybrid SF scaffolds that underwent the three different stimulation regime were tensile tested to failure following the protocol described in section 3.4.2.4. at the different time points (day 7, 14, 21 and 28). AL scaffolds cultured using the optimal stimulation regime would then be compared with statically cultured AL hybrid scaffolds, which served as the control group at similar time points. The load (N) and extension (mm) data was collected over 5 samples for each group and time point, and the failure load, elastic region stiffness, extension at maximum load and extent of toe region were determined after plotting the load displacement curves.

5.2.10. Statistical Analysis

Single factor ANOVA technique and post-hoc Tukey tests were used to assess the statistical significance of multiple comparisons. For pair-wise comparisons, two-tailed, unpaired Student's *t* tests were used. GraphPad Prism ver. 5 (GraphPad Software, Inc.,

CA, USA) was used to implement the statistical analysis. All data were expressed as means ± standard deviation (SD) and $p<0.05$ was considered statistically significant.

5.3. Results

The results obtained for the optimization of mechanical stimulation regime would be presented first under section 5.3.1. Upon determining the optimal stimulation regime, it would be evaluated fully with the static cultured control group, with the results being presented under section 5.3.2.

5.3.1. Results from Optimization of Mechanical Stimulation Regime

5.3.1.1. Cell Viability and Proliferation

Alamar Blue™ assay revealed that, as compared to the "continuous high" group, cell viability for AL scaffolds from the other two stimulation regimes ("continuous low" and "rehab") were significantly higher after 7 days of culture (Figure 5-2; $p<0.01$). "Rehab" group had significantly more viable cells on day 14 only when compared with the other two regimes ($p<0.01$). Scaffolds from the "rehab" group had 42% (day 7), 76% (day 14), 64% (day 21) and 62% (day 28) more cells when compared to the "continuous high" group ($p<0.01$) and 12% (day 14) more cells when compared to the "continuous low" group ($p<0.01$).

The proliferation trends for different stimulation regimes were also observed in Figure 5-2. There was consistent proliferation for constructs from the "continuous low" group up till day 21 ($p<0.05$), but for constructs from the "rehab" group, proliferation

was only found up till day 14 ($p<0.05$). Thereafter, there was no significant proliferation observed for the "rehab" group as percentage reduction of Alamar Blue reached a plateau. There was no significant proliferations in the "continuous high" group ($p>0.05$) within the same 28 days culture period.

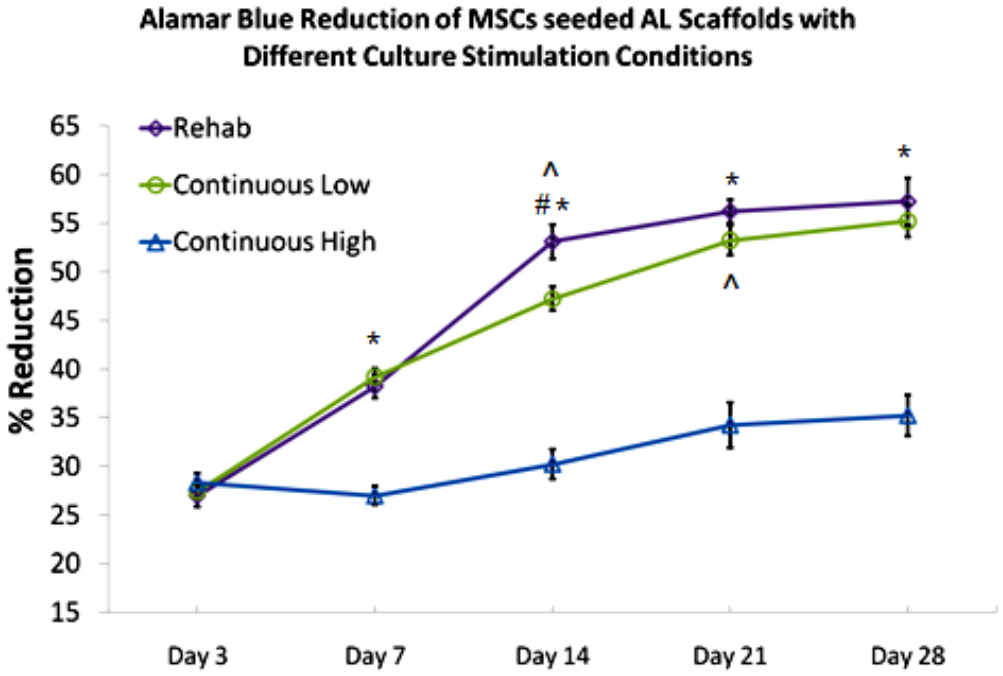

Figure 5-2: Alamar Blue™ assay illustrating consistent and significantly more viable cells in the "continuous low" and "rehab" groups compared to the "continuous high" group from day 7 onwards (*$p<0.01$, Student's t-test, n=5) with "rehab" having significantly more viable cells compared to both groups on day 14 only (#$p<0.01$, Student's t-test, n=5). Significant proliferation (^$p<0.05$, ANOVA and post-hoc Tukey tests, n=5) was observed in the "rehab" group up to day 14 and "continuous low" group up to day 21.

5.3.1.2. Collagen Synthesis

Insoluble collagen assay was performed to determine the amount of deposited collagen on the AL hybrid scaffolds that were mechanically stimulated by the various conditioning regime to qualitatively indicate the extent of ECM formation. This quantification assay revealed that there was significant increase ($p<0.05$) in collagen

production and deposition in both the "continuous low" and "rehab" groups over the culture duration (Figure 5-3) for both culture conditions. AL scaffolds subjected to "continuous high" stimulation regime, however, did not exhibit significant increase in collagen deposition through the experimental period ($p>0.05$).

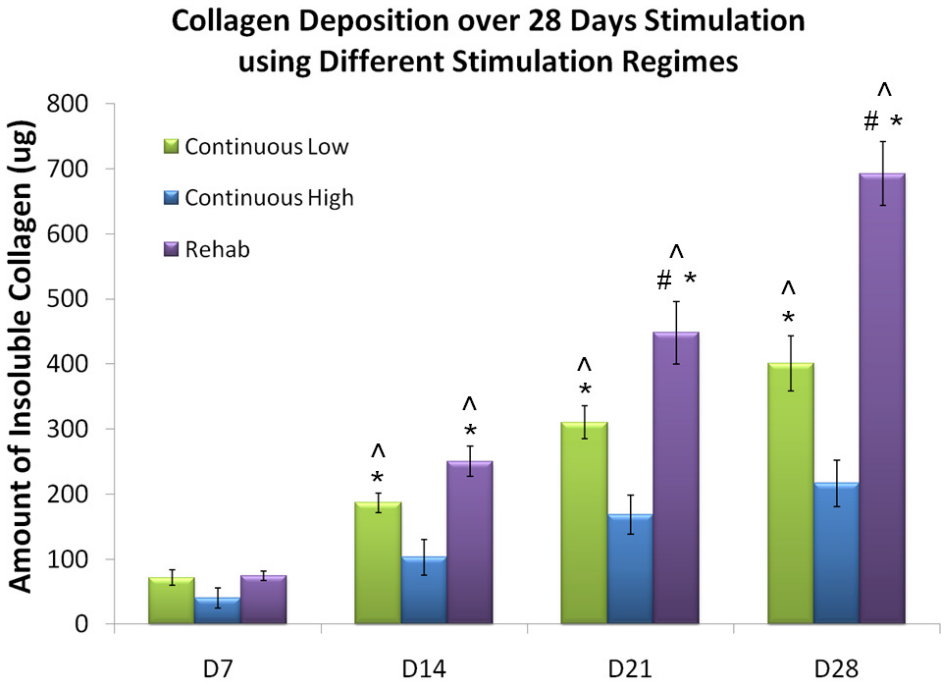

Figure 5-3: SirCol™ assay for amount of collagen deposited per scaffold sample. Significant increase in collagen deposition was observed in the "continuous low" and "rehab" groups as compared to the "continuous high" group from day 14 onwards (*p < 0.01, Student's t-test, n=3). Significantly more collagen was deposited in the "rehab" group as compared to the "continuous low" group from day 21 onwards (#p < 0.01, Student's t-test, n=3). Significant increase in collagen deposition was observed for "continuous low" and "rehab" respectively from day 14 onwards over the experimental period (^p<0.05 ANOVA and post-hoc Tukey tests, n=3).

Among the three stimulation regimes, significant difference was found in constructs stimulated by "continuous low" and "rehab" as compared to "continuous high" from day 14 onwards, with "continuous low" group having 85% and "rehab" group having 220% more collagen deposited at day 28 than "continuous high" group ($p<0.01$). Significantly more collagen was deposited in the "rehab" group from day 21 onwards when compared with the "continuous low" group (day 28: 73% more; $p<0.01$).

5.3.1.3. Histological Analysis

Masson's trichrome staining was performed on longitudinal and transverse sections of the central core portion of the AL hybrid scaffolds cultured in the three stimulation regimes after 14, 21 and 28 days of culture to assess ECM (specifically collagen) production, morphology and distribution within the scaffold qualitatively (Figure 5-4 and 5-5).

Consistent with previous observations, aligned ECM deposition was observed in the longitudinal sections of the AL hybrid scaffolds (Figure 5-4), regardless of the dynamic regime used. However, the density at which aligned ECM deposition and the consequent collagenous structure formation varied with the dynamic conditioning regime used. For the case of "continuous high" regime, very low cell and ECM density was observed throughout the AL scaffold construct from day 14 onwards. Although cell and ECM density increased over the experimental duration, with cell colonies of elongated morphologies forming by day 28, it was not sufficient for observable collagenous structure to be formed. On the contrary, aligned ECM depositions and collagenous structure formations (stained blue) were observed in the "continuous low" and "rehab" group, with the "rehab" group having thicker and denser collagenous structures formed by day 21. Extensive collagen deposition and fiber formation was demonstrated in the "rehab" group by day 28, with the formation of ligament-like microstructural "crimp" patterns in the collagen fibers. Aligned cells were also observed to be interspersed between the collagen fibers formed. Nevertheless, the collagen fibers were not as compact and dense as the native tissue, as voids were observed between the fragmented collagen fibers.

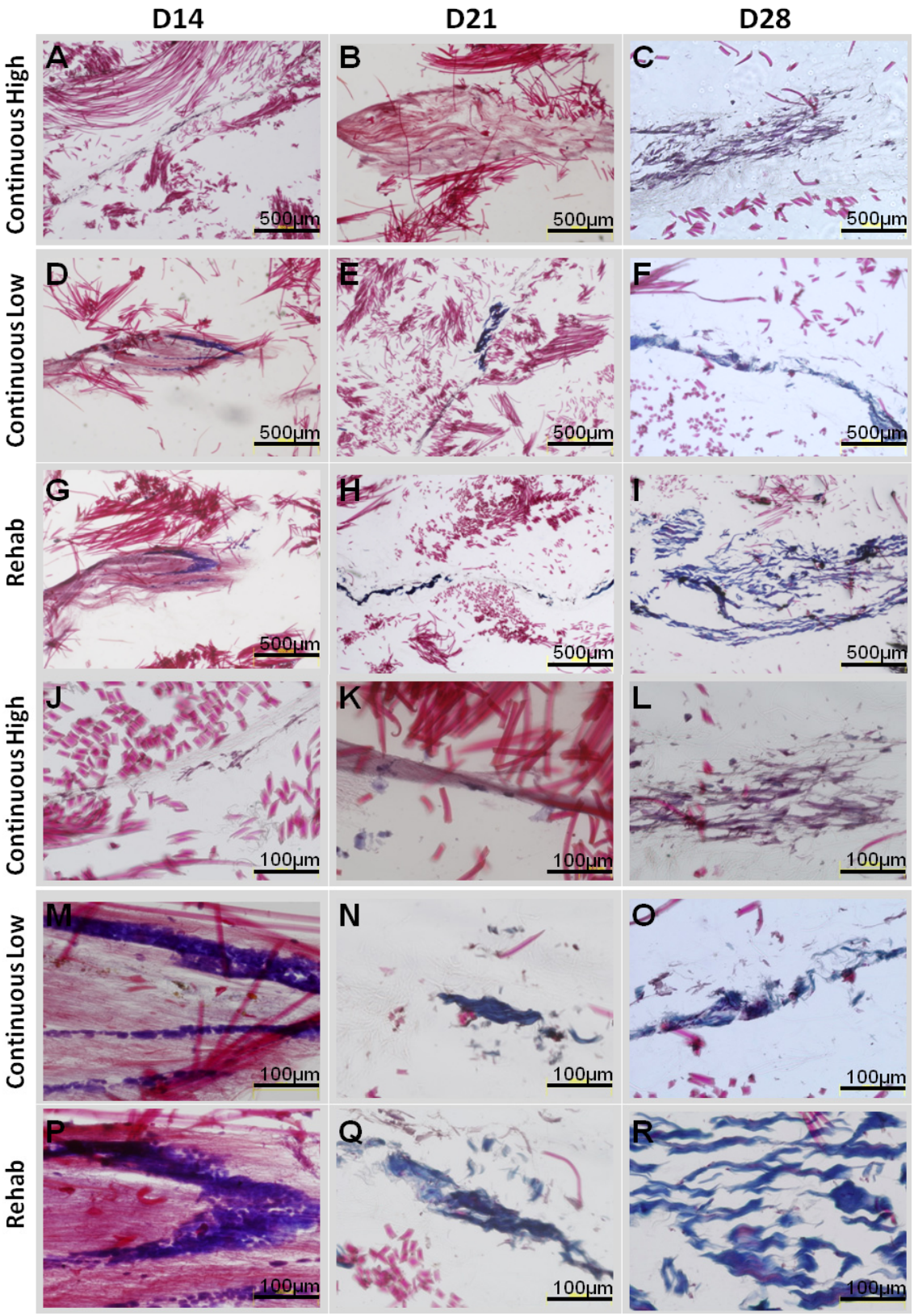

Figure 5-4: Longitudinal sections of Masson's trichrome stained AL hybrid scaffolds that underwent the different dynamic conditioning regime and observed at various timepoints. Magnification: (A-I) 40× and (J-R) 200×.

From the transverse sections (Figure 5-5), it was observed that the distribution of cells and the eventual collagenous structures were limited to the space in between adjacent layers of rolled-up hybrid scaffold stimulated by the "continuous low" and "rehab" regime since day 21 (Figure 5-5 E, F, H, I). As for the "continuous high" group, there was significantly less cells observed from the early day 14 stage, hence cellular and ECM structures were not observed readily throughout the scaffolds of this group through the experimental period. From these observations, it was thus deduced that infiltration of the cells through the AL-SFEF into the knitted SF component had been limited. Nevertheless, this phenomenon had in turn aided in concentrating the cells that were present and attached in the scaffold to a limited space, which eventually made it favorable for the formation of collagenous bands to occur.

As with the longitudinal sections, cell and ECM density had been very low in the "continuous high" group through the 28 days culture period. Sections from the "continuous low" and "rehab" group, on the other hand, showed collagen fiber band formation from day 21, with 87.6% significantly thicker collagen fibers formed in the "rehab" group as compared to the "continuous low" group at day 28 ("continuous low": 11.3 ± 2.0 μm and "rehab": 21.2 ± 4.7 μm; $p<0.01$). This indicated that the "rehab" stimulation regime provided dynamic cues that were more effective in triggering the formation of collagen fibers and continuously straining these fibers efficiently to achieve collagen fiber thickening and consequently tissue maturation.

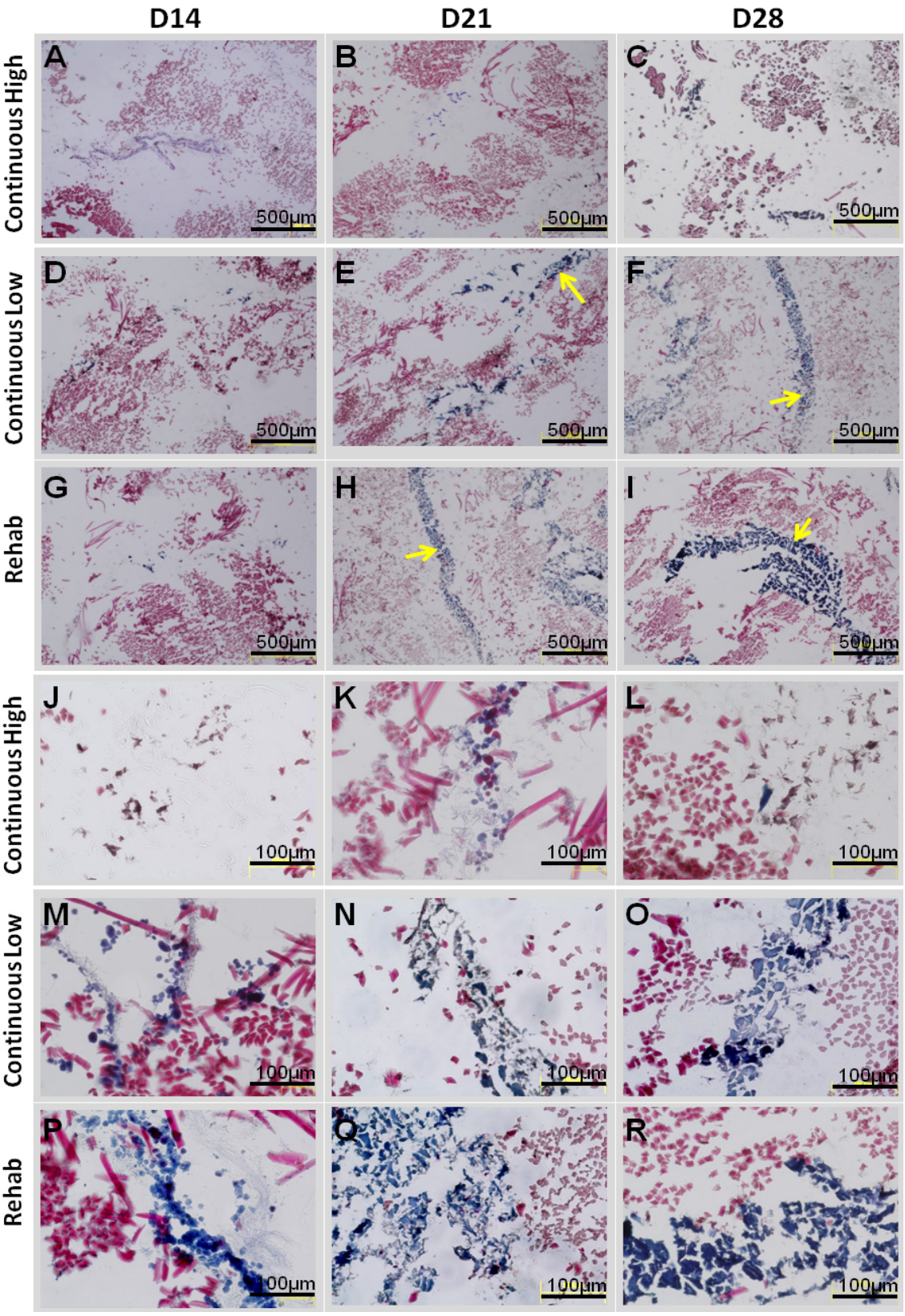

Figure 5-5: Longitudinal sections of Masson's trichrome stained AL hybrid scaffolds that underwent the different dynamic conditioning regime and observed at various timepoints. Arrows indicate the collagen bands formed within rolled-up scaffold. Magnification: (A-I) 40× and (J-R) 200×.

5.3.1.4. Gene Expression of Ligament-related ECM Proteins using Real-Time qRT-PCR

The expression of ligament-related genes in AL hybrid scaffolds conditioned via the different regimes were evaluated via real-time qRT-PCR. Results showed that gene expression across the targeted genes were up-regulated at all the time points tested in both the "continuous low" and "rehab" groups relative to the "continuous high" group (Figure 5-6). Specifically, there was no significant increase for the "continuous high" group in gene expression of the targeted genes throughout the experimental duration, except for expression in collagen I during the period from day 21 to day 28 (Figure 5-6A). When comparing between the "continuous low" and "rehab" groups, significantly higher expression in collagen I was found from day 14 onwards, collagen III from day 21 onwards, tenascin-C from day 21 onwards and tenomodulin from day 28 onwards. By day 28, all targeted genes were significantly expressed in the "rehab" group compared to the "continuous low" group (collagen I: 9.2% higher, collagen III 65.2% higher, tenascin-C: 70.5% higher, tenomodulin: 47.6% higher, $p<0.05$).

Interestingly, it was observed that the gene expression for collagen I of the "rehab" group decreased during the period between day 21 to day 28 but increased for the "continuous low" group within the same period (Figure 5-6A). A different set of observation was made for collagen III, whereby collagen III expression continued to increase from day 21 to day 28 in the "rehab" group but decreased for the "continuous low" group during the same period (Figure 5-6B).

For tenascin-C and tenomodulin, gene expressions plateaued for the "continuous low" group but continued to increase for the "rehab" group through the experimental period. It was thus indicative that the "rehab" regime had the capacity to stimulate consistently increasing gene expression especially for collagen III, tenascin-C and tenomodulin; of which, tenascin-C and tenomodulin are important ECM components necessary for ligament elasticity and collagen fiber maturation respectively.

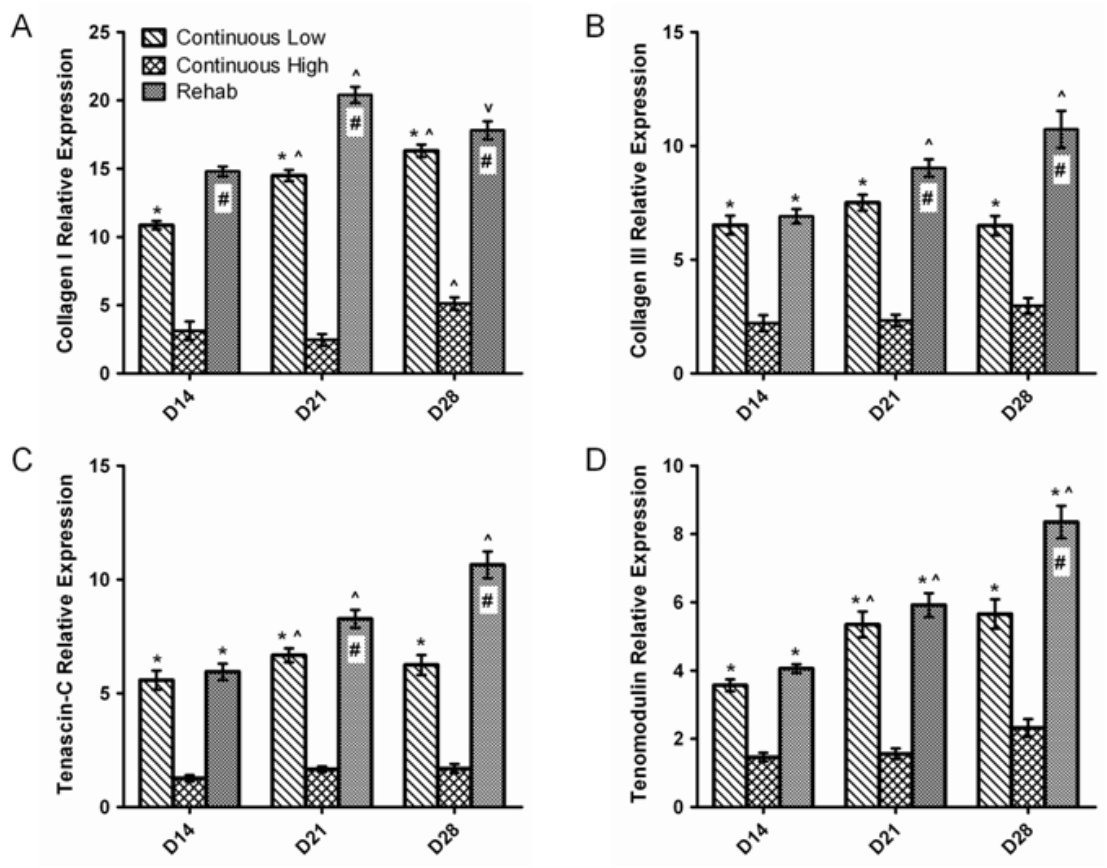

Figure 5-6: Gene expression for ligament-related ECM components were up-regulated in the "continuous low" and "rehab" groups as compared to the "continuous high" group (*p<0.05). Gene expression of "rehab" group was significantly higher than the "continuous low" group in all the targeted genes by day 28 (#p<0.05). Significant increase over the culture duration was observed for targeted genes of all groups except for collagen I in the "rehab" group at day 28 (^p<0.05 for increase and ^{v}p<0.05 for decrease). Levels were quantified using real time RT-PCR and were normalized to the housekeeping gene, GAPDH (n=3).

5.3.1.5. Tensile Properties of Dynamically Cultured AL Hybrid Scaffold using Different Stimulation Regimes

Dynamically cultured rolled-up hybrid scaffolds stimulated using the three different regimes were tested for their tensile properties at days 7, 14, 21 and 28, as tabulated in Table 5-2. The samples were tested to failure and ruptures were generally noted to initiate from the centre region of the entire gauge length, though exact rupture site was inconsistent across samples. Load-displacement curves plotted revealed the toe region, linear region, microfailure region and failure region, similar to that of native ACLs (Figure 5-7).

Table 5-2: Mechanical properties of dynamically cultured scaffold samples by different stimulation regimes (n=5, data: mean ± SD). ^p<0.05 when compared to the previous time point for each group respectively. #p<0.05 when the "rehab" group was compared to both the "continuous low" and "continuous high" groups at each time point.

Samples		Maximum load (N)	Stiffness (N/mm)	Extension at maximum load (mm)
Continuous Low	Day 7	144.33 ± 5.03	24.33 ± 1.40	11.46 ± 3.51
	Day 14	172.08 ± 6.28^	26.93 ± 2.40	10.99 ± 2.67
	Day 21	197.12 ± 14.54^	32.13 ± 3.20	11.26 ± 2.79
	Day 28	207.10 ± 12.07	38.23 ± 3.65^	13.15 ± 3.22
Continuous High	Day 7	127.33 ± 5.69	19.28 ± 2.20	9.25 ± 2.32
	Day 14	142.67 ± 3.21	24.55 ± 0.86^	9.89 ± 2.16
	Day 21	134.00 ± 5.57	25.66 ± 2.13	10.12 ± 3.12
	Day 28	162.00 ± 12.53	29.34 ± 3.11	10.26 ± 3.03
Rehab	Day 7	143.59 ± 5.07	25.18 ± 1.45	11.51 ± 2.58
	Day 14	192.83 ± 14.38^	35.15 ± 0.94^#	11.69 ± 3.52
	Day 21	227.26 ± 10.55^#	37.65 ± 2.32#	12.91 ± 3.09
	Day 28	238.08 ± 19.29#	44.44 ± 2.84^#	13.93 ± 2.16

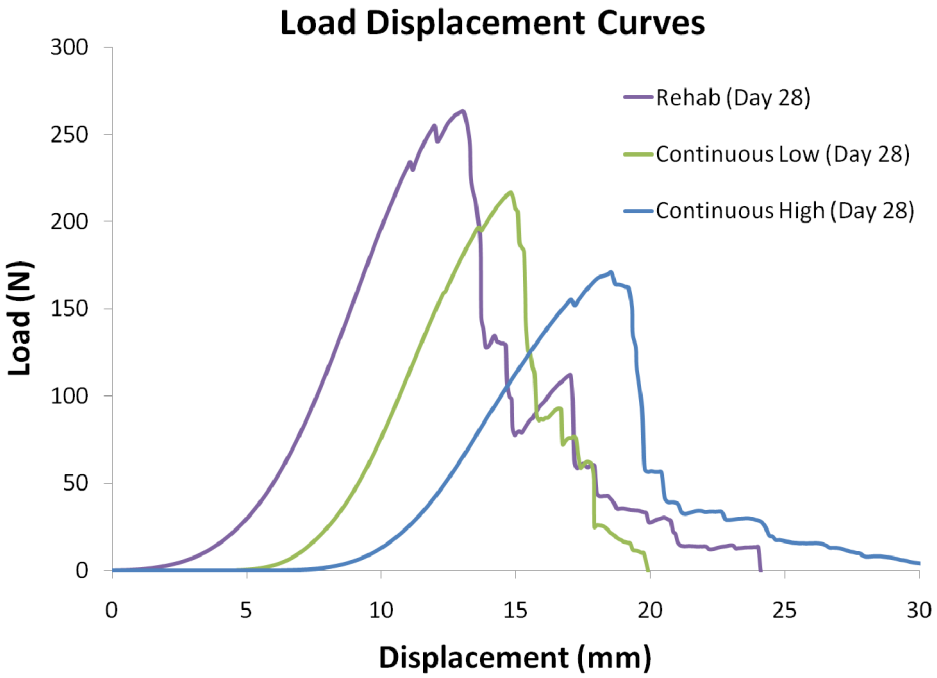

Figure 5-7: Representative load–displacement curves for AL hybrid scaffolds cultured in the different stimulation regimes at day 28.

Significant increase in the maximum load measured was observed in both the "continuous low" and "rehab" groups from days 14 ($p<0.05$) but this trend did not persist through the whole duration of the study as the increase from day 21 to day 28 was found to be insignificant for both groups ($p>0.05$; Table 5-2). The "continuous high" group did not exhibit any significant increase in the maximum load through the duration of this study ($p>0.05$). In terms of construct stiffness, significant increase was found after 28 days for the "continuous low" group and at 14 days for the "continuous high" group ($p<0.05$), which did not persist thereafter as the increase observed was not significantly different ($p>0.05$). For the "rehab" group, significant increase was found during the period from day 7 to day 14 and from day 21 to day 28 ($p<0.05$). No significant increase was found for the extension at maximum load through the experimental period for all three groups.

When the "rehab" group was compared with the other two stimulation regimes, significantly higher maximum load was found from day 21 onwards, with the "rehab" group being 15.0% stronger than the "continuous low" and 47.0% stronger than "continuous high" at day 28 ($p<0.05$; Table 5-2). The stiffness measured was also significantly more in the "rehab" group as compared to the other two regimes from as early as day 14 onwards, with the "rehab" group being 16.2% stiffer than the "continuous low" and 51.5% stiffer than "continuous high" at day 28 ($p<0.05$). Likewise, no significant difference were found when the extension at maximum load of the "rehab" group was compared with the other two groups at the various time points ($p>0.05$).

AL scaffolds cultured with "rehab" regime exhibited larger extents of toe region after 28 days of culture as compared to the "continuous high" regime ("rehab": 7.20 ± 2.13 mm, "continuous high": 3.60 ± 1.47 mm; $p<0.05$), while no significant differences were observed when compared to the "continuous low" group ("continuous low": 5.23 ± 1.32 mm; $p>0.05$).

5.3.2. Results from Characterization of the "Rehab" Mechanical Stimulation Regime

From the optimization study conducted using the three stimulation regimes, it was concluded that the "rehab" mechanical stimulation regime was more suitable for dynamic culture of the AL SF hybrid construct for tissue engineering of the ligament. Hence a full characterization of AL scaffolds cultured using this regime was done and compared with the static culture through 28 days period.

5.3.2.1. Cell Viability and Proliferation

Alamar Blue™ assay revealed that, as compared to the statically cultured AL scaffolds, cell viability was significantly higher when the MSC-seeded AL hybrid scaffolds were cultured in the "rehab" stimulation regime after 14 days of culture (Figure 5-8; $p<0.01$). Scaffolds from the "rehab" group had 20% (day 14), 14% (day 21) and 10% (day 28) more cells when compared to the statically cultured control group ($p<0.01$).

The proliferation trends were also observed to be significantly different between the two groups as shown in Figure 5-8. There was consistent proliferation for constructs that were statically cultured up till day 21 ($p<0.05$), but for constructs from the "rehab" group, proliferation was only found up till day 14 only ($p<0.05$). Thereafter, there was no significant proliferation observed for the "rehab" group as percentage reduction of Alamar Blue reached a plateau.

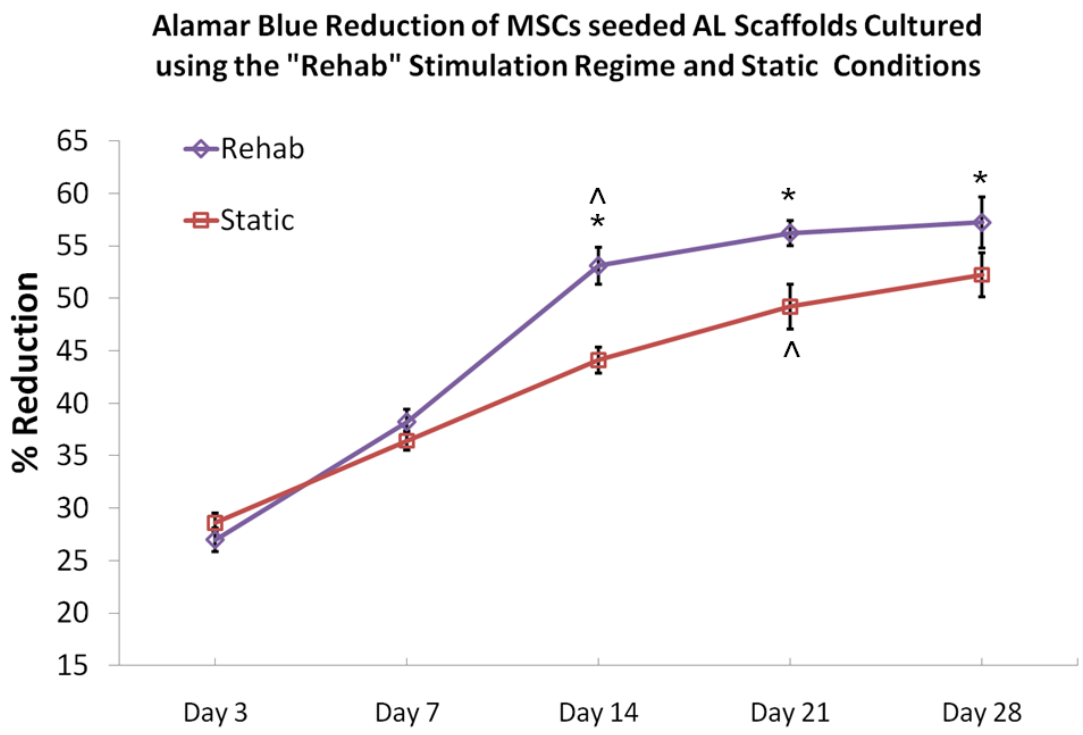

Figure 5-8: Alamar Blue™ assay illustrating consistent and significantly more viable cells in the "rehab" group compared to the statically cultured group from day 14 onwards (*p<0.01, Student's t-test, n=5)). Significant proliferation (^p<0.05, ANOVA and post-hoc Tukey tests, n=5) was observed in the "rehab" group up to day 14 and up to day 21 for statically cultured AL scaffolds.

5.3.2.2. Collagen Synthesis

Insoluble collagen assay was performed to determine the amount of deposited collagen on the AL hybrid scaffolds that were mechanically stimulated using the "rehab" conditioning regime to quantitatively indicate the extent of ECM formation. Statically cultured AL hybrid scaffolds were used as control. This quantification assay revealed that there was significant increase ($p<0.05$) in collagen production and deposition in the "rehab" group over the culture duration (Figure 5-9). However, for the statically cultured group, significant increase in collagen deposition was found from day 7 to day 14 only ($p<0.05$), with the production level reaching a plateau thereafter.

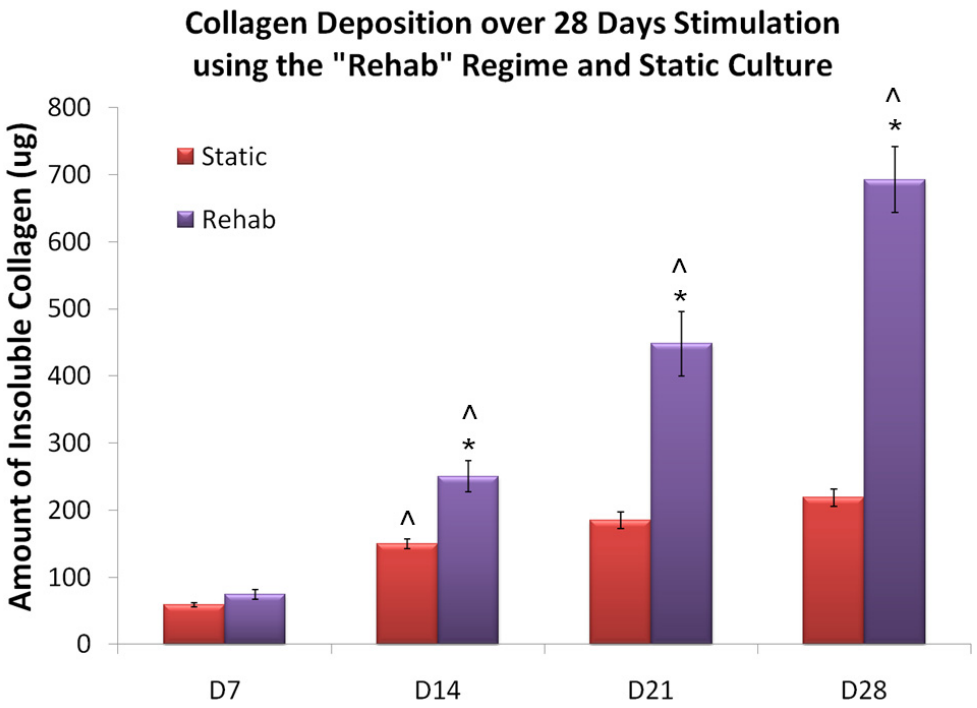

Figure 5-9: SirCol™ assay for amount of collagen deposited per scaffold sample. Significant increase in collagen deposition was observed in the "rehab" group as compared to the statically cultured group from day 14 onwards (*p < 0.01, Student's t-test, n=3). Significant increase in collagen deposition was observed consistently for the "rehab" group from day 14 onwards over the experimental period, while significant increase was only observed from day 7 to day 14 for the statically cultured group (^p<0.05 ANOVA and post-hoc Tukey tests, n=3).

When compared to the statically cultured constructs, significant difference was found in constructs stimulated by the "rehab" regime from day 14 onwards (day 14: 67% more, day 21: 143% more, day 28: 217% more; $p<0.01$).

5.3.2.3. Histological Analysis

Immunohistochemical staining was performed on the transverse sections of the central core portion of the AL hybrid scaffolds cultured in the "rehab" stimulation regime and static conditions after 28 days to assess for ligament-related ECM production, morphology and distribution within the scaffold qualitatively (Figure 5-10).

The immunohistochemical staining for type I collagen was strongly positive in the regenerated tissue of the "rehab" group. Type III collagen and tenascin-C on the other hand showed up less strongly in the "rehab" group. When referenced to the normal ligament, similar high composition of collagen I was observed compared to collagen III and tenascin-C, whereby 90% of the native ligament consists of collagen I, 9% collagen III and other proteoglycans [48]. The regenerated tissue using the "rehab" stimulation regime was thus consistent in composition with the ECM of native ligaments.

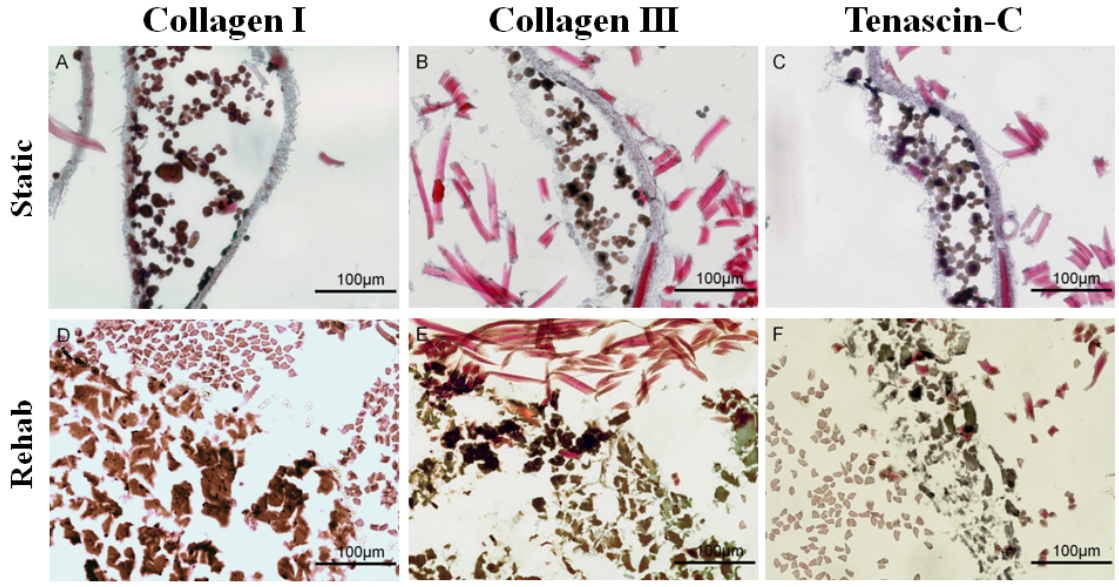

Figure 5-10: Transverse sections of immunochemical stained (collagen I, collagen III and tenascin-C) AL hybrid scaffolds that underwent the "rehab" conditioning regime and static culture as observed at day 28. Magnification: 200×.

It was also noted that thicker and denser collagen fibers were observed for the "rehab" group as compared to the static group after 28 days of culture. Nevertheless, the distribution of these collagenous structures were limited to the space in between adjacent layers of rolled-up hybrid scaffold and were sandwiched in between layers of AL-SFEF meshes as observed in both the groups.

5.3.2.4. Gene Expression of Ligament-related ECM Proteins using Real-Time qRT-PCR

The expression of ligament-related genes in AL hybrid scaffolds conditioned via the "rehab" conditioning regime was evaluated via real-time qRT-PCR. Results showed that gene expression across the targeted genes were up-regulated at all the time points tested in the "rehab" group relative to the statically cultured group (Figure 5-11). Specifically at day 28, collagen I was 117% higher, collagen III was 112% higher, tenascin-C was 338% higher, and tenomodulin 279% higher in the "rehab" group than the statically cultured group at the same time point.

For the statically cultured group, significant increase in gene expression was found in the period of day 14 till day 21for collagen I, tenascin-C and tenomodulin, of which tenascin-C and tenomodulin were down-regulated from day 21 to day 28, though with no significance ($p>0.05$). Collagen III was up-regulated by day 28 in the statically cultured group ($p<0.05$).

For the "rehab" group, up-regulation of all targeted genes was observed from day 14 onwards, with a significant down-regulation in collagen I after 21 days of dynamic culture. These results indicated that the "rehab" stimulation regime could stimulate sustained and consistent up-regulation of specific ligament genes as compared to the static culture conditions. This was especially so for tenascin-C and tenomodulin, which were consistently up-regulated in the "rehab" group to trigger collagen fiber build-up and thickening, leading to overall tissue maturation, as observed from the histological images.

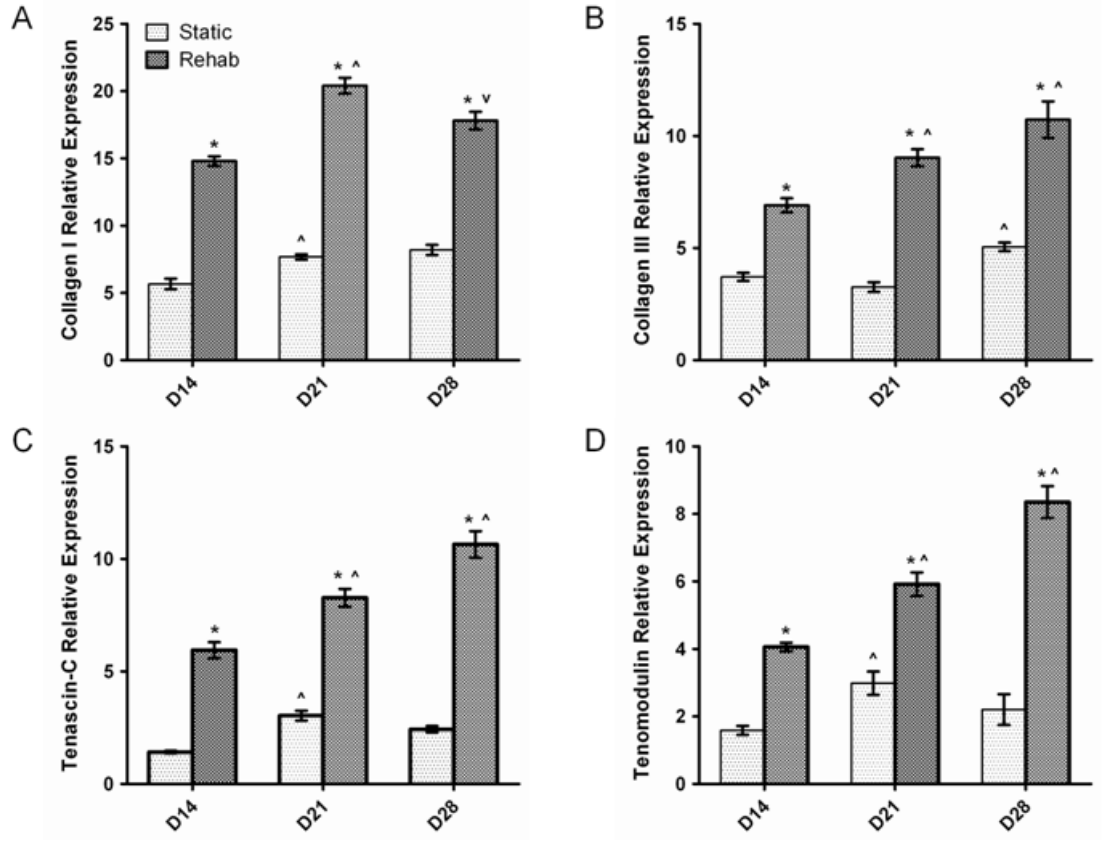

Figure 5-11: Gene expression for ligament-related ECM components were up-regulated in the "rehab" group as compared to the statically cultured group (*p<0.05). Significant increase over the culture duration was observed for targeted genes of the "rehab" group, except for collagen I at day 28 (^p<0.05 for increase and ^{v}p<0.05 for decrease). Levels were quantified using real time RT-PCR and were normalized to the housekeeping gene, GAPDH (n=3).

5.3.2.5. Western Blot Analysis

Protein expressions for collagen I, collagen III and tenascin-C were detected for the "rehab" group and the static control after 14, 21 and 28 days of culture (Figure 5-12). Analysis was performed on densitometric data of the optical intensity of each lane expressed in the Western blot membranes, which was normalized to statically cultured AL scaffolds at day 14.

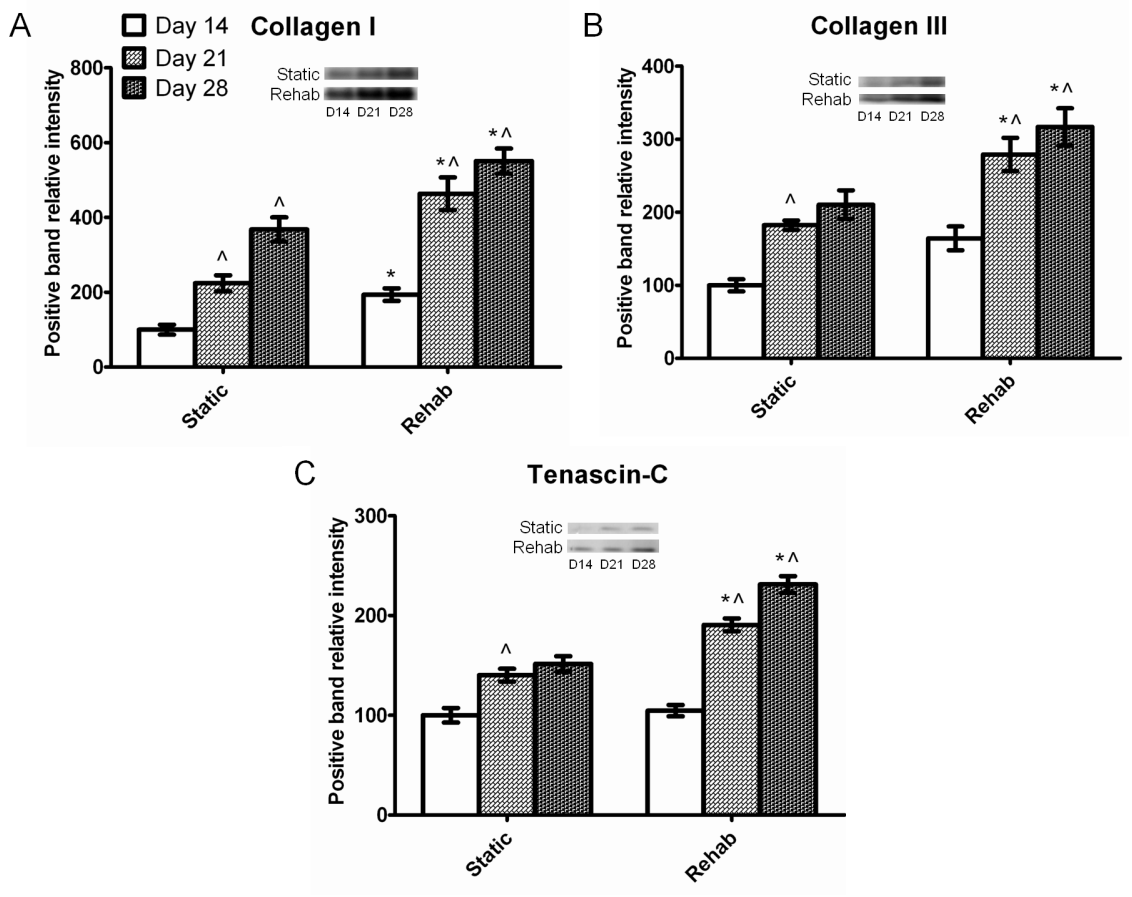

Figure 5-12: Western blot analysis of ligament-related ECM proteins produced by MSCs cultured on the AL scaffolds and dynamically ("rehab" regime) and statically cultured for 14, 21 and 28 days. The results were normalized to data obtained from AL scaffolds statically cultured for 14 days and evaluated on a relative basis for comparison between different samples (n=3). Significantly more type I collagen was produced in the "rehab" group than static group from day 14 onwards, while significance was observed for type III collagen and tenascin-C after 21 (*p < 0.05). Significant increases were found as compared to the previous time point in each group (^p<0.05).

The results demonstrated that the matrix of the cultured ligament analogues using the "rehab" regime composed mainly of type I and III collagen and tenascin-C, with collagen I being predominant as its expression was consistently higher in both dynamically and statically cultured AL scaffolds when compared to collagen III and tenascin-C. Significantly more collagen I was expressed in the "rehab" group than the static control from day 14 onwards (day 14: 93.4% more, day 21: 106.7% more, day 28:

49.7% more), while significance was found for collagen III and tenascin-C from day 21 onwards (on day 28: collagen III: 50.7% more and tenascin-C: 52.6% more; $p<0.05$).

For the static control, significant increase for collagen I was found through the 28 day study (day 14 to day 21: 124.1% more, day 21 to day 28: 64.1; $p<0.05$), while significant increases for collagen III and tenascin-C were only found from day 14 to 21 (collagen III: 82.2% more, tenascin-C: 40.2% more; $p<0.05$). No significant increase was found for these proteins thereafter ($p>0.05$). However for the "rehab" group, significant increase was found for all three targeted proteins through the experimental period ($p<0.05$). Similar trends were observed in the RT-PCR results for the "rehab" group as shown previously, except for collagen I which was shown to decrease in gene expression in the period of day 21 to day 28. The reason for the consistent increasing deposition of collagen I, as determined via Western blot analysis, was likely due to time lag between gene expression and the actual protein synthesis.

5.3.2.6. Tensile Properties of Dynamically Cultured AL Hybrid Scaffold using the "Rehab" Conditioning Regime

Dynamically cultured rolled-up hybrid scaffolds stimulated using the "rehab" regime and the statically cultured equivalents were tested for their tensile properties at days 7, 14, 21 and 28, as tabulated in Table 5-3. The samples were tested to failure and ruptures were generally noted to initiate from the centre region of the entire gauge length, though exact rupture site was inconsistent across samples. Load-displacement curves plotted revealed the toe region, linear region, microfailure region and failure region, similar to that of native ACLs (Figure 5-13).

Table 5-3: Mechanical properties of dynamically cultured scaffold samples using "rehab" stimulation regime (n=5, data: mean ± SD). ^p<0.05 when compared to the previous time point for each group respectively. #p<0.05 when the "rehab" group was compared to statically cultured group at each time point.

Samples		Maximum load (N)	Stiffness (N/mm)	Extension at maximum load (mm)
Static	Day 7	138.50 ± 9.19	23.29 ± 1.38	9.39 ± 2.89
	Day 14	158.00 ± 8.49	26.22 ± 0.92	12.45 ± 3.64
	Day 21	182.50 ± 9.19^	29.34 ± 2.32	11.84 ± 2.72
	Day 28	200.50 ± 10.61	34.23 ± 3.22	12.98 ± 2.93
Rehab	Day 7	143.59 ± 5.07	25.18 ± 1.45	11.51 ± 2.58
	Day 14	192.83 ± 14.38^#	35.15 ± 0.94^#	11.69 ± 3.52
	Day 21	227.26 ± 10.55^#	37.65 ± 2.32#	12.91 ± 3.09
	Day 28	238.08 ± 19.29#	44.44 ± 2.84^#	13.93 ± 2.16

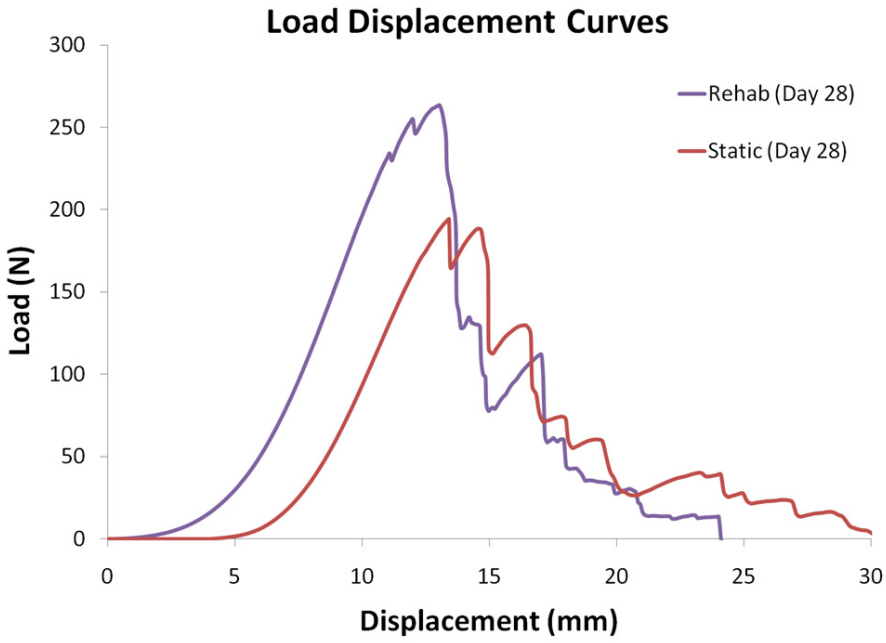

Figure 5-13: Representative load–displacement curves for AL hybrid scaffolds cultured in the "rehab" stimulation regime and static conditions at day 28.

When the "rehab" group was compared with the static control, significantly higher maximum load was found from day 14 onwards (day 14: 22.0%, day 21: 24.5%, day 28: 18.7%; $p<0.05$). The stiffness measured was also significantly more in the "rehab" group as compared to the statically cultured group from as early as day 14 onwards (day 14: 34.0%, day 21: 28.3%, day 28: 29.8%; $p<0.05$). No significant difference were found when the extension at maximum load of the "rehab" group was compared with the statically cultured group at the various time points ($p>0.05$).

AL scaffolds cultured with "rehab" regime exhibited larger extents of toe region after 28 days of culture as compared to the statically cultured group ("rehab": 7.20 ± 2.13 mm, static: 4.40 ± 1.11 mm; $p<0.05$).

5.4. Discussion

In this chapter, the "rehab" mechanical stimulation regime was compared with the other stimulation regimes that were executed continuously from day 3 post-seeding. The "high" and "low" stimulation profile were first identified based on the average physiological activity of the ligament in terms of the number of cycles per day obtained from pedometer results [262]. The onset of these stimulation profiles were then varied in the three stimulation regimes characterized. It was demonstrated that the "rehab" regime stimulated marked increase in cell viability as compared to the "continuous high" regime and supported initial MSC proliferation, which plateaued after 14 days of culture. The proliferation phase was then transited to the differentiation phase, whereby significantly higher collagen deposition was observed in the "rehab" group as compared "continuous low" and "continuous high" groups from day 21 onwards. This result was

supported qualitatively via histological evaluation, which illustrated higher levels of ligament-related ECM deposition, with formation of thicker collagen fibers by day 28 as compared to groups stimulated by the other two stimulation regimes and statically cultured constructs. Real-time qRT-PCR results also showed significantly higher expression for ligament-related genes, especially tenascin-C and tenomodulin, in the "rehab" group. Increased ligament-related ECM components were found for the "rehab" group and quantitatively ascertained to produce constructs of closer biochemical compositions to the native tissue. Such elevated production and deposition of fundamental ECM components was translated to superior functional aspects, whereby mechanically stronger and stiffer constructs were obtained as compared to the other stimulation regimes and static culture conditions tested. Therefore, with an appropriate temporal tissue conditioning at the respective phase of growth, as provided by the "rehab" regime, it was likely that seeded aligned MSCs could be induced to further synthesize collagen and ECM in a controlled *in vitro* environment for the regenerated construct to develop and become more mechanically robust before subjecting it to physiological environment.

5.4.1. Determination of the Onset of Specific Mechanical Stimulation Profiles in the Rehabilitative Approach

In the course of determining the appropriate onset for the implementation of mechanical stimulation, it was essential to understand the cellular response towards mechanical cues given at different stages of cell growth. Particularly, Chen *et al.* [245] found that MSCs' metabolic activity typically increased after 9 days of static culture

and that mechanically loading cell seeded matrices in the early stages of cell growth (1-3 days post-seeding) was detrimental. Excessively early mechanical stimulation was found to inhibit cell proliferation and differentiation instead of enhancing it, possibly due to the lack of initial cellular anchorage with the scaffold as ECM deposition were not established yet. It is thus a prerequisite to have sufficient cell-to-cell contact and cell-to-ECM interactions, through the formation of integrins, to gain the benefits of mechanical conditioning. As such, a 3 day static culture period was given to all the dynamically conditioned groups.

Thereafter, MSCs enter a proliferative phase during the period from day 3 to day 9. At the end of this phase, MSCs would up-regulate the expression of ECM-specific genes, such as collagen type I and fibronectin, to indicate the onset and progression of the differentiative phase [268-271]. It was often agreed that the onset for dynamic conditioning should only start from the initiation of this phase, which would be marked by increase in metabolic activity and up-regulation of ECM-specific genes, in order for cell survival and positive response to mechanical stimuli [268-271].

Nevertheless, in this study, we attempted to provide low intensity mechanical stimulation in the early proliferative phase with the aim to precondition the cells such that better cell-to-cell and cell-to-ECM linkages could be fostered, leading to improved response to the full dose of stimulation that would be effected later. This was motivated by the success of rehabilitation as a form of post-surgical treatment provided to patients with their ACLs replaced. Minimal loading of the newly replaced ACL was done to stimulate bone integration and prepare the replaced ACL for more intense activities in time to come. As shown by results obtained, proliferation was not adversely affected

with the implementation of the "low" intensity stimulation profile at day 4, instead, proliferation was shown to be comparable to that of statically cultured constructs.

With the onset of early low intensity stimulation, the high intensity stimulation profile could begin at day 7, which aid in stimulating marked increase in proliferation rate to day 14, which subsequently plateaued indicating the initiation of the differentiative phase. This was positively indicated by the up-regulation of ligament-related ECM genes and increased deposition of ECM components.

5.4.2. Suitability of the "Rehab" Regime for Prolonged Mechanical Stimulation

It was necessary to continuously provide this form of stimulation over an extended duration to assess its effectiveness. This was so as the cells would enter a phase of ECM maturation after the proliferative and differentiative phases. During this phase, cell proliferation would be restricted [268-271, 309-312] and it would then be necessary to continually provide specific differentiation signals, such as mechanical stimulations or growth factors, in order that the remaining cells would continue to proliferate and be metabolically active to continue ECM deposition [268]. Prolonged mechanical stimulation study as such would be important in determining if the "rehab" regime would be sufficient or excessive in the tissue maturation phase.

Indeed it was found from gene expression results that although type I collagen was more up-regulated than type III collagen throughout 28 days and showed an increasing trend in its expression through the first 21 days of culture, it was down-regulated on the

28th day, while collagen III gene expression was still increasing. It was favorable for collagen I to be expressed more than collagen III as this would better mimic the biochemical composition of healthy ligament, and indicate progressive tissue regeneration. Nevertheless, the down-regulation of collagen I and continuous up-regulation of collagen III on day 28 could indicate imminent scar tissue formation. The scar tissue is typically thicker and more cellular compared with the native tissue. It is usually formed at the injured sites for rapid closure of wound, and for the case of ligaments, to provide as an accelerated healing matrix with vasculature [9, 98]. The matrix is composed of disorganized collagen fibrils, constituted of higher percentages of collagen III than collagen I. Although the biochemical composition of the regenerated construct obtained using the "rehab" regime was not scar tissue like, the decrease in collagen I gene expression would be a concern of scar tissue development. This phenomenon could be attributed to the likelihood that the "high" intensity stimulation profile was not suitable for extended duration and a more complex rehabilitative regime might be necessary. It might be necessary to employ the "low" intensity profile once again after 28 days of stimulation (21 days of "high" intensity profile) to allow for tissue recuperation from excessive strain levels. The change towards a "low" intensity profile after 28 days was supported by the gene expression results for the "continuous low" group, which showed a drop, though not significant, in collagen III expression at day 28. This could then indicate that there was less tendency for scar tissue formation using this regime. Although it might seem that the "rehab" regime led to the possible formation of scar tissue and that the "continuous low" regime did not, it was still more advantageous to employ the "rehab" regime for accelerated regeneration of ligament.

Modification of the "rehab" regime to include recurring "low" and "high" intensity stimulating profiles would be interesting as future works.

Another reason for the decrease in collagen I expression could be the limited space available for tissue formation within the AL hybrid SF scaffold. This was so as cell proliferation and eventual collagen deposition was limited by the SFEF meshes to the space in between the adjacent layers of the rolled-up construct, which provided a negative feedback on the production of ECM components as a result. Therefore, a cell permeating electrospun SF mesh would be required. One way to achieve such a mesh is to use micropatterned electrical discharge or laser etching techniques, commonly used in the fabrication of microarrays, to form pits and holes in the SFEF mesh to allow improved cell infiltration into the knitted structure. This method would be discussed further in the recommendations section of the next chapter.

5.4.3. "Rehab" Stimulation Regime for Regenerated Ligament Tissue Maturation

In this study, the success of ligament tissue maturation was largely measured based on the expression of ligament-related genes. Specifically, tenascin-C, which is an ECM glycoprotein expressed abundantly during embryogenesis and regeneration of musculoskeletal tissues [313, 314], is associated with providing elasticity for mesenchymal tissues subjected to heavy tensile loading, while acting as an adaptor and modulator of cell-matrix interactions like cell adhesion and migration. The "rehab" stimulation regime was thus capable of stimulating its up-regulation to consequently support improvement in mechanical stiffness of the tissue. Tenomodulin, on the other

hand, is associated with ligament maturation via reducing individual collagen fibril diameter, as reported by Docheva et al. [299]. In their study, it was found that there was increase in maximal diameters of collagen fibrils, with large variations in fibril diameters compared to the original tissue, in tenomodulin-deficient mice. Its deficiency was therefore associated with formation of immature and mechanically weaker ligament tissues. Since the "rehab" regime could stimulate up-regulation of tenomodulin, it would be likely that the collagen fibrils that would be regenerated were of smaller calibers as well. With the smaller collagen fibrils, the overall tissue mechanical property would be improved and mimic more closely to the native tissue morphology.

Nevertheless, it should be noted that the calibers of collagen fibers (micron level), as opposed to the fibrils (nano level), should be increased such that the regenerated structure would be more mechanically viable. This was achieved by using the "rehab" regime in this study, as analysis of the histological images revealed that thicker collagen fibers were formed in the "rehab" group compared to the other stimulation groups. This observation, in association with the increased tenomodulin expression, would show that the resulting construct should be more matured and effectively stronger, with thick collagen fibers consisting of fine collagen fibrils. This had been positively shown by the significantly stronger and stiffer regenerated construct obtained via "rehab" stimulation regime as compared to the statically cultured equivalent. As the characterization of the ultrastructural state of regenerated collagen fibers had been limited in this study, future works should examine this aspect for more complete characterization of the deposited collagen structures.

Moreover, the use of rabbits' MSCs, like that of many other researchers who had used animal cells for bioreactor studies [257-259], was useful for preliminary assessment of the rehabilitative approach to dynamic conditioning of cell seeded constructs. However, future works should also focus on the use of human MSCs for the study of the optimal stimulation regime since human mechanical stimulation parameters were considered and used in this study. Although it had been shown that the rehabilitative approach, with parameters closely mimicking the human physiological values, improved tissue regeneration for rabbit cell based constructs, it was limited to only justifying that the approach was better than the other regimes tested. The actual parameters used might not be optimal and certainly not definitive in the absolute sense for human cells and clinical applications.

5.5. Concluding Remarks

The rehabilitative approach to providing dynamic conditions for regeneration of ligament tissue had been shown to be promising over the stimulation regimes that focused on supplementing leveled stimulation parameters. Proliferation was found for the earlier stages of the stimulation period, which transcended towards the differentiative phase in an accelerated manner after 14 days. Differentiation was marked by the increased collagen deposition, up-regulation of ligament-related genes and deposition of the corresponding ECM components. The "rehab" stimulation regime also triggered thicker collagen fibers formation and eventual superior mechanical strength and stiffness relative to the leveled stimulation regimes and static cultures. However, issues pertaining to limited cell and ECM infiltration, tendency of scar formation and the use of human MSCs instead of rabbit MSCs would need to be looked into in order for the AL hybrid SF scaffold and the "rehab" stimulation regime to be applicable for clinical applications.

Chapter 6

CONCLUSION AND RECOMMENDATIONS

6.1. Conclusion

A novel method of producing micron/submicron scale full SF aligned hybrid scaffold was developed in the PhD project. In the initial material assessments, it was shown that the SF material could be customized and fabricated to a knitted structure that had similar biomechanical characteristics as the native ligament and was suitable for functional tissue engineering of the tissue. The degumming process was also shown to be optimizable for SF mechanical properties retention via controlling parameters such as presence of mechanical agitation, duration, temperature and change of degumming solution, while ensuring that sericin was removed effectively. SF knits were optimally degummed in aqueous Na_2CO_3 with SDS (0.25% w/v each) at 100°C for 30 min in the presence of mechanical agitation. Highly aligned electrospun SF fibers could be obtained subsequently via the customized electrospinning setup, which consisted of a rotating grounded collector frame with two positively charged plates to limit the spinneret path. A well integrated hybrid SF scaffold structure could eventually be obtained via physical contractile forces generated from contraction of SFEF onto SF knit upon methanol treatment for SF crystallization.

Upon characterization of the MSC-seeded hybrid scaffolds, it was demonstrated that the aligned hybrid SF scaffold was capable of inducing prominent tenogenic differentiation due to its positive topographical cues that cause cellular and ECM alignment (hypothesis 1). With the addition of dynamic conditioning cues, enhanced tenogenic differentiation was effected due to its synergistic effect with the positive topographical cues of the aligned hybrid SF scaffold (hypothesis 2).

A novel rehabilitative approach to dynamically condition the cell seeded constructs was also conceived in this project. It was shown that the rehabilitative approach to dynamic conditioning allowed timely introduction of appropriate stimulation intensities, which allowed early introduction of mechanical cues to the MSCs to effect an accelerated differentiative profile towards ligament fibroblasts (hypothesis 3).

Through this study, it was thus demonstrated that the mechano-active AL hybrid SF scaffold was suitable providing mechanical functionality and topographical stimulation for tenogenic differentiation. When conditioned dynamically using a rehabilitative approach, the MSC-seeded construct would be able to develop into ligament-like structures more readily. This system thus showed promise and implication for future clinical ligament regenerative applications.

6.2. Recommendations for Future Work

6.2.1. Cell Migration Aided by SFEF Alignment

The positive topographical effects of AL-SFEF had been shown in this study via a series of characterizations done for the AL hybrid SF scaffold in both static and dynamic conditions. Other than providing cell guidance towards alignment and aligned ECM production, and stimulating positive topographical cues, the aligned SFEF component of the hybrid SF scaffold could aid in cell migration in the direction of fiber alignment. This phenomenon was shown in works performed by Schnell *et al.* [315] as they showed that the aligned electrospun poly-e-caprolactone and collagen/poly-ε-caprolactone blend that they produced could provide guidance for glial cell migration in the direction of the fiber alignment. Similarly, it would be likely that the AL-SFEF could provide an avenue for improved cell migration into the core of the scaffold. This would be especially useful when implantation of the hybrid scaffolds was to be involved as MSCs from the bone marrow cavity could preferentially migrate into the scaffold and specifically in the direction of SFEF alignment to further supplement the seeded MSCs. It would be interesting to characterize the rate of cell migration in both the *in vitro* and *in vivo* environment in the future.

6.2.2. Improvement of Cell Infiltration into the Hybrid SF Scaffold

From the histological assessments conducted for this study, it was noted that cell infiltration into the knitted structure had been limited. This could be due to the lack of

cell permeability in the SFEF meshes or that the static seeding technique, involving pipetting of cell suspension onto the scaffold surfaces, needed to be improved.

It was reported in several studies that low seeding efficiencies and non-uniform cell distributions with the scaffold were often associated with static seeding [316-319]. Consequently, many had turned to dynamic cell seeding techniques. This was usually done through the use of a bioreactor, and had been shown to improve seeding density, efficiency and uniformity compared to static approaches. As dynamic seeding systems could be readily integrated into bioreactor setups, this should be performed for future studies involving the use of the standalone bioreactor setup.

Cell permeability of the SFEF meshes could be improved via creating micropatterns of pits and holes in the electrospun mesh after fully integrating to form the hybrid scaffold. Such micropatterns could be achieved via the use of electrical discharge or laser etching techniques. Specifically, thermal energy generated by micropatterned electrical discharge arcs had been utilized to elevate temperature in localized regions to melt polymer electrospun fibers in the close vicinity. From the works conducted by Zeng *et al.* [320], microstructures as small as 20 μm could be created. Having controlled micro defects of these dimensions, the cell permeability of the SFEF meshes should be improved to allow infiltration of cells and ECM production in the knitted core of the hybrid scaffold. As such, future works should look at optimizing the density of these defects using such controllable methods to achieve regenerated constructs with uniform distribution of ECM and collagenous structures.

6.2.3. Sequential Release of Specific Growth Factors through Designed Incorporation into Electrospun Fibrous Meshes of Different Materials

The incorporated electrospun mesh of the hybrid scaffold could also be made as a composite structure in itself via the use different materials for electrospinning. The composed structure, as such, could be designed to have different degradation characteristics depending on the material used. With the different materials degrading at dissimilar rates during the course of tissue regeneration, it would then be possible to incorporate different growth factors into these different electrospun fibers, to achieve sequential release of the various growth factors at specific cellular growth phases.

For example, growth factor loaded PLGA and SF electrospun composite mesh could be designed and fabricated to allow initial release of bFGF to sustain proliferation of MSCs by preventing MSC differentiation during the cell expansion stage, and subsequent release of TGF-β to induce differentiation of MSCs, leading to increased expression of ECM proteins. Since PLGA degrades at a faster rate than that of SF, bFGF could be incorporated into PLGA electrospun fibers, while TGF-β incorporated into SF electrospun fibers. With culture, the PLGA would degrade earlier to release the loaded bFGF, while SF would be degraded later to release the loaded TGF-β (Figure 6-1).

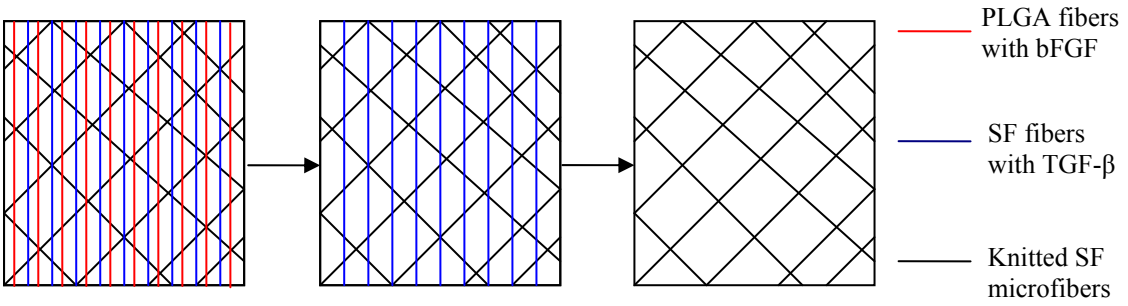

Figure 6-1: Schematic of gradual degradation of electrospun polymer fibers to sequentially release different growth factors

This form of sequential release of various growth factors had been shown to positively and more effectively stimulate the intended cellular activity at various stages of tissue regeneration than constant supplementation of all the growth factors throughout the culture period [321].

As such, release mechanism of the different growth factors from the targeted polymers would need to be understood in terms of the interplay between diffusion release and bulk release of the growth factors. Moreover, it would be essential to determine the respective degradation kinetics of growth factors loaded electrospun fibers and the dosage of growth factors that should be added for optimal cell proliferation and differentiation.

With this technology in place, it would then be possible in the future that controlled release of specific growth factors could be realized *in situ* at the implantation site via the implanted scaffold construct.

References

1. Vunjak-Novakovic G, Altman G, Horan R, Kaplan DL. Tissue engineering of ligaments. Annu Rev Biomed Eng 2004;6:131-156.
2. Martini F, Nath JL. Fundamentals of anatomy & physiology. 8th ed. San Francisco: Pearson/Benjamin Cummings, 2009.
3. Fan H, Liu H, Wong EJ, Toh SL, Goh JC. In vivo study of anterior cruciate ligament regeneration using mesenchymal stem cells and silk scaffold. Biomaterials 2008;29(23):3324-3337.
4. Ge Z, Yang F, Goh JC, Ramakrishna S, Lee EH. Biomaterials and scaffolds for ligament tissue engineering. J Biomed Mater Res A 2006;77(3):639-652.
5. Inouye K, Kurokawa M, Nishikawa S, Tsukada M. Use of Bombyx mori silk fibroin as a substratum for cultivation of animal cells. Journal of Biochemical and Biophysical Methods 1998;37(3):159-164.
6. Beynnon BD, Johnson RJ, Fleming BC, Peura GD, Renstrom PA, Nichols CE, et al. The effect of functional knee bracing on the anterior cruciate ligament in the weightbearing and nonweightbearing knee. Am J Sports Med 1997;25(3):353-359.
7. Sakane M, Fox RJ, Woo SL, Livesay GA, Li G, Fu FH. In situ forces in the anterior cruciate ligament and its bundles in response to anterior tibial loads. J Orthop Res 1997;15(2):285-293.
8. Matsumoto H, Suda Y, Otani T, Niki Y, Seedhom BB, Fujikawa K. Roles of the anterior cruciate ligament and the medial collateral ligament in preventing valgus instability. J Orthop Sci 2001;6(1):28-32.
9. Woo SL, Debski RE, Zeminski J, Abramowitch SD, Saw SS, Fenwick JA. Injury and repair of ligaments and tendons. Annu Rev Biomed Eng 2000;2:83-118.
10. Gianotti SM, Marshall SW, Hume PA, Bunt L. Incidence of anterior cruciate ligament injury and other knee ligament injuries: a national population-based study. J Sci Med Sport 2009;12(6):622-627.
11. Petrigliano FA, McAllister DR, Wu BM. Tissue engineering for anterior cruciate ligament reconstruction: a review of current strategies. Arthroscopy 2006;22(4):441-451.
12. Duthon VB, Barea C, Abrassart S, Fasel JH, Fritschy D, Menetrey J. Anatomy of the anterior cruciate ligament. Knee Surg Sports Traumatol Arthrosc 2006;14(3):204-213.
13. Laurencin CT, Freeman JW. Ligament tissue engineering: an evolutionary materials science approach. Biomaterials 2005;26(36):7530-7536.

14. Bach BR, Levy ME, Bojchuk J, Tradonsky S, Bush-Joseph CA, Khan NH. Single-incision endoscopic anterior cruciate ligament reconstruction using patellar tendon autograft - Minimum two-year follow-up evaluation. American Journal of Sports Medicine 1998;26(1):30-40.

15. Maletius W, Gillquist J. Long-term results of anterior cruciate ligament reconstruction with a Dacron prosthesis. The frequency of osteoarthritis after seven to eleven years. Am J Sports Med 1997;25(3):288-293.

16. Miller SL, Gladstone JN. Graft selection in anterior cruciate ligament reconstruction. Orthop Clin North Am 2002;33(4):675-683.

17. Strickland SM, MacGillivray JD, Warren RF. Anterior cruciate ligament reconstruction with allograft tendons. Orthop Clin North Am 2003;34(1):41-47.

18. Jorgensen U, Bak K, Ekstrand J, Scavenius M. Reconstruction of the anterior cruciate ligament with the iliotibial band autograft in patients with chronic knee instability. Knee Surg Sports Traumatol Arthrosc 2001;9(3):137-145.

19. Steenbrugge F, Verdonk R, Vorlat P, Mortier F, Verstraete K. Repair of chronic ruptures of the anterior cruciate ligament using allograft reconstruction and a ligament augmentation device. Acta Orthop Belg 2001;67(3):252-258.

20. Cooper JA, Jr., Sahota JS, Gorum WJ, 2nd, Carter J, Doty SB, Laurencin CT. Biomimetic tissue-engineered anterior cruciate ligament replacement. Proc Natl Acad Sci U S A 2007;104(9):3049-3054.

21. Liu H, Fan H, Wang Y, Toh SL, Goh JC. The interaction between a combined knitted silk scaffold and microporous silk sponge with human mesenchymal stem cells for ligament tissue engineering. Biomaterials 2008;29(6):662-674.

22. Sahoo S, Toh SL, Goh JC. A bFGF-releasing silk/PLGA-based biohybrid scaffold for ligament/tendon tissue engineering using mesenchymal progenitor cells. Biomaterials 2010;31(11):2990-2998.

23. Ma PX. Biomimetic materials for tissue engineering. Adv Drug Deliv Rev 2008;60(2):184-198.

24. Silver FH, Tria AJ, Zawadsky JP, Dunn MG. Anterior cruciate ligament replacement: a review. J Long Term Eff Med Implants 1991;1(2):135-154.

25. Li C, Vepari C, Jin HJ, Kim HJ, Kaplan DL. Electrospun silk-BMP-2 scaffolds for bone tissue engineering. Biomaterials 2006;27(16):3115-3124.

26. Teh TK, Toh SL, Goh JC. Optimization of the silk scaffold sericin removal process for retention of silk fibroin protein structure and mechanical properties. Biomed Mater 2010;5(3):035008.

27. Chen X, Qi YY, Wang LL, Yin Z, Yin GL, Zou XH, et al. Ligament regeneration using a knitted silk scaffold combined with collagen matrix. Biomaterials 2008;29(27):3683-3692.

28. Altman GH, Diaz F, Jakuba C, Calabro T, Horan RL, Chen J, et al. Silk-based biomaterials. Biomaterials 2003;24(3):401-416.

29. Minoura N, Aiba S, Gotoh Y, Tsukada M, Imai Y. Attachment and growth of cultured fibroblast cells on silk protein matrices. J Biomed Mater Res 1995;29(10):1215-1221.

30. Min BM, Lee G, Kim SH, Nam YS, Lee TS, Park WH. Electrospinning of silk fibroin nanofibers and its effect on the adhesion and spreading of normal human keratinocytes and fibroblasts in vitro. Biomaterials 2004;25(7-8):1289-1297.

31. Kim KH, Jeong L, Park HN, Shin SY, Park WH, Lee SC, et al. Biological efficacy of silk fibroin nanofiber membranes for guided bone regeneration. J Biotechnol 2005;120(3):327-339.

32. Van Eijk F, Saris DB, Riesle J, Willems WJ, Van Blitterswijk CA, Verbout AJ, et al. Tissue engineering of ligaments: a comparison of bone marrow stromal cells, anterior cruciate ligament, and skin fibroblasts as cell source. Tissue Eng 2004;10(5-6):893-903.

33. Lu HH, Cooper JA, Jr., Manuel S, Freeman JW, Attawia MA, Ko FK, et al. Anterior cruciate ligament regeneration using braided biodegradable scaffolds: in vitro optimization studies. Biomaterials 2005;26(23):4805-4816.

34. Cooper JA, Lu HH, Ko FK, Freeman JW, Laurencin CT. Fiber-based tissue-engineered scaffold for ligament replacement: design considerations and in vitro evaluation. Biomaterials 2005;26(13):1523-1532.

35. Ouyang HW, Goh JC, Thambyah A, Teoh SH, Lee EH. Knitted poly-lactide-co-glycolide scaffold loaded with bone marrow stromal cells in repair and regeneration of rabbit Achilles tendon. Tissue Eng 2003;9(3):431-439.

36. Ma Z, Kotaki M, Inai R, Ramakrishna S. Potential of nanofiber matrix as tissue-engineering scaffolds. Tissue Eng 2005;11(1-2):101-109.

37. Lee CH, Shin HJ, Cho IH, Kang YM, Kim IA, Park KD, et al. Nanofiber alignment and direction of mechanical strain affect the ECM production of human ACL fibroblast. Biomaterials 2005;26(11):1261-1270.

38. Ingber DE, Dike L, Hansen L, Karp S, Liley H, Maniotis A, et al. Cellular tensegrity: exploring how mechanical changes in the cytoskeleton regulate cell growth, migration, and tissue pattern during morphogenesis. Int Rev Cytol 1994;150:173-224.

39. Miller MD, Cooper DE, Warner JJP. Review of sports medicine and arthroscopy. 2nd ed. Philadelphia: W.B. Saunders, 2002.

40. Jakob R, Staubli HU, Schweizerische Gesellschaft fur Orthopadie . Orthopedic Study Group for the Knee. The Knee and the cruciate ligaments : anatomy, biomechanics, clinical aspects, reconstruction, complications, rehabilitation. Berlin ; New York: Springer-Verlag, 1992.

41. Jackson DW, Arnoczky SP, Woo SL, Frank CB, Simon TM. The Anterior cruciate ligament : current and future concepts. New York: Raven Press, 1993.

42. Nigg BM, Herzog W. Biomechanics of the musculo-skeletal system. 3rd ed. New Jersey: John Wiley & Sons, 2007.

43. Miller MD, Hart JA. Review of orthopaedics. 5th ed. Philadelphia, PA: Saunders / Elsevier, 2008.

44. Viidik A. Functional properties of collagenous tissues. Int Rev Connect Tissue Res 1973;6:127-215.

45. Yahia H. Ligaments and ligamentoplasties. Berlin ; New York: Springer, 1997.

46. Clark JM, Sidles JA. The interrelation of fiber bundles in the anterior cruciate ligament. J Orthop Res 1990;8(2):180-188.

47. Woo SL, Buckwalter JA. AAOS/NIH/ORS workshop. Injury and repair of the musculoskeletal soft tissues. Savannah, Georgia, June 18-20, 1987. J Orthop Res 1988;6(6):907-931.

48. Amiel D, Frank C, Harwood F, Fronek J, Akeson W. Tendons and ligaments: a morphological and biochemical comparison. J Orthop Res 1984;1(3):257-265.

49. Ker RF. The design of soft collagenous load-bearing tissues. J Exp Biol 1999;202(Pt 23):3315-3324.

50. Goh JC, Ouyang HW, Teoh SH, Chan CK, Lee EH. Tissue-engineering approach to the repair and regeneration of tendons and ligaments. Tissue Eng 2003;9 Suppl 1:S31-44.

51. Kastelic J, Galeski A, Baer E. The multicomposite structure of tendon. Connect Tissue Res 1978;6(1):11-23.

52. Harner CD, Livesay GA, Kashiwaguchi S, Fujie H, Choi NY, Woo SL. Comparative study of the size and shape of human anterior and posterior cruciate ligaments. J Orthop Res 1995;13(3):429-434.

53. Smith BA, Livesay GA, Woo SL. Biology and biomechanics of the anterior cruciate ligament. Clin Sports Med 1993;12(4):637-670.

54. Griffin LY. Rehabilitation of the injured knee. 2nd ed. St. Louis: : Mosby, 1995.

55. Jackson DW, Heinrich JT, Simon TM. Biologic and synthetic implants to replace the anterior cruciate ligament. Arthroscopy 1994;10(4):442-452.

56. Lee TQ, Woo SL. A new method for determining cross-sectional shape and area of soft tissues. J Biomech Eng 1988;110(2):110-114.

57. Dunn MG, Tria AJ, Kato YP, Bechler JR, Ochner RS, Zawadsky JP, et al. Anterior cruciate ligament reconstruction using a composite collagenous prosthesis. A biomechanical and histologic study in rabbits. Am J Sports Med 1992;20(5):507-515.

58. Danto MI, Woo SL. The mechanical properties of skeletally mature rabbit anterior cruciate ligament and patellar tendon over a range of strain rates. J Orthop Res 1993;11(1):58-67.

59. Lanza RP, Langer RS, Vacanti J. Principles of tissue engineering. 3rd ed. Amsterdam ; Boston: Elsevier Academic Press, 2007.

60. Feagin JA, Applewhite LB. The Crucial ligaments : diagnosis and treatment of ligamentous injuries about the knee. 2nd ed. New York: : Churchill Livingstone, 1994.

61. Noyes FR, Grood ES. The strength of the anterior cruciate ligament in humans and Rhesus monkeys. J Bone Joint Surg Am 1976;58(8):1074-1082.

62. Noyes FR, Butler DL, Paulos LE, Grood ES. Intra-articular cruciate reconstruction. I: Perspectives on graft strength, vascularization, and immediate motion after replacement. Clin Orthop Relat Res 1983(172):71-77.

63. Noyes FR, Butler DL, Grood ES, Zernicke RF, Hefzy MS. Biomechanical analysis of human ligament grafts used in knee-ligament repairs and reconstructions. J Bone Joint Surg Am 1984;66(3):344-352.

64. Noyes FR, Barber SD, Mangine RE. Bone-patellar ligament-bone and fascia lata allografts for reconstruction of the anterior cruciate ligament. J Bone Joint Surg Am 1990;72(8):1125-1136.

65. Azangwe G, Mathias KJ, Marshall D. Preliminary comparison of the rupture of human and rabbit anterior cruciate ligaments. Clin Biomech (Bristol, Avon) 2001;16(10):913-917.

66. Butler DL, Grood ES, Noyes FR, Zernicke RF. Biomechanics of ligaments and tendons. Exerc Sport Sci Rev 1978;6:125-181.

67. Cabaud HE. Biomechanics of the anterior cruciate ligament. Clin Orthop Relat Res 1983(172):26-31.

68. Nordin M, Frankel VH. Basic biomechanics of the musculoskeletal system. 3rd ed. Philadelphia: Lippincott Williams & Wilkins, 2001.

69. Hefti FL, Kress A, Fasel J, Morscher EW. Healing of the transected anterior cruciate ligament in the rabbit. J Bone Joint Surg Am 1991;73(3):373-383.

70. Jones RS, Nawana NS, Pearcy MJ, Learmonth DJ, Bickerstaff DR, Costi JJ, et al. Mechanical properties of the human anterior cruciate ligament. Clin Biomech (Bristol, Avon) 1995;10(7):339-344.

71. Sekiguchi H, Post WR, Han JS, Ryu J, Kish V. The effects of cyclic loading on tensile properties of a rabbit femur-anterior cruciate ligament-tibia complex (FATC). Knee 1998;5(3):215-220.

72. Takai S, Woo SL, Livesay GA, Adams DJ, Fu FH. Determination of the in situ loads on the human anterior cruciate ligament. J Orthop Res 1993;11(5):686-695.

73. Woo SLY, Hollis JM, Adams DJ, Lyon RM, Takai S. Tensile properties of the human femur-anterior cruciate ligament-tibia complex - The effects of specimen age and orientation. American Journal of Sports Medicine 1991;19(3):217-225.

74. Woo SLY, Newton PO, Mackenna DA, Lyon RM. A comparative-evaluation of the mechanical-properties of the rabbit medial collateral and anterior cruciate ligaments. Journal of Biomechanics 1992;25(4):377-386.

75. Woo SL, Livesay GA, Engle C. Biomechanics of the human anterior cruciate ligament. ACL structure and role in knee motion. Orthop Rev 1992;21(7):835-842.

76. Woo SL, Livesay GA, Engle C. Biomechanics of the human anterior cruciate ligament. Muscle stabilization and ACL reconstruction. Orthop Rev 1992;21(8):935-941.

77. Woo SL, Debski RE, Withrow JD, Janaushek MA. Biomechanics of knee ligaments. Am J Sports Med 1999;27(4):533-543.

78. Black J, Hastings GW. Handbook of Biomaterial Properties. London: Chapman & Hall, 1998.

79. Fu FH, Bennett CH, Lattermann C, Ma CB. Current trends in anterior cruciate ligament reconstruction. Part 1: Biology and biomechanics of reconstruction. Am J Sports Med 1999;27(6):821-830.

80. Monti RJ, Roy RR, Zhong H, Edgerton VR. Mechanical properties of rat soleus aponeurosis and tendon during variable recruitment in situ. J Exp Biol 2003;206(Pt 19):3437-3445.

81. Weiss JA, Gardiner JC. Computational modeling of ligament mechanics. Crit Rev Biomed Eng 2001;29(3):303-371.

82. Altman GH, Horan RL, Lu HH, Moreau J, Martin I, Richmond JC, et al. Silk matrix for tissue engineered anterior cruciate ligaments. Biomaterials 2002;23(20):4131-4141.

83. Lopez-Vazquez E, Juan JA, Vila E, Debon J. Reconstruction of the anterior cruciate ligament with a Dacron prosthesis. J Bone Joint Surg Am 1991;73(9):1294-1300.

84. Chen EH, Black J. Materials design analysis of the prosthetic anterior cruciate ligament. J Biomed Mater Res 1980;14(5):567-586.

85. Black J. Biological performance of materials : fundamentals of biocompatibility. 4th ed. Boca Raton: CRC Taylor & Francis, 2006.

86. Vena P, Gastaldi D, Contro R. A constituent-based model for the nonlinear viscoelastic behavior of ligaments. J Biomech Eng 2006;128(3):449-457.

87. Johnson GA, Livesay GA, Woo SL, Rajagopal KR. A single integral finite strain viscoelastic model of ligaments and tendons. J Biomech Eng 1996;118(2):221-226.

88. Weiss JA, Gardiner JC, Bonifasi-Lista C. Ligament material behavior is nonlinear, viscoelastic and rate-independent under shear loading. J Biomech 2002;35(7):943-950.

89. Hingorani RV, Provenzano PP, Lakes RS, Escarcega A, Vanderby R, Jr. Nonlinear viscoelasticity in rabbit medial collateral ligament. Ann Biomed Eng 2004;32(2):306-312.

90. Fu FH, Bennett CH, Ma CB, Menetrey J, Lattermann C. Current trends in anterior cruciate ligament reconstruction. Part II. Operative procedures and clinical correlations. Am J Sports Med 2000;28(1):124-130.

91. Maffulli N. Rupture of the Achilles tendon. J Bone Joint Surg Am 1999;81(7):1019-1036.

92. Schechtman H, Bader DL. Fatigue damage of human tendons. J Biomech 2002;35(3):347-353.

93. Lyon RM, Akeson WH, Amiel D, Kitabayashi LR, Woo SLY. Ultrastructural differences between the cells of the medial collateral and the anterior cruciate ligaments. Clinical Orthopaedics and Related Research 1991(272):279-286.

94. Nickerson DA, Joshi R, Williams S, Ross SM, Frank C. Synovial fluid stimulates the proliferation of rabbit ligament. Fibroblasts in vitro. Clin Orthop Relat Res 1992(274):294-299.

95. Witkowski J, Yang L, Wood DJ, Sung KL. Migration and healing of ligament cells under inflammatory conditions. J Orthop Res 1997;15(2):269-277.

96. Frank CB. Ligament Healing: Current Knowledge and Clinical Applications. J Am Acad Orthop Surg 1996;4(1):74-83.

97. Papageorgiou CD, Ma CB, Abramowitch SD, Clineff TD, Woo SL. A multidisciplinary study of the healing of an intraarticular anterior cruciate ligament graft in a goat model. Am J Sports Med 2001;29(5):620-626.

98. Woo SL, Vogrin TM, Abramowitch SD. Healing and repair of ligament injuries in the knee. J Am Acad Orthop Surg 2000;8(6):364-372.

99. Snook GA. A short history of the anterior cruciate ligament and the treatment of tears. Clin Orthop Relat Res 1983(172):11-13.

100. Salamone JC. Concise polymeric materials encyclopedia. Boca Raton: CRC Press, 1998.

101. Salamone JC. Polymeric materials encyclopedia. Boca Raton: : CRC Press, 1996.

102. Thomas NP, Turner IG, Jones CB. Prosthetic anterior cruciate ligaments in the rabbit. A comparison of four types of replacement. J Bone Joint Surg Br 1987;69(2):312-316.

103. Shino K, Inoue M, Horibe S, Nagano J, Ono K. Maturation of allograft tendons transplanted into the knee. An arthroscopic and histological study. J Bone Joint Surg Br 1988;70(4):556-560.

104. Johnson RJ, Beynnon BD, Nichols CE, Renstrom PA. The treatment of injuries of the anterior cruciate ligament. J Bone Joint Surg Am 1992;74(1):140-151.

105. McPherson GK, Mendenhall HV, Gibbons DF, Plenk H, Rottmann W, Sanford JB, et al. Experimental mechanical and histologic evaluation of the Kennedy ligament augmentation device. Clin Orthop Relat Res 1985(196):186-195.

106. Jackson DW, Windler GE, Simon TM. Intraarticular reaction associated with the use of freeze-dried, ethylene oxide-sterilized bone-patella tendon-bone allografts in the reconstruction of the anterior cruciate ligament. Am J Sports Med 1990;18(1):1-10; discussion 10-11.

107. Bolton CW, Bruchman WC. The GORE-TEX expanded polytetrafluoroethylene prosthetic ligament. An in vitro and in vivo evaluation. Clin Orthop Relat Res 1985(196):202-213.

108. Fujikawa K, Iseki F, Seedhom BB. Arthroscopy after anterior cruciate reconstruction with the Leeds-Keio ligament. J Bone Joint Surg Br 1989;71(4):566-570.

109. Greco RS. Implantation biology : the host response and biomedical devices. Boca Raton: : CRC Press, 1994.

110. Woods GW. Synthetics in anterior cruciate ligament reconstruction: a review. Orthop Clin North Am 1985;16(2):227-235.

111. Mody BS, Howard L, Harding ML, Parmar HV, Learmonth DJ. The ABC carbon and polyester prosthetic ligament for ACL-deficient knees. Early results in 31 cases. J Bone Joint Surg Br 1993;75(5):818-821.

112. Nau T, Lavoie P, Duval N. A new generation of artificial ligaments in reconstruction of the anterior cruciate ligament. Two-year follow-up of a randomised trial. J Bone Joint Surg Br 2002;84(3):356-360.

113. Guidoin MF, Marois Y, Bejui J, Poddevin N, King MW, Guidoin R. Analysis of retrieved polymer fiber based replacements for the ACL. Biomaterials 2000;21(23):2461-2474.

114. Woods GA, Indelicato PA, Prevot TJ. The Gore-Tex anterior cruciate ligament prosthesis. Two versus three year results. Am J Sports Med 1991;19(1):48-55.

115. Paavolainen P, Makisalo S, Skutnabb K, Holmstrom T. Biologic anchorage of cruciate ligament prosthesis. Bone ingrowth and fixation of the Gore-Tex ligament in sheep. Acta Orthop Scand 1993;64(3):323-328.

116. Markolf KL, Pattee GA, Strum GM, Gallick GS, Sherman OH, Nuys V, et al. Instrumented measurements of laxity in patients who have a Gore-Tex anterior cruciate-ligament substitute. J Bone Joint Surg Am 1989;71(6):887-893.

117. Kumar K, Maffulli N. The ligament augmentation device: an historical perspective. Arthroscopy 1999;15(4):422-432.

118. Richmond JC, Manseau CJ, Patz R, McConville O. Anterior cruciate reconstruction using a Dacron ligament prosthesis. A long-term study. Am J Sports Med 1992;20(1):24-28.

119. Schiavone Panni A, Fabbriciani C, Delcogliano A, Franzese S. Bone-ligament interaction in patellar tendon reconstruction of the ACL. Knee Surg Sports Traumatol Arthrosc 1993;1(1):4-8.

120. Lane JG, McFadden P, Bowden K, Amiel D. The ligamentization process: a 4 year case study following ACL reconstruction with a semitendinosis graft. Arthroscopy 1993;9(2):149-153.

121. Warren RF. Primary repair of the anterior cruciate ligament. Clin Orthop Relat Res 1983(172):65-70.

122. Espregueira M, Lopes JM, Castro C, Oliveira J. Time of remodelling of the patella tendon graft in anterior cruciate ligament surgery: an histological and immunohistochemical study in a rabbit model. The Knee 1998;5(1):9-19.

123. Zavras TD, Mackenney RP, Amis AA. The natural history of anterior cruciate ligament reconstruction using patellar tendon autograft. The Knee 1995;2(4):211-217.

124. Seedhom BB. Reconstruction of the anterior cruciate ligament. Proc Inst Mech Eng H 1992;206(1):15-27.

125. Arnoczky SP, Warren RF, Ashlock MA. Replacement of the anterior cruciate ligament using a patellar tendon allograft - an experimental-study. Journal of Bone and Joint Surgery-American Volume 1986;68A(3):376-385.

126. Shelton WR, Treacy SH, Dukes AD, Bomboy AL. Use of allografts in knee reconstruction: I. Basic science aspects and current status. J Am Acad Orthop Surg 1998;6(3):165-168.

127. Shelton WR, Treacy SH, Dukes AD, Bomboy AL. Use of allografts in knee reconstruction: II. Surgical considerations. J Am Acad Orthop Surg 1998;6(3):169-175.

128. Zimmerman MC, Contiliano JH, Parsons JR, Prewett A, Billotti J. The biomechanics and histopathology of chemically processed patellar tendon allografts for anterior cruciate ligament replacement. Am J Sports Med 1994;22(3):378-386.

129. Vasseur PB, Stevenson S, Gregory CR, Rodrigo JJ, Pauli S, Heitter D, et al. Anterior cruciate ligament allograft transplantation in dogs. Clin Orthop Relat Res 1991(269):295-304.

130. Jackson DW, Grood ES, Goldstein JD, Rosen MA, Kurzweil PR, Cummings JF, et al. A comparison of patellar tendon autograft and allograft used for anterior cruciate ligament reconstruction in the goat model. Am J Sports Med 1993;21(2):176-185.

131. Goldstein JD, Tria AJ, Zawadsky JP, Kato YP, Christiansen D, Silver FH. Development of a reconstituted collagen tendon prosthesis. A preliminary implantation study. J Bone Joint Surg Am 1989;71(8):1183-1191.

132. Jackson DW, Simon TM, Lowery W, Gendler E. Biologic remodeling after anterior cruciate ligament reconstruction using a collagen matrix derived from demineralized bone. An experimental study in the goat model. Am J Sports Med 1996;24(4):405-414.

133. Lee CH, Singla A, Lee Y. Biomedical applications of collagen. Int J Pharm 2001;221(1-2):1-22.

134. Liu SH, Yang RS, al-Shaikh R, Lane JM. Collagen in tendon, ligament, and bone healing. A current review. Clin Orthop Relat Res 1995(318):265-278.

135. McMaster WC. A histologic assessment of canine anterior cruciate substitution with bovine xenograft. Clin Orthop Relat Res 1985(196):196-201.

136. McMaster WC. Mechanical properties and early clinical experience with xenograft biomaterials. Bull Hosp Jt Dis Orthop Inst 1986;46(2):174-184.

137. van Steensel CJ, Schreuder O, van den Bosch BF, van Paassen HC, Menke HE, Voorhorst G, et al. Failure of anterior cruciate-ligament reconstruction using tendon xenograft. J Bone Joint Surg Am 1987;69(6):860-864.

138. Hawkins WL. Polymer stabilization. New York, 1971.

139. McCrum NG, Buckley CP, Bucknall CB. Principles of polymer engineering. 2nd ed. New York: Oxford University Press, 1997.

140. Puddu G, Cipolla M, Cerullo G, Franco V, Gianni E. Anterior cruciate ligament reconstruction and augmentation with PDS graft. Clin Sports Med 1993;12(1):13-24.

141. Brody GA, Eisinger M, Arnoczky SP, Warren RF. In vitro fibroblast seeding of prosthetic anterior cruciate ligaments. A preliminary study. Am J Sports Med 1988;16(3):203-208.

142. Lin VS, Lee MC, O'Neal S, McKean J, Sung KL. Ligament tissue engineering using synthetic biodegradable fiber scaffolds. Tissue Eng 1999;5(5):443-452.

143. Mooney DJ, Vacanti JP. Tissue engineering using cells and synthetic polymers. Transplantation Reviews 1993;7(3):153-162.

144. Naughton GK, Tolbert WR, Grillot TM. Emerging developments in tissue engineering and cell technology. Tissue Eng 1995;1(2):211-219.

145. Shieh SJ, Zimmerman MC, Parsons JR. Preliminary characterization of bioresorbable and nonresorbable synthetic fibers for the repair of soft tissue injuries. J Biomed Mater Res 1990;24(7):789-808.

146. Weiler A, Hoffmann RF, Stahelin AC, Helling HJ, Sudkamp NP. Biodegradable implants in sports medicine: the biological base. Arthroscopy 2000;16(3):305-321.

147. Dunn MG, Liesch JB, Tiku ML, Zawadsky JP. Development of fibroblast-seeded ligament analogs for ACL reconstruction. J Biomed Mater Res 1995;29(11):1363-1371.

148. Jackson DW, Simon TM. Tissue engineering principles in orthopaedic surgery. Clin Orthop Relat Res 1999(367 Suppl):S31-45.

149. Koski JA, Ibarra C, Rodeo SA. Tissue-engineered ligament: cells, matrix, and growth factors. Orthop Clin North Am 2000;31(3):437-452.

150. Butler DL, Goldstein SA, Guilak F. Functional tissue engineering: the role of biomechanics. J Biomech Eng 2000;122(6):570-575.

151. Dunn MG, Avasarala PN, Zawadsky JP. Optimization of extruded collagen fibers for ACL reconstruction. J Biomed Mater Res 1993;27(12):1545-1552.

152. Dunn MG, Maxian SH, Zawadsky JP. Intraosseous incorporation of composite collagen prostheses designed for ligament reconstruction. J Orthop Res 1994;12(1):128-137.

153. Laurencin CT, Ambrosio AM, Borden MD, Cooper JA, Jr. Tissue engineering: orthopedic applications. Annu Rev Biomed Eng 1999;1:19-46.

154. Horwitz EM, Le Blanc K, Dominici M, Mueller I, Slaper-Cortenbach I, Marini FC, et al. Clarification of the nomenclature for MSC: The International Society for Cellular Therapy position statement. Cytotherapy 2005;7(5):393-395.

155. Friedenstein AJ, Piatetzky S, II, Petrakova KV. Osteogenesis in transplants of bone marrow cells. J Embryol Exp Morphol 1966;16(3):381-390.

156. Friedenstein AJ, Petrakova KV, Kurolesova AI, Frolova GP. Heterotopic of bone marrow. Analysis of precursor cells for osteogenic and hematopoietic tissues. Transplantation 1968;6(2):230-247.

157. Pittenger MF, Mackay AM, Beck SC, Jaiswal RK, Douglas R, Mosca JD, et al. Multilineage potential of adult human mesenchymal stem cells. Science 1999;284(5411):143-147.

158. Muraglia A, Cancedda R, Quarto R. Clonal mesenchymal progenitors from human bone marrow differentiate in vitro according to a hierarchical model. J Cell Sci 2000;113 (Pt 7):1161-1166.

159. Mauney JR, Jaquiery C, Volloch V, Heberer M, Martin I, Kaplan DL. In vitro and in vivo evaluation of differentially demineralized cancellous bone scaffolds combined with human bone marrow stromal cells for tissue engineering. Biomaterials 2005;26(16):3173-3185.

160. Baddoo M, Hill K, Wilkinson R, Gaupp D, Hughes C, Kopen GC, et al. Characterization of mesenchymal stem cells isolated from murine bone marrow by negative selection. J Cell Biochem 2003;89(6):1235-1249.

161. Simmons PJ, Torok-Storb B. Identification of stromal cell precursors in human bone marrow by a novel monoclonal antibody, STRO-1. Blood 1991;78(1):55-62.

162. Jones E, McGonagle D. Human bone marrow mesenchymal stem cells in vivo. Rheumatology (Oxford) 2008;47(2):126-131.

163. Digirolamo CM, Stokes D, Colter D, Phinney DG, Class R, Prockop DJ. Propagation and senescence of human marrow stromal cells in culture: a simple colony-forming assay identifies samples with the greatest potential to propagate and differentiate. Br J Haematol 1999;107(2):275-281.

164. Colter DC, Class R, DiGirolamo CM, Prockop DJ. Rapid expansion of recycling stem cells in cultures of plastic-adherent cells from human bone marrow. Proc Natl Acad Sci U S A 2000;97(7):3213-3218.

165. Colter DC, Sekiya I, Prockop DJ. Identification of a subpopulation of rapidly self-renewing and multipotential adult stem cells in colonies of human marrow stromal cells. Proc Natl Acad Sci U S A 2001;98(14):7841-7845.

166. Phinney DG, Kopen G, Righter W, Webster S, Tremain N, Prockop DJ. Donor variation in the growth properties and osteogenic potential of human marrow stromal cells. J Cell Biochem 1999;75(3):424-436.

167. Banfi A, Muraglia A, Dozin B, Mastrogiacomo M, Cancedda R, Quarto R. Proliferation kinetics and differentiation potential of ex vivo expanded human bone marrow stromal cells: Implications for their use in cell therapy. Exp Hematol 2000;28(6):707-715.

168. Javazon EH, Colter DC, Schwarz EJ, Prockop DJ. Rat marrow stromal cells are more sensitive to plating density and expand more rapidly from single-cell-derived colonies than human marrow stromal cells. Stem Cells 2001;19(3):219-225.

169. Caplan AI. Adult mesenchymal stem cells for tissue engineering versus regenerative medicine. J Cell Physiol 2007;213(2):341-347.

170. Klyushnenkova E, Mosca JD, Zernetkina V, Majumdar MK, Beggs KJ, Simonetti DW, et al. T cell responses to allogeneic human mesenchymal stem cells: immunogenicity, tolerance, and suppression. J Biomed Sci 2005;12(1):47-57.

171. Bartholomew A, Sturgeon C, Siatskas M, Ferrer K, McIntosh K, Patil S, et al. Mesenchymal stem cells suppress lymphocyte proliferation in vitro and prolong skin graft survival in vivo. Exp Hematol 2002;30(1):42-48.

172. Le Blanc K, Tammik L, Sundberg B, Haynesworth SE, Ringden O. Mesenchymal stem cells inhibit and stimulate mixed lymphocyte cultures and mitogenic responses independently of the major histocompatibility complex. Scand J Immunol 2003;57(1):11-20.

173. Le Blanc K. Immunomodulatory effects of fetal and adult mesenchymal stem cells. Cytotherapy 2003;5(6):485-489.

174. Le Blanc K, Tammik C, Rosendahl K, Zetterberg E, Ringden O. HLA expression and immunologic properties of differentiated and undifferentiated mesenchymal stem cells. Exp Hematol 2003;31(10):890-896.

175. Krampera M, Glennie S, Dyson J, Scott D, Laylor R, Simpson E, et al. Bone marrow mesenchymal stem cells inhibit the response of naive and memory antigen-specific T cells to their cognate peptide. Blood 2003;101(9):3722-3729.

176. Maitra B, Szekely E, Gjini K, Laughlin MJ, Dennis J, Haynesworth SE, et al. Human mesenchymal stem cells support unrelated donor hematopoietic stem cells and suppress T-cell activation. Bone Marrow Transplant 2004;33(6):597-604.

177. Beyth S, Borovsky Z, Mevorach D, Liebergall M, Gazit Z, Aslan H, et al. Human mesenchymal stem cells alter antigen-presenting cell maturation and induce T-cell unresponsiveness. Blood 2005;105(5):2214-2219.

178. Le Blanc K, Rasmusson I, Sundberg B, Gotherstrom C, Hassan M, Uzunel M, et al. Treatment of severe acute graft-versus-host disease with third party haploidentical mesenchymal stem cells. Lancet 2004;363(9419):1439-1441.

179. Ringden O, Uzunel M, Rasmusson I, Remberger M, Sundberg B, Lonnies H, et al. Mesenchymal stem cells for treatment of therapy-resistant graft-versus-host disease. Transplantation 2006;81(10):1390-1397.

180. Aggarwal S, Pittenger MF. Human mesenchymal stem cells modulate allogeneic immune cell responses. Blood 2005;105(4):1815-1822.

181. Liu H, Fan H, Toh SL, Goh JC. A comparison of rabbit mesenchymal stem cells and anterior cruciate ligament fibroblasts responses on combined silk scaffolds. Biomaterials 2008;29(10):1443-1453.

182. Wise DL. Encyclopedic handbook of biomaterials and bioengineering. New York: : Marcel Dekker, 1995.

183. Agrawal CM, Niederauer GG, Athanasiou KA. Fabrication and Characterization of PLA-PGA Orthopedic Implants. Tissue Eng 1995;1(3):241-252.

184. Bastioli C, Rapra Technology Limited. Handbook of biodegradable polymers. Shrewsbury: Rapra Technology, 2005.

185. Cutright DE, Hunsuck EE. Tissue reaction to the biodegradable polylactic acid suture. Oral Surg Oral Med Oral Pathol 1971;31(1):134-139.

186. Mark JE. Physical properties of polymers handbook. 2nd ed. New York ; London: Springer, 2007.

187. Engelberg I, Kohn J. Physico-mechanical properties of degradable polymers used in medical applications: a comparative study. Biomaterials 1991;12(3):292-304.

188. Mark JE. Polymer data handbook. 2nd ed. New York: Oxford University Press, 2009.

189. Li S, McCarthy S. Further investigations on the hydrolytic degradation of poly (DL-lactide). Biomaterials 1999;20(1):35-44.

190. Lu L, Peter SJ, Lyman MD, Lai HL, Leite SM, Tamada JA, et al. In vitro and in vivo degradation of porous poly(DL-lactic-co-glycolic acid) foams. Biomaterials 2000;21(18):1837-1845.

191. Middleton JC, Tipton AJ. Synthetic biodegradable polymers as orthopedic devices. Biomaterials 2000;21(23):2335-2346.

192. Gopferich A. Mechanisms of polymer degradation and erosion. Biomaterials 1996;17(2):103-114.

193. Grizzi I, Garreau H, Li S, Vert M. Hydrolytic degradation of devices based on poly(DL-lactic acid) size-dependence. Biomaterials 1995;16(4):305-311.

194. von Burkersroda F, Schedl L, Gopferich A. Why degradable polymers undergo surface erosion or bulk erosion. Biomaterials 2002;23(21):4221-4231.

195. Meinel L, Betz O, Fajardo R, Hofmann S, Nazarian A, Cory E, et al. Silk based biomaterials to heal critical sized femur defects. Bone 2006;39(4):922-931.

196. Wang Y, Kim HJ, Vunjak-Novakovic G, Kaplan DL. Stem cell-based tissue engineering with silk biomaterials. Biomaterials 2006;27(36):6064-6082.

197. Fan H, Liu H, Toh SL, Goh JC. Anterior cruciate ligament regeneration using mesenchymal stem cells and silk scaffold in large animal model. Biomaterials 2009;30(28):4967-4977.

198. Moy RL, Lee A, Zalka A. Commonly used suture materials in skin surgery. Am Fam Physician 1991;44(6):2123-2128.

199. Vepari C, Kaplan DL. Silk as a Biomaterial. Prog Polym Sci 2007;32(8-9):991-1007.

200. Lotz B, Colonna Cesari F. The chemical structure and the crystalline structures of Bombyx mori silk fibroin. Biochimie 1979;61(2):205-214.

201. Marsh RE, Corey RB, Pauling L. An investigation of the structure of silk fibroin. Biochim Biophys Acta 1955;16(1):1-34.

202. Magoshi J, Magoshi Y, Nakamura S. Physical-properties and structure of silk. 7. Crystallization of amorphous silk fibroin induced by immersion in methanol. Journal of Polymer Science Part B-Polymer Physics 1981;19(1):185-186.

203. Inoue SI, Tanaka N, Magoshi Y, Magoshi J. Structure of filament spun by silkworm in different stages: Bombyx mori and wild silkworm. Abstracts of Papers of the American Chemical Society 2000;219:277-PHYS.

204. He SJ, Valluzzi R, Gido SP. Silk I structure in Bombyx mori silk foams. Int J Biol Macromol 1999;24(2-3):187-195.

205. Martel A, Burghammer M, Davies RJ, Riekel C. Thermal behavior of Bombyx mori silk: evolution of crystalline parameters, molecular structure, and mechanical properties. Biomacromolecules 2007;8(11):3548-3556.

206. Ohgo K, Bagusat F, Asakura T, Scheler U. Investigation of structural transition of regenerated silk fibroin aqueous solution by Rheo-NMR spectroscopy. J Am Chem Soc 2008;130(12):4182-4186.

207. Wen CM, Ye ST, Zhou LX, Yu Y. Silk-induced asthma in children: a report of 64 cases. Ann Allergy 1990;65(5):375-378.

208. Kurosaki S, Otsuka H, Kunitomo M, Koyama M, Pawankar R, Matumoto K. Fibroin allergy. IgE mediated hypersensitivity to silk suture materials. Nippon Ika Daigaku Zasshi 1999;66(1):41-44.

209. Rossitch E, Jr., Bullard DE, Oakes WJ. Delayed foreign-body reaction to silk sutures in pediatric neurosurgical patients. Childs Nerv Syst 1987;3(6):375-378.

210. Dewair M, Baur X, Ziegler K. Use of immunoblot technique for detection of human IgE and IgG antibodies to individual silk proteins. Journal of Allergy and Clinical Immunology 1985;76(4):537-542.

211. Zaoming W, Codina R, Fernandez-Caldas E, Lockey RF. Partial characterization of the silk allergens in mulberry silk extract. J Investig Allergol Clin Immunol 1996;6(4):237-241.

212. Soong HK, Kenyon KR. Adverse reactions to virgin silk sutures in cataract surgery. Ophthalmology 1984;91(5):479-483.

213. Morrow FA, Kogan SJ, Freed SZ, Laufman H. In vivo comparison of polyglycolic acid, chromic catgut and silk in tissue of the genitourinary tract: an experimental study of tissue retrieval and calculogenesis. J Urol 1974;112(5):655-658.

214. Nebel L, Rosenberg G, Tobias B, Nathan H. Autograft suture in peripheral nerves. Eur Surg Res 1977;9(3):224-234.

215. Peleg H, Rao UN, Emrich LJ. An experimental comparison of suture materials for tracheal and bronchial anastomoses. Thorac Cardiovasc Surg 1986;34(6):384-388.

216. Foschi D, Corsi F, Cellerino P, Rizzi A, Morandi E, Trabucchi E. Angiogenic effects of suture biomaterials. An experimental study in rats. Eur Surg Res 2001;33(1):16-20.

217. Setzen G, Williams EF, 3rd. Tissue response to suture materials implanted subcutaneously in a rabbit model. Plast Reconstr Surg 1997;100(7):1788-1795.

218. Bucknall TE, Teare L, Ellis H. The choice of a suture to close abdominal incisions. Eur Surg Res 1983;15(2):59-66.

219. Garcia-Fuentes M, Giger E, Meinel L, Merkle HP. The effect of hyaluronic acid on silk fibroin conformation. Biomaterials 2008;29(6):633-642.

220. Perez-Rigueiro J, Elices M, Llorca J, Viney C. Tensile properties of silkworm silk obtained by forced silking. Journal of Applied Polymer Science 2001;82(8):1928-1935.

221. Perez-Rigueiro J, Elices M, Llorca J, Viney C. Effect of degumming on the tensile properties of silkworm (Bombyx mori) silk fiber. Journal of Applied Polymer Science 2002;84(7):1431-1437.

222. Jiang P, Liu HF, Wang CH, Wu LZ, Huang JG, Guo C. Tensile behavior and morphology of differently degummed silkworm (Bombyx mori) cocoon silk fibres. Materials Letters 2006;60(7):919-925.

223. Freddi G, Berlin A, Tsukada M, Dubini Paglia E. Use of HP-size exclusion chromatography to study the degree of polymerization of silk (Bombyx mori) fibroin fibres. Sericologia 2000;40:363–373.

224. Gulrajani ML, Agarwal R, Chand S. Degumming of silk with fungal protease. Indian J Fibre Textile Res 2000; 25:138– 142.

225. Gulrajani ML, Gupta SV, Gupta A, Suri M. Degumming of silk with different protease enzymes. Indian J Fibre Textile Res 1996;21(270–5).

226. Gulrajani ML, Sen S, Soria A, Suri M. Efficacy of proteases on degumming of dupion silk. Indian J Fibre Textile Res 1998;23:52–58.

227. Nakpathom M, Somboon B, Narumol N. Papain Enzymatic Degumming of Thai Bombyx mori Silk Fibers. Journal of Microscopy Society of Thailand 2009; 23(1):142-146.

228. Chopra S, Chattopadhyay R, Gulrajani ML. Low stress mechanical properties of silk fabric degummed by different methods. J Textile Inst 1996;87(542–53).

229. Yamada H, Nakao H, Takasu Y, Tsubouchi K. Preparation of undegraded native molecular fibroin solution from silkworm cocoons. Materials Science & Engineering C-Biomimetic and Supramolecular Systems 2001;14(1-2):41-46.

230. Yang S, Leong KF, Du Z, Chua CK. The design of scaffolds for use in tissue engineering. Part I. Traditional factors. Tissue Eng 2001;7(6):679-689.

231. Hutmacher D, Woodfield T, Dalton P, Lewis J. Scaffold design and fabrication. In: Clemens van B, Peter T, Anders L, Jeffrey H, David FW, Ranieri C, et al., editors. Tissue Engineering. Burlington: Academic Press, 2008. p. 403-454.

232. Horan RL, Collette AL, Lee C, Antle K, Chen J, Altman GH. Yarn design for functional tissue engineering. Journal of Biomechanics 2006;39(12):2232-2240.

233. Lavoie P, Fletcher J, Duval N. Patient satisfaction needs as related to knee stability and objective findings after ACL reconstruction using the LARS artificial ligament. Knee 2000;7(3):157-163.

234. Ge Z, Goh JC, Lee EH. Selection of cell source for ligament tissue engineering. Cell Transplant 2005;14(8):573-583.

235. Jockenhoevel S, Zund G, Hoerstrup SP, Chalabi K, Sachweh JS, Demircan L, et al. Fibrin gel -- advantages of a new scaffold in cardiovascular tissue engineering. Eur J Cardiothorac Surg 2001;19(4):424-430.

236. Patrick CW, Mikos AG, McIntire LV. Frontiers in tissue engineering. Oxford, U.K. ; New York, NY, U.S.A.: Pergamon. Online. 1998. Available from URL: http://libproxy1.nus.edu.sg/login?url=http://www.sciencedirect.com/science/book/9780080426891

237. Sahoo S, Ouyang H, Goh JC, Tay TE, Toh SL. Characterization of a novel polymeric scaffold for potential application in tendon/ligament tissue engineering. Tissue Eng 2006;12(1):91-99.

238. Martin I, Wendt D, Heberer M. The role of bioreactors in tissue engineering. Trends Biotechnol 2004;22(2):80-86.

239. Bilodeau K, Mantovani D. Bioreactors for tissue engineering: focus on mechanical constraints. A comparative review. Tissue Eng 2006;12(8):2367-2383.

240. Chen HC, Hu YC. Bioreactors for tissue engineering. Biotechnol Lett 2006;28(18):1415-1423.

241. Altman GH, Lu HH, Horan RL, Calabro T, Ryder D, Kaplan DL, et al. Advanced bioreactor with controlled application of multi-dimensional strain for tissue engineering. J Biomech Eng 2002;124(6):742-749.

242. Abousleiman RI, Sikavitsas VI. Bioreactors for tissues of the musculoskeletal system. Adv Exp Med Biol 2006;585:243-259.

243. Noth U, Schupp K, Heymer A, Kall S, Jakob F, Schutze N, et al. Anterior cruciate ligament constructs fabricated from human mesenchymal stem cells in a collagen type I hydrogel. Cytotherapy 2005;7(5):447-455.

244. Altman GH, Horan RL, Martin I, Farhadi J, Stark PR, Volloch V, et al. Cell differentiation by mechanical stress. FASEB J 2002;16(2):270-272.

245. Chen J, Horan RL, Bramono D, Moreau JE, Wang Y, Geuss LR, et al. Monitoring mesenchymal stromal cell developmental stage to apply on-time mechanical stimulation for ligament tissue engineering. Tissue Eng 2006;12(11):3085-3095.

246. Lee IC, Wang JH, Lee YT, Young TH. The differentiation of mesenchymal stem cells by mechanical stress or/and co-culture system. Biochem Biophys Res Commun 2007;352(1):147-152.

247. Juncosa-Melvin N, Matlin KS, Holdcraft RW, Nirmalanandhan VS, Butler DL. Mechanical stimulation increases collagen type I and collagen type III gene expression of stem cell-collagen sponge constructs for patellar tendon repair. Tissue Eng 2007;13(6):1219-1226.

248. Fleming BC, Beynnon BD, Renstrom PA, Johnson RJ, Nichols CE, Peura GD, et al. The strain behavior of the anterior cruciate ligament during stair climbing: an in vivo study. Arthroscopy 1999;15(2):185-191.

249. Fleming BC, Beynnon BD, Renstrom PA, Peura GD, Nichols CE, Johnson RJ. The strain behavior of the anterior cruciate ligament during bicycling. An in vivo study. Am J Sports Med 1998;26(1):109-118.

250. Harrington IJ. A bioengineering analysis of force actions at the knee in normal and pathological gait. Biomed Eng 1976;11(5):167-172.

251. Morrison JB. Function of the knee joint in various activities. Biomed Eng 1969;4(12):573-580.

252. Morrison JB. The mechanics of the knee joint in relation to normal walking. J Biomech 1970;3(1):51-61.

253. Butler DL, Juncosa N, Dressler MR. Functional efficacy of tendon repair processes. Annu Rev Biomed Eng 2004;6:303-329.

254. Guilak F. Functional tissue engineering. New York: Springer, 2003.

255. Wang JH, Yang G, Li Z. Controlling cell responses to cyclic mechanical stretching. Ann Biomed Eng 2005;33(3):337-342.

256. Webb K, Hitchcock RW, Smeal RM, Li W, Gray SD, Tresco PA. Cyclic strain increases fibroblast proliferation, matrix accumulation, and elastic modulus of fibroblast-seeded polyurethane constructs. J Biomech 2006;39(6):1136-1144.

257. Raif el M, Seedhom BB, Pullan MJ, Toyoda T. Cyclic straining of cell-seeded synthetic ligament scaffolds: development of apparatus and methodology. Tissue Eng 2007;13(3):629-640.

258. Butler DL, Juncosa-Melvin N, Boivin GP, Galloway MT, Shearn JT, Gooch C, et al. Functional tissue engineering for tendon repair: A multidisciplinary strategy using mesenchymal stem cells, bioscaffolds, and mechanical stimulation. J Orthop Res 2008;26(1):1-9.

259. Jones BF, Wall ME, Carroll RL, Washburn S, Banes AJ. Ligament cells stretch-adapted on a microgrooved substrate increase intercellular communication in response to a mechanical stimulus. J Biomech 2005;38(8):1653-1664.

260. Joshi SD, Webb K. Variation of cyclic strain parameters regulates development of elastic modulus in fibroblast/substrate constructs. J Orthop Res 2008;26(8):1105-1113.

261. Grymes RA, Sawyer C. A novel culture morphology resulting from applied mechanical strain. In Vitro Cell Dev Biol Anim 1997;33(5):392-397.

262. Sequeira MM, Rickenbach M, Wietlisbach V, Tullen B, Schutz Y. Physical activity assessment using a pedometer and its comparison with a questionnaire in a large population survey. Am J Epidemiol 1995;142(9):989-999.

263. Montgomery JB, Steadman JR. Rehabilitation of the injured knee. Clin Sports Med 1985;4(2):333-343.

264. Henning CE, Lynch MA, Glick KR, Jr. An in vivo strain gage study of elongation of the anterior cruciate ligament. Am J Sports Med 1985;13(1):22-26.

265. Grodski M, Marks R. Exercises following anterior cruciate ligament reconstructive surgery: biomechanical considerations and efficacy of current approaches. Res Sports Med 2008;16(2):75-96.

266. Skinner HB, Wyatt MP, Stone ML, Hodgdon JA, Barrack RL. Exercise-related knee joint laxity. Am J Sports Med 1986;14(1):30-34.

267. Kirkley A, Mohtadi N, Ogilvie R. The effect of exercise on anterior-posterior translation of the normal knee and knees with deficient or reconstructed anterior cruciate ligaments. Am J Sports Med 2001;29(3):311-314.

268. Stein GS, Lian JB, Owen TA. Relationship of cell growth to the regulation of tissue-specific gene expression during osteoblast differentiation. FASEB J 1990;4(13):3111-3123.

269. Lian JB, Stein GS. Concepts of osteoblast growth and differentiation: basis for modulation of bone cell development and tissue formation. Crit Rev Oral Biol Med 1992;3(3):269-305.

270. Lian JB, Stein GS. The developmental stages of osteoblast growth and differentiation exhibit selective responses of genes to growth factors (TGF beta

1) and hormones (vitamin D and glucocorticoids). J Oral Implantol 1993;19(2):95-105; discussion 136-107.

271. Lian JB, Stein GS. Development of the osteoblast phenotype: molecular mechanisms mediating osteoblast growth and differentiation. Iowa Orthop J 1995;15:118-140.

272. Perez-Rigueiro J, Viney C, Llorca J, Elices M. Mechanical properties of single-brin silkworm silk. Journal of Applied Polymer Science 2000;75(10):1270-1277.

273. Somashekarappa H, Annadurai V, Sangappa, Subramanya G, Somashekar R. Structure-property relation in varieties of acid dye processed silk fibers. Materials Letters 2002;53(6):415-420.

274. Dunaway DL, Thiel BL, Viney C. Tensile mechanical property evaluation of natural and epoxide-treated silk fibers. Journal of Applied Polymer Science 1995;58(3):675-683.

275. Greenwald D, Shumway S, Albear P, Gottlieb L. Mechanical comparison of 10 suture materials before and after in vivo incubation. J Surg Res 1994;56(4):372-377.

276. Rutherford HA, Harris M. Concerning the existence of fractions of the sericin in raw silk. Journal of Research of the National Bureau of Standards 1940;24(4):415-421.

277. Takasu Y, Yamada H, Tsubouchi K. Isolation of three main sericin components from the cocoon of the silkworm, Bombyx mori. Biosci Biotechnol Biochem 2002;66(12):2715-2718.

278. Ki CS, Kim JW, Oh HJ, Lee KH, Park YH. The effect of residual silk sericin on the structure and mechanical property of regenerated silk filament. Int J Biol Macromol 2007;41(3):346-353.

279. Taketani I, Nakayama S, Nagare S, Senna M. The secondary structure control of silk fibroin thin films by post treatment. Applied Surface Science 2005;244(1-4):623-626.

280. Kawahara Y, Shioya M. Characterization of microvoids in mulberry and tussah silk fibers using stannic acid treatment. Journal of Applied Polymer Science 1999;73(3):363-367.

281. Robson RM. Microvoids in Bombyx mori silk. An electron microscope study. Int J Biol Macromol 1999;24(2-3):145-150.

282. Yamada K, Tsuboi Y, Itaya A. AFM observation of silk fibroin on mica substrates: morphologies reflecting the secondary structures. Thin Solid Films 2003;440(1-2):208-216.

283. Tsukada M, Freddi G, Monti P, Bertoluzza A, Kasai N. Structure and molecular-conformation of Tussah silk fibroin films - Effect of methanol. Journal of Polymer Science Part B-Polymer Physics 1995;33(14):1995-2001.

284. Cai S, Singh BR. Identification of beta-turn and random coil amide III infrared bands for secondary structure estimation of proteins. Biophys Chem 1999;80(1):7-20.

285. Chirgadze YN, Fedorov OV, Trushina NP. Estimation of amino acid residue side-chain absorption in the infrared spectra of protein solutions in heavy water. Biopolymers 1975;14(4):679-694.

286. Panilaitis B, Altman GH, Chen J, Jin HJ, Karageorgiou V, Kaplan DL. Macrophage responses to silk. Biomaterials 2003;24(18):3079-3085.

287. Terada S, Sasaki M, Yanagihara K, Yamada H. Preparation of silk protein sericin as mitogenic factor for better mammalian cell culture. Journal of Bioscience and Bioengineering 2005;100(6):667-671.

288. Tsubouchi K, Igarashi Y, Takasu Y, Yamada H. Sericin enhances attachment of cultured human skin fibroblasts. Biosci Biotechnol Biochem 2005;69(2):403-405.

289. Santin M, Motta A, Freddi G, Cannas M. In vitro evaluation of the inflammatory potential of the silk fibroin. J Biomed Mater Res 1999;46(3):382-389.

290. Reneker DH, Yarin AL. Electrospinning jets and polymer nanofibers. Polymer 2008;49(10):2387-2425.

291. Deitzel JM, Kleinmeyer J, Harris D, Tan NCB. The effect of processing variables on the morphology of electrospun nanofibers and textiles. Polymer 2001;42(1):261-272.

292. Stankus JJ, Guan J, Wagner WR. Fabrication of biodegradable elastomeric scaffolds with sub-micron morphologies. J Biomed Mater Res A 2004;70(4):603-614.

293. Fisher NI. Statistical analysis of circular data. Cambridge [England] ; New York, NY, USA: : Cambridge University Press, 1993.

294. Berens P. CircStat: A MATLAB Toolbox for Circular Statistics. Journal of Statistical Software 2009;31(10):1-21.

295. Cacou C, Palmer D, Lee DA, Bader DL, Shelton JC. A system for monitoring the response of uniaxial strain on cell seeded collagen gels. Med Eng Phys 2000;22(5):327-333.

296. Berry CC, Shelton JC, Bader DL, Lee DA. Influence of external uniaxial cyclic strain on oriented fibroblast-seeded collagen gels. Tissue Eng 2003;9(4):613-624.

297. Takagi M, Ueda K. Comparison of the optimal culture conditions for cell growth and tissue plasminogen activator production by human embryo lung cells on microcarriers. Appl Microbiol Biotechnol 1994;41(5):565-570.

298. Teh TK, Toh SL, Goh JC. Aligned Hybrid Silk Scaffold for Enhanced Differentiation of Mesenchymal Stem Cells into Ligament Fibroblasts. Tissue Eng Part C Methods 2011.

299. Docheva D, Hunziker EB, Fassler R, Brandau O. Tenomodulin is necessary for tenocyte proliferation and tendon maturation. Molecular and Cellular Biology 2005;25(2):699-705.

300. Li WJ, Mauck RL, Cooper JA, Yuan X, Tuan RS. Engineering controllable anisotropy in electrospun biodegradable nanofibrous scaffolds for musculoskeletal tissue engineering. J Biomech 2007;40(8):1686-1693.

301. Xu CY, Inai R, Kotaki M, Ramakrishna S. Aligned biodegradable nanofibrous structure: a potential scaffold for blood vessel engineering. Biomaterials 2004;25(5):877-886.

302. Baker BM, Mauck RL. The effect of nanofiber alignment on the maturation of engineered meniscus constructs. Biomaterials 2007;28(11):1967-1977.

303. Yim EK, Leong KW. Significance of synthetic nanostructures in dictating cellular response. Nanomedicine 2005;1(1):10-21.

304. Almarza AJ, Yang G, Woo SL, Nguyen T, Abramowitch SD. Positive changes in bone marrow-derived cells in response to culture on an aligned bioscaffold. Tissue Eng Part A 2008;14(9):1489-1495.

305. Hollister SJ, Maddox RD, Taboas JM. Optimal design and fabrication of scaffolds to mimic tissue properties and satisfy biological constraints. Biomaterials 2002;23(20):4095-4103.

306. Kuo CK, Tuan RS. Mechanoactive tenogenic differentiation of human mesenchymal stem cells. Tissue Eng Part A 2008;14(10):1615-1627.

307. Souryal TO, Moore HA, Evans JP. Bilaterality in anterior cruciate ligament injuries: associated intercondylar notch stenosis. Am J Sports Med 1988;16(5):449-454.

308. Viidik A. Simultaneous mechanical and light microscopic studies of collagen fibers. Z Anat Entwicklungsgesch 1972;136(2):204-212.

309. Moreau JE, Chen J, Bramono DS, Volloch V, Chernoff H, Vunjak-Novakovic G, et al. Growth factor induced fibroblast differentiation from human bone marrow stromal cells in vitro. J Orthop Res 2005;23(1):164-174.

310. Malaval L, Liu F, Roche P, Aubin JE. Kinetics of osteoprogenitor proliferation and osteoblast differentiation in vitro. J Cell Biochem 1999;74(4):616-627.

311. Choi JY, Lee BH, Song KB, Park RW, Kim IS, Sohn KY, et al. Expression patterns of bone-related proteins during osteoblastic differentiation in MC3T3-E1 cells. J Cell Biochem 1996;61(4):609-618.

312. Balint E, Lapointe D, Drissi H, van der Meijden C, Young DW, van Wijnen AJ, et al. Phenotype discovery by gene expression profiling: mapping of biological processes linked to BMP-2-mediated osteoblast differentiation. J Cell Biochem 2003;89(2):401-426.

313. Jarvinen TAH, Jozsa L, Kannus P, Jarvinen TLN, Kvist M, Hurme T, et al. Mechanical loading regulates tenascin-C expression in the osteotendinous junction. Journal of Cell Science 1999;112(18):3157-3166.

314. Jarvinen TAH, Jozsa L, Kannus P, Jarvinen TLN, Hurme T, Kvist M, et al. Mechanical loading regulates the expression of tenascin-C in the myotendinous junction and tendon but does not induce de novo synthesis in the skeletal muscle. Journal of Cell Science 2003;116(5):857-866.

315. Schnell E, Klinkhammer K, Balzer S, Brook G, Klee D, Dalton P, et al. Guidance of glial cell migration and axonal growth on electrospun nanofibers of poly-epsilon-caprolactone and a collagen/poly-epsilon-caprolactone blend. Biomaterials 2007;28(19):3012-3025.

316. Kim BS, Putnam AJ, Kulik TJ, Mooney DJ. Optimizing seeding and culture methods to engineer smooth muscle tissue on biodegradable polymer matrices. Biotechnol Bioeng 1998;57(1):46-54.

317. Holy CE, Shoichet MS, Davies JE. Engineering three-dimensional bone tissue in vitro using biodegradable scaffolds: Investigating initial cell-seeding density and culture period. Journal of Biomedical Materials Research 2000;51(3):376-382.

318. Bruinink A, Siragusano D, Ettel G, Brandsberg T, Brandsberg F, Petitmermet M, et al. The stiffness of bone marrow cell-knit composites is increased during mechanical load. Biomaterials 2001;22(23):3169-3178.

319. Li Y, Ma T, Kniss DA, Lasky LC, Yang ST. Effects of filtration seeding on cell density, spatial distribution, and proliferation in nonwoven fibrous matrices. Biotechnology Progress 2001;17(5):935-944.

320. Zeng H, Zhao Y. Microfabrication in electrospun nanofibers by electrical discharges. Sensors and Actuators A: Physical;In Press, Corrected Proof.

321. Moreau JE, Chen J, Horan RL, Kaplan DL, Altman GH. Sequential growth factor application in bone marrow stromal cell ligament engineering. Tissue Eng 2005;11(11-12):1887-1897.

322. Kastin AJ. Handbook of biologically active peptides. Amsterdam ; Boston: Academic Press, 2006. p. xliii, 1595 p., [1540] p. of col. plates.

323. Fan H, Liu H, Toh SL, Goh JC. Enhanced differentiation of mesenchymal stem cells co-cultured with ligament fibroblasts on gelatin/silk fibroin hybrid scaffold. Biomaterials 2008;29(8):1017-1027.

324. Bashur CA, Shaffer RD, Dahlgren LA, Guelcher SA, Goldstein AS. Effect of fiber diameter and alignment of electrospun polyurethane meshes on mesenchymal progenitor cells. Tissue Eng Part A 2009;15(9):2435-2445.

Appendix A. Method for determining elastic region

1. The data for the load and extension up to the first peak (load) were extracted.

2. The gradients between successive data points were calculated, such as that for g_1 and g_2 at two successive points shown in Figure A-1A.

3. The difference in gradients is calculated as a percentage of the first gradient using the formula

$$\text{Percent gradient change} = (g_2 - g_1)/ g_1 \times 100\ \%$$

4. The graph of x_2 (extension data point between the two gradients compared) versus the percent gradient change of the two gradients was plotted as shown in Figure A-1B.

5. From the graph of x_2 versus the percent gradient change, the region of best linearity was determined as the region with near zero gradient change. From the representative graph, this region is bounded by x = 4.0 mm and x = 7.5 mm.

6. If more than one region of linearity were found, the regions were compared using the correlation method to single out the more linear region.

7. The region selected was tested with the correlation formula to ensure a square of correlation factor of more than 0.99 (1.0 being a perfectly fitting straight line) could be obtained.

8. At the best linear region, a straight line was fitted using linear regression (least square method) and the gradient of the line would represent the stiffness of the elastic region (Figure A-1C).

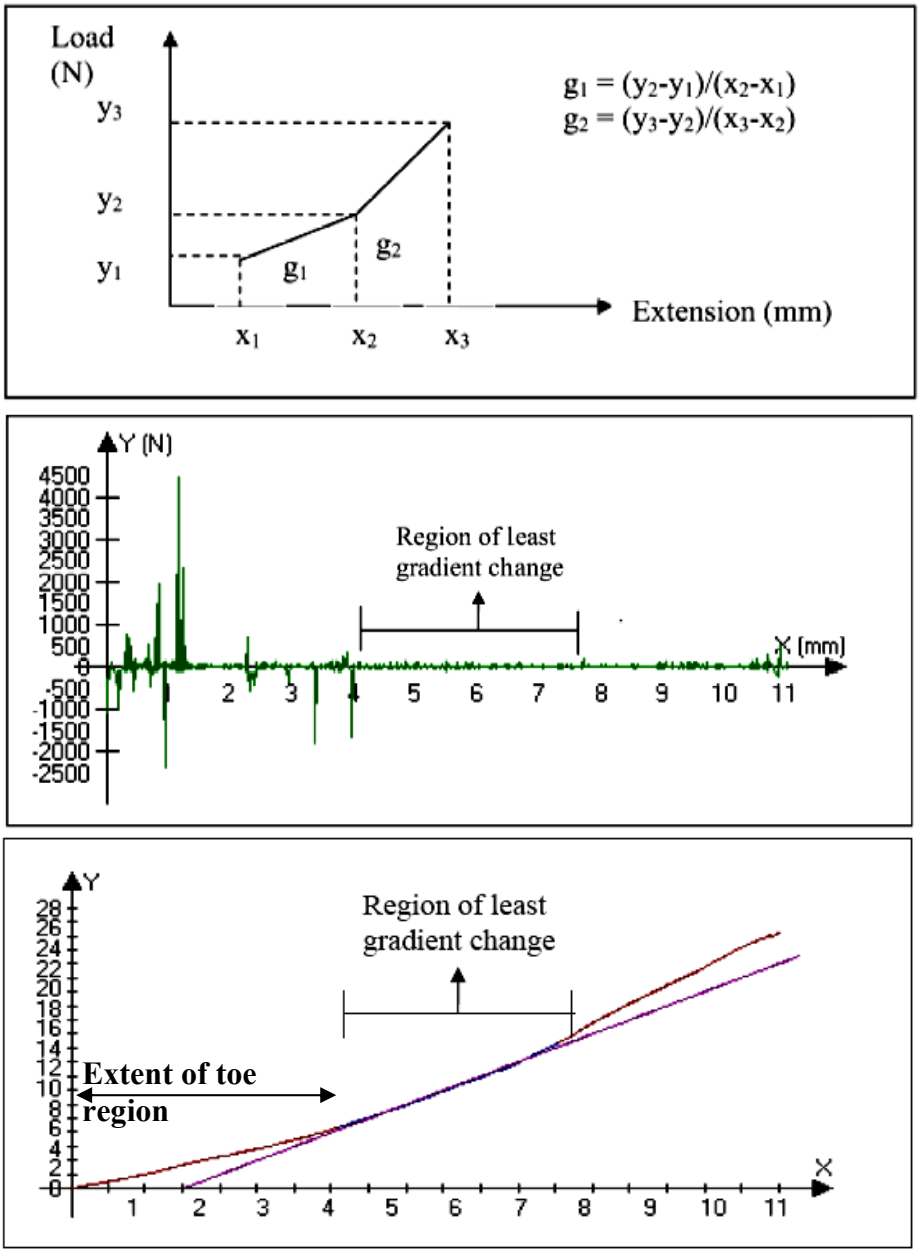

Figure A-1: (A) Method for calculation of gradient between two successive points (A). (B) Graph of percent gradient change versus the extension point to determine region of least gradient change. (C) The gradient of the best fitted straight line (blue) at the elastic liner region of the load-extension curve (red) yields the elastic stiffness of the tested construct.

To eliminate multi-factor contributions such as failure load and stiffness, toe region was determined based on the extent of displacement made with incremental stiffness changes before linear extension (Figure A-1C) instead of the absolute stiffness values involved. In other words, only the extent of the toe region, in terms of the extension, was evaluated and not the rate of stiffness change.

Appendix B1. Live/dead Hemocytometry

Cell attachment test was done to assess the cell density of the cell seeding suspension prior to cell seeding on scaffolds and also for assessing the cell adhesion post-seeding. The general method of cell counting is described as follows.

1. The hemocytometer and glass coverslip were first cleaned with 70% ethanol. The clean glass coverslip was then placed over the hemocytometer grooves and semi-silvered counting area.

2. Cells could be harvested by trypsinization of cell monolayers or of non-adherent cells in suspension. 40 µl of cell suspension was then mixed with 10 µl of Trypan Blue stain solution (Invitrogen Corporation, CA, USA) for dead cell exclusion. With the use of a micropipette, the cell suspension mixture was then transferred to the edge of the hemocytometer and allowed to spread evenly by capillary action.

3. Using the 10 × objective of a phase-contrast microscope, the number of cells in the 1 mm^2 area at the 4 corners of the hemocytometer grid (Figure A-2) were individually counted and averaged to obtain number of cells (n). Viable (unstained) and dead (stained blue) cells were distinguished during the counting.

4. Since the depth of the chamber is 0.1 mm and the area counted was 1 mm^2, the volume for cell suspension entrapped was 0.1 mm × 1.0 mm^2 = 0.1 mm^3 or 10^{-4} ml. Cell concentration was thus determined as follows:

   Cell concentration in cell suspension (cells/ml)

= Average cell number (n) × 10^4 × 5/4 (dilution factor resulting from addition of Trypan Blue staining solution)

Cell viability could be calculated using the following equation:

% cell viability

= [total viable cells (unstained) / total cells (stained + unstained)] × 100%

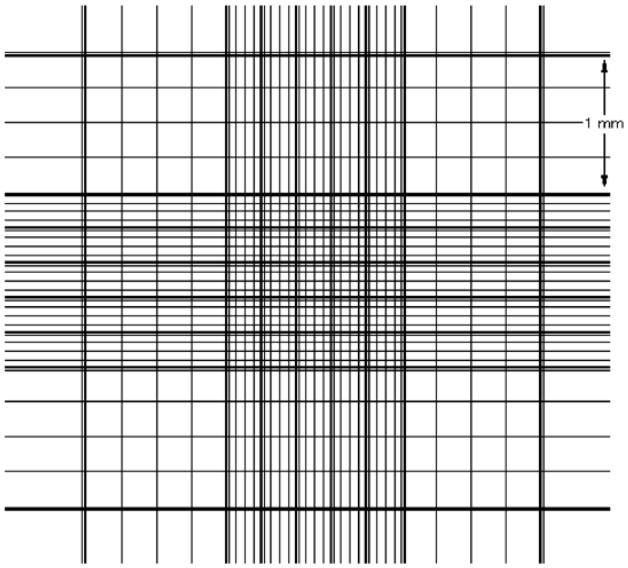

Figure A-2: Diagram for Hemocytometer (Counting Chamber).

Appendix B2. Alamar Blue™

Alamar Blue™, a soluble light sensitive dye, non-toxic and stable in culture medium, was used to assess the proliferation activity of the seeded cells on the scaffold as it monitored the reducing environment of the proliferating cell. It is composed of a blue dye, resazurin, which is reduced by the metabolic products of viable cells to form a fluorescent red dye called resorufin. The amount of resazurin (red) can be measured at 600nm absorbance wavelength while resorufin (blue) at 570nm wavelength. The percentage reduction of resazurin to resorufin, calculated with compensation for the culture medium background absorbance, reflects cell viability.

Alamar Blue mixture (10 %v/v) was first made with full culture medium. Upon aspirating the old medium from the scaffold culture chambers, 2 ml of the mixture was added to the scaffold, which was then incubated for 3 h at 37 °C. Negative control, which consisted of blank scaffold soaked in 2 ml Alamar Blue mix, was also incubated simultaneously. Care was taken to protect the Alamar Blue mix from light by wrapping with aluminium foil as the mixture is photosensitive. After the incubation, 200 µl of the Alamar Blue mix from each sample was transferred to a 96-well assay plate and measured for absorbance measured at 570/600 nm in a microplate reader (Sunnyvale, CA, USA). Percentage reduction of Alamar Blue, which indicated cellular proliferation, was then calculated as:

$$\%reduced = \frac{(\varepsilon_{ox}\lambda_2)(A\lambda_1) - (\varepsilon_{ox}\lambda_1)(A\lambda_2)}{(\varepsilon_{red}\lambda_1)(A'\lambda_2) - (\varepsilon_{red}\lambda_2)(A'\lambda_1)} \times 100$$, whereby

$(\varepsilon_{red}\lambda_1) = 155677$ (Molar extinction coefficient of reduced *Alamar Blue*™ at 570nm)

($\varepsilon_{red}\lambda_2$) = 14652 (Molar extinction coefficient of reduced *Alamar Blue*™ at 600nm)

($\varepsilon_{ox}\lambda_1$) = 80586 (Molar extinction coefficient of oxidized *Alamar Blue*™ at 570nm)

($\varepsilon_{ox}\lambda_2$) = 117216 (Molar extinction coefficient of oxidized *Alamar Blue*™ at 600nm)

($A\lambda_1$) = Absorbance of test wells at 570nm

($A\lambda_2$) = Absorbance of test wells at 600nm

($A'\lambda_1$) = Absorbance of negative control wells which contain medium plus *Alamar Blue*™ but to which no cells have been added at 570nm

($A'\lambda_2$) = Absorbance of negative control wells which contain medium plus *Alamar Blue*™ but to which no cells have been added at 600nm

Appendix B3. Texas Red-X Phalloidin/DAPI Fluorescence Staining

Phalloidin is a toxin isolated from the deadly *Amanita phalloides* mushroom. It is a bicyclic peptide that binds specifically to F-actin [322], making it a convenient tool to investigate the distribution of F-actin when labeled with fluorescent dyes such as the Texas Red®-X dye. Very often, DAPI is used for nuclear counterstain as it stands out vividly from other fluorescent probes used for other intracellular structures. DAPI stains nuclei specifically, with little or no cytoplasmic labeling.

Therefore, Texas Red-X Phalloidin/DAPI co-staining was utilized as a tool in this study to observe the cellular orientation, distribution and its interaction with the scaffold architecture. To achieve this, at each time point, cultured specimens were fixed in 4% paraformaldehyde for at least 15 min and permeabilized with 0.1% Triton-X100 in 1× PBS for 1 min. The F-actin filaments were stained with Texas Red®-X phalloidin (Molecular Probes, Invitrogen Corporation, CA, USA) diluted 1:100 in PBS for 15 min and nuclei stained with DAPI (Molecular Probes, Invitrogen Corporation, CA, USA) with working concentration of 300 nM in PBS for 5 min. Samples were thoroughly washed three times with PBS before inspection with laser scanning confocal microscopy (Zeiss LSM 510 Meta, Germany).

Appendix B4. Sircol™ Collagen Assay

The Sircol™ collagen assay (Biocolor Ltd., Newtownnabby, Ireland), a picrosirius-red based colorimetric dye-binding method specific for solubilized collagens, was used to measure the amount of collagen synthesized by the cell-scaffold construct or cell cultures. The assay does not require the isolation of collagens from other soluble tissue proteins and hence can be used to directly measure without any prior extraction or purification. Specifically, picrosirius-red, the Sircol dye reagent, selectively binds to the [Gly-X-Y]n tripeptide sequences in triple-helical collagens type I to V, and subsequently crosslinks and precipitates them. From this precipitate, the dye is released under strong alkaline conditions and its absorbance measured at 540nm. After comparison with collagen standards the amount of collagen in the sample is estimated. To ascertain that collagen detected was attributed to the cell-scaffold construct, collagen that was deposited in the constructs was extracted and tested, instead of the soluble form of collagen in medium.

The test was performed at the various time points for the different scaffold groups and cultured cells. Cultured scaffold specimens were finely cut and digested with 500 µl of pepsin solution (0.25 mg/ml). For cell culture controls, the cultured cells were first removed from the seeded 2-D tissue culture flask surface via mechanical cell scraping and suspended in PBS. After centrifugation of the cell suspension, 500 µl of pepsin solution (0.25 mg/ml) was added to the cell pellet likewise. Suspensions with the pepsin solution of the different specimens were then shaken at room temperature for 2 h. 1 ml of dye reagent was added to 200 µl of digested solution and mixed for another

30 min in room temperature. The pellet of dyed collagen was then precipitated by centrifugation at >10000 g for 10 min and then dissolved in 1 ml of releasing reagent. The absorbance of redissolved dye was measured in 96-well plates at absorbance wavelength of 540 nm in a Microplate Reader (TECAN Microplate Reader, Magellan Instrument Control and Data Analysis Software), from which the collagen amount in the 200 µl sample was derived by extrapolation from standard curve. This was then used to calculate the total amount of collagen in the sample based on the total volume of the sample after the pepsin digestion stage.

Appendix B5. Histological Assessments

Sections of seeded scaffolds of 8 μm thickness were made in both the longitudinal (along the lengthwise axis) and transverse sections (the circular profile) of the rolled-up scaffold. The cultured constructs were first fixed in 10 % neutral buffered formalin before being paraffin blocked for H&E and Masson's trichrome staining or frozen at -24 °C and cryosectioned for immunohistochemical staining. As it was of interest to examine the core of the hybrid scaffolds for cell morphology and continued viability over the study period, longitudinal or transverse sections were taken from the core and central region for histological evaluation. Sections were collected on a polylysine-coated glass slide before being stained using the various methods. Upon being mounted, the specimens were observed using a phase contrast microscopy (IX71 Inverted Research Microscope, Olympus Optical, Hamburg, Germany) and using an image analysis software (MicroImage v4.5.1, Olympus).

a. H&E Staining

Upon using xylene and ethanol mix to deparaffinize the sections, hydration was carried out using a reverse graded ethanol series (90% - 70% - 50%). After which, hematoxylin stain (Sigma-Aldrich St. Louis, USA) was applied for 5 min, followed by a rinse with tap water and soak in differentiation solution (Sigma-Aldrich St. Louis, USA) for 30 s. Care was taken during rinsing and soaking to prevent specimens from detaching from the slides. The sections were then soaked in eosin for 30 s before being dehydrated, cleared and mounted in Permount™ (Thermo Fisher Scientific Inc., MA, USA) with glass cover slips.

b. Masson's Trichrome Staining

Upon using xylene and ethanol mix to deparaffinize the sections, hydration was carried out using a reverse graded ethanol series (90% - 70% - 50%). After which, the sections were stained in Weigert's iron hematoxylin working solution (Sigma-Aldrich St. Louis, USA) for 10 min and rinsed with distilled water for 10 min thereafter. The sections were then stained in Biebrich scarlet-acid fuchsin solution (Sigma-Aldrich St. Louis, USA) for 15 min and rinsed with distilled water thereafter. Stain differentiation was carried out in phosphomolybdic-phosphotungstic acid solution for 15 min and without rinse, transferred to aniline blue solution and stain for 10 min. The sections were then rinsed briefly in distilled water and differentiated in 1 % acetic acid solution for 5 min. After rinsing in distilled water, sections were dehydrated, cleared and mounted in Permount™ (Thermo Fisher Scientific Inc., MA, USA) with glass cover slips.

c. Immunohistochemical Staining

Although the total amount of collagen deposited within the seeded constructs could be determined via Sircol™ collagen assays, the distribution of deposition for the specific proteins relative to the ECM structure was important for understanding their developmental states. Immunostaining was performed to detect the deposition of collagen type I and type III, and also tenascin-C, an ECM molecule abundantly present in tendons and ligaments relative to other tissue types. At the time of assessment, construct sections were cryosectioned as described and labeled with primary monoclonal antibodies (anti-collagen type I, type III and tenascin-C; Abcam Inc, MA,

USA) at a 1:500 dilution and left overnight at 4 °C. Subsequently, rinsing was performed before biotinylated goat anti-mouse antibodies (Lab Vision Corporation, CA) were administered at a 1:100 dilution for 1 h. After rinsing, the samples were then incubated with Streptavidin- Horseradish peroxidase (HRP) solution (IHC Select DAB Kit, Chemicon, Millipore Corporation, MA, USA), which bound to the biotin-labeled secondary antibody present on the tissue. Unbound enzyme was removed by washing. The chromogenic development reagent, 3, 3' diaminobenzidine (DAB substrate), was then added to react with the HRP attached to the HRP-streptavidin-biotin-antibody complex. The HRP activity on the chromogenic substrate resulted in the deposition of brown to black insoluble precipitate at those antigenic sites containing the specific epitopes recognized by the primary antibodies. After rinsing in distilled water, sections were dehydrated, cleared and mounted in Permount™ (Thermo Fisher Scientific Inc., MA, USA) with glass cover slips. Images were obtained by phase contrast microscopy (IX71 Inverted Research Microscope, Olympus, Germany).

Appendix B6. Real-time qRT-PCR

To assess tenogenic differentiation of the seeded MSCs, gene expression for ligament-related ECM proteins such as collagen type I, collagen type III, tenascin-C and tenomodulin was analyzed and evaluated for the different cultured constructs. At the different time points, total RNA was extracted from the cultured hybrid scaffolds or 2D cultures using the RNeasy Mini Kit® (Qiagen, Valencia, CA, USA) according to the vendor's protocol. RNA concentration was determined by using nanodrop (NanoDrop Technologies, Wilmington, DE, USA) and 200 ng RNA was used to synthesize cDNA with Iscript cDNA synthesis kit (Biorad Laboratories, Hercules, CA, USA). qRT-PCR was performed using QuantiTect SYBR-Green PCR kit (Qiagen, Valencia, CA, USA) to quantify the transcription level of ligament-related genes including collagen I, collagen III, tenascin-C and tenomodulin, using glyceraldehydes 3-phosphate dehydrogenase (GAPDH) as reference genes. The primer sequences used, as summarized in Table A-1, were obtained from published literature [22, 323, 324] and were synthesized by Aitbiotech Pte Ltd (Singapore). cDNA (1 μl) from each sample was mixed with 10.0 ml of QuantiTect SYBR Green PCR master mix, 0.25 ml of each primer, and 8.50 ml of RNase-free water. Quantitative real-time PCR reactions were carried out and monitored using a Stratagene Mx3000P system (Agilent Technologies, Inc., CA, USA). Reaction was done at 95°C for 15 min, followed by amplification for 40 cycles, which included a denaturation step at 95°C for 15 s and an extension step at 60°C for 1 min. The amplification was performed in duplicates and transcription level of the target genes were normalized to GAPDH prior to analysis using the $2^{\Delta Ct}$ formula with reference to undifferentiated MSCs (P3).

Table A-1: Real-time RT-PCR primer sequences.

Primer	Forward primer sequences	Reverse primer sequences
Collagen I (α2)[a]	5'-GCATGTCTGGTTAGGAGAAACC-3'	5'-ATGTATGCAATGCTGTTCTTGC-3'
Collagen III (α1)[a]	5'-AAGCCCCAGCAGAAAATTG-3'	5'-TGGTGGAACAGCAAAAATCA-3'
Tenascin-C[b]	5'-TCTCTGCACATAGTGAAAAACAATACC-3'	5'-TCAAGGCAGTGGTGTCTGTGA-3'
Tenomodulin[c]	5'-CCCACAAGTGAAGGTGGAGAA-3'	5'-AACAGTAACCTCTCTCATCCAGCAT-3'
GAPDH[a]	5'-GACATCAAGAAGGTGGTGAAGC-3'	5'-CTTCACAAAGTGGTCATTGAGG-3'

[a] Col I, Coll III and GAPDH sequences obtained from [22]

[b] Tenascin-C sequences obtained from [323]

[c] Tenomodulin sequences obtained from [324]

Appendix B7. Western Blot

The relative amounts of specific proteins of interest were obtained from Western blot analysis of the cultured scaffolds. At the various time points, cultured hybrid scaffold groups were digested with pepsin (200 mg/mL in 0.5 N acetic acid; Sigma-Aldrich, St. Louis, USA) for 72 h at 4°C for total protein extraction. Upon pepsin inactivation using 10 N NaOH, the protein extract was concentrated using a Microcon 30 centrifugal filter (30,000Mw cutoff, Millipore Co., Bedford, MA, USA). The concentrated protein extracts of each sample was then individually mixed with laemmli buffer and 50 mM Dithiothreitol (DTT) solution, put to 3-8% SDS-PAGE, and blotted onto nitrocellulose membranes. Subsequently, Western blot was carried out using the Western blot kit following vendor's protocol (Zymed Laboratories, Invitrogen, CA, USA). Firstly, the membranes were blocked with blocking buffer for 1 h and incubated at 4°C overnight with diluted (1:500) primary monoclonal antibodies. The specific primary antibodies used were mouse anti-type I collagen, anti-type III collagen, and anti-tenascin-C monoclonal antibody (Abcam Inc, MA, USA). The membranes were then washed with washing buffer five times before incubating with secondary antibodies diluted to 1:200 in blocking buffer for 30 min. After washing with washing buffer again, the membranes were incubated with enhanced chemiluminescence (ECL) working solution for 5 min. Band signals were detected and relative band intensities were obtained and compared among the specimen groups.

Appendix C. Bioreactor Environmental Feedback Control Mechanism

The mechanism to maintain chamber temperature at 37°C was as follows. Temperature probe measured the temperature in the bioreactor chamber. The temperature of the medium was directly proportional to the resistance value measured. This information was fed to the Data Acquisition Card (DAC) which communicated the information to the software in the computer. When the temperature registered was lower than the preset value (37°C), the software instructs to send a small voltage of 24 V to energize a relay in the control panel. This closed the circuit for the heaters and the water temperature rose consequently. This could be described in the following schematic (Figure A-3) with the optimized parameter listed in Table A-2.

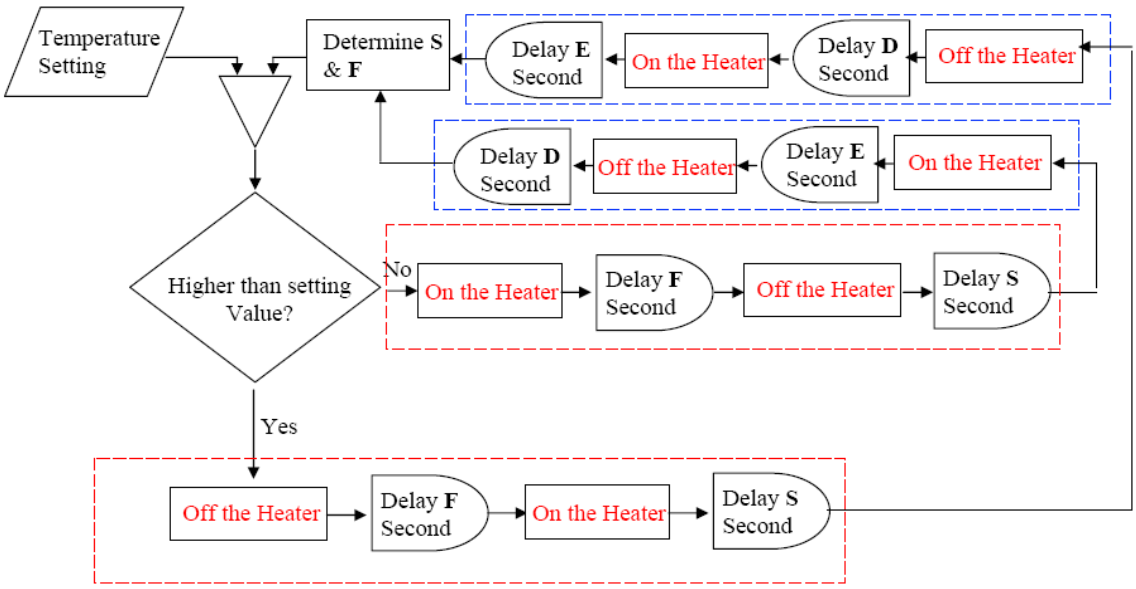

Figure A-3: Schematic of Temperature Control.

Table A-2: Optimized control parameters for temperature control of (A) chambers and (B) water bath.

$\Delta T = |Setting - Measurement|$

(A)

For Chamber 1, 2 & 3	F(s)	S (s)
$\Delta T > 6.0°$	7	0
$6.0° \geq \Delta T > 2.0°$	6	0
$2.0° \geq \Delta T > 0.2°$	4	0
$\Delta T \leq 0.2°$	1	0

(Note: Delay time D= 15 s, Delay time E = 0s)

(B)

For Water Bath Temperature	F(s)	S (s)
$\Delta T > 6.0°$	10	0
$6.0° \geq \Delta T > 2.0°$	9	0
$2.0° \geq \Delta T > 0.2°$	6	0
$\Delta T \leq 0.2°$	1	0

(Note: Delay time D= 10 s, Delay time E = 0s)

For pH control, the pH probe measured the pH value from the medium reservoir and sent it to the DAC which communicated the information to the software in the computer. If the pH reading was higher than the preset value (pH 7.4), the software would instruct to open the CO_2 solenoid valve. If the reading pH value was lower than preset value, the software would instruct to open the release valve. This could be illustrated in the following schematic (Figure A-4) with optimized parameters listed in Table A-3.

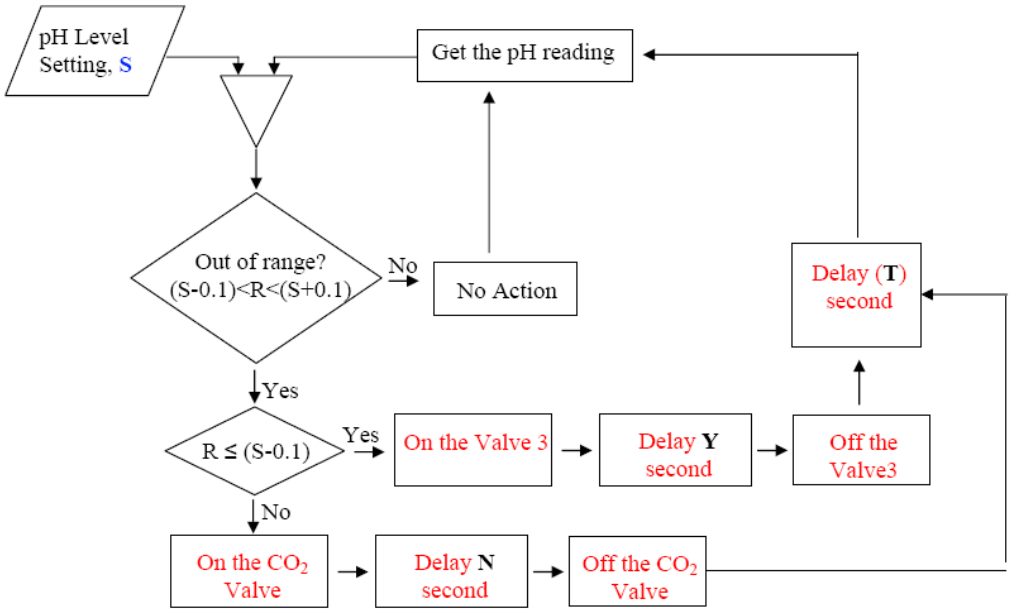

Figure A-4: Schematic of pH Control.

Table A-3: Optimized control parameters for pH control of (A) release valve and (B) CO_2 valve.

Delay Time T = 20s

(A) To calculate Y (for Release valve)

ΔT= S - R	Y(s)
ΔT > 2.0	12
2.0 ≥ ΔT > 1.0	10
1.0 ≥ ΔT > 0.5	8
0.5 ≥ ΔT > 0.1	6
0.1 ≥ ΔT	3

(B) To calculate N (for CO_2 valve)

ΔT= R-S	N(s)
ΔT > 2.0	8
2.0 ≥ ΔT > 1.0	6
1.0 ≥ ΔT > 0.5	4
0.5 ≥ ΔT > 0.1	2
0.1 ≥ ΔT	1

For oxygen control, the system instructed to open O_2 valve when the measured DO value was lower than preset value (30%). When the measured value was higher than

preset value, the system would open the release valve. This process is illustrated in the schematic shown in Figure A-5. The duration at which solenoid valves were opened would depend on the extent of correction to be made, which was optimized as shown in Table A-4.

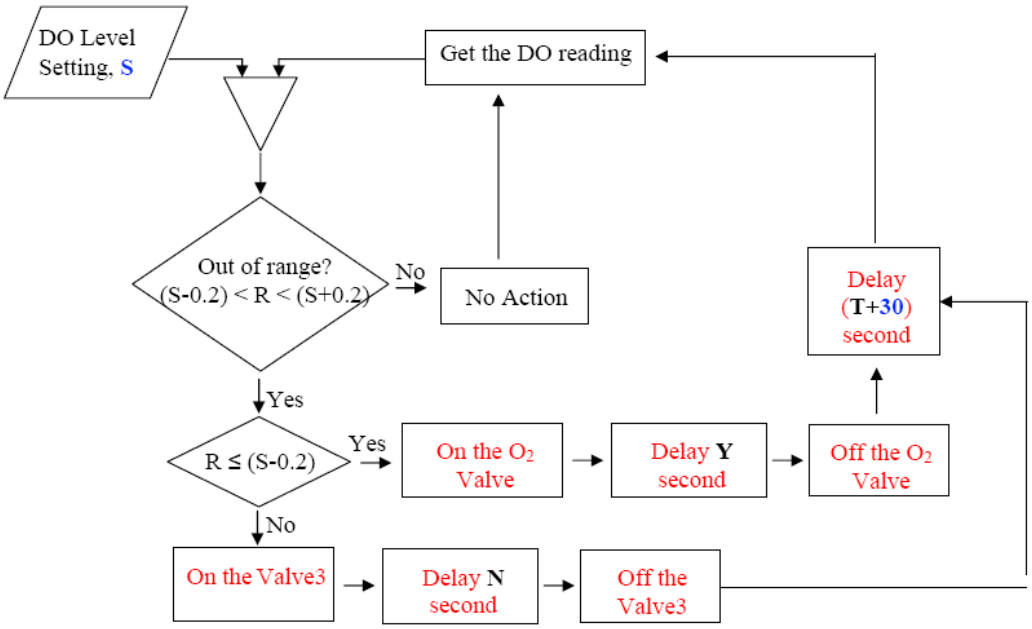

Figure A-5: Schematic of O_2 Control.

Table A-4: Optimized control parameters for O_2 control of (A) O_2 valve and (B) release valve.

Delay Time T = 20s

(A) To calculate Y (for O_2 valve)

ΔT= S - R	Y(s)
ΔT > 5.0	9
5.0 ≥ ΔT > 3.0	7
3.0 ≥ ΔT > 1.0	4
1.0 ≥ ΔT > 0.5	3
0.5 ≥ ΔT	1

(B) To calculate N (for Release valve)

ΔT= R-S	N(s)
ΔT > 5.0	15
5.0 ≥ ΔT > 3.0	10
3.0 ≥ ΔT > 1.0	8
1.0 ≥ ΔT > 0.5	5
0.5 ≥ ΔT	3